цена свободная
price – not fixed

индекс 80568
80568 Index

https://journals.vsu.ru/kcmt/about

ISSN 1606-867X
eISSN 2687-0711

Конденсированные среды и межфазные границы

РЕЦЕНЗИРУЕМЫЙ НАУЧНЫЙ ЖУРНАЛ

Condensed Matter and Interphases

Kondensirovannye Sredy i Mezhfaznye Granitsy

PEER-REVIEWED SCIENTIFIC JOURNAL

Том / Vol. 23, № / No. 3
2021

Condensed Matter and Interphases
Kondensirovannye sredy i mezhfaznye granitsy

Peer-reviewed scientific journal
Published since January 1999
Periodicity: Quarterly
Volume 23, No. 3, 2021

Full-text version is available in the Russian language on the website: https://journals.vsu.ru/kcmf

Condensed Matter and Interphases (Kondensirovannye Sredy i Mezhfaznye Granitsy) publishes articles in Russian and English dedicated to key issues of condensed matter and physicochemical processes at interfaces and in volumes.

The mission of the journal is to provide open access to the results of original research (theoretical and experimental) at the intersection of contemporary condensed matter physics and chemistry, material science and nanoindustry, solid state chemistry, inorganic chemistry, and physical chemistry, and to share scientific data in the **following sections**: atomic, electron, and cluster structure of solids, liquids, and interphase boundaries; phase equilibria and defect formation processes; structure and physical and chemical properties of interphases; laser thermochemistry and photostimulated processes on solid surfaces; physics and chemistry of surface, thin films and heterostructures; kinetics and mechanism of formation of film structures; electrophysical processes in interphase boundaries; chemistry of surface phenomena in sorbents; devices and new research methods.

The journal accepts for publication: reviews, original articles, short communications by leading Russian scientists, foreign researchers, lecturers, postgraduate and undergraduate students.

FOUNDER AND PUBLISHER:
Voronezh State University

The journal is registered by the Russian Federal Service for Supervision of Communications, Information Technology and Mass Media, Certificate of Registration ПИ № ФС77-78771 date 20.07.2020

The journal is included in the List of peer reviewed scientific journals published by the Higher Attestation Commission in which major research results from the dissertations of Candidates of Sciences (PhD) and Doctor of Science (DSc) degrees are to be published. Scientific specialties of dissertations and their respective branches of science are as follows: 02.00.01 – Inorganic Chemistry, 02.00.04 – Physical Chemistry, 02.00.05 – Electrochemistry, 02.00.21 – Solid State Chemistry (Chemical sciences); 01.04.07 – Condensed Matter Physics (Physical Sciences)

The journal is indexed and archived in: Russian Scientific Index Citations, Scopus, Chemical Abstract, EBSCO, DOAJ, CrossRef

Editorial Board and Publisher Office:
1 Universitetskaya pl., Voronezh 394018
Phone: +7 (432) 2208445
https://journals.vsu.ru/kcmf/about
E-mail: kcmf@main.vsu.ru

Signed for printing 30.09.2021

Price – not fixed

Subscription is available using the unified catalogue "Russian Press", subscription index 80568

When reprinting the materials, a reference to the Condensed Matter and Interphases must be cited

The journal's materials are available under the Creative Commons "Attribution" 4.0 Global License

© Voronezh State University, 2021

EDITOR-IN-CHIEF:
V. N. Semenov, DSc in Chemistry, Professor (Voronezh)

VICE EDITORS-IN-CHIEF:
E. P. Domashevskaya, DSc in Physics and Mathematics, Professor (Voronezh)
P. Volovitch, DSc, Professor (Paris, France)

EDITORIAL BOARD:
N. N. Afonin, DSc in Chemistry, Professor (Voronezh)
V. I. Vasil'eva, DSc in Chemistry, Associate Professor (Voronezh)
A. V. Vvedenskii, DSc in Chemistry, Professor (Voronezh)
V. V. Gusarov, DSc in Chemistry, Associate Member of the RAS (St. Petersburg)
V. E. Guterman, DSc in Chemistry, Professor (Rostov-on-Don)
B. M. Darinskii, DSc in Physics and Mathematics, Professor (Voronezh)
V. P. Zlomanov, DSc in Chemistry, Professor (Moscow)
V. M. Ievlev, DSc in Physics and Mathematics, Full Member of the RAS (Moscow)
A. D. Izotov, DSc in Chemistry, Associate Member of the RAS (Moscow)
O. A. Kozaderov, DSc in Chemistry, Associate Professor (Voronezh)
A. I. Marchakov, DSc in Chemistry, Professor (Moscow)
I. Ya. Mittova, DSc in Chemistry, Professor (Voronezh)
V. V. Nikonenko, DSc in Chemistry, Professor (Krasnodar)
O. V. Ovchinnikov, DSc in Physics and Mathematics, Professor (Voronezh)
S. N. Saltykov, DSc in Chemistry, Associate Professor (Lipetsk)
V. F. Selemenev, DSc in Chemistry, Professor (Voronezh)
V. A. Terekhov, DSc in Physics and Mathematics, Professor (Voronezh)
E. A. Tutov, DSc in Chemistry, Associate Professor (Voronezh)
P. P. Fedorov, DSc in Chemistry, Professor (Moscow)
V. A. Khonik, DSc in Physics and Mathematics, Professor (Voronezh)
V. A. Shaposhnik, DSc in Chemistry, Professor (Voronezh)
A. B. Yaroslavtsev, DSc in Chemistry, Associate Member of the RAS (Moscow)

INTERNATIONAL MEMBERS OF THE EDITORIAL BOARD:
M. B. Babanly, DSc in Chemistry, Associate Member of the ANAS (Baku, Azerbaijan)
T. Bellezze, DSc (Ancona, Italy)
R. M. Mane, DSc (Kolhapur, India)
Nguyen Anh Tien, PhD in Chemistry, Associate Professor (Ho Chi Minh City, Vietnam)
V. V. Pan'kov, DSc in Chemistry, Professor (Minsk, Belarus)
F. Scholz, DSc, Professor (Greifswald, Germany)
M. S. Wickleder, DSc, Professor (Cologne, Germany)
V. Sivakov, DSc (Jena, Germany)

EXECUTIVE SECRETARY:
V. A. Logacheva, PhD in Chemistry (Voronezh)

ISSN 1606-867X (Print)
ISSN 2687-0711 (Online)
Конденсированные среды и межфазные границы / Condensed Matter and Interphases. 2021, 23(3)

CONTENTS

Semenov V. N.
A special message from the editor-in-chief of the Condensed Matter and Interphases journal to the readers in connection with the anniversary of Ya. A. Ugai 307

REVIEW

Mittova I. Ya., Sladkopevtsev B. V., Mittova V. O.
Nanoscale semiconductor and dielectric films and magnetic nanocrystals – new directions of development of the scientific school of Ya. A. Ugai "Solid state chemistry and semiconductors" Review 309

Semenov V. N., Naumov A. V.
Interaction of metal sulphides in films deposited from solutions of thiourea coordination compounds. Review 337

Semenova G. V., Zavrazhnov A. Yu.
The development of methods for the research and synthesis of solid phases by the scientific school of Ya. A Ugai. Review 353

ORIGINAL ARTICLES

Vasil'ev M. G., Vasil'ev A. M., Izotov A. D., Kostin Yu. O., Shelyakin A. A.
Technological features of the method of liquid-phase epitaxy when growing InP/GaInAsP heterostructures 374

Vorob'eva V. P., Zelenaya A. E., Lutsyk V. I., Lamueva M. V.
A 3D computer model of the CaO-MgO-Al_2O_3 *T-x-y* diagram at temperatures above 1300 °C 380

Jaloliddinzoda M., Marenkin S. F., Ril' A. I., Vasil'ev M. G., Izotov A. D., Korkin D. E.
Synthesis of bulk crystals and thin films of the ferromagnetic MnSb 387

Kaul A. R., Nygaard R. R., Ratovskiy V. Yu., Vasiliev A. L.
TSF-MOCVD – a novel technique for chemical vapour deposition on oxide thin films and layered heterostructures 396

Kostryukov V. F., Balasheva D. S., Parshina A. S.
Creation of thin films on the surface of InP with a controlled gas-sensitive signal under the influence of PbO + Y_2O_3 compositions 406

Sanygin V. P., Pashkova O. N., Izotov A. D.
Structure and chemical composition of grain boundaries in the magnetic semiconductor GaSb<Mn> 413

Spiridonova T. S., Solodovnikov S. F., Kadyrova Yu. M., Solodovnikova Z. A., Savina A. A., Khaikina E. G.
Double molybdates of silver and monovalent metals 421

Tomina E. V., Sladkopevtsev B. V., Serikov D. V., Mittova I. Ya.
Activation of film growth on indium phosphide by pulsed photon treatment 432

Khort A. M., Yakovenko A. G., Syrov Yu. V.
An integral feature of porous silicon and its classification

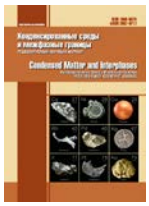

ISSN 1606-867X (Print)
ISSN 2687-0711 (Online)
Condensed Matter and Interphases
Kondensirovannye Sredy i Mezhfaznye Granitsy
https://journals.vsu.ru/kcmf/

A special message from the editor-in-chief of the Condensed Matter and Interphases journal to the readers in connection with the anniversary of Ya. A. Ugai

Dear colleagues and readers!

On September 20, 2021 we celebrate the 100th anniversary of the birth of an outstanding scientist and teacher of Voronezh State University, DSc in Chemistry, Professor Yakov Aleksandrovich Ugai, the founder of a new priority branch of science "The chemistry of semiconductors". Yakov Aleksandrovich was the founder and head of the leading scientific school “Solid state chemistry and semiconductors”. The school has had more than 650 studies (including certificates of authorships and patents) published in central domestic periodicals: Proceedings of the USSR Academy of Sciences and RAS, Russian Chemical Reviews, Russian Journal of Inorganic Chemistry, Russian Journal of Physical Chemistry, Russian Journal of General Chemistry, Inorganic Materials, Journal of Applied Chemistry, Semiconductors, Solid-state Physics and in foreign press. In addition, 7 monographs have been published, including: Shevchenko V. Ya., Ugai Ya. A., et al. “Crystallochemical problems of semiconductors”. M.: Science, 1975. 132 p., Ugai Ya. A., Goncharov E. G., Semenova G. V., et al. “Phase equilibria between phosphorus, arsenic, antimony, and bismuth”. M.: Science, 1989. 204 p.

The first studies by Yakov Aleksandrovich and his colleagues on the identification of new semiconductor substances (Proceedings of the USSR Academy of Sciences 1961–1965, Russian Journal of Inorganic Chemistry 1962–1964) have laid the foundations for a scientifically grounded classification of semiconductors. (Ugai Ya. A. “Introduction to the chemistry of semiconductors”. M.: High School, 1965. 332 p. and 1975. 300 p.).

The idea of the dependence of the properties of solids, not only on the qualitative and quantitative composition, but also on their crystallochemical

structure, runs like a golden thread in all the textbooks of Ya. A. Ugai, intended for students of chemical faculties of classical universities (Ya. A. Ugai "General chemistry". M.: High School, 1977. 408 p. and 1984. 438 p.). He was one of those who redefined the concepts and problems of inorganic chemistry relating to the solid state of matter. (Ya. A. Ugai "Inorganic Chemistry". M.: High School, 1989. 463 p.). His textbook "General and Inorganic Chemistry". M.: High School, 1997. 527 p. was reprinted several times from 1997 to 2007. This textbook is still in demand, not only in the leading universities of Russia, but also abroad.

For his research on the chemical thermodynamics of semiconductors as part of a group of scientists in 1981, Ya. A. Ugai was awarded the USSR National Prize in Science. Ya. A. Ugai took an active part in the certification of scientific personnel, for more than two decades he was a member of the expert committee on inorganic chemistry of the State Commission for Academic Degrees of the USSR and the Russian Federation. For more than 10 years he was the head of the doctoral dissertation board on chemical sciences of Voronezh State University and was a member of the editorial board of the journal "Inorganic materials" of the Russian Academy of Sciences.

From 1962 to 1966 he was the head of the Department of Semiconductor Chemistry, the first of its kind in the USSR, which he created. From 1975 to 1984 he was the vice-rector for research of Voronezh State University, at the same time he was the head of the Department of General and Inorganic Chemistry. He was awarded the Order of Friendship of Peoples. In 1995, the city council elected him as a Distinguished Citizen of Voronezh.

Yakov Aleksandrovich was the supervisor of more than 70 PhD students, out of which 9 people obtained DSc degree. Ya. A. Ugai was a bright, outstanding personality: highly erudite, cheerful, and possessed encyclopaedic knowledge. Until now, there are legends about his lectures, which were attended by both his students, who became teachers, and employees of other faculties and universities. In addition to the excellent, clear presentation of the main material, he kept the attention of the audience alive and always found the opportunity and time to share facts regarding the history of chemistry and the biography of scientists.

The staff of the Faculty of Chemistry, his students, and followers try to preserve all the traditions laid down by Yakov Aleksandrovich Ugai, as evidenced by the articles of this anniversary issue of the journal, which cover topics related to materials science in solid state chemistry and inorganic and physical chemistry.

Editor-in-chief of the journal "Kondensirovannye sredy i mezhfaznye granitsy = Condensed matters and interphases", Dean of the Chemical Faculty of Voronezh State University, DSc in Chemistry, Professor V. N. Semenov

Translated by Valentina Mittova

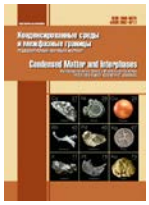

ISSN 1606-867X (Print)
ISSN 2687-0711 (Online)
Condensed Matter and Interphases
Kondensirovannye Sredy i Mezhfaznye Granitsy
https://journals.vsu.ru/kcmf/

Review

Review article
https://doi.org/10.17308/kcmf.2021.23/3524

Nanoscale semiconductor and dielectric films and magnetic nanocrystals – new directions of development of the scientific school of Ya. A. Ugai "Solid state chemistry and semiconductors". Review

I. Ya. Mittova[1], B. V. Sladkopevtsev[1], V. O. Mittova[2]

[1]*Voronezh State University,*
1 Universitetskaya pl., Voronezh 394018, Russian Federation

[2]*Voronezh State Medical University named after N. N. Burdenko,*
12 Studencheskaya Street, Voronezh 394036, Russian Federation

Abstract

New directions of development of the scientific school of Yakov Aleksandrovich Ugai "Solid state chemistry and semiconductors" were considered for the direction "Study of semiconductors and nanostructured functional films based on them", supervised by I. Ya. Mittova. The study of students and followers of the scientific school of Ya. A. Ugai cover materials science topics in the field of solid-state chemistry and inorganic and physical chemistry. At the present stage of research, the emphasis is being placed precisely on nanoscale objects, since in these objects the main mechanisms of modern solid-state chemistry are most clearly revealed: the methods of synthesis - composition - structure (degree of dispersion) - properties. Under the guidance of Professor I. Ya. Mittova DSc (Chem.), research in two key areas is conducted: "Nanoscale semiconductor and dielectric films" and "Doped and undoped nanocrystalline ferrites". In the first area, the problem of creating high-quality semiconductor and dielectric nanoscale films on $A^{III}B^{V}$ by the effect reasonably selected chemostimulators on the process of thermal oxidation of semiconductors and/or directed modification of the composition and properties of the films. They present the specific results achieved to date, reflecting the positive effect of chemostimulators and modifiers on the rate of formation of dielectric and semiconductor films of the nanoscale thickness range and their functional characteristics, which are promising for practical applications.

Nanomaterials based on yttrium and lanthanum orthoferrites with a perovskite structure have unique magnetic, optical, and catalytic properties. The use of various approaches to their synthesis and doping allowing to control the structure and properties in a wide range. In the field of magnetic nanocrystals under the supervision of Prof. I. Ya. Mittova studies of the effect of a doping impurity on the composition, structure, and properties of nanoparticles of yttrium and lanthanum orthoferrites by replacing the $Y(La)^{3+}$ and Fe^{3+} cations are carried out. In the Socialist Republic of Vietnam one of the talented students of Prof. I. Ya. Mittova, Nguyen Anh Tien, performs studies in this area. To date, new methods for the synthesis of nanocrystals of doped and undoped ferrites, including ferrites of neodymium, praseodymium, holmium, etc. have been developed.

Keywords: Semiconductors, Dielectrics, Magnetic nanocrystals, Ferrites, Nanoscale films, Nanocrystals

Acknowledgements: the authors are grateful to Full Member of the Russian Academy of Sciences V. M. Ievlev for providing the opportunity for further creative development of research within the framework of the scientific school, for their support and assistance.

For citation: Mittova I. Ya., Sladkopevtsev B. V., Mittova V. O. Nanoscale semiconductor and dielectric films and magnetic nanocrystals - new directions of development of the scientific school of Ya. A. Ugai "Solid state chemistry and semiconductors". *Kondensirovannye sredy i mezhfaznye granitsy = Condensed Matter and Interphases*. 2021;23(3): 309–336. https://doi.org/10.17308/kcmf.2021.23/3524

Для цитирования: Миттова И. Я., Сладкопевцев Б. В., Миттова В. О. Наноразмерные полупроводниковые и диэлектрические пленки и магнитные нанокристаллы – новые направления развития научной школы Я. А. Угая «Химия твердого тела и полупроводников». *Конденсированные среды и межфазные границы*. 2021;23(3): 309–336. https://doi.org/10.17308/kcmf.2021.23/3524

✉ Irina Ya. Mittova, e-mail: imittova@mail.ru
© Mittova I. Ya., Sladkopevtsev B. V., Mittova V. O., 2021

The content is available under Creative Commons Attribution 4.0 License.

1. Introduction

New research of the scientific school of Ya. A. Ugai "Solid state chemistry and semiconductors" [1] in the subdivision "Study of semiconductors and nanostructured functional films based on them", supervised by I. Ya. Mittova, are developing in a number of directions "in breadth and depth". They are performed by both the followers of Yakov Aleksandrovich's work and by the "students of followers", which is reflected in Table 1. In fact, we can talk about a deeper scientific continuity, since Yakov Aleksandrovich defended his Ph.D. thesis on the physical and chemical analysis of salt systems under the guidance of Prof. A. P. Palkin, who, in turn, was a student of Full Member of the Russian Academy of Sciences N. S. Kurnakov. The coverage of modern materials science topics in the field of solid-state chemistry and inorganic and physical chemistry as developed by students and followers of the scientific school of Ya. A. Ugai, his "scientific children, grandchildren, and great-grandchildren" can be seen in Table 1. Here one cannot fail to mention one of the most talented, beloved, and successful students of Ya. A. Ugai, Evelina Domashevskaya. For many years she was the Head of the Department of Solid-State Physics and Nanostructures of Voronezh State

Table 1. Defence of thesis

No.	Thesis	Full name of the applicant	Title of dissertation	Year of defence
1	2	3	4	5
Scientific advisor/consultant Prof. I. Ya. Mittova				
1	Doctorate	Natalia Ivanovna Ponomareva	Formation of functional layers on semiconductors by chemical vapour deposition from organoelement compounds	2004
2	Doctorate	Alexander Mikhailovich Samoilov	Directed synthesis of lead telluride films doped with gallium and indium with the controlled content of impurity atoms and deviation from stoichiometry	2006
3	Doctorate	Viktor Fedorovich Kostryukov	Combined effect of chemostimulants on the thermal oxidation of gallium arsenide	2011
4	Doctorate	Elena Viktorovna Tomina	Chemically stimulated oxidation of GaAs and InP under the action of d-metals (Ni, Co, V), their oxides and oxide compositions	2017
5	PhD	Tatiana Alexandrovna Gadebskaya	Growth kinetics and some properties of doped oxide films on silicon	1983
6	PhD	Natalia Ivanovna Ponomareva	Interaction of chlorides of elements of III, IV and V groups with the surface of silicon and gallium arsenide in an oxidizing atmosphere	1984
7	PhD	Victoria Vladimirovna Pukhova	Interactions in Si-E_xS_y structures (E = In, Ge, Pb, Sb, Bi) and GaAs-E_xS_y(E = In, Pb, Sb) during their thermal oxidation	1986
8	PhD	Vera Vasilievna Sviridova	Thermal oxidation of gallium arsenide and indium phosphide in the presence of impurity oxides	1995
9	PhD	Irina Vladimiovna Kuznetsova	Phase formation processes in alumina ceramics modified with oxides of copper, nickel and boron	1995
10.	PhD	Elena Viktorovna Tomina	Thermal oxidation of gallium arsenide and indium phosphide with the participation of chlorides and oxochlorides of elements of groups IV - VI	1997
11	PhD	Viktor Fedorovich Kostryukov	Nonlinearity of the combined effect of lead, antimony and bismuth oxides on the thermal oxidation of gallium arsenide	2000
12	PhD	Olga Anatolyevna Pinyaeva	Chemostimulating effect of chromium derivatives on thermal oxidation of gallium arsenide	2001

End of Table 1

1	2	3	4	5
13	PhD	Olga Vladimirovna Artamonova	Synthesis of nanoceramic materials based on zirconium dioxide stabilized with indium oxide	2004
14	PhD	Alexey Sergeevich Sukhochev	Solid-phase interactions during the thermal oxidation of Me/GaAs and MeO/GaAs structures (Me = Fe, Co, Ni)	2006
15	PhD	Irina Alexandrovna Donkareva	Localization regions of interactions between activator oxides during the thermal oxidation of gallium arsenide	2006
16	PhD	Petr Konstantinovich Penskoy	Thermal oxidation of GaAs under the influence of Sb_2O_3, Bi_2O_3, MnO, MnO_2 chemostimulant compositions with inert components Ga_2O_3, Al_2O_3, Y_2O_3	2009
17	PhD	Nguyen Anh Tien	Synthesis, structure and properties of $La(Y)_{1-x}Sr(Ca)_xFeO_3$ (x = 0.0; 0.1; 0.2; 0.3) nanopowders	2009
18	PhD	Alexander Alexandrovich Lapenko	Evolution of nanoscale film and island structures Me/InP (GaAs) and Me_xO_y/ InP (GaAs) (Me = V, Co) during thermal oxidation	2010
19	PhD	Dinh Van Tac	Sol-gel synthesis and properties of nanocrystalline ferrites based on Y_2O_3-Fe_2O_3 system	2012
20	PhD	Boris Valdimirovich Sladkopevtsev	Influence of the methods for the formation of V_xO_y/InP structures on the features of their thermal oxidation and the composition of the films	2013
21	PhD	Alexey Alekseevich Samsonov	Thermal oxidation of InP modified by deposited compositions of NiO+PbO, V_2O_5+PbO oxides	2013
22	PhD	Maria Viktorovna Berezhnaya	Effect of zinc and barium on the structure and properties of $YFeO_3$ and $LaFeO_3$-based nanopowders synthesized by the sol-gel method	2019
Scientific adviser prof. N. I. Ponomareva				
23	PhD	Pavel Ivanovich Manelyak	Influence of an anolyte disinfectant solution on the stability of geometric shapes of silicone imprints (joint supervision with DSc in Medical Sciences, Professor Edward Sarkisovich Kalivrajian, now deceased)	2009
24	PhD	Elena Viktorovna Budakova	Clinical and experimental substantiation of the use of an isoprene-styrene thermoplastic elastomer for basic removable laminar dentures (joint supervision with DSc in Medical Sciences, Professor Edward Sarkisovich Kalivrajian, now deceased)	2009
25	PhD	Tatiana Dmitrievna Poprygina	Synthesis, structure, and properties of hydroxyapatite and the composites and coatings based on it	2012
Scientific adviser Prof. A. M. Samoilov				
26	PhD	Mikhail Konstantinovich Sharov	Synthesis and properties of lead telluride films doped with gallium on silicon substrates	2000
27	PhD	Sergey Vladimirovich Belenko	One-step synthesis of gallium-doped PbTe/Si films with a specified composition and optimized functional parameters	2013

University, and now she is a professor of this department. The scientific school created by her "Atomic and electronic structure of solid state and nanostructures" is widely known not only in Russia, but also around the world. Undoubtedly, a great contribution in the formation of our scientific school was made by such outstanding students of Yakov Aleksandrovich as Associate Professor E. M. Averbakh (his first graduate student), professor V. Z. Anokhin, Associate Professors V. R. Pshestanchik and V. L. Gordin, who have unfortunately passed away. All of them laid the foundations for the study of objects that were new for that time, thin films of various functional purposes on semiconductors. New objects of research are mainly nanoscale, since in this area the main regularity of modern solid-state chemistry is most visibly and clearly manifested: synthesis method – composition – structure (degree of dispersion) – properties. This choice was due to the need to establish new fundamental laws of solid-state chemistry, the requirements of modern materials science, reflected in the current List of Critical Technologies (Technologies for the Production and Processing of Functional Nanomaterials) and the List of Priority Areas for the Development of Science, Technology and Engineering in the Russian Federation (Industry of Nanosystems).

2. Nanoscale semiconductors and dielectric films

Prospects for the development of all spheres of human activity are unambiguously associated with the improvement of microelectronic and nanoelectronic element bases. A variety of properties of $A^{III}B^{V}$ type semiconductors determines their widespread use in devices for various technical purposes: for the production of the variety of optoelectronic devices in the infrared and visible ranges, high-speed electronic and powerful microwave devices [2].

One of the main tasks of the targeted formation of heterostructures on $A^{III}B^{V}$ with the desired properties is the production of high-quality dielectric and semiconductor films of nanometer thickness and the improvement of the properties of the interfaces. The creation of high-quality heterostructures on $A^{III}B^{V}$ by thermal oxidation is complicated by the mechanisms of ongoing processes, due to the implementation of a negative communication channel between the stages of component-wise oxidation in the case of InP, the enrichment of films with unoxidized indium, and the segregation of arsenic in the elementary state at the inner interface of the heterostructure for GaAs [3]. Thermal oxidation of $A^{III}B^{V}$ with the simultaneous action of interface modifiers and growing films, allowing to control their composition, nanostructure and properties, and chemostimulating agents promoting the accelerated formation of films with a decrease in the operating parameters of the process and blocking the negative communication channel of the intrinsic thermal oxidation of $A^{III}B^{V}$, allows achieving acceptable optical and electrophysical characteristics and to control the nanostructure of films, which is one of the factors determining their properties.

High-quality thermal oxide films on InP can be used in the development of highly efficient and cheap photoconverters of natural and linearly polarized radiation based on InP. Gallium arsenide, along with indium phosphide, is the most promising material for the production of next generation microwave integrated circuits [4].

The emergence of gallium arsenide microelectronics resulted in the creation of efficient and high-power injection lasers and LEDs in the wavelength range of 600-900 nm based on GaAs/GaAlAs heterostructures. Indium phosphide turned out to be a necessary component of more complex heteroepitaxial structures. As a result of these studies, InP technology arose and was rapidly developed, which currently constitutes a significant portion of micro- and optoelectronics. Laser diodes based on InP/InGaPAs/InP are a key element of optoelectronics for fiber-optic communication, processing, data storage, etc., since they cover the ranges of the highest optical fibre transparency (wavelengths 1.3 and 1.55 μm) [5]. In modern commercial and technical cable communications (intercomputer communications, long-distance telephony, local networks, etc.), these heterolasers are mainly used.

The energy parameters of the single-crystal phase of InP and GaAs are very close to the parameters of single-crystal silicon, which allows the manufacture of hybrid integrated electronics

devices compatible with silicon [6]. In addition to the production technology of microwave integrated circuits [4, 7, 8], heterostructures based on indium phosphide and gallium arsenide find many other applications, for example, as photodetectors [9, 10], in field-effect transistors based on Gatestacktechnology [11], memory cells [12], optoelectronic devices [13], in solar cells [14].

Wide-gap and optically transparent gallium phosphide is the main material for the creation of light-emitting diodes, photodetectors, photodetectors; it is promising for the development of high-temperature electronics devices capable of operating at temperatures significantly exceeding the reached limits of modern temperature sensors [15–17]. The unique optical properties of GaP single crystals are used to manufacture optical lenses and lenses for lasers [13]. However, any practical application of GaP requires the formation of various functional films (conductive, dielectric, antireflection, etc.) on its surface, which is undoubtedly associated with a number of technical difficulties. The use of gallium phosphide as waveguides and optical lenses for lasers is usually associated with the encapsulation of GaP single crystals in layers of a material with a lower refractive index (nGaP < 3.3), i.e., antireflection. Usually, AlGaP is used as the deposited material, which is well matched in lattice size with GaP [18].

Separately, it is necessary to highlight the areas of research associated with the formation of $A^{III}B^{V}$ metal oxide semiconductor heterostructures by various methods. Among them are ZnO/InP heterostructures used to create optoelectronic devices and acoustic sensors [19, 20]; SnO_2/InP with certain electrophysical properties, allowing their use as gas-sensitive sensors [21, 22]; multilayer heterostructures with a manganese dioxide layer with promising magnetic characteristics [23]. The range of synthesis methods used for such heterostructures is extremely wide: aerosol pyrolysis, molecular beam epitaxy, magnetron sputtering, CVD processes, etc. However, now, the idea of multipurpose control of the formation of functional nanoscale films on the surface of $A^{III}B^{V}$ semiconductors by dopants remains practically unrealized. This approach allows fine adjustment of the kinetics and mechanism of the synthesis processes of these objects and the variation of their composition, nanostructure, and, consequently, their properties within wide limits.

In the modern world, the demand for portable gas sensors is increasing due to the need for their widespread use in various branches of technology (for the prevention of explosions, fires) and for the control of environmental pollution. All these circumstances stimulated the development of research in the field of semiconductor gas sensors around the world. However, the study of the physical and chemical processes underlying the operation of sensors is still far from complete. Namely, the understanding of these processes allowed creating a new generation of highly efficient, reliable, and economical devices based on sensor elements. Among the materials studied, nanocrystalline tin dioxide has found the greatest practical application [24–27]. In addition to tin dioxide materials, other oxide materials are also studied (In_2O_3, ZnO, MoO_3, Ga_2O_3), which may be of interest for creating chemical sensors. Indium oxide is characterized by its high sensitivity, fast response, a convenient range of resistance variation, and a sufficiently low temperature for detecting oxidizing and reducing gases in air [24]. The data [28, 29] and the results of studies [30] suggest that the decisive role in the exceptional sensory properties of In_2O_3 belongs to the high mobility of surface oxygen, which is characteristic for this oxide. There is an adsorption-competitive mechanism of the sensory response, which is associated with the displacement of oxygen from the surface with the subsequent adsorption of the detected gas molecules on the active sites of indium oxide. However, the low-dimensional structure of a single semiconducting metal oxide obtained by various methods does not solve the problem of selectivity and stability of the sensor material.

Therefore, it becomes necessary to alloy the oxide. It was shown in the study [24] that $Fe_2O_3 \cdot In_2O_3$ thin films exhibit maximum sensitivity to ozone at an operating temperature of 370 °C. In addition, the number of studies in which it was proposed to use multicomponent systems based on indium oxide with additives of other metal oxides ZnO – In_2O_3, MgO – In_2O_3, In_2O_3–SnO_2 for the detection of chlorine in air is currently increasing [31, 32]. Attention is also paid to sensors based on copper oxide [33–35].

A significant disadvantage of the materials presented in the literature by various authors for the production of sensors is the high operating temperature (above 200 °C). This disadvantage can be offset by creating materials of mixed compositions [35].

The main direction of the development of our ideas, continuing the development of the considered section of the scientific school, is the use of chemostimulators and modifiers of the interface and growing films in the process of $A^{III}B^{V}$ oxidation for the control of the rate of their formation, composition, nanostructure, and properties [36–39]. The solution to the problem of creating high-quality semiconductor and dielectric films of nanometer scale thickness on $A^{III}B^{V}$ is possible when changing the mechanism of thermal oxidation of these semiconductors from intrinsic to chemostimulated by influencing the process using reasonably selected chemostimulators and/or directed modification of the composition and properties of the films. The participation of chemostimulators in the oxidation process ensures the occurrence of new interface reactions with kinetically coupled and heterogeneous catalytic stages. In this case, the kinetic blocking of negative communication channels between the stages of oxidation of components A^{III} and B^{V} due to the creation of new, positive channels with the participation of chemostimulators, the temperature and time of the synthesis process are reduced with a simultaneous modification of the composition and properties of functional films of nanometer thickness in the case of a chemostimulator with a modifying effect. We have previously shown [40–42] that the use of only modifiers of the inner interface and the films themselves already prevents the evaporation of the volatile component and degradation of the inner interface, reduce the density of surface states at the inner interface of the heterostructure, and control the structure and surface relief at the nanoscale. Naturally, the use of the combined action of a chemostimulator and a modifier is the most effective approach to solving this scientific problem. Based on many years of research, we have developed 2 methods for introducing a chemostimulator (modifier) into an oxidizing environment: directly in the process of thermal oxidation of a semiconductor through the gas phase (method 1) and preliminary application to the surface, after which thermal oxidation of an already formed heterostructure occurs (method 2). At the same time, depending on the effect on the semiconductor surface, is the process of applying a chemostimulator (modifier), in the framework of method 2 we used two methods: method 1 (hard method) magnetron or vacuum-thermal deposition on the semiconductor surface and method 2 (soft method) of aerosol deposition or centrifugation. There is no noticeable effect on the semiconductor surface during the creation of the heterostructure using method 2 [43, 44].

The use of modifiers in combination with chemostimulators, in addition to blocking the diffusion of component A into the film in the unoxidized state and chemical bonding of component B at the inner interface, provides control over the growth rate, nanostructure, and properties of thermal oxide films and allows the development of new processes for the formation of functional nanosized dielectric and semiconductor films on $A^{III}B^{V}$ semiconductors. The combined use of growth chemostimulators and modifiers is especially important in the formation of nanoscale films of a given thickness, when in the process of oxidation using only a chemostimulating agent due to the small thickness of the synthesized samples, the positive effect of the chemostimulator may not be fully realized [45, 46]. Chemostimulating and modifying agents can be introduced during the oxidation of semiconductors in one compound. In particular, with the chemical deposition of sulphides (PbS, Sb_2S_3, etc.) on the surface of semiconductors, during the oxidation of the formed heterostructures, the cation-forming element capable of the transit transfer of oxygen to the substrate components provides the rapid formation of the film by the catalytic or transit mechanism, partially performing the modifying function during its doping. The main modifying role is played by the anionic agent, influencing the characteristics of the internal interface, the composition, and, consequently, the characteristics of the films. The change in the composition of the films in the processes of oxidation of sulphide/semiconductor heterostructures according to the sulphide –

sulphate – oxosulphate – oxide scheme allows obtaining a whole spectrum of their different characteristics. The effectiveness of the effect of sulphur on the properties of the internal interface of a thermal oxide film with a semiconductor was demonstrated by preliminary treatment of the substrate surface in sulphur vapour [47, 48].

The use of complex compounds such as manganese and bismuth vanadate phosphates in the processes of chemically stimulated $A^{III}B^{V}$ oxidation demonstrated a positive effect [49, 50], since manganese and bismuth oxides previously were demonstrated as effective chemostimulators of thermal oxidation of $A^{III}B^{V}$, in which the cation has a pronounced chemo-stimulating activity, and the anion can provide ready-made fragments of growing oxide films such as PO_4^{3-} groups or groups that are isostructural to them.

The use of chemostimulators and/or modifiers is promising for the stepwise synthesis of nanoscale films on $A^{III}B^{V}$ in combination with different types of activation of their action, heat treatment or pulsed photonic treatment, which expands the possibilities of controlling the rate of formation of films, their composition, structure, and properties [43, 44, 51].

Some of the specific results achieved to date reflecting the positive effect of chemostimulators and modifiers on the rate of formation of dielectric and semiconductor films of the nanoscale thickness range and their functional characteristics that have prospects for practical application are summarized in Table 2.

The main fundamental results achieved by the scientific group under the supervision of DSc in Chemistry, Professor I. Ya. Mittova, which includes DSc in Chemistry E. V. Tomina and V. F. Kostryukov, PhD in Chemistry B. V. Sladkopevtsev and A. A. Samsonov, PhD students and students, are as follows:

1. The concept of the multifunctional effect of chemostimulators-modifiers, often in one compound and in a single process, was proposed. Schemes were also proposed for the mechanisms of thermal oxidation processes of $A^{III}B^{V}$ under the influence of simple and complex compounds and their compositions as a physicochemical basis for the development of new processes for the formation of semiconductor and dielectric films on $A^{III}B^{V}$ with a given growth rate and target characteristics. The specificity of catalytic processes in new nonequilibrium systems with solid-phase thin-film catalysts, reagents, and products has been revealed. The nature of the synergistic effects of the joint action of the chemostimulators deposited on the surface of $A^{III}B^{V}$ semiconductors and modifiers of the processes of oxidation of heterostructures was established [36–38,52–55].

2. The nonlinear effects of the influence of binary compositions of oxide-chemostimulators on the formation of thin films on GaAs and InP were established and quantitatively interpreted using the concept of relative partial and integral thicknesses [39, 56–64].

3. The dependence of the nonlinear effect of the combined action of chemostimulators on the oxidation state of the element forming one of the oxides of the composition was revealed, both paired with the oxide of another element, and with the oxide of the same element, but in a different oxidation state [59, 65, 66].

4. The nature and spatial localization of binding stages under the combined action of chemostimulators on the thermal oxidation of GaAs and InP, responsible for the observed nonlinear effects, have been established [67–71].

5. The fundamental possibility of the additive effect of a composition of oxides, one of which is an inert component, on the process of thermal oxidation of GaAs has been proved [72–78].

6. The presence of a sensor signal for the presence of reducing gases in the atmosphere for of thin films synthesized on the surface of GaAs and InP by chemically stimulated thermal oxidation under the influence of both individual chemostimulating oxides and their compositions was established [79–82].

7. Methods for precision doping of thin films on the surface of GaAs and InP have been developed [81, 83, 84].

8. Methods were developed for the synthesis of nano-sized nanostructured oxide films on InP and GaAs using a V_2O_5 gel allowing to modify the surface of semiconductors under mild conditions, characterized by their efficiency and ease of implementation, variability of the composition, the thickness and morphology of deposited layers of oxide dopants over a wide range [43, 51, 85, 86].

Table 2. Multifunctionality of the action of chemostimulants and modifiers in the processes of synthesis of nanoscale films on $A^{III}B^{V}$

Characteristics of the object		Oxidation mode, T, °C / t, min	EAE, kJ/mol Stage 1 / Stage 2	Oxidation mechanism	Relative increase in film thickness compared to intrinsic oxidation (% or times)	The composition of the films	The result of the impact	Resistivity (ρ), breakdown voltage (E)	Properties of the synthesized films
Chemo-stimulant	Semicon-ductor								
Modifiers									
Method - introduction through the gas phase									
$AlPO_4$	InP	475–550/10–60	153	intrinsic	120%	$AlPO_4$, $InPO_4$,	modification		
Method – surface application – hard methods									
SnO_2	InP	475–550/10–60	48	intrinsic	–	$In(PO_3)_3$, P_2O_5, In_2O_3, SnO_2, $Sn_3(PO_4)_2$	modification	$\rho = 9.0 \cdot 10^6$ Ohm·cm	semiconductor
Superposition modifier + modifier									
SnO_2/InP + $AlPO_4$	InP	530/10–60		intrinsic	–	$AlPO_4$, $InPO_4$, $Sn_3(PO_4)_2$	modification	$\rho = 8.5 \cdot 10^7$ Ohm·cm	semiconductor
Chemostimulants									
Method – surface application – hard methods									
MnO_2	GaAs	450–550/10–60	95	transit	up to 7.5 times	Ga_2O_3, As_2O_5, MnO_2	chemo-stimulation	$\rho = 1.2' 10^{10}$ Ohm·cm; $E = 5.2 \cdot 10^6$ V/cm	dielectric
	InP	450–550/10–60	180	transit	up to 2.1 times	In_2O_3, $InPO_4$, Mn_2O_3, MnO_2	chem-ostimulation	$\rho = 6.3 \cdot 10^8$ Ohm·cm; $E = 7 \cdot 10^6$ V/cm	dielectric
Superposition chemostimulant + modifier									
Method – surface application – soft methods									
$BiP_xV_{1-x}O_4$	InP	490–570/5–60	51	transit-catalytic	62 – 248%	$BiVO_4$, $InPO_4$ $BiPO_4$, V_2O_5	chemo-stimulation and modification		
$Mn_3(P_xV_{1-x}O_4)_2$	GaAs	490–550/5–60	156	transit	up to 220%	$MnAsO_4$, $Mn_3(VO_4)_2$, $Mn_3(PO_4)_2$, GaAs, $GaAsO_4$	chemo-stimulation and modification		

Method – application to the surface and simultaneous introduction from the gas phase								
MnO_2/InP+ $Mn_3(PO_4)_2$ [d]	InP	450–550/10–60	110	transit	up to 240%	$In(PO_3)_3$, $Mn_2P_2O_7$, MnO, Mn_2O_3, $Mn_3(PO_4)_2$, $MnPO_4$	chemo-stimulation and modification	$\rho = 1.5 \cdot 10^{10}$ Ohm·cm	dielectric
Superposition of chemostimulant + inert component									
Sb_2O_3+Y_2O_3	GaAs	530/10–40		transit	2–6 times	Ga_2O_3, As_2O_3, Sb_2O_3	chemo-stimulation	$\rho = 1.5 \cdot 10^6$ Ohm×cm	Semiconductor with gas sensitivity
PbO + Y_2O_3	InP	560/10–60		transit	2–4 times	In_2O_3, $InPO_4$, PbO	chemo-stimulation	$\rho = 1.5 \cdot 10^6$ Ohm×cm	Semiconductor with gas sensitivity
Superposition chemostimulant + chemostimulant									
PbO + Bi_2O_3	GaAs	530/10–40		transit	2–4 times	Ga_2O_3, As_2O_3, PbO, Bi_2O_3	chemo-stimulation	$\rho = 1 \cdot 10^6$ Ohm×cm	Semiconductor with gas sensitivity
Sb_2O_3 + V_2O_5	GaAs	530/10–40		transit	3–6 times	Ga_2O_3, As_2O_3, Sb_2O_3, V_2O_5	chemo-stimulation	$\rho = 1 \cdot 10^6$ Ohm×cm	Semiconductor with gas sensitivity
PbO + V_2O_5	InP	560/10–60		transit	2–4 times	In_2O_3, $InPO_4$, PbO, V_2O_5	chemo-stimulation	$\rho = 1 \cdot 10^6$ Ohm×cm	Semiconductor with gas sensitivity
Standards									
	GaAs, standard-1	450–550/10–60	110	intrinsic	–	As, Ga_2O_3, As_2O_3	–	$\rho = 1 \cdot 10^5$ Ohm×cm	Semiconductor
	InP, standard-2	450–550/10–60	270	intrinsic	–	In, In_2O_3, $InPO_4$	–	Ohmic conductivity	Conductive

9. Studies of the chemically stimulated thermal oxidation of GaAs and InP have established the decisive influence of the physicochemical nature of the chemostimulator, the procedure and the method of its introduction into the system on the mechanism of the process. It was shown that the introduction of an oxide chemostimulator through the gas phase and its application by soft methods on the semiconductor surface causes the transit mechanism of oxidation. The application of compounds providing a renewable cyclicity of the process by rigid methods provides a synchronous catalytic mechanism for the process. Data on the dependence of the composition, thickness, and rate of formation of films, their morphology on the procedure and method of introducing various chemostimulators-modifiers into the system were obtained [46, 51, 86–90].

10. The high efficiency of the application of the spectral ellipsometry method for determination of the thickness and optical constants of nanoscale films of complex compositions, grown as a result of thermal oxidation of InP and GaAs under the influence of chemostimulators-modifiers was proved [81, 91–94].

11. It was found that magnetron sputtering is the optimal method for the formation of oxide heterostructures (V_2O_5, MnO_2, etc.)/ semiconductor efficiently blocking the diffusion of unoxidised indium into the film during thermal oxidation in comparison with mild methods of modifying the semiconductor surface. Weakly absorbing films with a low content of unoxidised indium, no more than 1–2%, have been synthesized [89, 93].

12. Chemically stimulated oxidation of indium phosphide with a nanosized layer of bismuth vanadate phosphate on the surface led to a significant decrease in EAE (~ 50 kJ/mol) as compared to the intrinsic oxidation of InP (~ 270 kJ/mol), which indicates a significant chemostimulating effect of a complex chemostimulators on the thermal oxidation process of InP due to the decomposition of a complex chemostimulator-modifier with the formation of oxides-chemostimulators, as well as isostructural phosphate and vanadate fragments embedding in the forming film. The presence of V_2O_5 in films with a significant decrease in EAE and a large relative increase in the thickness of the films throughout the entire process suggest the presence of the catalytic component of the oxidation mechanism [95]. The composition and optical properties of the films confirm the effective blocking of the diffusion of unoxidised indium into the forming films, which favourably affects their functional properties. The chemically stimulated oxidation of gallium arsenide with a nanosized layer of manganese vanadate phosphate on the surface proceeds by a transit mechanism as was evidenced by the EAE value of the process (about 150 kJ/mol), comparable by an order of magnitude with that of the reference oxidation of InP (~ 270 kJ/mol). According to the XRD results, a chemostimulator with a pronounced catalytic mechanism of action (V_2O_5), originally present in vanadate-phosphate was not revealed in films, which indicates the absence of a catalyst regeneration cycle: $V_2O_5 \leftrightarrow VO_2$. Vanadate-phosphates of bismuth and manganese act simultaneously as both chemostimulators and modifiers of the thermal oxidation process, acting according to the transit mechanism for heterostructures on GaAs and according to transit-catalytic mechanism for heterostructures on InP, and leading to an acceleration of the process up to 220–248% (see Table 2). Thermal oxidation of InP with magnetron deposited nanoscale layers of the MnO_2chemostimulator and the simultaneous introduction of a chemostimulator-modifier $Mn_3(PO_4)_2$ through the gas phase led to an increase in the growth rate of the films up to 240% compared with the intrinsic oxidation of InP, the absence of under-oxidized indium in the films, the high content of a whole spectrum of phosphates (XRD, IRS, AES, USXES, SE), and, as a consequence, their dielectric characteristics (resistivity up to 10^{10} Ohm·cm, see Table 2).

The traditions established by the scientific school of Professor Yakov Aleksandrovich Ugai are continued by DSc in Chemistry, Professor A. M. Samoilov [96-101].

The main objectives of these studies are the investigation of the fundamental physicochemical properties of semiconductor systems with sensor properties and the improvement of methods for the directed synthesis of hetero- and nanostructures based on these materials for the achievement of optimal values of their functional parameters.

The focus of studies is on multicomponent narrow-bandgap $A^{IV}B^{VI}$ semiconductors capable of efficiently detecting electromagnetic radiation in the terahertz and infrared regions of the spectrum [102–115], as well as wide-bandgap transparent metal oxides, which are promising for the creation of gas sensors and ultraviolet radiation sensors [116–129]. The study of these materials is currently carried out in several directions: the investigation of fundamental physicochemical properties, which are fundamental for the functioning of these systems as sensor materials [102, 103, 105, 109–112]; methods for the synthesis of PbTe thin films were optimized based on the data on the solubility of Ga and In in PbTe<Ga> and PbTe<In> with high sensitivity to IR radiation [104, 106, 111, 124, 125].

The obtained experimental data on the thermal stability and crystal structure of palladium (II) oxide allowed developing methods for the synthesis of nanostructures with different morphological organization, which demonstrated high sensitivity to toxic gases with oxidizing properties as well as good speed and stability of the sensory response over time [120–123]. The results of calculating the region of nonstoichiometry of nanocrystalline PdO films [127–129] in the future will allow finding the optimal conditions for the synthesis of nanostructures with high selectivity for detecting poisonous and explosive gases with oxidizing and reducing properties in atmospheric air [126].

The materials science traditions of the school were developed somewhat unexpectedly in the studies of DSc in Chemistry, Professor N. I. Ponomareva by the development of new methods for the synthesis of hydroxyapatite (HA) composites, allowing to obtain particles included in a biopolymer matrix. Since the properties of both HA itself and composites based on it depend on the particle size, the research task was to obtain nano-HA. It was shown that with the dropwise mixing of the reagents and the addition of alizarin red, promoting the formation of centres of induced crystallization, the rate of formation of stoichiometric HA in an aqueous solution increased by more than 100 times in comparison with the reference process. Synthesis of GA in a model body fluid (SBF) leads to the formation of type A carbonate hydroxyapatite corresponding to the formula $Ca_{10}(PO_4)_6(CO_3)_{0.5x}(OH)_{2-x}$, where $x < 2$ (EPXMA, IRS), which was explained by the presence of a bicarbonate ion in SBF and carbon dioxide in the air [130, 131]. A method for the synthesis of nano-HA in drops of microemulsions prepared on the basis of toluene/octane and water with the addition of AOT as a surfactant has been developed, and it was shown that the particles had needle shape (length 10–20 nm and width 2–4 nm) and were covered with an amorphous shell. It was found that in the formation of HA composites with biopolymers, the determining factors are the presence of carboxyl, hydroxyl, and sulpho groups in the used biopolymers and the negative surface charge of the polymers. An excess of calcium ions increased the degree of binding of these organic components with HA and significantly increased the hardness of composites (up to 260 MN/m^2) [132–134]. N. I. Ponomareva et al. Proposed a new economically viable method for the formation of bioactive coatings on the surface of titanium by the deposition of carbonate films from the solution with their subsequent transformation into phosphate and hydroxyapatite films [133–137]. The authors provided recommendations for the impregnation of HA with carbon implants [138, 139].

3. Doped and undoped nanocrystalline yttrium and lanthanum ferrites

The development of research in the field of semiconductor and dielectric films of the nanoscale thickness range by the followers of the scientific school of Ya. A. Ugai naturally spread to the area of magnetic nanocrystals. The increased interest in nanomaterials based on yttrium and lanthanum orthoferrites with a perovskite structure was caused by their unique magnetic, optical, and catalytic properties [140, 141] and the ability to control their structure and properties through doping over a wide range.

Among the methods for obtaining nanosized REE ferrites, the sol-gel method is widely used, allowing nanopowders with a narrow particle size distribution to be formed at relatively low temperatures using simple and inexpensive equipment. Variations of the sol-gel method include the polymer-gel process, in which the formation of a gel is achieved by introducing a water-soluble polymer into the initial solution followed by

evaporation, and the Pechini method (citrate-gel), which uses citric acid, ethylene glycol, or polyvinyl alcohol [142–144]. Hydrothermal treatment of precipitated yttrium and iron (III) hydroxides makes it possible to obtain single crystals of yttrium ferrite [145, 146], microcrystalline [147, 148] and nanocrystalline powders [147, 149, 150] by selecting the appropriate precursors, pH of the medium, and conditions of hydrothermal treatment. The mechanism of the formation of yttrium ferrite nanopowders under the conditions of glycine-nitrate combustion is described in [151, 152]. The synthesized particles are characterized by a rhombic and hexagonal structure with a particle size of 30 to 53 nm and 6 to 14 nm, respectively. It was found that the phase composition and average crystallite size are significantly influenced by the glycine/nitrate ratio, which determines the combustion temperature.

By the method of decomposition of alkoxide complexes, yttrium orthoferrite nanopowders are formed at a temperature of 680 °C and exhibit weak ferromagnetism [153]. One of the modern methods for the synthesis of ferrite nanocrystals is microwave synthesis. The method for the synthesis of vanadate and ferrite precipitation from a solution of precursors under the influence of microwave radiation is characterized by the simplicity of implementation, economy, and high synthesis rate. Microwave radiation stimulates the decomposition of salt precursors, the dehydration and synthesis of target products is due to the uniformity and high rate of microwave heating and acceleration of the processes of "nucleation" under the influence of "non-thermal" effects [154].

Effective absorption of microwave radiation requires the presence in the substance of either dipoles that can reorient and rotate under microwave action, or free charge carriers that can move when the microwave field is applied. Water molecules located in the crystal lattice of crystalline hydrates-precursors have a significant dipole moment. The decomposition of the used crystalline hydrates in a microwave field proceed to oxides, since the formation of an oxide product begins before the removal of all water contained in the system.

Compared to traditional heating methods, microwave heating has several undoubted advantages: during microwave heating, the walls of the vessel are not heated, only the reaction mixture is heated. As a result of this: the reaction time was reduced (by 10-1000 times); directed activation of reacting molecules was carried out; there wee no side processes of destruction on the walls of the vessel, the overheating of the solvent above the boiling point was absent; the flow of energy stopped after the termination of the reaction [155, 156].

Microwave exposure followed by ultrasonic treatment of synthesized $YFeO_3$ and $BiFeO_3$ samples using sodium hydroxide as a precipitant allowed synthesizing chemically homogeneous nanopowders with a significant decrease in the energy intensity of the process. The resulting $YFeO_3$ and $BiFeO_3$ particles had a nearly spherical shape, they were characterized by a small size dispersion in the range of 20–100 nm [157, 158].

The change in the magnetic properties of doped ferrites was caused by several reasons: a change in the size and shape of particles, a distortion of the crystal lattice due to the difference in ionic radii, a change in the valence state of iron upon the introduction of a dopant, and the appearance of oxygen nonstoichiometry.

Studies of the effect of a doping impurity on the composition, structure, and properties of yttrium orthoferrite nanoparticles can be divided into two directions: substitution of the Y^{3+} and Fe^{3+} cation. We are working in both directions.

During the first stage of research, it was shown that the substitution of Y^{3+} by La^{3+} in yttrium ferrite nanopowders synthesized by coprecipitation led to an increase in magnetization from 0.041 A·m^2/ kg for x = 0 to 0.231 A·m^2/ kg for x = 0.4 and a decrease in the coercive force, which indicates a significant contribution of crystal lattice distortion in the formation of the magnetic properties of the material [159]. This effect was found even in the case of isovalent substitution, and in this case, it was due to the size factor.

The change in the magnetic properties in the case of heterovalent substitution was due not only to size factors, but also due to a change in the valence state of iron for compensation of the charge and the appearance of oxygen nonstoichiometry.

Data obtained by doping yttrium ferrite with some doubly charged cations are presented by

us in [160–162]. Sol-gel synthesis of $Y_{1-x}A_xFeO_3$ samples (where A – Ca^{2+}, Sr^{2+}, Cd^{2+}) is based on the processes of co-deposition of cations and annealing in a muffle furnace at a temperature of 750 °C for 1 h. Doping with Ca^{2+} and Cd^{2+} cations with ionic radius slightly exceeding the ionic radius of Y^{3+}, led to a decrease in the particle size, specific magnetization, and coercive force. Decrease in D_{av} was explained by the appearance of internal stresses, limiting the growth of crystals [163]. Despite the deviation from Goldschmidt's rule [164], the substitution of Y^{3+} with strontium cations is possible and causes a significant increase in the coercive force from 3.98 kA/m (x = 0) up to 409.94 kA/m (x = 0.3), i.e. the formation of a new type of magnetic material, a hard magnetic ferromagnet.

It could be assumed that the doping of yttrium ferrite with barium cations would lead to a strong increase in the magnetic characteristics due to the incorporation of Ba^{2+} into position of Y^{3+} (since $r(Ba^{2+}) > r(Y^{3+})$ [165]), and the introduction of Zn^{2+} can change the magnetic properties both in the direction of decreasing (since zinc cations have a small radius) and increasing their value in the case of substitution of iron cations with Zn^{2+} ions. Indeed, in the studies of our team it was shown [165, 166] that the substitution of La^{3+} or Y^3 cations in orthoferrites by doubly charged Zn^{2+} and Ba^2 caused the distortion of the crystal lattice, a change in the valence state of iron, which, in turn, affects the strength of the exchange interaction and leads to a change in physicochemical properties, which expands the scope of the synthesized materials. Thus, nanocrystalline powders $(1-x)$ $YFeO_{3-d}$: xZn^{2+} and $(1-x)LaFeO_{3-\delta}$: xZn^{2+}, which are characterized by weak ferromagnetism, are promising materials for the production of devices requiring rapid re-magnetization of the sample with minimal energy consumption, for example, when creating transformer coils, and, nanopowders $(1-x)YFeO_{3-d}$: xBa^{2+} and $(1-x)$ $LaFeO_{3-\delta}$: xBa^{2+} can be used to solve the problem of increasing the density of media for the magnetic recording of information, since they are magnetically hard materials. It was shown that the doping of nanocrystalline yttrium ferrite powders with zinc by coprecipitation followed by heat treatment causes a nonmonotonic decrease in the crystallite size from 60 ± 6 nm x = 0 to 50 ± 4 nm x = 0.2 (XRD), contributes to an increase in the specific magnetization from 0.242 A m^2/kg for x = 0 to 0.556 A m^2/kg for x = 0.2 (in the field 1250 kA/m). The presence of $ZnFe_2O_4$ impurities in the samples led to an increase in the ferromagnetic character of the samples.

It was found that the developed technique for the synthesis [167] of $(1-x)YFeO_{3-\delta}$: xBa^{2+} nanopowders led to the formation of particles with a size of 30 ± 2 nm for x = 0 to 55 ± 5 for x = 0.1 (XRD), characterised by the presence of a soft magnetic and magnetic hard sublattice within the same chemical phase.

In our studies [168], a method for the sol-gel synthesis of $LaFeO_3$ using an aqueous solution of ammonia as a precipitant was demonstrated, lanthanum ferrite was doped with calcium and strontium. It was found that the introduction of Ca^{2+} into the ferrite lattice caused an increase in the average crystallite diameter from 30 nm for $LaFeO_3$ up to 50 nm, in the case of Sr^{2+} it was up to 70 nm. Doping with calcium and strontium cations led to an increase in the coercive force and specific magnetization of the samples. The change in the magnetic properties of lanthanum ferrite upon doping with doubly charged cations was caused by the partial transition of Fe^{3+} in Fe^{4+}, as well as distortion of the crystal lattice due to the difference in the ionic radii of La^{3+} and the dopant. With an equal content of Ca^{2+} and Sr^{2+} cations in the composition of the samples, the magnetic properties were different: $H_c(La_{0.7}Ca_{0.3}FeO_3) < H_c(La_{0.7}Sr_{0.3}FeO_3)$, a $J(La_{0.7}Ca_{0.3}FeO_3) > J(La_{0.7}Sr_{0.3}FeO_3)$.

The complexity of the formation of lanthanum ferrite nanopowders doped with zinc and barium is due to the large difference in the ionic radii of lanthanum and the dopant introduced. However, despite the narrow homogeneity region, single-phase samples with a complex magnetic structure were obtained [169, 170]. The maximum degree of doping of lanthanum ferrite with zinc was x_{real} = 0.07. As the amount of the introduced dopant increased, the unit cell volume nonmonotonically increased from 240.634 Å^3 (x = 0) up to 242.245 Å^3 (x = 0.2) and the average crystallite size increased from 58 (x = 0) to 123 nm (x = 0.2), which was due to the incorporation of Zn ions^{2+} into the position of Fe^{3+}, since $r(Zn^{2+}) > r(Fe^{3+})$. $(1-x)LaFeO_{3-\delta}$: xZn^{2+}

nanoparticles, depending on the composition, possess different types of magnetic ordering: antiferromagnetic and ferrimagnetic. The doping of $YFeO_3$ nanopowders with Zn^{2+} cations with a radius of less than Y^{3+}, should negatively affect the magnetization and coercive force. However, the formation of nanocrystals, characterized by a complex distribution of the doping cation was observed. The formation of particles with the structure "crystal core - amorphous shell" led to the arrangement of a part of the dopant ions in the form of an amorphous shell of zinc oxide. The increase in specific magnetization (1-x) $YFeO_{3-\delta}$: xZn^{2+} with an increase in the amount of Zn^{2+} was due to the reorientation of the magnetic moments of iron ions, as was observed in the study [171]. The distortion of the crystal lattice was insignificant, therefore, in this case, it did not significantly affect the properties. The enhancement of the ferromagnetic character of the material was also due to the presence of zinc ferrite in the spinel phase [166]

The introduction of Ba^{2+} cations into a $LaFeO_3$ lattice in the position of La^{3+} caused an increase in the parameters of the crystal lattice and the average particle diameter from 25 (x = 0) up to 42 nm (x = 0.1). The maximum nominal doping level was x = 0.1 (XRD). The synthesized particles exhibited the properties of a hard magnetic ferromagnet with a wide hysteresis loop. The non-monotonic change in the magnetic characteristics was due to the formation of a complex magnetic structure combining a hard magnetic and soft magnetic sublattice.

Thus, as in the case of yttrium ferrite, the doping of lanthanum ferrite with doubly charged barium and zinc cations led to the formation of materials exhibiting different magnetic properties, which allows using them for the production of information storage devices [165, 166, 169, 170]

Changes in the magnetic properties of yttrium ferrite upon doping with doubly charged cations were caused by several factors: first, due to the difference in ionic radii of Y^{3+} and dopant, distortion of the crystal lattice occurred and the particle size changed; secondly, such doping refers to heterovalent isomorphic transformations, which resulted in the formation of Fe^{4+} cations, i.e., a double exchange interaction of Fe^{3+}–O^{2-}–Fe^{4+} occurred, holes which were charge carriers in the transition from the Fe^{4+} ion to Fe^{3+} ion through the p-orbital of oxygen were generated [172]. It was shown in studies [159, 161] that upon the doping of lanthanum ferrite, an increase in the magnetization can be caused by similar reasons. The absence of such an interaction in perovskite $Y_{1-x}La_xFeO_3$ [159] explains its lower magnetization compared to $Y_{1-x}Cd_xFeO_3$ [161] with the same degree of substitution, since with an increase in the cadmium content, although the size of the resulting particles $Y_{1-x}Cd_xFeO_3$ decreased, their magnetization increased monotonically. Therefore, the compensation described above probably has a stronger effect on the magnetization than a change in particle size.

It should be noted that the data available in the literature on the effect of zinc on the size of nanocrystals and the magnetic properties of $LaFeO_3$ nanopowders are very controversial. In studies [173, 174], the possibility to substitute La^{3+} cations with Zn^{2+} cations in lanthanum orthoferrite synthesized by the coprecipitation method was shown. A decrease in the crystal lattice volume with an increase in the dopant concentration led to an increase in the orthorhombic distortion of the $LaFeO_3$ perovskite lattice, which caused an increase in magnetization.

In studies [175, 176], the results of the synthesis of $LaFe_{1-x}Zn_xO_3$ nanopowders by the gel combustion method were presented, the mechanism of incorporation of the dopant and the effect on the magnetic structure of the material were described. The introduction of Zn^{2+} instead of Fe^{3+} led to the transformation of Fe^{3+} – Fe^{4+} and the formation of oxygen vacancies in the perovskite structure, which changed the angle and length of the Fe-O bonds. The structural analysis showed that zinc doping causes oxygen nonstoichiometry in the system. This can change the valence state of Fe^{3+} and hence the magnetization [176].

The doping of lanthanum ferrite with zinc, regardless of the preparation method and the position of the dopant in the perovskite lattice (in the position of La^{3+} or Fe^{3+}) led to the formation of particles with a complex magnetic structure: an antiferromagnetic core - a ferromagnetic shell, as was evidenced by the shift of the hysteresis loop towards a negative field strength [174–176].

Due to the fact that the difference between the radii of La^{3+} – Zn^{2+} is much higher than that of Fe^{3+} – Zn^{2+}, the substitution of iron cations by zinc is more likely. This was proved by us for $(1–x)LaFeO_{3–\delta}$: xZn^{2+} nanopowders synthesized by co-deposition followed by annealing in a muffle furnace [170]. The substitution of some Fe^{3+} ions with Zn^{2+} ions led to the formation of a material with a complex magnetic structure. By controlling the amount of dopant introduced, it was possible to obtain materials with antiferromagnetic (for x = 0; 0.075; 0.15) or ferrimagnetic (x = 0.05; 0.1; 0.2) properties.

Lower specific magnetization for samples of yttrium ferrite doped with Zn^{2+}, Cd^{2+}, Ca^{2+}, Sr^{2+}, Ba^{2+} cations compared with $(1–x)LaFeO_{3–\delta}$:xE^{2+}, indicates a significant contribution of the effect of double exchange interaction on the magnetic properties of the material. The magnitude of the magnetization and coercive force of lanthanum ferrite nanopowders doped with doubly charged cations depends on the difference in ionic radii, i.e., on the distortion of the crystal lattice. With an increase in the dopant content, the dependence of the magnetization on the particle size has not been established. Consequently, the above compensation and the structure factor seem to have a stronger effect on magnetization than a change in the particle size of the studied yttrium and lanthanum ferrites. The described results can be used to obtain composite materials [177, 178]. In addition, the detected inclusions of the ferromagnetic Fe_2O_3, $BaFe_2O_4$, $ZnFe_2O_4$ phases show that the synthesized samples are promising for creating granular structures [179, 180].

From the described above information, a complex mechanism for the incorporation of zinc into the lattices of yttrium and lanthanum ferrites can be proposed, and, based on the difference in atomic radii, it is most likely to be incorporated into the place of iron. However, as shown above, this statement is far from clear. Such transition elements as manganese and nickel should occupy positions of iron in the structure, since they are quite similar in their properties. The corresponding studies belong to the above-mentioned second direction. A significant increase in the magnetic parameters of $YFeO_3$ nanoparticles was observed upon doping with magnetic ions Mn^{3+}, as shown in [181]. It is believed that the magnetic moment of the Mn^{3+} ion is higher than Fe^{3+} in oxides of the perovskite type, and this should be the reason for the increase in magnetic moments with an increase in the amount of dopant in $YFe_{1-x}Mn_xO_3$ [182]. In addition, the enhancement of antiferromagnetic ordering is due to distortions in the crystal lattice. In studies [183, 184] the results of doping of yttrium and lanthanum ferrite powders with nickel Ni^{2+} by successive precipitation using an aqueous solution of potassium hydroxide are presented [184]. The single-phase of $YFe_{1-x}Ni_xO_3$ (x = 0–0.25) samples is achieved at a temperature of 800 °C for 1 h, respectively (XRD). With an increase in the content of the dopant Ni to x = 0.3 after annealing at 800 °C for 1 h, in addition to $YFeO_3$, NiO and Y_2O_3 impurity phases are formed. With an increase in Ni^{2+} content in the $YFeO_3$ lattice from x = 0.1 to 0.25, a decrease in the coercive force from 1332.6 to 887.9 Oe was observed, while the values of excess magnetization M_r and saturation magnetization M_s increased: from $1.8\cdot10^{-1}$ up to $3.2\cdot10^{-1}$ emu/g and 0.67 to 1.18 emu/g, respectively.

The introduction of Ni^{2+} cations into the $LaFeO_3$ lattice in the position of Fe^{3+} causes a decrease in the parameters of the crystal lattice and a decrease in average particle diameter from 28.72 (x = 0) to 23.59 nm (x = 0.25). For $LaFe_{1-x}Ni_xO_3$ samples with an increase in the content of Ni^{2+} dopant from x = 0 to 0.25, an increase in the coercive force from 42.53 Oe to 160.76 Oe was observed, while the values of excess magnetization M_r and saturation magnetization M_s decreased: from $1.0\cdot10^{-2}$ up to $3.8\cdot10^{-4}$ emu/g and from 0.24 10° up to $0.74\cdot10^{-4}$ emu/g [183]. It was found that an increase in the content of the dopant Ni^{2+} in $YFeO_3$ and $LaFeO_3$ lattices allows varying the value of the coercive force (H_c) and saturation magnetization (M_s), which expands new possibilities of using doped yttrium and lanthanum ferrites in a strong magnetic field.

In the study [185], $YFe_{1-x}Mn_xO_3$ (x = 0.1; 0.2; 0.3; 0.4) perovskite nanopowders were synthesized by chemical coprecipitation using 5% KOH as the precipitating reagent. The introduction of manganese ions into the $YFeO_3$ lattice using the proposed method led to an increase in the parameters of the crystal lattice (b = 7.7373÷7.5194 Å, c = 5.3014 ÷ 5.2592 Å); unit cell

volume (V = 229.425÷224.4012 Å), average particle size (D_{XRD} = 23.6081÷22.9449 nm). An increase in the coercive force (H_c = 56.94÷150.95 Oe) and residual magnetization (M_r = 0.23–0.50 emu/g) with an increase in the dopant content was revealed.

Nanocrystalline $La_{1-x}Cd_xFeO_3$ (x = 0, 0.05, 0.1, 0.15, 0.2) powders, characterized by a narrow region of homogeneity x_{max} = 0.09 (EPXMA, XRD) were synthesized by co-deposition followed by thermal annealing at 950 °C for 1 h. Introduction of Cd^{2+} cations led to a decrease in the average crystallite size from 10–70 nm for x = 0 to 5–60 nm for x = 0.1 (TEM). The synthesized nanocrystals exhibited the properties of ferrimagnets [186].

In this direction, the work related to the section of the scientific school of Ya. A. Ugai, continue abroad. Thus, in the Socialist Republic of Vietnam, Nguyen Anh Tien, who defended his PhD thesis in Russia under the supervision of I. Ya. Mittova, is the Head of the Department of General and Inorganic Chemistry of Ho Chi Minh City University of Education, and with his colleagues and co-authors successfully conducts research into the synthesis and characterization of ferrite nanocrystals. The studies are being carried out in co-authorship with Russian colleagues (a scientific group led by I. Ya. Mittova) in accordance with the Memorandum of Understanding, concerning the program for the development of cooperation in the field of higher education, signed between Voronezh State University and Ho Chi Minh City University of Education. To date, new methods for the synthesis of nanocrystals of doped and undoped ferrites, including REE ferrites (neodymium, praseodymium, holmium, etc.) by solution methods have been developed; the regularities of changes in magnetic properties depending on the synthesis method, particle size, physicochemical nature of the dopant, and the level of doping have been established [187-192]. This research has been repeatedly supported by internal grants from the Socialist Republic of Vietnam.

In our country, studies that continue the foundations and traditions of the scientific school of Ya. A. Ugai, supported by the following grants and Programs (Head Researcher – Prof. I. Ya. Mittova):

1. Soros Fund No. NZN000 + NZN300.

2. STP "Scientific research of higher education in priority areas of science and technology", subprogram (208) – electronics, project code 01.01.004.

3. Grant of the Ministry of Education E00-5.0-363 (registration number 01.2.00104702).

4. STP Research of the Higher School in the priority areas of science and technology.

5. Federal Program "Universities of Russia – Basic Research" (grants No. 06.01.07, No. UR.06.01.020, No. UR.06.01.001).

6. Basic Research Program in Radio Engineering and Electronics (Grant No. 97-5-1.1-32).

7. RFBR No. 02-03-32418: Chemically stimulated oxidation of $A^{III}B^{V}$ semiconductors during the formation of heterostructures.

8. RFBR No. 03-03-96500-r2003tschr_a – Nonlinear effects in the processes of chemically stimulated synthesis of dielectric oxide layers on $A^{III}B^{V}$.

9. RFBR No. 06-03-96338_r_center_a – Effect of chemostimulators on the kinetics and mechanism of thermal oxidation of semiconductors $A^{III}B^{V}$ in the formation of thin films and heterostructures.

10. RFBR No. 09-03-97552-r_center_a – Catalytic and transit solid-phase interactions in nanosystems based on semiconductor materials.

11. RFBR 10-03-00949-a – Size effects in the processes of synthesis of oxide layers on GaAs and InP.

12. RFBR No. 13-03-00705-a – Role of V_2O_5 as an oxidation catalyst, interface modifier and the nanostructure of functional nanometer films on InP and GaAs.

13. RFBR No. 16-43-360595 p_a – Modification of the surface of GaAs, GaP and InP as a method of controlling the nanostructure, optical and electrophysical properties of oxide films of nanometer thickness range for microelectronics.

14. RFBR No. 18-03-00354_a – Development of the fundamental principles of chemically controlled synthesis of functional nanoscale films on semiconductors A^3B^5 for opto- and microelectronics, gas-sensitive sensors.

15. Analytical departmental target program (No. G.R. 01200602176) "Development of the scientific potential of higher education" within the framework of program action 1 "Conducting fundamental research within the framework

of thematic plans" "Development of synthesis methods and establishment of the mechanism for the formation of nanoscale layers, nanopowders and crystals of semiconductor, dielectric and magnetic materials".

16. Project of the Ministry of Education and Science of the Russian Federation: Goverment Order 3.1673.2011.

17. Government Order for higher education institutions in the area of scientific research for 2014-2016 (projects No. 673, 225).

18. RFBR grant No. 20-33-90048 "Formation mechanisms, structural features and properties of carbon-containing nanocomposites based on nanocrystalline ferrites with a perovskite-like structure" ("Postgraduate students").

Postgraduate student Kopeichenko E. I. (scientific advisor – Proffessor I. Ya. Mittova) won the competition for the best scientific projects carried out by young scientists under the supervision of scientists with PhD and DSc degrees in scientific organisations of the Russian Federation (RFBR grant No. 19-33-50104 mol_nr "Mobility").

The Russian Academy of Natural Sciences issued a certificate to I. Ya. Mittova as the head of the scientific school "Control of synthesis processes, composition and properties of functional (semiconductor, dielectric, para- and ferromagnetic) nanoscale films, magnetic nanocrystals and nanophosphors by chemostimulators and dopants "(Russian Academy of Natural Sciences, certificate No. 01165, "Leading scientific schools. – Moscow: Publishing House of the Academy of Natural Sciences, 2018. – Vol. 11. – 132 p.; Mittova Irina Yakovlevna, p. 81; http://www.famous-scientists.ru/school/1393"), which is the embodiment of the

РОССИЙСКАЯ АКАДЕМИЯ ЕСТЕСТВОЗНАНИЯ

СЕРТИФИКАТ

№ 01165

ПРИСВОЕНО ПОЧЕТНОЕ ЗВАНИЕ

ОСНОВАТЕЛЬ НАУЧНОЙ ШКОЛЫ

Миттовой Ирине Яковлевне

Научная школа: Управление процессами синтеза, составом и свойствами функциональных (полупроводни-ковых, диэлектрических, пара- и ферромагнитных) наноразмерных пленок, магнитных нанокристаллов и нанолюминофоров посредством хемостимуляторов и допантов

ПРЕЗИДЕНТ
д.м.н., профессор,
академик РАЕ
М.Ю.Ледванов

МОСКВА 2017

ideas of Ya. A. Ugai, his students and followers in the study of semiconductors and nanostructured functional films based on them, their spread to the field of new challenges and scientific trends of today.

Author contributions

All authors made an equivalent contribution to the preparation of the publication.

Conflict of interests

The authors declare that they have no known competing financial interests or personal relationships that could have influenced the work reported in this paper.

References

1. Sidorkin A. S. *Vedushchie nauchnye shkoly* [Leading scientific schools]. Voronezh: Voronezhskii gosudarstvennyi universitet Publ.; 2001. 172 p. (In Russ.)

2. Mikhailova M. P., Moiseev K. D., Yakovlev Y. P. Discovery of III–V semiconductors: Physical properties and application semiconductors. *Semiconductors*. 2019;53(3): 273–290. https://doi.org/10.1134/S1063782619030126

3. Wilmsen C. W. Oxide layers on III—V compound semiconductors. *Thin Solid Films*. 1976;39(1-2-3): 105-117. https://doi.org/10.1016/0040-6090(76)90628-3

4. Oktyabrsky S., Ye P. *Fundamentals of III-V Semiconductor MOSFETs*. Springer Science LCC; 2013. 447 p.

5. Moorthy S. B. K. *Thin film structures in energy applications*. Springer; 2015. 292 p.

6. Bolkhovityanov Yu. B., Pchelyakov O. P. GaAs epitaxy on Si substrates: modern status of research and engineering. *Physics-Uspekhi*. 2008;51: 437–456. http://dx.doi.org/10.1070/PU2008v051n05ABEH006529

7. Engström O. *The MOS System*. Cambridge University Press: 2014. 216 p.

8. Aderstedt E., Medugorac I., Lundgren P. High-gain MOS tunnel emitter transistors. *Solid-State Electronics*. 2002;46(4): 497–500. https://doi.org/10.1016/S0038-1101(01)00298-2

9. Chistokhin I. B., Zhuravlev K. S. SVCh-fotodetektory dlya analogovoi optovolokonnoi svyazi [Microwave photodetectors for analog fiber optic communication]. *Uspekhi Prikladnoi Fiziki*. 2015;3(1): 85–94. Available at: https://advance.orion-ir.ru/UPF-15/1/UPF-3-1-85.pdf (In Russ.)

10. Li Sheng S. *Semiconductor physical electronics. Second Edition*. Springer-Verlag New York; 2006. 708 p.

11. Arbiol J., Xiong Q. *Semiconductor nanowires: materials, synthesis, characterization and applications*. Elsevier Ltd.; 2015. 554 p.

12. Bachhofer H., Reisinger H., Bertagnolli E., Philipsborn von H. Transient conduction in multidielectric silicon–oxide–nitride–oxide semiconductor structures. *Journal of Applied Physics*. 2011;89(5): 2791-2800. https://doi.org/10.1063/1.1343892

13. Ahmad S. R., Cartwright M. *Laser ignition of energetic materials*. John Wiley & Sons Ltd.; 2015. 425 p.

14. Ünlü H., Horing N. J. M., Dabowski J. *Low-dimensional and nanostructured materials and devices*. Springer Science LCC; 2015. 674 p.

15. Biksei M. P., Dobrovol'skii Yu. G., Shabashkevich B. G. Fotopriemnik ul'trafioletovogo izlucheniya na osnove fosfida galliya [Photodetector of ultraviolet radiation based on gallium phosphide]. *Prikladnaya Fizika*. 2005;4: 97–100. Available at: https://applphys.orion-ir.ru/appl-05/05-4/PF-05-4-97.pdf (In Russ.)

16. Dobrovol'skii Yu. G. Fotodiod na osnove GaP s povyshennoi chuvstvitel'nost'yu v korotkovolnovoi oblasti UF-spektra [GaP based photodiode with increased sensitivity in the short wavelength region of the UV spectrum]. *Tekhnologiya i konstruirovanie v elektronnoi apparature*. 2012;5: 31–34. Available at: http://dspace.nbuv.gov.ua/bitstream/handle/123456789/51709/07-Dobrovolskii.pdf?sequence=1 (In Russ.)

17. Sobolev M. M., Nikitin V. G., High-temperature diode formed by epitaxial GaP layers *Technical Physics Letters*. 1998;24(5): 329–331. https://doi.org/10.1134/1.1262110

18. Aleshkin V. Ya., Dubinov A. A., Afonenko A. A. Oscillations at a difference frequency in the middle and far infrareds in GaP semiconductor waveguides. *Technical Physics*. 2006;51(9): 1207–1209. https://doi.org/10.1134/S1063784206090167

19. Purica M., Budianu E., Rusu E. Heterojunction with ZnO polycrystalline thin films for optoelectronic devices applications. *Microelectronic Engineering*. 2000;51–52: 425–431. https://doi.org/10.1016/S0167-9317(99)00492-X

20. Bang K. H., Hwang D. K., Park M. C., Ko Y. D., Yun I., Myoung J. M. Formation of *p*-type ZnO film on InP substrate by phosphor doping. *Applied Surface Science*. 2003;210(3–4): 177–182. https://doi.org/10.1016/S0169-4332(03)00151-X

21. Thilakan P., Kumar J. Reactive thermal deposition of indium oxide and tin-doped indium oxide thin films on InP substrates. *Thin Solid Films*. 1997;292(1-2): 50–54. https://doi.org/10.1016/S0040-6090(96)08943-2

22. Kim T. W., Lee D. U., Yoon Y. S. Microstructural, electrical, and optical properties of SnO_2 nanocrystalline thin films grown on InP (100) substrates for applications as gas sensor devices. *Journal of Applied Physics*. 2000;88: 3759. https://doi.org/10.1063/1.1288021

23. Lee D. J., Park C. S., Lee C. J., Song J. D., Koo H. C., Yoon C. S., Yoon I. T., Kim H. S., Kang T. W., Shon Y. Enhanced ferromagnetism by preventing antiferromagnetic MnO_2 in InP:Be/Mn/InP:Be triple layers fabricated using molecular beam epitaxy. *Current Applied Physics*. 2014;14(4): 558–562. https://doi.org/10.1016/j.cap.2014.01.017

24. Belysheva T. V, Bogovtseva L. P., Gutman E. E. Primenenie metallooksidnykh poluprovodnikovykh geterosistem dlya gazovogo analiza [Application of metal oxide semiconductor heterosystems for gas analysis]. *Mezhdunarodnyi nauchnyi zhurnal al'ternativnaya energetika i ekologiya*. 2003;S1: 128. Available at: https://www.elibrary.ru/item.asp?id=12879078

25. Rumyanceva M. N., Safonova O. V., Bulova M. N., Ryabova L. I., Gas'kov A. M. Gazochuvstvitel'nye materialy na osnove dioksidov olova [Gas sensitive materials based on tin dioxides]. *Sensor*. 2003;2: 8–33. (In Russ.)

26. Rembeza S. I., Svistova T. V., Rembeza E. S., Borsyakova O. I. The microstructure and physical properties of thin SnO_2 films. *Semiconductors*. 2001;35: 762–765. https://doi.org/10.1134/1.1385709

27. Lekshmy S. S., Joy K. Structural and optoelectronic properties of indium doped SnO_2 thin films deposited by sol gel technique. *Journal of Materials Science: Materials in Electronics*. 2014;25(4): 1664–1672. https://doi.org/10.1007/s10854-014-1781-x

28. Lugin G., Zharskii I. M. Ispol'zovanie termoelektricheskikh effektov tonkikh plenok oksidov indiya i olova dlya sozdaniya gazovykh sensorov [The use of thermoelectric effects of thin films of indium and tin oxides to create gas sensors]. *Mikrosistemnaya Tekhnika*. 2001;10: 10–14. Available at: https://www.elibrary.ru/item.asp?id=8970862 (In Russ.)

29. Ivanovskaya M., Bogdanov P., Faglia G., Sberveglieri G. Properties of Thin Film and Ceramic Sensors fot the Detection of CO and NO_2. *Proc. of Int. Metting "Eurosensors XIII"*. 1999. p. 145–148.

30. Belysheva T. V., Bogovtseva L. P., Gutman E. E. In_2O_3 films modified with gold as selective sensors of CO in air. *Russian Journal of Applied Chemistry*. 2000;73(12): 2070–2073.

31. Miyata T., Hikosaka T., Minami T. High sensitivity chlorine gas sensors using multicomponent transparent conducting oxide thin films. *Sensors and Actuators*. 2000;69(1-2): 16–21. https://doi.org/10.1016/S0925-4005(00)00301-4

32. Miyata T., Minami T., Shimokawa K., Kakumu T., Ishii M. New materials consisting of multicomponent oxides for thin film gas sensors. *Journal of the Electrochemical Society*. 1997;144(7): 2432–2436. https://doi.org/10.1117/12.352810

33. Petrov V. V., Nazarova T. N., Kopylova N. F., Zabluda O. V., Kiselev I., Bruns M. Issledovanie fiziko-himicheskih i elektrofizicheskih svojstv, gazochuvstvitel'nyh harakteristik nanokompozitnyh plenok sostava SiO_2-SnO_x-CuO_y [Investigation of physicochemical and electrophysical properties, gas-sensitive characteristics of nanocomposite films of the composition SiO_2-SnO_x-CuO_y]. *Nano- i mikrosistemnaya tekhnika*. 2010;8: 15–21. Available at: https://www.elibrary.ru/item.asp?id=15260225 (In Russ.)

34. Mingqing Y., Junhui H., Xiaochun H., Chunxiao Y., Zhenxing C., Yingqiang Z., Guomin Z. Copper oxide nanoparticle sensors for hydrogen cyanide detection: Unprecedented selectivity and sensitivity. *Sensors and Actuators B*. 2011;155(2): 692–698. https://doi.org/10.1016/j.snb.2011.01.031

35. Satyendra S., Yadava B. C., Rajiv P., Bharat B., Jae R. Synthesis of nanorod sand mixed shaped copper ferrite and their applications as liquefied petroleum gas sensor. *Applied Surface Science*. 2011;257(24): 10763–10770. http://dx.doi.org/10.1016/j.apsusc.2011.07.094

36. Mittova I. Ya. Influence of the physicochemical nature of chemical stimulators and the way they are introduced into a system on the mechanism of the thermal oxidation of GaAs and InP. *Inorganic Materials*. 2014;50(9): 874–881. https://doi.org/10.1134/S0020168514090088

37. Tomina E. V., Mittova, I. Y., Zelenina, L. S. Thermal oxidation as a method of formation of nanoscale functional films on AIIIBV semiconductors: influence of deposited metal layers. *Kondensirovannye sredy i mezhfaznye granitsy = Condensed Matter and Interphases*. 2018;20(1): 6–24. https://doi.org/10.17308/kcmf.2018.20/472 (In Russ., abstract in Eng.)

38. Tomina E. V., Mittova I. Ya., Sladkopevtsev B. V., Kostryukov V. F., Samsonov A. A., Tretyakov N. N. Thermal oxidation as a method of formation of nanoscale functional films on $A^{III}B^{V}$ semiconductors: chemostimulated influence of metal oxides: overview. *Kondensirovannye sredy i mezhfaznye granitsy = Condensed Matter and Interphases*. 2018;20(2): 184–203. https://doi.org/10.17308/kcmf.2018.20/522 (In Russ., abstract in Eng.)

39. Kostryukov V. F., Mittova I. Y., Tomina E. V., Sladkopevtsev B. V., Parshina A. S., Balasheva D. S. Nonlinear effects of oxides of p- and d-elements' coactions in formation of thin films on the GaAs and InP surfaces overview. *Kondensirovannye sredy i mezhfaznye granitsy = Condensed Matter and Interphases*. 2018;20(4): 506–536. https://doi.org/10.17308/kcmf.2018.20/625 (In Russ., abstract in Eng.)

40. Mittova I. Ya., Tomina E. V., Golovenko N. A., Agapov B. L. Formation of thermal oxide layers on InP in the presence of $SbCl_3$ in the gas phase. *Inorganic Materials*. 1993;29(5): 514–516. Available at: https://www.elibrary.ru/item.asp?id=27651233

41. Mittova I. Ya., Pukhova V. V., Klement'eva I. F., Semenov V. N., Kashkarov V. M. Poluchenie

termicheskim okisleniem struktur GaAs/Bi_2S_3 i svoistva dielektricheskikh plenok na GaAs[Thermal oxidation of GaAs/Bi_2S_3 structures and properties of dielectric layers on GaAs]. *Izvestiya Akademii nauk SSSR. Neorganicheskie Materialy*. 1988;24(9): 1431–1434. Available at: https://www.elibrary.ru/item.asp?id=27454116

42. Kostryukov V. F., Mittova I. Ya., Sladkopevtsev B. V., Parshina A. S., Balasheva D. S. The role of $BiPO_4$ introduced through the gas phase in the process of creating thin films on the surface of InP. *Kondensirovannye sredy i mezhfaznye granitsy = Condensed Matter and Interphases*. 2019;21(2): 215–224. https://doi.org/10.17308/kcmf.2019.21/759 (In Russ., abstract in Eng.)

43. Sladkopevtsev B. V., Tomina E. V., Mittova I. Ya., Dontsov A. I., Pelipenko D. I. On the thermal oxidation of V_xO_y–InP heterostructures formed by the centrifugation of vanadium(V) oxide gel. *Journal of Surface Investigation. X-ray, Synchrotron and Neutron Techniques*. 2016;10(2): 335–340. https://doi.org/10.1134/S102745101602018X

44. Sladkopevtsev B. V., Mittova I. Ya., Tomina E. V., Burtseva N. A. Growth of vanadium oxide films on InP under mild conditions and thermal oxidation of the resultant structures. *Inorganic Materials*. 2012;48(2): 161–168. https://doi.org/10.1134/S0020168512020173

45. Mittova I. Ya., Tretyakov N. N., Kostryukov V. F., Sladkopevtsev B. V. Thermal oxidation of GaAs under action of V_2O_5–MnO_2 oxide chemostimulating mixture with particles size of 50–150 μm. *Russian Journal of General Chemistry*. 2016;86(5): 995–1000. https://doi.org/10.1134/S1070363216050017

46. Tret'yakov N. N., Mittova I. Ya., Sladkopevtsev B. V., Samsonov A. A., Andreenko S. Yu. Vliyanie magnetronno napylennogo sloya MnO_2 na kinetiku termooksidirovaniya InP, sostav i morfologiyu sintezirovannykh plenok [Influence of a magnetron-deposited MnO_2 layer on the kinetics of thermal oxidation of InP, composition and morphology of the synthesized films]. *Neorganicheskie materialy*. 2017;53(1): 41–48. https://doi.org/10.7868/S0002337X17010171 (In Russ.)

47. Tarasova O. S., Dontsov A. I., Sladkopevtsev B. V., Mittova I. Ya. The effect of sulphur vapour treatment on the speed of InP thermal oxidation, composition, surface morphology, and properties of films. *Kondensirovannye sredy i mezhfaznye granitsy = Condensed Matter and Interphases*. 2019;21(2): 296–305. https://doi.org/10.17308/kcmf.2019.21/767 (In Russ., abstract in Eng.)

48. Mittova I. Ya., Sladkopevtsev B. V., Dontsov A. I., Syrov Yu. V., Kovaleva A. S., Tarasova O. S. Thermal oxidation of a single-crystal GaAs surface treated in sulfur vapor. *Inorganic Materials*. 2021;57(7): 663–668. https://doi.org/10.1134/S002016852107013X

49. Mittova I. Y., Sladkopevtsev B. V., Ilyasova N. A., Tomina E. V., Dontsov A. I., Tarasova O. S. The effect of certain complex chemostimulators and modifiers on InP thermal oxidation. *Kondensirovannye sredy i mezhfaznye granitsy = Condensed Matter and Interphases*. 2020;22(2): 245-256. https://doi.org/10.17308/kcmf.2020.22/2851

50. Tomina E. V., Sladkopevtsev B. V., Dontsov A. I., Perfileva L. I., Mittova I. Y. Influence of nanoscale layers of the $Mn_3(P_{0.1}V_{0.9}O_4)_2$ chemostimulator-modifier on the process of thermal oxidation of GaAs, its composition, and morphology of the resulting films. *Kondensirovannye sredy i mezhfaznye granitsy = Condensed Matter and Interphases*. 2020;22(1): 116–123. https://doi.org/10.17308/kcmf.2020.22/2535

51. Mittova I. Y., Tomina E. V., Sladkopevtsev B. V., Dontsov A. I. Effect of different types of annealing on the thermal oxidation of V_xO_y/InP structures formed by the deposition of vanadium(V) oxide gel on the phase composition and morphology of films. *Journal of Surface Investigation. X-ray, Synchrotron and Neutron Techniques*. 2014;8: 941–949. https://doi.org/10.1134/S1027451014050140

52. Mittova I. Ya., Tomina E. V., Lapenko A. A., Khorokhordina A. O. Solid-state reactions during thermal oxidation of vanadium-modified GaAs surfaces. *Inorganic Materials*. 2004;40(5): 441–444. https://doi.org/10.1023/B:INMA.0000027588.78546.af

53. Mittova I. Ya., Tomina E. V., Lapenko A. A., Sladkopevtsev B. V. Kataliticheskoe deistvie vanadiya i ego oksida (V) v protsessakh oksidirovaniya poluprovodnikov $A^{III}B^{V}$. [Catalytic action of vanadium and its oxide (V) in the processes of oxidation of $A^{III}B^{V}$ semiconductors]. *Nanosystems: Physics, Chemistry, Mathematics*. 2012;3(2): 116–138. Available at: https://www.elibrary.ru/item.asp?id=17881315 (In Russ.)

54. Ievlev, V. M., Mittova, I. Y., Samsonov, A. A., Tomina E. V., Kashkarov V. M. Catalytic effect of a nanolayer of the (V_2O_5 + PbO) composite in the thermal oxidation of InP crystals. *Doklady Chemistry*. 2007;417: 277–281. https://doi.org/10.1134/S0012500807120014

55. Mittova I. Y., Sladkopevtsev B. V., Samsonov A. A., Tomina E. V., Andreenko S. Y., Kostenko P. V. Growth and properties of nanofilms produced by the thermal oxidation of MnO_2/InP under the effect of $Mn_3(PO_4)_2$. *Inorganic Materials*. 2019;55(9): 915–919 https://doi.org/10.1134/S0020168519090073

56. Mittova I. Ya., Pshestanchik V. R., Kostryukov V. F. Nonlinear effect of the joint action of activators on thermal oxidation of gallium arsenide. *Doklady Physical Chemistry*. 1996;349(4-6): 196–198. Available at: https://www.elibrary.ru/item.asp?id=13233187

57. Mittova I. Ya., Pshestanchik V. R., Kostryukov V. F., Kuznetsov N. T. Alternating nonlinearity of the joint activating effect of binary mixtures of *p*-element oxides on the chemically activated thermal

GaAs oxidation. *Doklady Chemistry*. 2001;378(4-6): 165-167. https://doi.org/10.1023/A:1019238812687

58. Mittova I. Ya., Pshestanchik V. R., Pinyaeva O. A., Kostryukov V. F., Skorokhodova S. M. Nonadditive oxides influence in (CrO_3-PbO) and (CrO_3-V_2O_5) compositions as activators of thermal oxidation of gallium arsenide. *Doklady Chemistry*. 2002;385(4-6): 212–214. https://doi.org/10.1023/A:1019998719921

59. Mittova I. Ya., Pshestanchik V. R., Kostryukov V. F., Donkareva I. A., Saratova A. Yu. Chemostimulated GaAs thermal oxidation under the joint action of manganese (IV) oxide with lead (II) oxide and vanadium (V) oxide. *Russian Journal of Inorganic Chemistry*. 2004;49(7) 991–994. Available at: https://elibrary.ru/item.asp?id=13464912

60. Mittova I. Ya., Kostryukov V. F., Donkareva I. A., Pshestanchik V. R., Lopatin S. I., Saratova A. Yu. Nonlinear effects of MnO + PbO and MnO + V_2O_5 compositions on GaAs thermal oxidation. *Russian Journal of Inorganic Chemistry*. 2005;50(6): 869–873. Available at: https://elibrary.ru/item.asp?id=13487639

61. Mittova I. Ya., Pshestanchik V. R., Kuznetsova I. V., Kostryukov V. F., Skorokhodova S. M., Medvedeva K. M. Vliyanie razmera chastits aktivatorov na protsess termooksidirovaniya GaAs pod vozdeistviem kompozitsii PbO + V_2O_5 [Influence of the particle size of activators on the process of thermal oxidation of GaAs under the influence of PbO + V_2O_5 compositions]. *Zhurnal neorganicheskoi khimii*. 2005;50(10): 1603–1606. Available at: https://elibrary.ru/item.asp?id=9153646 (In Russ.)

62. Mittova I. Ya., Kostryukov V. F. GaAs thermal oxidation activated by the coaction of p-block oxides. *Nanosystems: Physics, Chemistry, Mathematics*. 2014;5(3): 417–426. Available at: http://www.mathnet.ru/links/8364620026a0f40f5d8a284be0ba04bf/nano872.pdf

63. Tret'yakov N. N., Mittova I. Ya., Kozik V. V., Sladkopevtsev B. V., Kostryukov V. F., Studenikina Yu. I. Opredelenie tolshchiny i fazovogo sostava plenok, sintezirovannykh khemostimulirovannym termooksidirovaniem InP pod vozdeistviem kompozitsii oksidov V_2O_5+MnO_2 raznogo sostava [Determination of the thickness and phase composition of films synthesized by chemically stimulated thermal oxidation of InP under the influence of a composition of V_2O_5 + MnO_2 oxides of different compositions]. *Izvestiya vysshikh uchebnykh zavedenii. Fizika*. 2014;57(7-2): 186–191. Available at: https://elibrary.ru/item.asp?id=23184836 (In Russ.)

64. Mittova I. Y., Tretyakov N. N., Kostryukov V. F., Sladkopevtsev B. V. Combined influence of chemostimulator oxides V_2O_5 and MnO_2 introduced via the gas phase on InP thermal oxidation. *Russian Journal of General Chemistry*. 2015;85(4): 796–801. https://doi.org/10.1134/S1070363215040040

65. Mittova I. Ya., Kostryukov V. F., Donkareva I. A., Penskoi P. K., Pinyaeva O. A., Pshestanchik V. R. MnO + MnO_2 mixture as a nonadditive activator of GaAs thermal oxidation. *Russian Journal of General Chemistry*. 2005;50(1): 15–19. Available at: https://elibrary.ru/item.asp?id=13497054

66. Losev V. N., Kudrina Yu. V., Trofimchuk A. K., Komozin P. N. Sorption of ruthenium (III) and ruthenium (IV) on silica gels chemically modified with mercapto and disulfide groups. *Russian Journal of Inorganic Chemistry*. 2005;50(4): 577–581. Available at: https://elibrary.ru/item.asp?id=13481209

67. Mittova I. Ya., Pshestanchik V. R., Kostryukov V. F., Donkareva I. A. Prostranstvennaya lokalizatsiya vzaimodeistvii mezhdu soedineniyami-aktivatorami pri khemostimulirovannom termooksidirovanii GaAs [Space localisation of linking interactions between activating compounds at the course of chemically stimulated GaAs thermal oxidation]. *Doklady akademii nauk*. 2002;386(4): 499–501. Available at: https://elibrary.ru/item.asp?id=44462420 (In Russ.)

68. Mittova I. Ya., Pshestanchik V. R., Kostryukov V. F., Donkareva I. A. Mutual effect of activators on chemostimulated GaAs thermal oxidation with spatially separated coupling stages. *Russian Journal of Inorganic Chemistry*. 2003;48(4): 480–482. Available at: https://elibrary.ru/item.asp?id=13436411

69. Kostryukov V. F., Pshestanchik V. R., Donkareva I. A., Agapov B. L., Mittova I. Ya., Lopatin S. I. Role of solid- and gas-phase interactions in the coaction of the oxides in MnO_2 + PbO and MnO_2 + V_2O_5 compositions activating the thermal oxidation of GaAs. *Russian Journal of Inorganic Chemistry*. 2007;52(10): 1498–1502. https://doi.org/10.1134/S0036023607100038

70. Mittova I. Ya., Kostryukov V. F., Pshestanchik V. R., Donkareva I. A., Agapov B. L. Contribution from the solid-phase interactions of activating oxides to their nonlinear joint effect on the thermal oxidation of GaAs. *Russian Journal of Inorganic Chemistry*. 2008;53(7): 1018–1023. https://doi.org/10.1134/S0036023608070085

71. Kostryukov V. F., Donkareva I. A., Pshestanchik V. R., Agapov B. L., Mittova I. Ya., Lopatin S. I. GaAs thermal oxidation with participation of spatially separated activator oxides (MnO + PbO and MnO + V_2O_5). *Russian Journal of Inorganic Chemistry*. 2008;53(8): 1182–1186. https://doi.org/10.1134/S0036023608080056

72. Mittova I. Ya., Lopatin S. I., Pshestanchik V. R., Kostryukov V. F., Sergeeva A. V., Penskoi P. K. Rol' inertnogo komponenta Ga_2O_3 v kompozitsii s oksidom-aktivatorom Sb_2O_3 v protsesse khemostimulirovannogo okisleniya GaAs [role of an inert component Ga_2O_3 in the composition with the activator oxide Sb_2O_3 in chemostimulated GaAs oxidation]. *Zhurnal neorganicheskoi khimii*. 2005;50(10): 1599–1602.

Available at: https://elibrary.ru/item.asp?id=9153645 (In Russ.)

73. Penskoi P. K., Kostryukov V. F., Pshestanchik V. R., Mittova I. Ya. Effekt sovmestnogo vozdeistviya kompozitsii khemostimulyatorov (Sb_2O_3, Bi_2O_3, MnO_2) s inertnym komponentom (Al_2O_3) v protsesse termooksidirovaniya arsenida galliya [Effect of the combined effect of chemostimulant compositions (Sb_2O_3, Bi_2O_3, MnO_2) with an inert component (Al_2O_3) during thermal oxidation of gallium arsenide]. *Doklady akademii nauk*. 2007;414(6): 765–767. Available at: https://elibrary.ru/item.asp?id=9533571 (In Russ.)

74. Penskoi P. K., Pshestanchik V. R., Kostryukov V. F., Agapov B. V., Mittova I. Ya., Kuznetsova I. V. Nonadditive linearity in the chemostimulating effect of activator oxides + dlient compositions on GaAs thermal oxidation. *Russian Journal of Inorganic Chemistry*. 2008;53(2): 186–191. https://doi.org/10.1007/s11502-008-2006-0

75. Penskoi P. K., Mittova I. Ya., Kostryukov V. F., Kononova E. Yu., Reutova E. A. Vliyanie inertnogo komponenta $A1_2O_3$ v kompozitsiyakh s oksidami-aktivatorami (Sb_2O_3, Bi_2O_3, MnO_2) na protsess termooksidirovaniya GaAs [The influence of inert component Al_2O_3 in mixtures with oxide activators (Sb_2O_3, Bi_2O_3, MnO_2) on the process of thermal oxidation of GaAs surface]. *Kondensirovannye sredy i mezhfaznye granitsy*. 2008;10(3): 236–243. Available at: https://elibrary.ru/item.asp?id=11688570 (In Russ.)

76. Penskoi P. K., Kostryukov V. F., Pshestanchik V. R., Mittova I. Ya., Kutsev S. V., Kuznetsova I. V. Effect of inert components (Y_2O_3, Al_2O_3, and Ga_2O_3) on the chemistimulating effect of the Sb_2O_3 activator of GaAs thermal oxidation. *Russian Journal of Inorganic Chemistry*. 2009;54(10): 1564–1570. https://doi.org/10.1134/S0036023609100118

77. Kozhevnikova T. V., Penskoi P. K., Kostryukov V. F., Mittova I. Y., Kuznetsova I. V., Kutsev S. V. Role of an inert component in compositions with manganese (II) and manganese (IV) oxides in studying nonlinear effects in gaas thermal oxidation. *Russian Journal of Inorganic Chemistry*. 2010;55(12): 1857–1862. https://doi.org/10.1134/S0036023610120077

78. Kozhevnikova T. V., Penskoi P. K., Kostryukov V. F., Mittova I. Ya., Agapov B. L., Kuznetsova I. V., Kutsev S. V. Termicheskoe okislenie GaAs pod vozdeistviem kompozitsii Sb_2O_3, Bi_2O_3, MnO, MnO_2 i V_2O_5 s oksidami alyuminiya i ittriya [Thermal oxidation of gaas under influence of compositions of Sb_2O_3, Bi_2O_3, MnO, MnO_2 and V_2O_5 with oxides of aluminium and yttrium]. *Kondensirovannye sredy i mezhfaznye granitsy = Condensed Matter and Interphases*. 2010;12(3): 212–225. Available at: https://elibrary.ru/item.asp?id=15574165 (In Russ.)

79. Penskoi P. K., Salieva E. K., Kostryukov V. F., Rembeza S. I., Mittova I. Ya. Gazochuvstvitel'nost' slabolegirovannykh sloev, poluchennykh okisleniem GaAs v prisutstvii PbO i Bi_2O_3 [Gas-sensitivity of the light-alloyed layers. Obtained by the oxidation of GaAs in the presence of PbO and Bi_2O_3]. *Vestnik VGU Seriya Khimiya. Biologiya. Farmatsiya*. 2008;1: 26–31. Available at: https://elibrary.ru/item.asp?id=11615172 (In Russ.)

80. Kostryukov V. F., Mittova I. Ya. Ammonia response of thin films grown on GaAs using PbO + Bi_2O_3 mixtures. *Inorganic Materials*. 2015;51(5): 425–429. https://doi.org/10.1134/S0020168515040056

81. Kostryukov V. F., Mittova I. Ya., Dimitrenko A. A. Chemically stimulated synthesis of gas-sensing films on the surface of GaAs. *Inorganic Materials*. 2017;53(5): 451–456. https://doi.org/10.1134/S0020168517050132

82. Kostryukov V. F., Mittova I. Ya., Ali Saud Gas-sensing properties of thin films grown on the surface of InP single crystals by thermal oxidation. *Inorganic Materials*. 2020;56(1): 66–71. https://doi.org/10.1134/S0020168520010070

83. Kostryukov V. F., Mittova I. Ya. Method for precision doping of thin films on gallium arsenide surface: *Patent No 2538415 RF*. Claim. 17.07.2013. Publ. 10.01.2015. Byul. №2013133382/28 1.

84. Kostryukov V.F., Mittova I. Ya., Sladkopevtsev B. V. Method of precision doping thin films on InP surface: *Patent No 2632261 RF*. Claim. 17.12.2015. Publ. 03.10.2017. Byul. №28.

85. Sladkopevtsev B. V., Tomina E. V., Mittova I. Ya., Tretyakov N. N. Method of creating nano-sized nanostructured oxide films on InP with application of vanadium pentaxide gel: *Patent No 2550316 RF*. Claim. 30.12.2013. Publ. 10.05.2015. Byul. № 13

86. Tomina E. V., Sladkopevtsev B. V., Mittova I. Ya., Zelenina L. S., Dontsov A. I., Tretyakov N. N., Gudkova Yu. N., Belashkova Yu. A. Effect of surface V_2O_5 nanolayers on the thermal oxidation kinetics of GaAs and the composition and morphology of resulting films. *Inorganic Materials*. 2015;51(11): 1138–1142. https://doi.org/10.1134/S0020168515110126

87. Mittova I. Y., Tomina E. V., Lapenko A. A., Sladkopevtsev B. V. Synthesis and catalytic performance of V_2O_5 nanoislands produced on the surface of InP crystals by electroexplosion. *Inorganic Materials*. 2010;46(4): 383–388. https://doi.org/10.1134/S0020168510040114

88. Mittova I. Ya., Tomina E. V., Tret'yakov N. N., Sladkopevtsev B. V. Zavisimost' mekhanizma khemostimuliruyushchego deistviya V_2O_5 ot sposoba vvedeniya ego v sistemu pri termooksidirovanii InP [Dependence of the mechanism of the chemostimulating action of V_2O_5 on the method of its introduction into the system during thermal oxidation of InP.]. *Kondensirovannye sredy i mezhfaznye granitsy = Condensed Matter and Interphases*. 2013;15(3): 305–311. Available at: https://www.elibrary.ru/item.asp?id=20296106 (In Russ.)

89. Tretyakov N. N., Mittova I. Ya., Sladkopevtsev B. V., Agapov B. L., Pelipenko D. I., Mironenko S. V. Surface morphology, composition, and structure of nanofilms grown on InP in the presence of V_2O_5. *Inorganic Materials*. 2015;51(7): 655-660. https://doi.org/10.1134/S002016851507016X

90. Mittova I. Ya., Sladkopevtsev B. V., Tomina E. V., Samsonov A. A., Tretyakov N. N., Ponomarenko S. V. Preparation of dielectric films via thermal oxidation of MnO_2/GaAs. *Inorganic Materials*. 2018;54(11): 1085–1092. https://doi.org/10.1134/S0020168518110109

91. Shvets V. A., Rykhlitskii, S. V., Mittova, I. Ya., Tomina E. V. Analysis of the optical and structural properties of oxide films on InP using spectroscopic ellipsometry. *Technical Physics*. 2013;58: 1638–1645. https://doi.org/10.1134/S1063784213110248

92. Mittova I. Ya., Tomina E. V., Sladkopevtsev B. V., Tret'Yakov N. N., Lapenko A. A., Shvets V. A. High-speed determination of the thickness and spectral ellipsometry investigation of films produced by the thermal oxidation of InP and V_xO_y/InP structures. *Inorganic Materials*. 2013;49(2): 179–184. https://doi.org/10.1134/S0020168513020143

93. Mittova I. Ya., Tomina E. V., Samsonov A. A., Sladkopevtsev B. V., Tret'yakov N. N., Shvets V. A. Determination of the thickness and optical constants of nanofilms produced by the thermal oxidation of InP with V_2O_5, V_2O_5 + PbO, and NiO + PbO chemical stimulator layers grown by magnetron sputtering. *Inorganic Materials*. 2013;49(10): 963–970. https://doi.org/10.1134/S0020168513100075

94. Kostryukov V. F., Mittova I. Ya., Shvets V. A., Tomina E. V., Sladkopevtsev B. V., Tret'yakov N. N. Spectral ellipsometry study of thin films grown on GaAs by chemically stimulated thermal oxidation. *Inorganic Materials*. 2014;50(9): 882–887. https://doi.org/10.1134/S0020168514090052

95. Sladkopevtsev B. V., Mittova I. Ya., Tomina E. V., Zabolotskaya A. V., Samsonov A. A., Dontsov A. I. Osobennosti kinetiki i mekhanizma formirovaniya plenok pri oksidirovanii geterostruktur V_2O_5/InP, sformirovannykh metodami reaktivnogo magnetronnogo raspyleniya i elektricheskogo vzryva provodnika [Features of kinetics and mechanism of films formation in oxidation of V_2O_5/InP heterostructures, formed by reactive magnetron sputtering and electric explosion of conductor]. *Izvestiya vysshikh uchebnykh zavedenii. Fizika*. 2014;57(7-2): 148–153. Available at: https://www.elibrary.ru/item.asp?id=23184829 (In Russ.)

96. Ugai Ya. A., Samoilov A. M., Synorov Yu. V., Yatsenko O. B., Zuev D. V. Poluchenie tonkikh plenok tellurida svintsa na kremnievykh podlozhkakh [Preparation of thin films of lead telluride on silicon substrates]. *Neorganicheskie materialy*. 1994;30(7): 898-902. Available at: https://elibrary.ru/item.asp?id=35103015 (In Russ.)

97. Ugai Y. A., Samoylov A. M., Sharov M. K., Tadeev A. V. Crystal microstructure of PbTe/Si and PbTe/SiO_2/Si thin films. *Thin Solid Films*. 1998;336(1-2): 196–200. https://doi.org/10.1016/S0040-6090(98)01278-4

98. Ugai Ya. A., Samoilov A. M., Synorov Yu. V., Yatsenko O. B. Electrical properties of thin PbTe films on Si substrates. *Inorganic Materials*. 2000;36(5): 449–453. https://doi.org/10.1007/BF02758045

99. Ugai Ya. A., Samoilov A. M., Sharov M. K., Arsenov A. V., Buchnev S. A. Vyrashchivanie plenok PbTe, legirovannykh galliem v protsesse ikh rosta, na Si-podlozhkakh pri pomoshchi modifitsirovannogo metoda "goryachei stenki" [Growing of PbTe films doped with gallium during their growth on Si substrates using a modified "hot wall" method.]. *Poverkhnost'. Rentgenovskie, sinkhrotronnye i neitronnye issledovaniya*. 2002;3: 28–34. (In Russ.)

100. Ugai Ya. A., Samoylov A. M., Buchnev S. A., Synorov Yu. V., Sharov M. K. Ga doping of thin PbTe films on Si substrates during growth. *Inorganic Materials*. 2002;38(5): 450–456. https://doi.org/10.1023/A:1015410703238

101. Ugai Ya. A., Samoylov A. M., Sharov M. K., Yatsenko O. B., Akimov B. A. Transport properties of Ga-doped PbTe thin films on Si substrates. *Inorganic Materials*. 2002;38(1): 12–16. https://doi.org/10.1023/A:1013687024227

102. Samoylov A. M., Buchnev S. A., Khoviv A. M., Dolgopolova E. A., Zlomanov V. P. Comparative study of point defects induced in PbTe thin films doped with Ga by different techniques. *Materials Science in Semiconductor Processing*. 2003;6(5-6): 481–485. https://doi.org/10.1016/j.mssp.2003.07.014

103. Samoylov A. M., Khoviv A. M., Buchnev S. A., Synorov Yu. V., Dolgopolova E. A. Crystal structure and electrical parameters of In-doped PbTe/Si films prepared by modified HWE technique. *Journal of Crystal Growth*. 2003;254(1-2): 55–64. https://doi.org/10.1016/S0022-0248(03)01022-4

104. Samoilov A. M., Buchnev S. A., Synorov Yu. V., Agapov B. L., Khoviv A. M. Vyrashchivanie modifitsirovannym metodom "goryachei stenki" plenok PbTe, legirovannykh In neposredstvenno v protsesse sinteza [Preparation of PbTe thin films doped with indium on Si substrates by modified "hot wall" technique]. *Poverkhnost'. Rentgenovskie, sinkhrotronnye i neitronnye issledovaniya*. 2004;1: 86-94. Available at: https://elibrary.ru/item.asp?id=17662304 (In Russ.)

105. Samoilov A. M., Buchnev S. A., Dolgopolova E. A., Khoviv A. M., Synorov Yu. V. Structural perfection of pbte films doped with indium during growth on Si substrates. *Inorganic Materials*. 2004;40(4): 349-354. https://doi.org/10.1023/B:INMA.0000023953.49486.2a

106. Dolgopolova E. A., Samoilov A. M., Synorov Yu. V., Khoviv A. M. Sintez legirovannykh In plenok PbTe s kontroliruemym soderzhaniem primesnykh atomov i otkloneniem ot stekhiometrii [Synthesis of In-doped PbTe films with controlled content of impurity atoms and deviation from stoichiometry]. *Poverkhnost'. Rentgenovskie, sinkhrotronnye i neitronnye issledovaniya*. 2008;10: 17–22. Available at: https://elibrary.ru/item.asp?id=11533187 (In Russ.)

107. Belenko S. V., Dolgopolova E. A., Samoilov A. M., Synorov Yu. V., Sharov M. K. Oblast' rastvorimosti galliya v plenkakh tellurida svintsa, vyrashchennykh na kremnievykh podlozhkakh [Gallium solubility region in lead telluride films grown on silicon substrates]. *Poverkhnost'. Rentgenovskie, sinkhrotronnye i neitronnye issledovaniya*. 2010;2: 99–108. Available at: https://elibrary.ru/item.asp?id=13044799 (In Russ.)

108. Sharov M. K, Yatsenko O. B., Samoilov A. M. Elektrofizicheskie svoistva monokristallov tellurida svintsa, legirovannogo bromom [Electrophysical properties of single crystals of lead telluride doped with bromine.]. *Poverkhnost'. Rentgenovskie, sinkhrotronnye i neitronnye issledovaniya.* 2010;7: 77–79. Available at: https://elibrary.ru/item.asp?id=15142184 (In Russ.)

109. Samoylov A. M., Agapov B. L., Belenko S. V., Dolgopolova E. A., Khoviv A. M. Electrical properties and mechanisms of the point defect formation in PbTe(In) films prepared by modified "Hot Wall" technique. *Functional Materials*. 2011;18(1): 29–36. Available at: https://elibrary.ru/item.asp?id=18002406

110. Samoylov A. M., Belenko S. V., Dolgopolova E. A., Khoviv A. M., Synorov Y. V. The solubility region of Ga in PbTe films prepared on Si-substrates by modified "Hot Wall" technique. *Functional Materials*. 2011;18(2): 181–188. Available at: https://www.elibrary.ru/item.asp?id=18002278

111. Samoylov A. M., Belenko S. V., Sharov M. K., Dolgopolova E. A., Zlomanov V. P. The deviation from a stoichiometry and the amphoteric behaviour of Ga in PbTe/Si films. *Journal of Crystal Growth*. 2012;351(1): 149–154. https://doi.org/10.1016/j.jcrysgro.2012.01.042

112. Naumov A. V., Samoilov A. M., Lopatin S. I. Thermodynamic functions of mixing the melts in the Ga-Pb system. *Russian Journal of General Chemistry*. 2013;83(1): 26–31. https://doi.org/10.1134/S1070363213010040

113. Samoilov A. M., Belenko S. V., Siradze B. A., Toreev A. S., Dontsov A. I., Filonova I. V. Plotnosti dislokatsii v plenkakh PbTe, vyrashchennykh na podlozhkakh Si (100) i BaF_2 (100) modifitsirovannym metodom «goryachei stenki» [Dislocation densities in PbTe films grown on Si (100) and BaF_2 (100) substrates by the modified hot wall method]. *Kondensirovannye sredy i mezhfaznye granitsy = Condensed Matter and Interphases*. 2013;15(3): 322-331. Available at: https://elibrary.ru/item.asp?id=20296109 (In Russ., abstract in Eng.)

114. Akimov A. N., Klimov A. E., Samoilov A. M., Shumskii V. N., Epov V. S. Zavisimost' kinetiki fototoka v plenkakh $Pb_{x-1}Sn_xTe$ ot urovnya osveshcheniya i vremeni ekspozitsii [Dependence of photocurrent kinetics in $Pb_{x-1}Sn_xTe$ films on illumination intensity and duration of exposure]. *Kondensirovannye sredy i mezhfaznye granitsy = Condensed Matter and Interphases*.. 2013;15(4): 378–381. Available at: https://elibrary.ru/item.asp?id=20931228 (In Russ., abstract in Eng.)

115. Samoilov A. M., Belenko S. V., Sharov M. K., Lopatin S. I., Synorov Y. V. Synthesis of films in the system Ga-Pb with precision control over quantitative composition. *Russian Journal of General Chemistry*. 2015;85(10): 2242–2251. https://doi.org/10.1134/S1070363215100059

116. Marikutsa A. V., Rumyantseva M. N., Gaskov A. M., Samoylov A. M. Nanocrystalline tin dioxide: Basics in relation with gas sensing phenomena. Part I. Physical and chemical properties and sensor signal formation. *Inorganic Materials*. 2015;51(13): 1329–1347. https://doi.org/10.1134/S002016851513004X

117. Ievlev V. M., Kushchev S. B., Sinel'nikov A. A., Soldatenko S. A., Ryabtsev S. V., Bosykh M. A., Samoilov A. M. Struktura geterosistem plenka SnO_2–ostrovkovyi kondensat metalla (Ag, Au, Pd) [Structure of heterosystems SnO_2 film – island condensate of metal (Ag, Au, Pd)]. *Neorganicheskie materialy*. 2016;52(7): 757–764. https://doi.org/10.7868/S0002337X1607006X (In Russ.)

118. Ryabtsev S. V., Shaposhnik A. V., Samoilov A. M., Sinel'nikov A. A., Soldatenko S. A., Kushchev S. B., Ievlev V. M. Tonkie plenki oksida palladiya dlya gazovykh sensorov [Palladium Oxide Thin Films for Gas Sensors]. *Doklady Akademii nauk, seriya Fizicheskaya khimiya*. 2016;470(5): 550–553. https://doi.org/10.7868/s0869565216290168 (In Russ.)

119. Marikutsa A. V., Rumyantseva M. N., Gaskov A. M., Samoylov A. M. Nanocrystalline tin dioxide: Basics in relation with gas sensing phenomena. Part II. Active centers and sensor behavior. *Inorganic Materials*. 2016;52(13): 1311–1338. https://doi.org/10.1134/S0020168516130045

120. Ievlev V. M., Ryabtsev S. V., Shaposhnik A. V., Samoylov A. M., Kuschev S. B., Sinelnikov A. A. Ultrathin films of palladium oxide for oxidizing gases detecting. *Procedia Engineering*. 2016;168: 1106–1109. https://doi.org/10.1016/j.proeng.2016.11.357

121. Ryabtsev S. V., Ievlev V. M., Samoylov A. M., Kuschev S. B., Soldatenko S. A. Microstructure and electrical properties of palladium oxide thin films for oxidizing gases detection. *Thin Solid Films*. 2017;636: 751–759. https://doi.org/10.1016/j.tsf.2017.04.009

122. Samoylov, A. M., Gvarishvili, L. J., Ivkov, S. A., Pelipenko, D. I., Badica, P. Two-stage Synthesis of palladium (II) oxide nanocrystalline powders for gas sensor. *Research & Development in Material Sciences*.

2018;8(2): 1–7. https://doi.org/10.31031/RDMS.2018.08.000682

123. Ievlev V. M., Ryabtsev S. V., Samoylov A. M., Shaposhnik A. V., Kuschev S. B., Sinelnikov A. A. Thin and ultrathin films of palladium oxide for oxidizing gases detection. *Sensors and Actuators B: Chemical*. 2018;255(2): 1335–1342. https://doi.org/10.1016/j.snb.2017.08.121

124. Samoilov A. M., Kuz'minykh O. G., Synorov Yu. V., Ivkov S. A., Agapov B. L., Belonogov E. K. Morfologiya poverkhnosti plenok PbTe/Si (100), sintezirovannykh modifitsirovannym metodom "goryachei stenki" [Surface morphology of PbTe/Si (100) films synthesized by modified "hot wall" epitaxy technique]. *Kondensirovannye sredy i mezhfaznye granitsy = Condensed Matter and Interphases*. 2018;20(1): 102–114. https://doi.org/10.17308/kcmf.2018.20/483 (In Russ., abstracy in Eng.)

125. Samoylov A. M., Kuzminykh O. G., Belonogov E. K., Agapov B. L., Synorov Y. V., Belenko S. V. Growth kinetics and microstructure of PbTe films produced on Si and BaF_2 substrates by a modified hot-wall method. *Inorganic Materials*. 2018;54(4): 338-348. https://doi.org/10.1134/S002016851804012X

126. Samoylov A. M., Ryabtsev S. V., Popov V. N., Badica P. Palladium (II) oxide nanostructures as promising materials for gas sensors. In book: *Novel Nanomaterials Synthesis and Applications*. Edited by George Kyzas. UK, London: IntechOpen Publishing House; 2018. 211–229 p. https://doi.org/10.5772/intechopen.72323

127. Samoylov A. M., Ryabtsev S. V., Chuvenkova O. A, Ivkov S. S., Sharov M. K., Turishchev S. Yu. Crystal structure and surface phase composition of palladium oxides thin films for gas sensors. In book: *SATF 2018. Science and Applications of Thin Films, Conference & Exhibition. Proceeding Book.*: *17 to 21 September 2018*. Turkey: Izmir, Izmir Institute of Technology; 2018. p. 43–56.

128. Samoylov A. M., Ivkov S. A., Pelipenko D. I., Sharov M. K., Tsyganova V. O., Agapov B. L., Tutov E. A., Badica P. Structural changes in palladium nanofilms during thermal oxidation. *Inorganic Materials*. 2020;56(10): 1020–1026. https://doi.org/10.1134/S0020168520100131

129. Samoilov A. M., Pelipenko D. I., Kuralenko N. S. Raschet oblasti nestekhiometrii nanokristallicheskikh plenok oksida palladiya (II) [Calculation of the nonstoichiometry area of nanocrystalline palladium (II) oxide films]. *Kondensirovannye sredy i mezhfaznye granitsy = Condensed Matter and Interphases*. 2021;23(1): 62–72. https://doi.org/10.17308/kcmf.2021.23/3305

130. Ponomareva N. I., Poprygina T. D., Lesovoi M. V., Karpov S. I. Effect of alizarin red S on the formation of hydroxyapatite crystals. *Russian Journal of General Chemistry*. 2008;78(4): 521-526. https://doi.org/10.1134/S1070363208040038

131. Ponomareva N. I., Poprygina T. D., Karpov S. I., Lesovoi M. V., Agapov B. L. Mikroemul'sionnyi sposob polucheniya gidroksiapatita [Microemulsion method for producing hydroxyapatite]. *Zhurnal obshchei khimii*. 2010;80(5): 735–738. (In Russ.)

132. Ponomareva N. I., Poprygina T. D., Lesovoi M. V., Karpov S. I., Agapov B. L. Issledovanie kompozitov gidroksiapatita s biopolimerami [The investigation of hydroxyapatite-biopolymer composites *Kondensirovannye sredy i mezhfaznye granitsy = Condensed Matter and Interphases*. 2009;11(3): 239–243. Available at: https://elibrary.ru/item.asp?id=12971539 (In Russ.)

133. Ponomareva N. I., Poprygina T. D., Lesovoi M. V., Sokolov Yu. V., Agapov B. L. Crystal structure and composition of hydroxyapatite biocomposites prepared at excess of calcium ions. *Russian Journal of General Chemistry*. 2009;79(2): 186–190. https://doi.org/10.1134/S1070363209020030

134. Ponomareva N. I., Poprygina T. D., Karpov S. I., Sokolov Yu. V. Issledovanie mikrotverdosti kompozitov gidroksiapatita s biopolimerami [Investigation of microhardness of composites of hydroxyapatite with biopolymers]. *Vestnik VGU, Seriya «Khimiya. Biologiya. Farmatsiya»*. 2012;2: 45–50. (In Russ.)

135. Ponomareva N. I., Poprygina T. D., Lesovoi M. V., Sokolov Yu. V. Vliyanie primesei zheleza na poluchenie i kharakteristiki apatitovykh pokrytii titanovykh implantantov [The influence of iron admixtures on the synthesis and characteristics of apatite coatings of titanium implants]. *Sistemnyi analiz i upravlenie v biomeditsinskikh sistemakh*. 2010;9(2) 448–451. Available at: https://elibrary.ru/item.asp?id=14749925

136. Ponomareva N. I., Poprygina T. D., Kashkarov V. M., Lesovoi M. V. Calcite and apatite coatings on titanium. *Russian Journal of Inorganic Chemistry*. 2011;56(11): 1713–1716. https://doi.org/10.1134/S0036023611110209

137. Ponomareva N. I., Poprygina T. D. Procedure for application of coating on items out of titanium: *Patent No. 2453630 RF*. Claim. 11.01.2011. Publ. 20.06.2012. Byul. No 17.

138. Ponomareva N. I., Poprygina T. D., Ponomarev Yu. A., Soldatenko S. A. A study of resorption of the hydroxyapatite in the composition of impregnated carbon implants. *Russian Journal of General Chemistry*. 2012;82(9): 1472–1475. https://doi.org/10.1134/S1070363212090022

139. Ponomareva N. I., Poprygina T. D., Karpov S. I., Samodai V. G. Vliyanie ionov margantsa na sintez i kharakteristiki gidroksiapatita v sostave impregnirovannykh uglerodistykh implantatov [Effect of manganese ions on the synthesis and characteristics of hydroxyapatite in the composition of impregnated

carbon implants]. *Aprobatsiya*. 2013;5(8): 21–23. Available at: https://elibrary.ru/item.asp?id=23216891

140. Xu C., Yang Y., Wang S., Duan W., Gu B., Bellaiche L. Anomalous properties of hexagonal rare-earth ferrites from first principles. *Physical Review B*. 2014;89(20): 205122. https://doi.org/10.1103/PhysRevB.89.205122

141. Mahalakshmi S., SrinivasaManja K., Nithiyanantham S. Electrical properties of nanophase ferrites doped with Rare Earth Ions. *Journal of Superconductivity and Novel Magnetism*. 2014;27(9): 2083–2088. https://doi.org/10.1007/s10948-014-2551-y

142. Fahlman B. *Materials Chemistry*. Springer; 2007. 485 p.

143. Gusev A. I. *Nanomaterials, nanostructures, nanotechnologies*. Moscow: Fizmatlit Publ.; 2005. 416 p. (In Russ.)

144. Maiti R. Basu S., Chakravorty D. Synthesis of nanocrystalline $YFeO_3$ and its magnetic properties. *Journal of Magnetism and Magnetic Materials*. 2009;321(19): 3274–3277. https://doi.org/10.1016/j.jmmm.2009.05.061

145. Kolb E. D. The hydrothermal growth of rare earth orthoferrites. *Journal of Applied Physics*. 1968;39(2): 1362–1364. https://doi.org/10.1063/1.1656305

146. Cheng Z. X., Shen H., Xu J., Liu P., Zhang S. J., Wang J. L., Wang X. L., Dou S. X. Magnetocapacitance effect in nonmultiferroic $YFeO_3$ single crystal. *Journal of Applied Physics*. 2012;111(3): 34103.1-5. https://doi.org/10.1063/1.3681294

147. Racu A. V., Ursu D. H., Kuliukova O. V., Logofatu C., Leca A., Miclau M. Direct low temperature hydrothermal synthesis of $YFeO_3$ microcrystals. *Materials Letters*. 2015;140(1): 107–110. https://doi.org/10.1016/j.matlet.2014.10.129

148. Duan L., Jiang G.-J., Peng W., Cheng M., Wang X.-J. Influence of reaction conditions on the phase composition, particle size and magnetic properties of $YFeO_3$ microcrystals synthesized by hydrothermal method. *Journal of Synthetic Crystals*. 2015;44(8): 2144-2149.

149. Popkov V. I., Almjasheva O. V. Formation mechanism of $YFeO_3$ nanoparticles under the hydrothermal condition. *Nanosystems: Physics, Chemistry, Mathematics*. 2014;5(5): 703–708. Available at: https://www.elibrary.ru/item.asp?id=22415667

150. Tang P., Sun H., Chen H., Cao F. Hydrothermal processing-assisted synthesis of nanocrystalline $YFeO_3$ and its visible-light photocatalytic activity. *Current Nanoscience*. 2012;8(1): 64–67. https://doi.org/10.2174/1573413711208010064

151. Popkov V. I., Almjasheva O. V., Gusarov V. V. The investigation of the structure control possibility of nanocrystalline yttrium orthoferrite in its synthesis from amorphous powders. *Russian Journal of Applied Chemistry*. 2014;87(10): 1417–1421. https://doi.org/10.1134/S1070427214100048

152. Popkov V. I., Almjasheva O. V. Yttrium orthoferrite $YFeO_3$ nanopowders formation under glycine-nitrate combustion conditions. *Russian Journal of Applied Chemistry*. 2014;87(2): 167–171. https://doi.org/10.1134/S1070427214020074

153. Mathur S., Veith M., Rapalaviciute R., Shen H., Goya G. F., Martins Filho W. L., Berquo T. S. Berquo Molecule derived synthesis of nanocrystalline $YFeO_3$ and investigations on its weak ferromagnetic behavior. *Chemistry of Materials*. 2004;16(10): 1906–1913. https://doi.org/10.1021/cm0311729

154. Tretyakov Yu. D. Development of inorganic chemistry as a fundamental for the design of new generations of functional materials. *Russian Chemical Reviews*. 2004;73(9): 831–846. https://doi.org/10.1070/RC2004v073n09ABEH000914

155. Niepce C. J., Stuerga D., Caillot T., Clerk J.P., Granovsky A., Inoue M., Perov N., Pourroy G. The magnetic properties of magnetic nanoparticles produced by microwave flash synthesis of ferrous alcoholic solutions. *IEEE Transactions on Magnetics*. 2002;38(51): 2622–2624. https://doi.org/10.1109/TMAG.2002.801963

156. Zou J., Gong W., Ma J., Li L., Jiang J. Efficient catalytic activity $BiFeO_3$ nanoparticles prepared by novel microwave-assisted aynthesis. *Journal of Nanoscience and Nanotechnology*. 2015;15(2): 1304–1311. https://doi.org/10.1166/jnn.2015.9074

157. Tomina E. V., Mittova I. Y., Stekleneva O. V., Kurkin N. A., Perov N. S., Alekhina Y. A. Microwave synthesis and magnetic properties of bismuth ferrite nanopowder doped with cobalt. *Russian Chemical Bulletin*. 2020;69(5): 941–946. https://doi.org/10.1007/s11172-020-2852-1

158. Tomina E. V., Darinskii B. M., Mittova I. Y., Boikov N. I., Ivanova O. V., Churkin V. D. Microwave-assisted synthesis of $YCo_xFe_{1-x}O_3$ nanocrystals. *Inorganic Materials*. 2019;55(4): 390–394. https://doi.org/10.1134/S0020168519040150

159. Din' V. T., Mittova V. O., Mittova I. Ya. Vliyanie soderzhaniya lantana i temperatury otzhiga na razmer i magnitnye svoistva nanokristallov $Y_{1-x}La_xFeO_3$, poluchennykh zol' – gel' metodom [Influence of lanthanum content and annealing temperature on the size and magnetic properties of $Y_{1-x}La_xFeO_3$ nanocrystals obtained by the sol – gel method]. *Neorganicheskie materialy*. 2011;47(5): 590–595. Available at: https://www.elibrary.ru/item.asp?id=16339649 (In Russ.)

160. Nguen A. T., Mittova I. Ya., Solodukhin D. O., Al'myasheva O. V., Mittova V. O., Demidova S. Yu. Zol'-gel' formirovanie i svoistva nanokristallov tverdykh rastvorov $Y_{1-x}Ca_xFeO_3$ [Sol-gel formation and properties of nanocrystals of $Y_{1-x}Ca_xFeO_3$ solid solutions]. *Zhurnal*

neorganicheskoi khimii. 2014;59(2): 166–171. https://doi.org/10.7868/S0044457X14020159 (In Russ.)

161. Din' V. T., Mittova V. O., Al'myasheva O. V., Mittova I. Ya. Cintez i magnitnye svoistva nanokristallicheskogo $Y_{1-x}Cd_xFeO_{3-\delta}$ ($0 \leqslant x \leqslant 0.2$) [Synthesis and magnetic properties of nanocrystalline $Y_{1-x}Cd_xFeO_{3-\delta}$ ($0 \leqslant x \leqslant 0.2$)]. *Neorganicheskie materialy*. 2011;47(10): 1251–1256. Available at: https://www.elibrary.ru/item.asp?id=16893013 (In Russ.)

162. Nguyen A. T. Synthesis, structure and properties of nanopowders $La(Y)_{1-x}Sr(Ca)_xFeO_3$ (x = 0.0; 0.1; 0.2; 0.3). *Diss. Cand. Chem. Sciences* / Voronezh: Voronezh State University; 2009. 153 p. Available at: https://www.dissercat.com/content/sintez-struktura-i-svoistva-nanoporoshkov-lay1-xsrcaxfeo3-x-00-01-02-03 (In Russ.)

163. Polezhaeva O. S., Dolgopolova E. A., Baranchikov A. E., Ivanov V. K., Tret'yakov Yu. D. Sintez nanokristallicheskikh tverdykh rastvorovna osnove dioksida tseriya, dopirovannogo RZE [Synthesis of nanocrystalline solid solutions based on cerium dioxide doped with REE]. *Kondensirovannye sredy i mezhfaznye granitsy = Condensed Matter and Interphases*. 2010;12(2): 154–159. Available at: https://www.elibrary.ru/item.asp?id=15176050 (In Russ., abstract in Eng.)

164. Batsanov S. S. *Strukturnaya khimiya. Fakty i zavisimosti* [Structural chemistry. Facts and dependencies]. M.: Dialog – MGU Publ.; 2000. 292 p. (In Russ.)

165. Berezhnaya M. V., Al'myasheva O. V., Mittova V. O., Nguyen A. T., Mittova I. Ya. Sol-gel synthesis and properties of $Y_{1-x}Ba_xFeO_3$ nanocrystals. *Russian Journal of General Chemistry*. 2018;88(6): 1349–1349. https://doi.org/10.1134/S1070363218060464

166. Berezhnaya M. V., Mittova I. Ya., Perov N. S., Al'myasheva O. V., Nguyen A. T., Mittova V. O., Bessalova V. V., Viryutina E. L. Production of zinc-doped yttrium ferrite nanopowders by the sol–gel method. *Russian Journal of Inorganic Chemistry*. 2018;63(6): 742–746. https://doi.org/10.1134/s0036023618060049

167. Mittova I. Ya., Solodukhin D. O., Mittova V. O., Demidova S. Yu., Knurova M. V. Method for obtaining nanocrystalline magnetic powder of doped yttrium orthoferrite: *Patent No No 2574558 RF*. Claim. 04.12.2013. Publ. 10.02.2016. Byul. No 4.

168. Nguen A. T., Mittova V. O., Mittova I. Ya., Din' V. T. Synthesis of $La_{1-x}Sr(Ca)_xFeO_3$ (x = 0; 0.1; 0.2; 0.3) nanopowders by the sol-gel method. *Kondensirovannye sredy i mezhfaznye granitsy = Condensed Matter and Interphases*. 2010;12(1): 56–60. Available at: https://www.elibrary.ru/item.asp?id=15164382 (In Russ., abstract in Eng.)

169. Berezhnaya M. V., Perov N. S., Almjasheva O. V., Mittova V. O., Nguyen A. T., Mittova I. Ya., Druzhinina L. V., Alekhina Yu. A. Synthesis and magnetic properties of barium-doped nanocrystal lanthanum orthoferrite. *Russian Journal of General Chemistry*. 2019;89(3): 480–485. https://doi.org/10.1134/s1070363219030198

170. Knurova M. V., Mittova I. Ya., Perov N. S., Al'myasheva O. V., Tien N. A., Mittova V. O., Bessalova V. V., Viryutina E. L. Effect of the degree of doping on the size and magnetic properties of nanocrystals $La_{1-x}Zn_xFeO_3$ synthesized by the sol–gel method. *Russian Journal of Inorganic Chemistry*. 2017;62(3): 281–287. https://doi.org/10.1134/s0036023617030081

171. Lin Q., Xu J., Yang F., Yang X., He Y. The influence of Ca substitution on $LaFeO_3$ nanoparticles in terms of structural and magnetic properties. *Journal of Applied Biomaterials & Functional Materials*. 2018;16(1S): 17–25. https://doi.org/10.1177/2280800017753948

172. Belov K. P. *Magnitostriktsionnye yavleniya i ikh tekhnicheskie prilozheniya* [Magnetostrictive phenomena and their technical applications]. M.: Nauka Publ.; 1987. 160 p. (In Russ.)

173. Mukhopadhyay K., Mahapatra A. S., Chakrabarti P. K. Multiferroic behavior, enhanced magnetization and exchange bias effect of Zn substituted nanocrystalline $LaFeO_3$ ($La_{(1-x)}Zn_xFeO_3$, x=0.10, and 0.30). *Journal of Magnetism and Magnetic Materials*. 2013;329: 133–141. https://doi.org/10.1016/j.jmmm.2012.09.063

174. Mukhopadhyay K., Mahapatra A. S., Chakrabarti P. K. Enhanced magneto-electric property and exchange bias effect of Zn substituted $LaFeO_3$ ($La_{0.50}Zn_{0.50}FeO_3$). *Materials Letters*. 2015;159: 9–11. https://doi.org/10.1016/j.matlet.2015.06.059

175. Bhat I., Husain S., Khan W. Structural and dielectric properties of $LaFe_{1-x}Zn_xO_3$ ($0 \leqslant x \leqslant 0.3$). *AIP Conference Proceedings*. 2013;1512: 968–969. https://doi.org/10.1063/1.4791364

176. Bhat I., Husain S., Khan W., Patil S. I. Effect of Zn doping on structural, magnetic and dielectric properties of $LaFeO_3$ synthesized through sol–gel auto-combustion process. *Materials Research Bulletin*. 2013;48(11): 4506–4512. https://doi.org/10.1016/j.materresbull.2013.07.028

177. Almjasheva O. V., Tomkovich M. V., Gusarov V. V., Smirnov A.V., Fedorov B.A. structural features of ZrO_2-Y_2O_3 and ZrO_2-Gd_2O_3 nanoparticles formed under hydrothermal conditions. *Russian Journal of General Chemistry*. 2014;84(5): 804–809. https://doi.org/10.1134/S1070363214050028

178. Tugova E. A., Gusarov V. V. Structure peculiarities of nanocrystalline solid solutions in $GdAlO_3$ — $GdFeO_3$ system. *Nanosystems: Physics, Chemistry, Mathematics*. 2013;4(3): 352-356. Available at: https://www.elibrary.ru/item.asp?id=19412861

179. Marenkin S. F., Izotov A. D., Fedorchenko I. V., Novotortsev V. M. Manufacture of magnetic granular

structures in semiconductor-ferromagnet systems. *Russian Journal of Inorganic Chemistry*. 2015;60(3): 295-300. https://doi.org/10.1134/S0036023615030146

180. Gupta A. K., Gupta M. Synthesis and surface engineering of iron oxide nanoparticles for biomedical applications. *Biomaterials*. 2005;26(18): 3995–4021. https://doi.org/10.1016/j.biomaterials.2004.10.012

181. Shen H., Xu J., Jin M., Jiang G. Influence of manganese on the structure and magnetic properties of $YFeO_3$ nanocrystal. *Ceramics International*. 2012;38(2): 1473–1477. https://doi.org/10.1016/j.ceramint.2011.09.030

182. Ma Y., Wu Y. J., Lin Y. Q., Chen X. M. Microstructures and multiferroic properties of $YFe_{1-x}Mn_xO_3$ ceramics prepared by spark plasma sintering. *Journal of Materials Science: Materials in Electronics*. 2010;21(8): 838–843. https://doi.org/10.1007/s10854-009-0004-3

183. Nguyen T. A., Pham V. N. T., Le H. T., Chau D. H., Mittova V. O. Tr Nguyen L. T., Dinh D. A., Hao T. V. N., Mittova I. Ya. Crystal structure and magnetic properties of $LaFe_{1-x}Ni_xO_3$ nanomaterials prepared via a simple co-precipitation method. *Ceramics International*. 2019;45(17): 21768–21772. https://doi.org/10.1016/j.ceramint.2019.07.178

184. Nguyen A. T., Pham V., Chau D. H., Mittova V. O., Mittova I. Ya., Kopeychenko E. I., Nguyen L. T. Tr., Bui V. X., Nguyen A. T. P. Effect of Ni substitution on phase transition, crystal structure and magnetic properties of nanostructured $YFeO_3$ perovskite. *Journal of Molecular Structure*. 2020;1215: 12829. https://doi.org/10.1016/j.molstruc.2020.128293

185. Nguyen A. T., Pham V. N. T., Nguyen T. T. L., Mittova V. O., Vo Q. M., Berezhnaya M. V., Mittova I. Ya, Do Tr. H., Chau H. D. Crystal structure and magnetic properties of perovskite $YFe_{1-x}Mn_xO_3$ nanopowders synthesized by co-precipitation method. *Solid State Sciences*. 2019;96: 105922. https://doi.org/10.1016/j.solidstatesciences.2019.06.011

186. Kopeichenko E. I., Mittova I. Ya., Perov N. C., Nguen A. T., Mittova V. O., Alekhina Yu. A., Fam V. Sintez, sostav i magnitnye svoistva nanoporoshkov ferrita lantana, dopirovannogo kadmiem [Synthesis, composition and magnetic properties of cadmium-doped lanthanum ferrite nanopowders]. *Neorganicheskie materialy*. 2021;57(4): 388–392. https://doi.org/10.31857/S0002337X21040072 (In Russ.)

187. Nguyen T. A., Berezhnaya M. V., Mittova I. Y., Viryutina E. L., Pham T. L., Nguyen L. T. T., Mittova V. O., Vo M. Q., Do H. T. Synthesis and magnetic characteristics of neodymium ferrite powders with perovskite structure. *Russian Journal of Applied Chemistry*. 2019;92(4): 498–504. https://doi.org/10.1134/S1070427219040050

188. Nguyen T. A., Pham V., Pham T. L., Nguyen L. T. T., Mittova I. Ya., Mittova V. O., Lan N. V., Nguyen B. T. T., Bui V. X., Viryutina E. L. Simple synthesis of $NdFeO_3$ nanoparticles by the co-precipitation method based on a study of thermal behaviors of Fe (III) and Nd (III) hydroxides. *Crystals*. 2020;10(3): 219. https://doi.org/10.3390/cryst10030219

189. Nguyen A. T., Nguyen V. Y., Mittova I. Ya., Mittova V. O., Viryutina E. L., Hoang C. Ch. T., Nguyen Tr. L. T., Bui X.V., Do T. H. Synthesis and magnetic properties of $PrFeO_3$ nanopowders by the co-precipitation method using ethanol. *Nanosystems: Physics, Chemistry, Mathematics*. 2020;11(4): 463–473. https://doi.org/10.17586/2220-8054-2020-11-4-468-473

190. Nguyen A. T., Tran H. L. T., Nguyen Ph. U. T., Mittova I. Ya., Mittova V. O., Viryutina E. L., Nguyen V. H., Bui X. V., Nguyen T. L. Sol-gel synthesis and the investigation of the properties of nanocrystalline holmium orthoferrite. *Nanosystems: Physics, Chemistry, Mathematics*. 2020;11(6): 698–704. https://doi.org/10.17586/2220-8054-2020-11-6-698-704

191. Nguyen A. T., Nguyen T. D., Mittova V. O., Berezhnaya M. V., Mittova I. Ya. Phase composition and magnetic properties of $Ni_{1-X}Co_XFe_2O_4$ nanocrystals with spinel structure, synthesized by co-precipiation. *Nanosystems: Physics, Chemistry, Mathematics*. 2017;8(3): 371–377. https://doi.org/10.17586/2220-8054-2017-8-3-371-377

192. Nguyen T. A., Nguyen L. T. Tr., Bui V. X., Nguyen D. H. T., Lieu H. D., Le L. M. T., Pham V. Optical and magnetic properties of $HoFeO_3$ nanocrystals prepared by a simple co-precipitation method using ethanol. *Journal of Alloys and Compounds*. 2020;834: 155098. https://doi.org/10.1016/j.jallcom.2020.155098

Information about the authors

Irina Ya. Mittova, DSc in Chemistry, Professor at the Department of Materials Science and the Industry of Nanosystems, Voronezh State University, Voronezh, Russian Federation; e-mail: imittova@mail.ru. ORCID iD: https://orcid.org/0000-0001-6919-1683.

Boris V. Sladkopevtsev, PhD in Chemistry, Associate Professor, Department of Materials Science and the Industry of Nanosystems, Voronezh State University, Voronezh, Russian Federation; e-mail: dp-kmins@yandex.ru. ORCID iD: https://orcid.org/0000-0002-0372-1941.

Valentina O. Mittova, PhD in Biology, Associate Professor, Department of Biochemistry, Voronezh State Medical University named after N. N. Burdenko, Voronezh, Russian Federation; e-mail: vmittova@mail.ru. ORCID iD: https://orcid.org/0000-0002-9844-8684.

Received 22 June 2021; Approved after reviewing 15 July 2021; Accepted for publication 15 August 2021; Published online 25 September 2021.

Translated by Valentina Mittova
Edited and proofread by Simon Cox

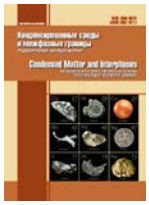

ISSN 1606-867X (Print)
ISSN 2687-0711 (Online)
Condensed Matter and Interphases
Kondensirovannye Sredy i Mezhfaznye Granitsy
https://journals.vsu.ru/kcmf/

Review

Review article
https://doi.org/10.17308/kcmf.2021.23/3525

Interaction of metal sulphides in films deposited from solutions of thiourea coordination compounds. Review

V. N. Semenov✉, **A. V. Naumov**

Voronezh State University,
1 Universitetskaya pl., Voronezh 394018, Russian Federation

Abstract

Metal sulphides are highly important for the technology of semiconductor film materials. The potential of these compounds has not been exhausted yet when it comes to creating optoelectronic devices, solar cells, and luminescent devices based on them. The goal of this work was to determine the nature of interaction of sulphides in polycrystalline layers of CdS–Me_mS_n, where Me are metals of groups I–VII of the periodic table. Cadmium sulphide was chosen as the common component of all studied systems due to the great photoelectric and luminescent properties of this well-studied material.

It was shown that using aerosol spray pyrolysis of the solutions of thiourea complexes, we can obtain solid solutions and chemical compounds of CdS–Me_mS_n at temperatures not exceeding 500 °C. The main electric, optical, and luminescent properties of the layers were described.

It was established that the use of aerosol spray pyrolysis of the solutions of thiourea coordination compounds allows significantly expanding the areas of solubility during the formation of solid sulphide solutions. The specific character of solid-phase interaction and nonequilibrium of the processes occurring during the deposition of layers allow avoiding structural incompatibility of the components expressed in the form of typical factors, such as the non-uniformity of crystal structure, differences in the chemical nature of the components, and discrepancies in sizes of substituting/penetrating atoms.

Under such conditions of deposition of films (the lower threshold of deposition temperatures is determined by the temperature of decomposition of the most thermally stable thiourea coordination compound and does not exceed 250 °C), the solid-phase interactions of most sulphides cannot be achieved. Therefore, the interaction occurs at the moment of thermal destruction of complex compounds due to the emerging valence opportunities of their structural fragments.

Keywords: Metal sulphides, Thiocarbamide coordination compounds, Polycrystalline films, Aerosol spray pyrolysis, Solid-phase interaction

For citation: Semenov V. N., Naumov A. V. Interaction of metal sulphides in films deposited from solutions of thiourea coordination compounds. Review. *Kondensirovannye sredy i mezhfaznye granitsy = Condensed Matter and Interphases*. 2021;23(3): 337–352. https://doi.org/10.17308/kcmf.2021.23/3525

Для цитирования: Семенов В. Н., Наумов А. В. Взаимодействие сульфидов металлов в пленках, осажденных из растворов тиомочевинных координационных соединений. Обзор. *Конденсированные среды и межфазные границы*. 2021;23(3): 337–352. https://doi.org/10.17308/kcmf.2021.23/3525

✉ Viktor N. Semenov, e-mail: deanery@chem.vsu.ru
© Semenov V. N., Naumov A. V., 2021

The content is available under Creative Commons Attribution 4.0 License.

1. Introduction

In 1962, the first Department of Semiconductor Chemistry in the USSR was opened at the Faculty of Chemistry of Voronezh State University, and in 1965 the "Vysshaya shkola" publishing house published Yakov A. Ugai's textbook for chemistry and physics students of higher educational institutions "Introduction to semiconductor chemistry" [1]. In 1965, Yakov Ugai defended his doctoral dissertation in chemistry on the topic "A study in the field of semiconductor phases based on antimony, arsenic, and phosphorus". Apart from $A^{III}B^{V}$ compounds that are by their nature coordinate compounds in a solid state, he also studied such semiconductors as $A^{II}B^{IV}$, $A^{II}B^{VI}$, $A^{I}B^{V}$, and others. For his series of works on chemical semiconductor thermodynamics, in 1981 Y. A. Ugai was granted an honorary title of the USSR National Prize laureate in the field of science, the first such title in the history of VSU.

Yakov Ugai was the founder and long-standing head of the scientific school of chemical study of semiconductors. At first, all studies were conducted on massive crystals, but the needs of modern microelectronics required the miniaturisation of devices, so the interest to thin-film technologies increased. VSU's Department of General and Inorganic Chemistry started working on synthesis and study of the properties of semiconductor films. Among the promising methods of deposition of wide-band semiconductor films was aerosol spray pyrolysis (ASP, originally named the method of "solution spray"). Evgeny M. Averbakh, Viktor N. Semenov, and Oleg B. Yatsenko, employees of the department, began working on the application of this method for the deposition of metal sulphides. Over the past years, we have continued exploring this topic in line with the scientific field developed by Y. A. Ugai in 1960s.

Metal sulphides with promising optical, electrical, and luminescent properties are indeed highly important for the film technology of semiconductor materials. A number of devices were created based on them, such as radiation receivers and converters, thermal resistors, etc. At the same time, the potential of these materials has not been exhausted yet when it comes to creating optoelectronic devices, solar cells, and luminescent devices based on them.

In this regard, there is a promising chemical method of obtaining the films of metal sulphides based on thermal destruction of *thiourea coordination compounds* (TCC). Thermal destruction was conducted by spraying aqueous solutions of coordination compounds on a heated substrate, which is the technological basis of aerosol spray pyrolysis [2]. The conditions for the growth of polycrystalline layers of metal sulphides were created. This method can be used for the deposition of metal sulphides of groups III(*a*)–V(*a*) (Ga, In, Sn, Pb, Bi), transition metals I(*b*)–II(*b*) (Cu, Ag, Cd, Zn), and groups VI(*b*)–VIII(*b*) (Cr, Mn, Fe) of the periodic system (Table. 1).

The method offers great possibilities for the formation of thin-film compositions both on dielectric (quartz, sitall) and transparent conductor (doped SnO_2) substrates. Thus, using only a "spray" technology, we obtained heterostructures $SnO_2/Cd_xZn_{1-x}S/Cu_{2-x}S$ that are able to work as photoelectric converters [3]. Recently, it has been found that using thiourea as a sulphidising reagent without changing the deposition method, some sulphides (In_3S_4, $CuInS_2$) can be obtained not only on glass-shaped but also on single-crystal substrates, including silicon, gallium arsenide, indium phosphide, and other $A^{III}B^{V}$ [4–6]. Such films have a number of specific features, the principal of which is their expressed orientation in relation to the substrate.

From the point of view of chemistry of sulphides and applied tasks of inorganic material science, it is important that using ASP, we can obtain layers of sulphides of different metals with random bulk composition. Also, depending on the nature of sulphides and conditions of deposition, the interaction of the components in the layers varies from the formation of a simple heterophasic mixture to limited solid solutions and chemical compounds of sulphides. It is notable that the release of such compounds and solid solutions on a substrate occurs at relatively low temperatures. Aerosol of TCCs dissolved in water decomposes in the range of temperatures 250–500 °C, however, in order to dope, for example, cadmium sulphide with activators (Cu, Mn, etc.), it is sufficient to introduce the corresponding addition of Cu^{2+} and Mn^{2+} salts to the TCC solution [$Cd(thio)_2Cl_2$]. The study of solid-phase interactions of sulphides in films deposited using ASP has become a separate

Table 1. Physical properties of metal sulphides deposited from solutions of thiourea coordination compounds using ASP

Sulphide		E_g, eV	E_{pc}, eV	E_{pl}, eV	σ, cm/m	ρ, g/cm³
I	$Cu_{1.76}S$	1.8	–	–	$8\cdot10^{4}$	–
	Ag_2S	1.2	–	–	$6\cdot10^{-1}$	–
II	**CdS**	**2.4**	**2.3–2.6 ***	**1.48 1.58 1.70**	**$(0.2–11.2)\times10^{-7}$ ***	**4.82**
	ZnS	3.60	3.5	2.65	$8\cdot10^{-7}$	4.25
III	Ga_2S_3	2.85	3.11	1.80	$3\cdot10^{-8}$	3.45
	In_2S_3	2.3	2.3	1.66 2.3 2.8	$1\cdot10^{-3}$	4.60
IV	SnS	1.2	–	–	$1\cdot10^{-2}$	–
	SnS_2	2.2	2.3	–	$1\cdot10^{-5}$	4.80
	PbS	0.4	0.8 1.1	–	$1\cdot10^{-1}$	7.45
V	Bi_2S_3	1.4	1.46	–	$1\cdot10^{-3}$	7.10
VI	Cr_2S_3	1.1	–	–	$4\cdot10^{-2}$	–
VII	MnS	2.5	–	–	$5\cdot10^{-6}$	–
VIII	FeS_2	1.3	–	–	$6\cdot10^{-3}$	–

Designations: E_g is band gap; E_{pc} is photoconductivity band; E_{pl} is photoluminescence band; σ is specific electric conductivity; ρ is density.

* Depending on the initial TCC

task. It includes: *a)* determining the mechanisms of deposition of "mixed" layers and formation of phases with different chemical nature in them and *b)* the dependences of properties of "mixed" layers on the composition and nature of solid-phase interactions.

In this work we discuss the properties of films of sulphide systems with the participation of cadmium sulphide. The goal of the work was to determine the nature of interaction of sulphides in the CdS–Me_mS_n layers. Cadmium sulphide was chosen as the common component of all the studied systems due to its great photoelectric and luminescent properties of this well-studied material.

2. Formation of metal sulphides from thiourea coordination compounds

The idea of aerosol spray pyrolysis is simple and involves the following. We chose the cation-forming salts that are soluble in some solvent (usually it is water, more rarely ethanol or mixtures of ethanol and water) and reagents that are required for the delivery of the anion former. The obtained solution was sprayed on a heated substrate where after the evaporation of the solvent (or with the participation of the solvent) the components decomposed, leaving a layer of the most thermally stable substance forming a film on the substrate. Thiourea (thiocarbamide, $SC(NH_2)_2$) is a promising sulphidising agent used to obtain the films of metal sulphides. This is due to a number of reasons, among which are low temperatures of the start of aerosol decomposition (from 200 to 300 °C) and high coordination affinity of thiourea to cations of various metals [7]. It was reliably established that the deposition of sulphide films in the studied method occurred through the stage of formation of a coordination compound of thiocarbamide with a metal salt.

TCCs of metals are various in their composition and structure, thermal stability, and mechanisms of thermal destruction. It should be noted that we only refer to true coordination compounds (CC) with the participation of thiourea which is able to produce ionic complexes and inclusion compounds with a number of *s*- and *p*-elements [7]. Apparently, these compounds did not result in the formation of the corresponding sulphides due to the ion-dipole nature of chemical bonds

as compared to true TCCs. In the latter ones, thiourea is always coordinated through an atom of sulphur of thiocarbamide group (S=C) and can act both as terminal and bridge ligands (in such compounds as $[Cu(thio)_2Cl]$, $[Bi(thio)_3Cl_3]$, etc.) [7, 8]. The existence of covalent bonds of Me-S determines the mechanism of sulphide formation by direct introduction of sulphur atoms into the composition of the immediate environment of the metal atom. This explains the great difference of the method of obtaining sulphides from TCCs from hydrolytic methods.

In the complexes with coordination number of 4, such as cadmium, copper, and zinc complexes, the central atom was in the state of sp^3- hybridisation, so the configuration of its immediate environment can be considered to be a distorted tetrahedral one. The configuration of the immediate environment meant the position of atoms that were directly related to the complexing agents by covalent bonds. It should be noted that molecules or ions of thiocarbamide coordination compounds have low symmetry. For instance, particle $[Cd(thio)_2Cl_2]$ had a symmetry of either point group $\boldsymbol{C}_2$ (in this case it was chiral), or point group $\boldsymbol{C}_S$ [8, 10–11]. At the same time, the symmetry of the immediate environment was increased and could be described by point groups $\boldsymbol{C}_{2v}$ – in such structures as $[Cd(thio)_2Hal_2]$ (here Hal – is halogen); $\boldsymbol{C}_{3v}$ – in such structures as $[Cu(thio)_3Cl]$; $\boldsymbol{T}_d$ – in such structures as $[Cd(thio)_4]^{2+}$. Analysis of the composition and structure of the coordination compounds that acted as the starting material for the formation of the sulphide phase, allowed drawing a fundamental conclusion that fragments of the sulphide structure started forming in the inner sphere. In case of S→Me coordination with the use of p_y AO S, the order of the C–S bond may decrease (Scheme (1), Fragment I). It is well-known [7] that S-coordination of thiourea causes a shift in the frequencies of valence bonds ν_{CS} into the long-wave region, while frequencies ν_{CN} and δ_{NCN}, by contrast, shift to the short-wave region of the IR spectrum. Thus, the decrease of the order and weakening of the C–S bond with simultaneous reinforcement of the C–N bonds in the TCCs created conditions for the elimination of the organic residue in case of thermal excitation (Scheme (1), Fragment II).

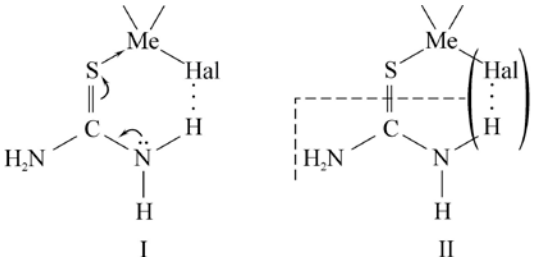

I II (1)

The immediate environment of the complexing agent influenced the formation of various point defects in the metal sulphide lattice. As we know, there is always a variability of complex forms in the solutions of metal salt, and their distribution depends on the composition (gross composition) of the solution. Previous experimental and theoretical studies [12–13] provide a better understanding of this distribution in case of different cadmium salts. Depending on the nature of the salt and composition of the solution, different coordination forms may dominate, and in addition to molecules of thiocarbamide the inner sphere may include anions of Cl^-, Br^-, I^-, CH_3COO^-, and, under certain circumstances, SO_4^{2-}. Therefore, the immediate environment of a cadmium atom may include atoms of sulphur, halogens, and oxygen, and in case of thermal destruction some of the Cd–Hal or Cd–O bonds remain, and defects Hal_S^+ and O_S are formed in the sulphide lattice [14–15]. The use of coordination compounds with an inner coordination sphere saturated with thiocarbamide, such as $[Cd(thio)_4]F_2$, allowed obtaining sulphides with the composition that is very close to stoichiometric, and the introduction of additives of selenium-$(SeC(NH_2)_2)$ and tellurium carbamide $(TeC(NH_2)_2)$ allowed doping metal sulphides with selenides and tellurides.

The influence of the composition and structure of starting coordination compounds on the crystal structure of deposited sulphides is of great interest. Thus, depending on the covalent radius of halide ligands in the $[Cd(thio)_2Cl_2]$, $[Cd(thio)_2Br_2]$, $[Cd(thio)_2I_2]$ series, the structure of the deposited cadmium sulphide changed from wurtzite to sphalerite. In case of a complex compound $[Cd(thio)_2(ac)_2]$ (ac is ion acetate), the wurtzite modification of cadmium sulphide was deposited together with the sphalerite one, while in case of the compounds with the inner coordination sphere saturated with thiocarbamide $[Cd(thio)_4](NO_3)_2$ and $[Cd(thio)_4]SO_4$, a sulphide of mostly sphalerite

modification was formed [11, 14]. Thus, point symmetry and the composition of the inner sphere of thiocarbamide complexes influenced the spatial symmetry and defect structure of metal sulphides, which allowed purposefully influencing a number of properties of films.

Another important aspect of the influence of the processes of formation of complexes on the properties of sulphide films is a possibility to control the state of oxidation of the cation-forming metal with a variable oxidation state. In this context, a typical example is copper sulphide (I) obtained from thiocarbamide coordination compounds of copper.

The formation of complexes of copper chloride (II) with thiocarbamide is associated with redox processes, as a result of which copper (II) is reduced to copper (I) [7, 16]. The process is preceded by the coordination of a thiocarbamide molecule, and such mutual influence of ligands leads to a homolytic break in the Cu–Cl bond in the inner sphere of the complex [17–18]:

$$(NH_2)_2C{=}S{-}Cu{\leftarrow}Cl \quad \rightarrow \quad (NH_2)_2C{=}S{-}Cu^{\cdot} + Cl^{\cdot}$$

(the scheme shows a part of the coordination environment of the copper ion). In [17] it is assumed that the separated radicals of $Cl^{\cdot}$ oxidise water, and the overall scheme of the process is as follows:

$$4CuCl_2 + 4SC(NH_2)_2 + 2H_2O \rightarrow$$
$$\rightarrow 4[Cu(SC(NH_2)_2)]Cl + 4HCl + O_2.$$

The displacement of chlorine anions into the inner sphere was achieved by the increase in the ratio of concentrations of C_{thio}/C_{CuCl_2}, which allowed increasing to some extent the portion of copper (II) in the solution. The processes similar to those described above also occurred in case of ferrous chloride (III), where, as we proved experimentally, the oxidation state of Fe^{2+} was stabilised in the presence of thiocarbamide. Thus, by varying the concentration of metal salt and thiocarbamide in the solution, we can regulate the oxidation state of the cation-forming metal.

It should be noted that if doping sulphides with anion formers, substitutes in the anion sublattice were achieved by the introduction of the complexes of corresponding ligands to the inner sphere, then doping with cation formers can be achieved by the introduction of the additives of salts of corresponding metals to the initial solution. As a rule, in this case, a substitutional solid solution is formed at first, and then an interstitial solid solution is formed [19]. Thus, we obtained the luminescent layers of CdS and ZnS, activated by Cu^{2+} and Mn^{2+} ions, as well as Cl^- and Br^- [19–21].

Therefore, unique conditions for predicting the properties of sulphides and controlling them were created during the synthesis of metal sulphides from thiocarbamide coordination compounds.

The processes occurring when the aerosol solution reaches the heated substrate are complex and are characterised by significant nonequilibrium. The behaviour of the solvent in a dispersed, quickly heated medium of aerosol has not been thoroughly studied. According to our studies, a series of approximations can be used that suggest either instant evaporation of the solvent similar to quenching, or gradual evaporation that leads to the concentration of the solution, the change in the distribution of coordination forms, and, finally, to the release of crystals of the complexes that are subject to thermal destruction.

Thermal destruction of thiocarbamide complexes is thought to occur due to the thermal excitation of the C–S bond in the coordinated molecule of thiocarbamide [9]. At the same time, there is an opinion that the excitation of this bond was caused by negative charge fluctuation that was localised on the complex upon the destruction of hydrogen bonds in the crystal of coordination compound when it was melted [22]. However, despite the differences in the opinions on the nature of elementary act of thermal destruction, we can formulate the principal concepts characterising this process.

As it was noted before, in the IR spectra of all thiocarbamide complexes we observed a shift in the stretching vibration bonds of the C–S and C–N bonds to the long-wave and short-wave regions respectively, as compared to the position of the bands of the uncoordinated molecule of thiocarbamide. Such changes in the spectrum were due to the redistribution of the electron density in the $SC(NH_2)_2$ molecule that was related to the metal ion through the sulphur atom. The order of the C–S bond in a "free" molecule of thiocarbamide was 1.5, but in case of coordination to the metal ion it decreased to around 1. The order of the

C–N bond, on the contrary, increased due to the involvement of non-separated electron pairs of nitrogen atoms in π-conjugation. Analysis of the IR spectroscopic data allowed stating that as a result of thermal influence on a thiocarbamide complex, such redistribution of the electron density became even deeper, which led to the destruction of the complex due to the disassociation of the C–S bond (Scheme (1)). This scheme showed only the main features of the process and did not provide a full description of pyrolysis, complicated by a series of transformations of the organic residue [23].

The pyrolitic break-down of the C–S bonds may be preceded by the stages of isomerisation of complexes and transformations both occurring in the inner sphere and related to the appearance of ligands in the inner sphere. The transformations in the inner sphere may be associated with the changes in the denticity of ligands (for example, a decrease in the denticity of ligand SO_4^{2-} in the $[Cd(thio)_2$*bi*-$SO_4]$ complex), while the appearance of ligands in the inner sphere can be considered as the formation of intermediates with the lowered coordination number. For instance, during the thermal destruction of the $[Cd(thio)_2I_2]$ compound we discovered an intermediate compound $[Cd(thio)I_2]$ formed as a result of elimination and appearance of one molecule of thiocarbamide in the inner sphere [24]:

$$[Cd(thio)_2I_2] \rightarrow [Cd(thio)I_2] + thio.$$

This can be explained by the mutual influence of the ligands, in particular, by steric difficulties caused by the significant covalent radius of iodine atoms located in the neighbouring vertices of the distorted tetrahedron.

The conducted studies allowed determining the following main features of the synthesis of metal sulphides using TCCs (quoted in [2]).

1. The influence of the TCC structure on the structural defect of the sulphide, including both its impurity and internal disorder caused by the existence of a genetic bond between the immediate environment of the complexing agent in the TCC and the first coordination sphere of the cation former in the sulphide lattice.

2. The dependence of the crystal-chemical structure of sulphide phase allowing polymorphism or forming several stoichiometrically similar independent phases on the symmetry of TCC.

3. The possibility to control the oxidation state of metal in a solution and, therefore, the content of the corresponding phase in a film based on the change in the structure of thiourea coordination compounds by replacement or intentional choice of acidoligands.

3. CdS – $Cu_{2-x}S$ and CdS – Ag_2S systems

The CdS–$Cu_{2-x}S$ system is of interest due to the fact that cadmium sulphide is an electronic semiconductor, while copper sulphides are hole semiconductors, and electrical conductivity of polycrystalline CdS and $Cu_{2-x}S$ may differ by ~ 10^6 times. Such conditions result in some interesting electrical effects observed in thin polycrystalline layers that contain semiconductor phases with different electrophysical properties.

Under the conditions allowing joint deposition of cadmium and copper sulphides as macrohomogeneous layers (T ≈ 350 °C), the phase of the $Cu_{1.76}S$ digenite is deposited that contains four-coordinated atoms of copper in tetrahedral voids of the thickest packings of S atoms [25].

According to X-ray phase analysis, the interaction in mixed layers containing CdS and $Cu_{1.76}S$ is reduced to the limited solubility which does not exceed 5 mol% both on the part of cadmium sulphide or copper sulphide. However, as the results of electrophysical measurements show, such an interaction is of more complex nature. The non-monotonic dependence of electrical conductivity of films on the composition with a minimum in the region of 5 mol% $Cu_{1.76}S$ (fig. 1) indicated the presence of limited solubility on the part of CdS, although the extrema position should not be directly linked to the position of the border of the region of solid solutions. According to photoluminescent data [19], substitutional solid solutions CdS(Cu) were formed with the concentration of copper up to 0.1 at%, and the appearance of acceptor centres Cu_{Cd}^- should result in the compensation of the *n*-conductivity of CdS. When doping cadmium sulphide with copper additives greater than 0.1 at%, Cu atoms started penetrating into interstitial sites, thus forming Cu_i^+ donor centres. Being relatively small donors [27], these centres were ionised at normal temperatures:

$$Cu_i \rightarrow Cu_i^+ + e^-,$$

creating a reverse effect. Based on the suggestion about the change of mechanism of solubility of small

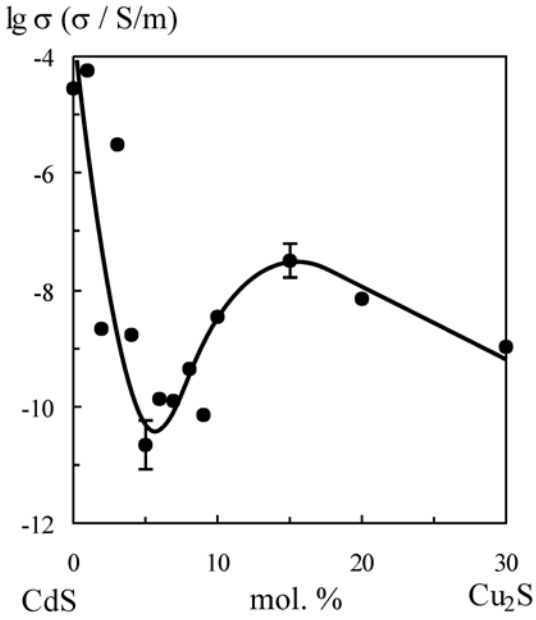

Fig. 1. Dependence of specific electric conductivity of CdS–$Cu_{1.76}S$ films on the composition on the part of CdS

amounts of copper in CdS, the minimum of electrical conductivity near bulk composition of 5 mol% $Cu_{1.76}S$ can be explained by the release of substitutional solid solutions and further penetration when crossing the concentration bulk threshold of 5 mol%. With such concentration the second phase (*p*-$Cu_{1.76}S$) was almost compensated, and film properties were determined by the main phase of *n*-CdS.

The described mechanism of behaviour of impurities is apparently typical for other sulphides that are poorly soluble in cadmium sulphide and do not form chemical bonds with it. Based on the data of X-ray phase analysis, in the films of the CdS–Ag_2S system we found solid solutions with the region of existence < 1 mol% on the part of CdS and ~ 5 mol% on the part of Ag_2S. At the same time, the minima of electrical conductivity accompanying the formation of solid solutions were noticeably shifted in relation to those borders that were determined by X-ray phase analysis. Extreme behaviour of electrical conductivity near 50-60 mol% Ag2S was specific for heterophase films and could be related to an increase in the dissipation of carriers at grain boundaries. In such cases, the extrema on "composition – property" diagrams should not be associated with the chemical interaction of the components in the thin layer. From the point of view of current carrier behaviour, a polycrystalline film is a system of randomly placed potential pits and barriers, which is markedly expressed in case of mixed films. Multiple experimental data showed that the effects related to the appearance of such nonperiodic potential became noticeable near equimolar (bulk) compositions when the microstructure of a film was most imperfect.

4. CdS–ZnS system

This system is one of the most important on the practical level, thus it attracts the close attention of researchers [28–30]. When studying the specific features of the interaction in this system, it should be taken into account that in case of using TCCs [$Zn(thio)_2Cl_2$] and [$Cd(thio)_2Cl_2$], zinc sulphide is deposited in a sphalerite modification, while cadmium sulphide is deposited in a modification with the wurtzite lattice [2, 11]. Due to this circumstance, the continuous solubility between hexagonal CdS and cubic ZnS was eliminated. Indeed, the analysis of concentration dependences of properties (Fig. 2) showed typical features of the change of nature of dependence with the compositions of about 18 and 80 mol% ZnS. Therefore, three "composition – property" sections were found on the curves, which indicated the formation of limited solid solutions based on hexagonal CdS on the one hand and cubic ZnS on the other hand. The limited solubility was confirmed by the data of X-ray phase analysis (Fig. 3a), according to which the structure changed from wurtzite (CdS) to sphalerite (ZnS) when the total amount of zinc sulphide in a film increased.

At the same time, photoluminescence spectra of CdS–ZnS films showed a continuous shift of the band within the range of 1.4–2.4 eV accompanied by a non-monotonic change in its intensity. Maximum radiation intensity was observed for the equimolar composition 50 mol%. Apart from the "main" band shifting according to Fig. 2a, there were also radiation bands 520 and 830 nm. They were related to the presence of oxygen in sulphides ZnS and CdS and were not shifted when the composition was changed. The introduction of oxygen during the process of deposition of layers was related not only to the common influence of an oxidising atmosphere where the layer grew, but also to the need to compensate for structural distortions [31]. This, in its turn, led to the inclusion of a greater amount of oxygen for the films approaching an equimolar composition. It is notable that the

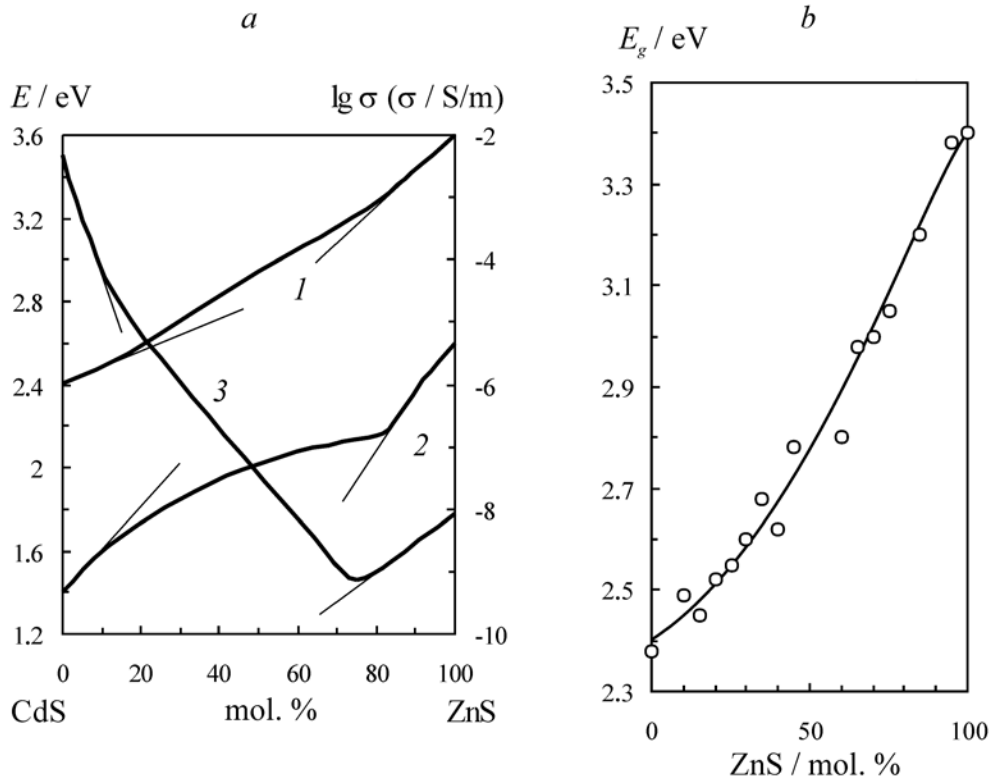

Fig. 2. Concentration dependences of the optical band gap (*1*), spectral position of the luminescence maximum (*2*), and specific electrical conductivity (*3*) of the CdS–ZnS films deposited from chloride (*a*) and acetate (*b*) coordination compounds

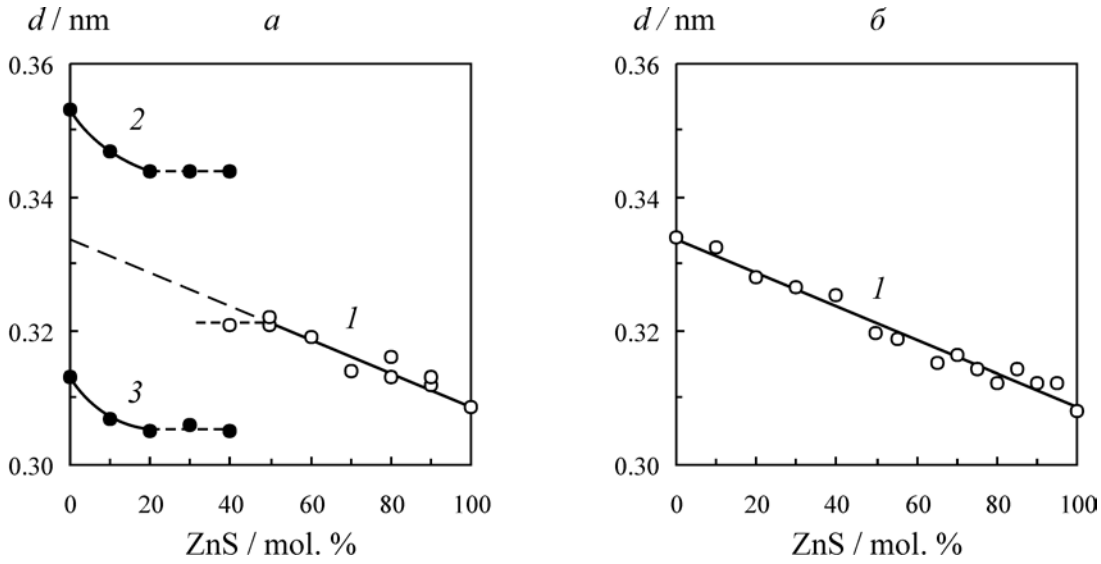

Fig. 3. Concentration dependences of the interplanar distances for the solid solutions of the CdS–ZnS system deposited from chloride (*a*) and acetate (*b*) coordination compounds *1*) reflection 111 for a cubic solid solution; *2)* reflection 100 for a hexagonal solid solution; *3)* reflection 101 for a hexagonal solid solution [11]

layers obtained at high temperatures (500 °C) and containing more than 50–60 % ZnS turned out to be X-ray amorphous. We can assume that the inclusions of the ZnO phase under the conditions of oxygenation of a film contributed to the amorphisation. The spectral position of the band of intrinsic conductivity changed only according to the change in the band gap.

It was possible to deposit a series of CdS–ZnS solid solutions in the form of films when using coordination compounds, the thermal destruction of which resulted in the release of a cubic sphalerite modification of cadmium sulphide. An acetate complex $[Cd(thio)_2(ac)_2]$ can be used for that purpose [11]. As Fig. 2b shows, the nature of the dependence of the band gap on the composition changed: the dependence became smooth, without typical sharp curves which would be indicative of reaching the boundaries of the homogeneity region and the decomposition of a solid solution. Interplanar distance d_{111} for these films changed continuously and linearly together with the composition according to Vegard's law (Fig. 3b). An example of the CdS–ZnS system is important as it showed the influence of coordination precursors not only on semiconductor properties but also on polymorphic modifications of sulphides that can exist in several crystalline forms. This way various phase states and different solid-phase solubility in the deposited layers were realised.

5. CdS – Ga_2S_3 system

The solubility of cadmium sulphide in Ga_2S_3, discovered from the data on concentration dependences of the optical band gap, electric conductivity σ, and pycnometric density ρ was evaluated as ~ 5 mol% CdS. The most reliable data on the range of the area of existence of solid solutions on the part of CdS were obtained from the concentration dependence of density and interplanar distance *d* (Fig. 4). The nature of changes in these parameters near pure CdS indicates the limited solubility within 5 mol% Ga_2S_3. The existence of the $CdGa_2S_4$ compound described in previous studies in the films of the CdS–Ga_2S_3 system cannot be conclusively established despite the satisfactory coincidence of some characteristics of the films of equimolar composition with the characteristics of this compound.

6. CdS – In_2S_3 system

A chemical compound with a spinel structure, $CdIn_2S_4$, was found in this system [32]. The extrema appearing at 50 mol% In_2S_3 on concentration dependences of the band gap and pycnometric density of CdS–In_2S_3 films also confirmed the existence of this compound (Fig. 5). The main

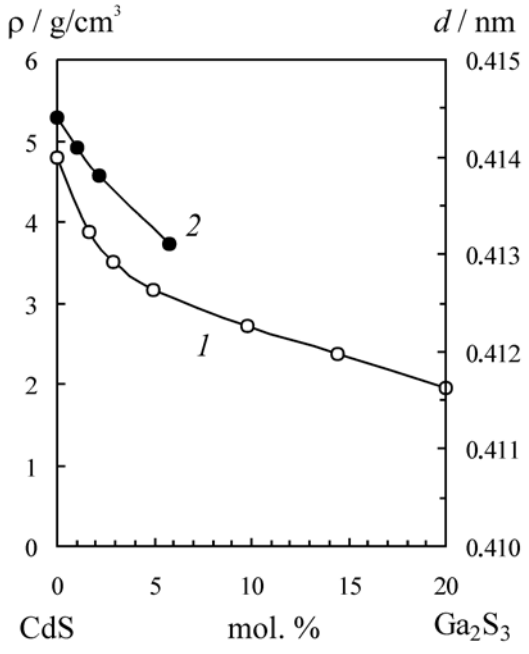

Fig. 4. Density (*1*) and lattice parameter (*2*) of the CdS–Ga_2S_3 films

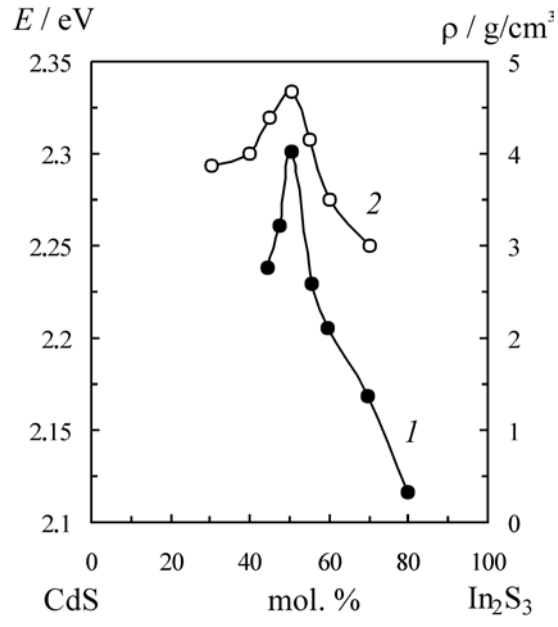

Fig. 5. Concentration dependences of the band gap (*1*) and density (*2*) of films of the CdS–In_2S_3 system

characteristics of the $CdIn_2S_4$ compound are presented in Table 2.

The range of existence of solid solutions with indium sulphide according to the data of X-ray phase analysis can reach 45 mol% CdS, while with cadmium sulphide it did not exceed 2 mol% In_2S_3. The behaviour of electrical conductivity with a sharp minimum near 2.5 mol% In_2S_3 (Fig. 6) was typical, which definitely indicated the formation of limited solid solutions.

The spectral position of luminescence bands did not depend on the composition of CdS–In_2S_3 films (Fig. 7); the centres of radiative recombinations typical for CdS, apparently, did not change significantly when the bulk composition changed. Only a redistribution of intensities occurred, which can be associated both with the change in the amount of centres and the redistribution of recombination flows involving these centres [33].

7. CdS–SnS and CdS–SnS_2 systems

Redox processes do not occur in the solutions of chlorides of tin (II) and (IV) and thiourea, unlike salts of copper (II) and iron (III). The preservation of the oxidation state of tin allowed obtaining the layers of SnS and SnS_2 sulphides directly using the corresponding chlorides for the synthesis of $[Sn(thio)_2Cl_2]$ and $[Sn(thio)_4]Cl_4$ complexes in acidic (for the suppression of hydrolysis) aqueous solutions. It should be noted that other metals (Ga^{3+}, In^{3+}, Cr^{3+}) require the same method of oxidation to suppress hydrolysis. However, a strongly acidic environment had a negative effect

Table 2. Some properties of the $CdMe_2S_4$ compounds deposited in thin layers from the solutions of thiourea coordination compounds

Sulphide	E_g, eV	E_{pc}, eV	E_{pl}, eV	σ, cm/m	ρ, g/cm³	Identification
$CdIn_2S_4$	2.3	2.3	1.53 1.70	$3\cdot10^{-2}$	4.7	XRD
$CdBi_2S_4$	1.4	2.1–1.5	–	$3.2\cdot10^{-1}$	7.0	XRD
$CdCr_2S_4$	2.1	–	–	$3.6\cdot10^{-3}$	4.1	XRD

Designations: E_g is the band gap; E_{pc} is the photoconductivity band; E_{pl} is the photoluminescence band; σ is the specific electric conductivity; ρ is the density.

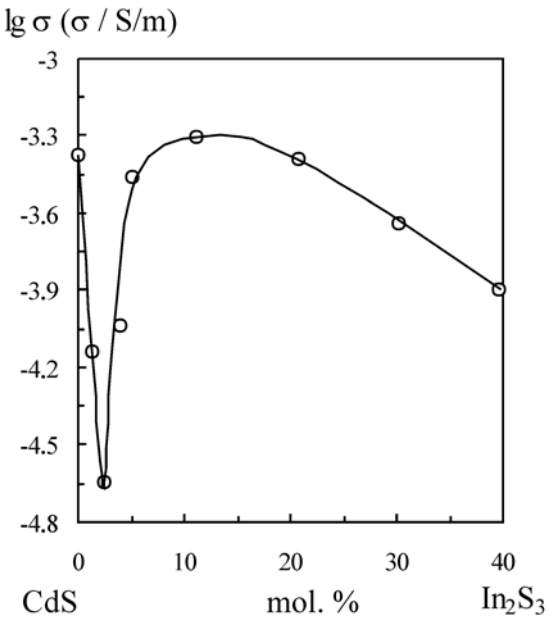

Fig. 6. Dependence of specific electric conductivity of CdS–In_2S_3 films on the composition on the part of CdS

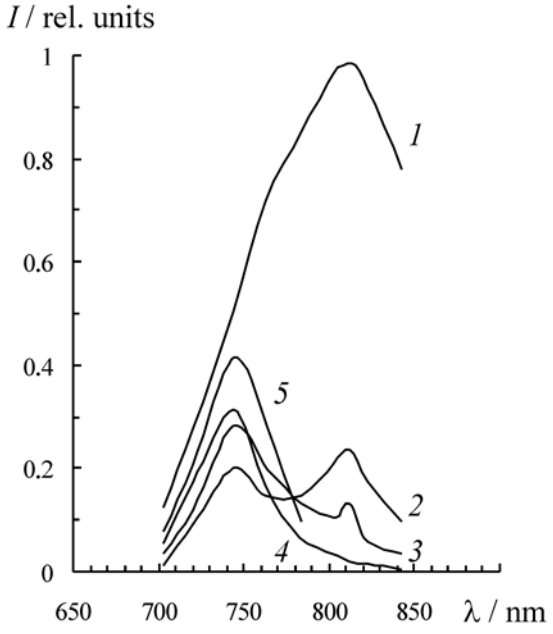

Fig. 7. Photoluminescence spectra of films of the CdS–In_2S_3 system: *1* – 0; *2* – 10; *3* – 50; *4* – 90; *5* – 100 mol% In_2S_3

on the formation of coordination compounds due to the S-protonation of the $SC(NH_2)_2$ molecule competing with the formation of complexes. Thus, in order to obtain "cadmium sulphide – tin (II), (IV) sulphides" films, the pH of the solutions was gradually increased in accordance with the growth of the content of tin salts.

The dependence of the band gap on the composition for the CdS–SnS films showed sudden changes near the compositions of 5 and 95 mol% SnS. Specific electric conductivity had the extrema at the same points. Such behaviour of properties may indicate the formation of limited solid solutions. Indeed, XRD showed the existence of solid solutions near CdS and SnS with homogeneity regions no less than 5 mol%. Photoconductive films can be obtained up to the composition of 70 mol% of tin sulphide. The maximum of photosensitivity significantly shifted to the long-wave region from the value of 515 nm typical for intrinsic photoconductivity of pure CdS (E_g = 2.4 eV).

The films of the CdS–SnS_2 system are of interest as they contain wide-band semiconductors with similar band gap values ($E_{g(SnS2)}$ = 2.2 eV) that are photosensitive in the visible region of the spectrum. Despite the heterophasic nature of the mixed films, it was possible to obtain the samples with a continuously shifting absorption edge due to the superposition of the spectra of individual phases (Fig. 8). The sharp dependence of the edge position on the composition near pure components indicated their solubility. This was also confirmed by the structure of the absorption spectra that looked like $h\nu\alpha \sim (h\nu - E_g)^{1/2}$ for the compositions in the region of 0–10 mol% SnS_2 and $\alpha \sim (h\nu - E_g)^{3/2}$ in the region of 95–100 mol% SnS_2. The first one was characterised by cadmium sulphide (direct permitted transition), the second one was characterised by tin sulphide (indirect permitted transition $\Gamma \rightarrow L$).

The concentration dependence of the photosensitivity maximum point E_{pc} correlated with the dependence of the band gap in the regions of solubility of sulphides (Fig. 8). The additions of tin (IV), similar to other heterovalent impurities (Bi), resulted in a short-wave shift of the photosensitivity band of cadmium sulphide. The change in E_{pc} in the region of the equimolar composition may be indicative of a wide homogeneity region of the intermediate phase of

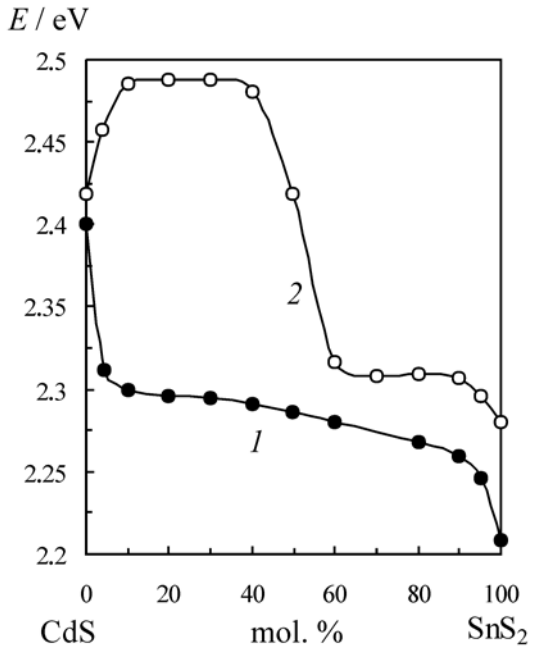

Fig. 8. Dependences of the observed optical band gap (*1*) and spectral position of the photosensitivity maximum (*2*) of CdS–SnS_2 films on the composition

the berthollide type, although X-ray phase analysis did not show any certain presence of chemical compounds in the CdS–SnS_2 films. This issue requires further investigation.

8. CdS–Bi_2S_3 system

The analysis of the data of X-ray diffraction allowed establishing the existence of a $CdBi_2S_4$ compound [34] in the films of the CdS–Bi_2S_3 system. The properties of the compound are presented in Table 2. It is assumed that cadmium sulphide dissolves in bismuth sulphide through the penetration of cadmium atoms into the interstitial space of the Bi_2S_3 structure. At the same time, on the part of cadmium sulphide, the most probable mechanism is the replacement of cadmium nodes with the atoms of bismuth. The areas of existence of solid solutions according to the results of X-ray phase analysis and indirect methods were determined by the values of 1 mol% Bi_2S_3 on the part of CdS and 5 mol% CdS on the part of Bi_2S_3.

The formation of the only compound in the CdS–Bi_2S_3 system was confirmed by the existence of maxima on concentration dependences of the properties at coordinates corresponding to the $CdBi_2S_4$ composition (Fig. 9). In this case, the extreme behaviour of electric conductivity is

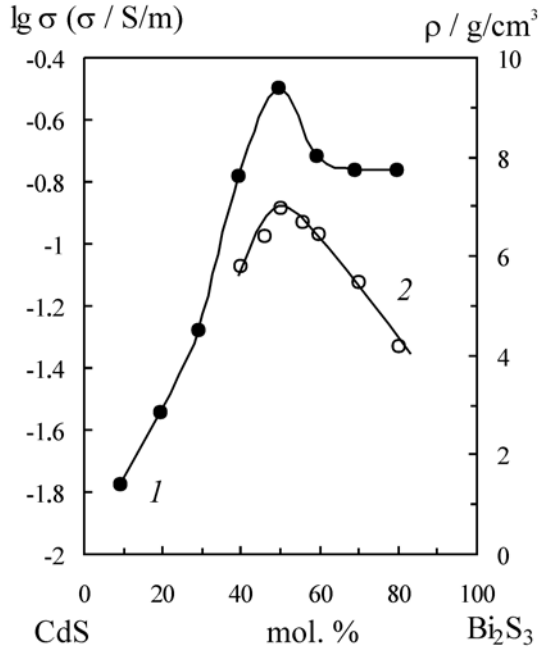

Fig. 9. Concentration dependences of the specific electric conductivity (*1*) and density (*2*) of films of the CdS–Bi_2S system

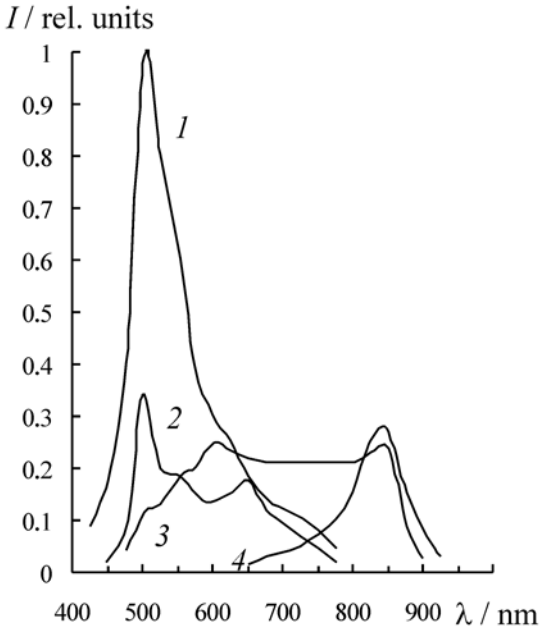

Fig. 10. Photoconductivity spectra of films of the CdS–Bi_2S_3 system: *1* – 0; *2* – 40; *3* – 50; *4* – 100 mol% Bi_2S_3

informative when it comes to the identification of a chemical compound, as it is "duplicated" by the specific features of other properties and the data of X-ray phase analysis.

The monotonic dependence of the optical band gap can be associated with the fact that the position of the edge of the fundamental absorption was determined by the most narrow-bandgap semiconductor, especially if there was a great difference between the band gaps. It can be said that the most narrow-bandgap material "masked" the optical properties of the film on the whole. Remarkably, it did not occur, for instance, in case of CdS–In_2S_3 films as both sulphides composing the film had very close values of bandgap.

The photosensitivity of the CdS–Bi_2S_3 layers with equimolar composition was considerably different from the photosensitivity of films of other alloys. In this case, the spectral distribution of photosensitivity was characterised by an extended gap (Fig. 10) that, apparently, had a complex structure and consisted of several unresolved bands belonging to the $CdBi_2S_4$ compound.

9. CdS–Cr_2S_3 system

Solid-phase interactions in the thin films of the CdS–Cr_2S_3 system are similar to the studied interactions in CdS–Bi_2S_3 films [35]. This primarily applies to the existence of a compound with the $CdCr_2S_4$ composition (Table. 2). We should also take into account similar behaviour of the dependences of film properties on the composition that include experimental points for the composition corresponding to the compound (Fig. 11). A non-specific concentration dependence of the optical band gap can be explained by the fact that the narrow-bandgap chromium sulphide ensured the main absorption by a heterophasic film.

It appeared that the introduction of chromium sulphide created the centres of non-radiative recombination that were rather effective and significantly reduced the lifetime of nonequilibrium carriers. Indeed, when the content of Cr_2S_3 increased, we observed a very sudden drop in the intensity of the near IR luminescence of CdS, on the one hand, and significant reduction of a photoresponse, on the other hand. The influence of oxygen that was included in the structure of the film and eliminates the distortion of the crystal lattices had an effect on the shift of the photosensitivity maximum to the short-wave region. This effect was evidently related to the increase of ionicity of the bond during the interaction of solid components of a film with oxygen. Nevertheless, in addition to

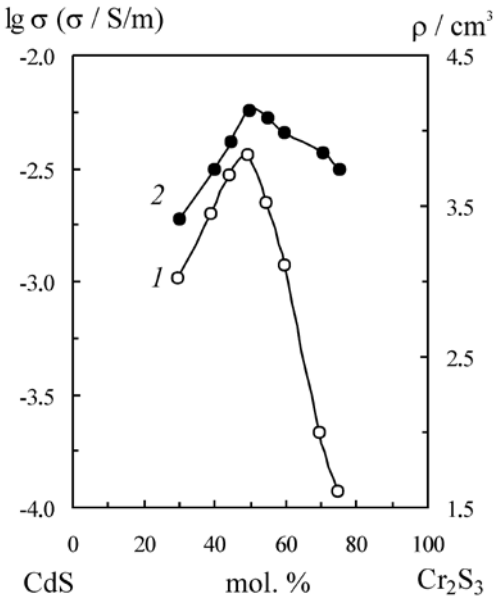

Fig. 11. Concentration dependences of the specific electric conductivity (*1*) and density (*2*) of films of the $CdS–Cr_2$ system

the described reduction of intensity, we can also note a shift of the luminescence band in near IR region that indicates the solubility of chromium sulphide in cadmium sulphide.

10. $CdS–FeS_2$ system

As it was noted before, partial reduction of Fe^{3+} to the oxidation state of Fe^{2+} occurred in solutions of iron (III) salts in the presence of thiourea. This process led to the deposition of iron sulphides FeS and FeS_2 depending on the composition of the initial solution and the temperature of the substrate. The conditions were found (the temperature of the substrate 300 °C, 4x and more excess of thiourea in relation to the ferrous salt ($FeCl_3$)) for the release of a phase of pyrite FeS_2 that is rather perfect in structure and its optical and electric properties.

There was no significant solubility in the $CdS–FeS_2$ system neither on the part of CdS or on the part of FeS_2. The luminescence intensity typical for cadmium sulphide decreased sharply as soon as small amounts of iron were added. Unlike the additions of Cr^{3+}, there was no shift in the bands in the luminescence spectra.

The concentration dependence of specific electric conductivity of films with an expressed maximum at the ratio of the components $CdS:FeS_2$ = 1:2 apparently cannot clearly indicate the presence of the compound due to the reasons mentioned above ($CdS–Ag_2S$ system). The results of the X-ray phase analysis allowed stating with greater certainty that no compounds were formed in the $CdS–FeS_2$ system. Therefore, the $CdS–FeS_2$ system is an example of almost total lack of interaction between the components.

11. Conclusion

The possibility to obtain solid solutions and chemical compounds of sulphides in the process of deposition considerably enriches the ASP method. The studied systems showed almost all types of interactions, and the formation of compounds with cadmium sulphide was typical for sulphides of Me_2S_3 metals of groups III, V, and VI. The formation of solid solutions with CdS was established almost in all systems, although mutual solubility was low for sulphides of metals of groups I (Ag) and VIII (Fe). The greatest range of the area solid solutions was observed in the $CdS–In_2S_3$ system where the solubility of cadmium sulphide in In_2S_3 reached the value of 45 mol%.

Therefore, it was possible to vary the properties of films using specific features of solid solution interactions of sulphides. Photoluminescence of the layers based on CdS allowed observing the ways of controlling a certain property (Table 3). There are possibilities for the activation of luminescence and shift of the bands as well as for the change of intensities of the bands without changing their spectral position.

When interpreting the mechanism of formation of solid solutions and compounds of sulphides, it should be taken into account that multicore thiourea complexes with dissimilar cores were not found in the solutions with various complexing agents. This indicates an independent existence of complexes in the solution, although we cannot make assumptions about their independent thermal decomposition within the use of ASP method. The conditions of the deposition of films did not involve a direct solid-phase interaction of the released sulphides with the formation of solid solutions and chemical compounds. The lowest threshold of deposition temperatures was determined by the temperature of decomposition of the most thermally stable TCC and did not exceed 250 °C. Diffusion coefficients in solids

Table 3. The nature of the photoluminescence spectra of films of the CdS–Me_mS_n systems

Activation of cadmium sulphide luminescence with small additions of an activator metal	CdS – $Cu_{2-x}S$, CdS – MnS
Continuous shift of the band in the whole range of compositions 0–100 mol%	CdS – ZnS
Continuous shift of the band, probably, within the limited range of solubility	CdS – Cr_2S_3
Two luminescence bands with a variable ratio of intensities	CdS – In_2S_3
"Quenching" of luminescence	CdS – Cr_2S_3, CdS – FeS_2

were low at such temperatures. If metal sulphides were released independently during the thermal destruction of complexes, solid-phase interactions of most sulphides could not be realised. Therefore, the interaction occurred at the moment of thermal destruction of complex compounds right on the substrate due to the emerging valence opportunities of their structural fragments.

Author contributions

Semenov V. N. - scientific leadership, research concept, conducting research and methodology development, writing of text, final conclusions.

Naumov A. V. - research concept, conducting research and methodology development, writing of text, final conclusions.

Conflict of interests

The authors declare that they have no known competing financial interests or personal relationships that could have influenced the work reported in this paper.

References

1. Ugai Ya. A. *Vvedenie v khimiyu poluprovodnikov* [Introduction to Semiconductor Chemistry]. Moscow: Vysshaya shkola Publ.; 1965. 339 p. (In Russ.)

2. Naumov A. V., Semenov V. N., Averbakh E. M. Tiomochevinnye koordinatsionnye soedineniya v protsessakh sinteza sul'fidov metallov [Thiourea coordination compounds in the synthesis of metal sulfides]. *Khimicheskaya promyshlennost' (Russian Chemical Industry*). 2003;80(2): 17–26. Available at: https://elibrary.ru/item.asp?id=23712470 (In Russ.)

3. Semenov V. N., Ostapenko O. V., Levin M. N. Geterostruktury $Cd_xZn_{1-x}S/Cu_2S$ dlya nazemnykh fotoelektricheskikh preobrazovatelei, sformirovannye iz tiokarbamidnykh kompleksov [$Cd_xZn_{1-x}S/Cu_2S$ heterostructures for ground-based photovoltaic converters formed from thiocarbamide complexes]. *Kondensirovannye sredy i mezhfaznye granitsy = Condensed Matter and Interphases*. 2002;4(1): 55–58. Available at: https://elibrary.ru/item.asp?id=23713361 (In Russ.)

4. Sergeeva A. V., Naumov A. V., Semenov V. N., Sokolov Yu. V. Phase composition and microstructure of In_2S_4 and $CuInS_2$ films grown on silicon by spray pyrolysis. *Inorganic Materials*. 2007;43(10): 1046–1049. https://doi.org/10.1134/S0020168507100032

5. Naumov A. V., Sergeeva A. V., Semenov V. N. Structure and reflection spectra of $In_{3-x}S_4$(111)/mono-Si и $In_{3-x}S_4$(111)/SiO_2/mono-Si films. *Inorganic Materials*. 2015;51(12): 1205-1212. https://doi.org/10.1134/s0020168515110060

6. Naumov A. V., Sergeeva A. V., Semenov V. N. Oriented $In_{3-x}S_4$ films on the (100) surface of Si, GaAs, and InP single crystals. *Inorganic Materials*. 2017;53(6): 560–567. https://doi.org/10.1134/s0020168517060127

7. Vorob'ev-Desyatovskii N. V., Kukushkin Yu. N., Sibirskaya V. V. Soedineniya tiomocheviny i ee kompleksov s solyami metallov [Compounds of thiourea and its complexes with metal salts]. *Koordinatsionnaya khimiya (Russian Journal of Coordination Chemistry)*.1985;11(10): 1299 – 1328. (In Russ.)

8. Kharitonov Yu. Ya., Brega V. D., Ablov A. V. IK-spektry pogloshcheniya i normal'nye kolebaniya kompleksov metallov s tiomochevinoi [IR absorption spectra and normal vibrations of metal complexes with thiourea]. *Zhurnal neorganicheskoi khimii (Russian Journal of Inorganic Chemistry*). 1974;19(8): 2166- 2168. (In Russ.)

9. Dutault F., Lahaye J. Formation de sulfure de cadmium a partir d'une solution aqueuse de thiouree et de chlorure de cadmium. *Bulletin de la Société chimique de France*. 1980;1(5): 236 – 240. (In French)

10. Naumov A. V., Nechaev I. V., Samofalova T. V., Semenov V. N. Structure and properties of thiocarbamide complexes of cadmium and zinc according to the results of a quantum-chemical calculation. *Russian Journal of Applied Chemistry*. 2010;83(6): 974–977. https://doi.org/10.1134/s107042721006008x

11. Naumov A. V., Samofalova T. V., Semenov V. N., Nechaev I. V. Thiourea complexes in synthesis of $Cd_{1-x}Zn_xS$ solid solutions. *Russian Journal of Inorganic Chemistry*. 2011;56(4): 621–627. https://doi.org/10.1134/s0036023611040218

12. Ugai Ya. A., Semenov V. N., Averbakh E. M. Issledovanie vzaimodeistviya solei kadmiya s

tiomochevinoi pri poluchenii plenok sul'fida kadmiya [Study of the interaction of cadmium salts with thiourea in the preparation of cadmium sulfide films]. *Zhurnal prikladnoi khimii (Journal of Applied Chemistry of the USSR)*. 1988;(11): 2409–2414. Available at: https://elibrary.ru/item.asp?id=23712458 (In Russ.)

13. Semenov V. N., Vlasenko N. V. Protsessy kompleksoobrazovaniya v sistemakh tiomochevina – kadmievaya sol' kislorodsoderzhashchei kisloty [Complexation processes in thiourea чев cadmium salt of oxygen-containing acid systems.]. *Zhurnal neorganicheskoi khimii (Russian Journal of Inorganic Chemistry)*. 1992;37(4): 929–933. Available at: https://elibrary.ru/item.asp?id=28931801

14. Naumov A. V., Semenov V. N., Goncharov E. G. Properties of CdS films prepared from thiourea complexes of cadmium salts. *Inorganic Materials*. 2001;37(6): 539–543. https://doi.org/10.1023/a:1017594228500

15. Naumov A. V., Meteleva Yu. V., Sermakasheva N. L., Semenov V. N., Novikov G. F. Luminescence and HF photoconductivity of cadmium and zinc sulfides obtained from thiocarbamide coordination compounds. *Journal of Applied Spectroscopy*. 2002;69(1): 120–125. Available at: https://elibrary.ru/item.asp?id=5028730

16. Ugai Ya. A., Semenov V. N., Averbakh E. M. Vliyanie kompleksoobrazovaniya na poluchenie plenok sul'fida medi iz vodnogo rastvora tiomocheviny i khlorida medi pul'verizatsiei [Effect of complexation on the preparation of copper sulfide films from an aqueous solution of thiourea and copper chloride by pulverization]. *Russian Journal of Inorganic Chemistry*. 1981;26(1): 271–273. Available at: https://elibrary.ru/item.asp?id=28887544 (In Russ.)

17. Gazho Ya. Vzaimnoe vliyanie ligandov, struktura i svoistva kompleksov medi (II) [Mutual influence of ligands, structure and properties of copper (II) complexes]. *Russian Journal of Inorganic Chemistry*. 1977;22(11): 2936–2944. (In Russ.)

18. Semenov V. N., Naumov A. V. Complexation and redox processes in aqueous solutions of copper (II) chloride and thiourea. *Russian Journal of Inorganic Chemistry*. 2001;46(3): 367–370. Available at: https://elibrary.ru/item.asp?id=13371854.

19. Semenov V. N, Sushkova T. P., Klyuev V. G. Lyuminestsentnye svoistva plenok CdS, legirovannogo med'yu, poluchennykh raspyleniem rastvorov na nagretuyu podlozhku [Luminescent properties of copper-doped CdS films obtained by sputtering solutions onto a heated substrate]. *Inorganic Materials*. 1993;29(3): 323–326. Available at: https://elibrary.ru/item.asp?id=23712453 (In Russ.)

20. Semenov V. N, Klyuev V. G., Kushnir M. A. Spektral'no-lyuminestsentnye svoistva plenok, poluchennykh raspyleniem rastvorov tiomochevinnykh kompleksov kadmiya na nagretuyu podlozhku [Spectral and luminescent properties of films obtained by sputtering solutions of thiourea complexes of cadmium on a heated substrate]. *Journal of Applied Spectroscopy*. 1993;59(1–2): 114–119. Available at: https://elibrary.ru/item.asp?id=23319124 (In Russ.)

21. Lukin A. N., Samofalova T. V., Semenov V. N., Naumov A. V. Lyuminestsentsiya, fotoprovodimost' i opticheskie svoistva plenok $Cd_xZn_{1-x}S$ [Luminescence, photoconductivity and optical properties of $Cd_xZn_{1-x}S$ films]. *Russian Physics Journal*. 2011(2/2): 211–215. Available at: https://elibrary.ru/item.asp?id=17394968 (In Russ.)

22. Makurin Yu. N., Zhelonkin N. A. Zaryadovoe sostoyanie i mekhanizm termoliza tiomochevinnogo kompleksa kadmiya [Charge state and the mechanism of thermolysis of the thiourea complex of cadmium]. *Inorganic Materials*. 1994;30(2): 279–280. (In Russ.)

23. Ugai Ya. A., Semenov V. N., Averbakh E. M., Shamsheeva I. L. Thermal decomposition of diclorodithioureacadmium(II). *Russian Journal of General Chemistry*. 1986;56(9): 1945–1950. Available at: https://elibrary.ru/item.asp?id=28890314 (In Russ.)

24. Semenov V. N., Naumov A. V. Thermal decomposition of cadmium thiourea coordination compounds. *Russian Journal of General Chemistry*. 2001;71: 495–499. https://doi.org/10.1023/A:1012306512566

25. Naumov A. V., Semenov V. N., Lukin A. N., Goncharov E G. Phase composition of copper sulfide films produced from copper salt–thiourea complexes. *Inorganic Materials*. 2002;38: 271–273. https://doi.org/10.1023/A:1014779018372

26. Semenov V. N., Zolotukhina L. A. Physical properties of the thin CdS–Cu_2S films. *Inorganic Materials*. 1992;28(7): 1370–1373. Available at: https://elibrary.ru/item.asp?id=28931821 (In Russ.)

27. Burcus I., Zet Gh., Ghreghei M. Studies on the Realization of CdS and Cu_xS Thin photoconductor films by liquid phase reaction method. *Bull. Inst. Politechn. Iasi. Sec. 1*. 1983;29(1–4): 79–86.

28. Semenov V. N., Sushkova T. P., Klyuev V. G. Fotolyuminestsentnye svoistva legirovannykh plenok $Cd_xZn_{1-x}S$ [Photoluminescent properties of doped $Cd_xZn_{1-x}S$ films]. *Physics, Chemistry and Mechanics of Surfaces*. 1994(7): 60–64. Available at: https://elibrary.ru/item.asp?id=23725261 (In Russ.)

29. Klyuev V. G., Semenov V. N., Kustov A. I. Fotoaktivnost' tonkoplenochnykh tverdykh rastvorov $Cd_xZn_{1-x}S$ [Photoactivity of $Cd_xZn_{1-x}S$ thin-film solid solutions]. *Surface Investigation: X-Ray, Synchrotron and Neutron Techniques*. 2001(4): 101–103. Available at: https://elibrary.ru/item.asp?id=23723780 (In Russ.)

30. Meteleva Yu. V., Semenov V. N., Klyuev V. G., Smerek S. A. Luminescent properties of polycrystalline $Cd_{0.5}Zn_{0.5}S$ films prepared from thiourea complexes.

Inorganic Materials. 2001;37: 1224–1227. https://doi.org/10.1023/A:1012909621867

31. Morozova N. K., Kuznetsov V. A. Sul'fid tsinka. Poluchenie i opticheskie svoistva [Zinc sulphide. Receiving and optical properties]. Moscow: Nauka Publ.; 1987. 200 p. (In Russ.)

32. Semenov V. N., Ostapenko O. V., Lukin A.N. Physical properties of CdS–In_2S_3 thin films. *Inorganic Materials*. 2000;36: 111–113. https://doi.org/10.1007/BF02758007

33. Fok M. V. *Vvedenie v kinetiku lyuminestsentsii kristallofosforov* [Introduction to the kinetics of luminescence of crystal phosphors]. Moscow: Nauka Publ.; 1964. 284 p. (In Russ.)

34. Semenov V. N., Ostapenko O. V., Lukin A. N. Solid-state reactions in CdS–Bi_2S_3 thin films. *Inorganic Materials*. 2000;36: 1197–1199. https://doi.org/10.1023/A:1026665211338

35. Semenov V. N., Ostapenko O. V., Klyuev V. G. Poluchenie i svoistva plenok sistemy CdS–Cr_2S_3 [Preparation and properties of films of the CdS–Cr_2S_3 system]. *Surface Investigation: X-Ray, Synchrotron and Neutron Techniques*. 2000(4): 37–40. Available at: https://elibrary.ru/item.asp?id=28925164

Information about the authors

Victor N. Semenov, DSc in Chemistry, Professor, Head of the Department of General and Inorganic Chemistry, Voronezh State University, Voronezh, Russian Federation; e-mail: semenov@chem.vsu.ru. ORCID iD: https://orcid.org/0000-0002-4247-5667.

Alexander V. Naumov, PhD in Chemistry, Assistant Professor, Department of General and Inorganic Chemistry, Voronezh State University, Voronezh, Russian Federation; e-mail: aither@bk.ru. ORCID ID: 0000-0002-1313-8573.

Received 17 June 2021; Approved after reviewing 15 July 2021; Accepted for publication 15 August 2021; Published online on 25 September 2021.

Translated by Marina Strepetova
Edited and proofread by Simon Cox

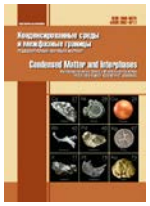

ISSN 1606-867X (Print)
ISSN 2687-0711 (Online)
Condensed Matter and Interphases
Kondensirovannye Sredy i Mezhfaznye Granitsy
https://journals.vsu.ru/kcmf/

Review

Review article
https://doi.org/10.17308/kcmf.2021.23/3526

The development of methods for the research and synthesis of solid phases by the scientific school of Ya. A Ugai. Review

G. V. Semenova✉, **A. Yu. Zavrazhnov**

Voronezh State University,
1 Universitetskaya pl., Voronezh 394018, Russian Federation

Abstract

The scientific school founded by Yakov A. Ugai has existed at Voronezh State University for over fifty years. One of its focus areas has been the development of physics and chemistry for obtaining solid phases in systems with volatile components. This determined the necessity to develop methods for the investigation of vapour pressure (tensimetric methods). This article only focuses on some of the works by the VSU staff dedicated to the study and construction of *P-T-x* diagrams. This review analyses phase equilibria and the nature of the intermediate phases in the $A^{IV} – B^{V}$, $A^{IV} – B^{V} – C^{V}$, and $A^{III} – B^{VI}$ systems. Owing to the special nature of the cation-cation and anion-anion bonds, these compounds have highly specific properties that make them promising materials (2D materials in particular). The article presents an overview of works devoted to the construction of *P-T-x* diagrams and the investigation of defect formation processes in binary and ternary systems based on $A^{IV}B^{V}$ compounds. It should be emphasised that the known techniques needed updating due to the high values of vapour pressure. This allowed conducting experiments at pressures of about 35-40 atmospheres. The study of the A^{III} - B^{VI} systems, on the contrary, is complicated by low values of vapour pressure over indium and gallium chalcogenides and the complex composition of the vapour. For such systems the auxiliary component method was developed. The possibilities of its application are wide and are not limited to $A^{III}B^{VI}$ compounds. A new method for nonstoichiometry regulation was developed and applied using non-destructive selective chemical transport reactions (i.e. with the participation of an auxiliary component). This method is based on the introduction or removal of one of the sample components by means of a selective chemical transport reaction. In conclusion, the development of methods for the research and synthesis of intermediate phases with variable compositions (properties) was analysed based on the example of the discussed systems.

Keywords: Phase equilibria, Tensimetric methods, $A^{IV}B^{V}$ compounds, Indium and gallium chalcogenides, Phase diagrams

For citation: G. V. Semenova, A. Yu. Zavrazhnov The development of methods for the research and synthesis of solid phases by the scientific school of Ya. A Ugai. Review. *Kondensirovannye sredy i mezhfaznye granitsy = Condensed Matter and Interphases.* 2021;23(3): 353–373. https://doi.org/10.17308/kcmf.2021.23/3526

Для цитирования: Семенова Г. В., Завражнов А. Ю. Развитие методов исследования и синтеза твердых фаз в научной школе Я. А. Угая. Обзор. *Конденсированные среды и межфазные границы*. 2021;23(3): 353–373. https://doi.org/10.17308/kcmf.2021.23/3526

✉ Galina V. Semenova, e-mail: semenova@chem.vsu.ru
© G. V. Semenova, A. Yu. Zavrazhnov, 2021

The content is available under Creative Commons Attribution 4.0 License.

1. Introduction

In 1981, Yakov Ugai was awarded with the USSR National Prize in Science and Technology for a series of studies in the area of chemical thermodynamics of semiconductors. This event honoured the contributions of the Voronezh school of inorganic chemists founded by him in the development of a new direction, semiconductor chemistry [1]. It was at Voronezh State University that Ya. A. Ugai established the country's first department of semiconductor chemistry and works aimed at the search for new materials and the study of their properties were conducted. Unique experimental units created by the department staff allowed exploring the nature of phase equilibria in complex systems with volatile components (phosphorus, arsenic, and sulphur) and to construct phase diagrams for such systems. Until now, some of these data are still unique and are quoted in international handbooks [2, 3]. The contribution of Yakov A. Ugai identified research areas in the field of physics and chemistry for obtaining solid-phase materials.

2. Phase equilibria in systems based on elements of groups IV and V in the periodic system

The research into $A^{IV}B^{V}$ compounds hold an important place among the studies dedicated to the nature of phase equilibria in binary systems with volatile components carried out under the leadership of Ya. A. Ugai. Unlike the commonly known classes of $A^{III}B^{V}$, $A^{II}B^{VI}$, and $A^{I}B^{VII}$ compounds, these compounds belong to the class of so called abnormally constructed phases. They are formed by elements located in adjacent groups of the periodic system, which are largely similar in their physical and chemical nature. Owing to the special nature of the cation-cation and anion-anion bonds in silicon and germanium phosphides and arsenides (as well as in indium and gallium monochalcogenides, which will be discussed in the second part of the article), they have highly specific properties. Silicon and germanium pnictogenides are semiconductors and have interesting optical and electrical properties [4,5]. However, there was clearly insufficient interest in this group of compounds due to the difficulty in synthesising high-quality crystals and a lack of information about phase diagrams which largely determine the set of production methods.

Owing to many years of research by the closest disciple and colleague of Ya. A. Ugai, Evgeny G. Goncharov, and other staff, this interesting class of compounds was finally characterised. They studied the properties of silicon and germanium phosphides and arsenides and constructed phase diagrams of the respective systems. It was shown that Si – As and Ge – As systems are characterised by two intermediate phases with the AB and AB_2 composition. Additionally, germanium arsenides and silicon monoarsenide melt congruently, and $SiAs_2$ decomposes by a peritectic reaction [6–9]. It was revealed that the Si – P system has two intermediate phases of phosphide and silicon diphosphide which melt congruently [10, 11], while the germanium-phosphorus system is characterised by a single intermediate phase of GeP which decomposes by a peritectic reaction [12–14]. It should be noted that such studies were made possible owing to a variety of techniques developed by the authors. They include using steel counter pressure chambers for the synthesis of samples, graphitisation of quartz ampoules, the introduction of an indifferent solvent and a number of other methods that distinguished the Voronezh school.

For the neighbouring elements in the periodic system the electronegativity values are close enough, and this factor does not play a major role. In this case, the peculiarities of component interactions are largely determined by the size factor. Hence the higher stability of silicon phosphides, the congruent nature of melting of silicon and germanium phosphides and arsenides, and the appearance of decomposing phases in Si – As, Ge – P systems. This is also reflected in the nature of the formation of defects in these phases, which is characterised by the dominant role of antistructural defects (e.g., Ge'_{As} and $As^{\bullet}_{Ge}$ in the Ge - As system) [15–19]. The study of the processes leading to the formation of defects enabled the electrophysical properties of these materials to be explained [20, 21]. These studies led to the development of a platform for obtaining high-quality crystals with reproducible properties.

The studies of $A^{IV}B^{V}$ compounds were continued with the research of systems involving another element of the fourth group, tin. The

data on phase equilibria in these systems are actually based on a few studies, mostly relating to compositions rich in tin. The data on vapour pressure of volatile components in these systems are extremely scarce and controversial. On the other hand, in recent years, there have been a large number of publications dedicated to tin phosphides used as negative electrode materials for lithium-ion batteries and for the creation of thermoelectric materials [22–33].

Three intermediate phases were detected in the Sn – P system: Sn_4P_3 decomposes at 823 K into two liquids of different compositions with a content of phosphorus of 22.5 and 47.0 mol%; Sn_3P_4 phase melts without decomposition at 833 K, and SnP_3 also decomposes by a synthetic schema. However, no specific experimental data have been provided [2]. It should be noted that the reference information on the phase equilibria in the Sn-P system is mainly based on one study [34]. In their research, the authors used visual polythermal method, which cannot fully evaluate the complex physical and chemical nature of the phases. Sn_4P_3, Sn_3P_4, SnP_3 phases have a similar crystal structure with the $R\bar{3}m$ space group similar to the structure of elements in the arsenic subgroup. This fact, together with the high reactivity and volatility of phosphorus, challenges the production of tin phosphides: due to similar atom coordination, a transition from one phase to another is possible even under slight changes in the conditions of synthesis. It was repeatedly mentioned that it was difficult to form the Sn_3P_4 phase. Despite the variation of the synthesis conditions, the resulting sample often contained Sn_4P_3 impurities. They only managed to produce the Sn_3P_4 compound as a result of the prolonged low-temperature annealing of stoichiometric amounts of tin and phosphorus.

The study of the Sn – P system by X-ray diffraction, differential thermal analysis, SEM, and EPXMA showed that within the concentration range of 43–70 mol% of P there is only one invariant equilibrium with the participation of the higher phosphide of $L_2 \leftrightarrow Sn_4P_3 + SnP_3$ [35–38]. The temperature of the eutectic horizontal was determined to be 824 K. As a result of prolonged annealing of alloys at temperatures below 673 K, the alloys with the content of phosphorus of 43–57 mol% were heterophasic mixtures of the Sn_4P_3 and Sn_3P_4 phosphides and Sn_3P_4 and SnP_3 were the samples with the greatest content of phosphorus. On the contrary, if the Sn_3P_4 phase was initially recorded in the samples, the high-temperature annealing at a temperature of 773 K led to its decomposition into the adjacent phases of Sn_4P_3 and SnP_3. In particular, the Sn_3P_4 sample, produced as a result of two-temperature synthesis, decomposed completely under such heat treatment. Thus, a conclusion was made about the peritectoid decomposition of the Sn_3P_4 phosphide. The use of high-temperature *in situ* spectrophotometry of saturated phosphorus vapour over alloys of the Sn – P system allowed estimating the concentration of this component in the vapour and calculating the pressure value. For the first time, the *P-T-x* diagram was constructed (Fig. 1) [39–41].

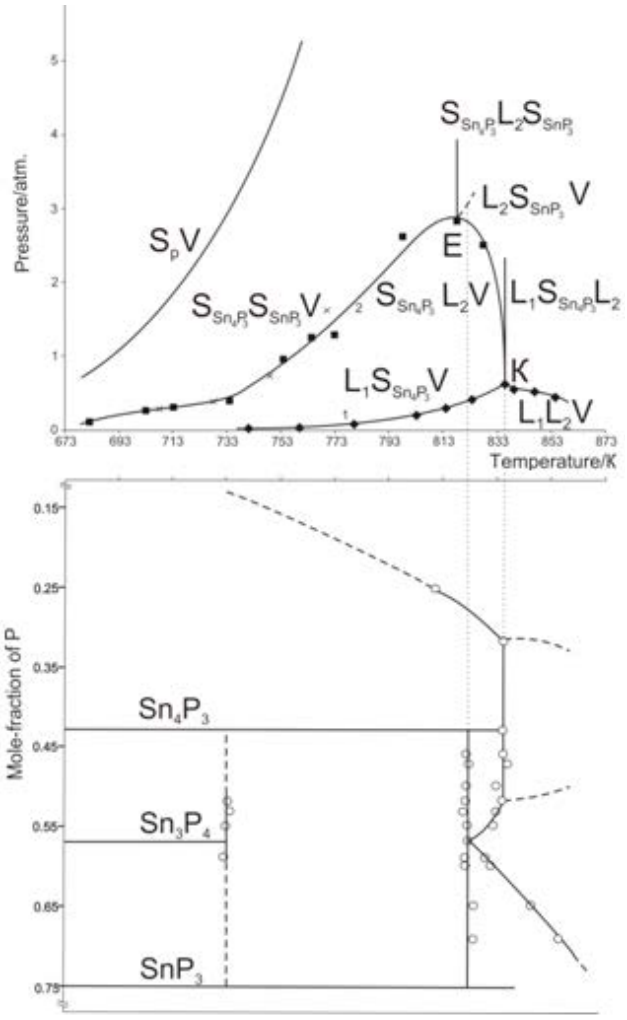

Fig. 1. *P-T-x* diagram of the Sn–P: (a) *P-T*; (b) *T-x* projection

Silicon and germanium phosphides and arsenides were used as solid phase diffusants upon the doping of elemental semiconductors. These compounds are of great practical value for two reasons: their anisotropic electrophysical characteristics resulting from the low-symmetry structure; and their layered crystal structure which allows for the intercalation of ions and molecules into the interlayer space. However, despite the obtained physical and chemical information about the $A^{IV}B^{V}$ compounds, their application as semiconductor materials did not become widespread.

The discovery of graphene provoked a considerable interest in 2D semiconductor materials [42–46]. From this point of view, using the $A^{IV}B^{V}$ compounds characterised by a layered structure with weak van der Waals bonds between the layers, is promising. The presence of volatile components makes it challenging to synthesise such compounds, which is why [42] attempted to obtain 2D samples of silicon phosphide in the presence of bismuth or tin. In the latter case, Sn-doped materials with peculiar semiconductor properties were obtained. However, the lack of information about the phase equilibria in the A^{IV}–B^{V}–Bi and A^{IV}–B^{V}–Sn ternary systems makes further research in this area rather problematic.

Phase diagrams were built for the Bi –$GeAs_2$ and Bi–GeAs polythermal cross sections of the Ge – As – Bi system [47]. It was established that in the ternary system there was a L ↔ GeAs + Bi + Ge eutectic and a L + $GeAs_2$ ↔ GeAs + Bi peritectic four-phase transformations which occurred at a temperature of 542 and 548 K, respectively. It was shown that the four-phase processes in the ternary system occurred in the areas of concentrations with a high content of bismuth. Therefore, bismuth may be used as an indifferent solvent. However, due to the flat shape of the liquidus surface, a great amount of its additions is required to reduce the temperature of the alloy synthesis.

The nature of the phase diagram of the Sn – As – Ge system is more complex [48–52]. Fig. 2 shows a topological equilibrium diagram that illustrates phase transformations and successive (with decreasing temperature) crystallisation processes in the Ge–As–Sn system. The polythermal cross sections SnAs – GeAs and SnAs – $GeAs_2$ can perform phase subsolidus demarcation of the state diagram of the Sn – As – Ge system. However, they are not quasibinary. There are also non-variant peritectic equilibria L + $GeAs_2$ ↔ GeAs + SnAs (838 K) and L + As ↔ SnAs + $GeAs_2$ (843 K) in the system. Comparing the form of the polythermal cross sections of Sn–GeAs [49] and Bi–GeAs [47], it can be concluded that even small additions of tin significantly soften the conditions for obtaining germanium arsenide, however, the possibility of a Sn_4As_3 auxiliary phase makes tin a less attractive solvent as compared to bismuth, which acts as an indifferent solvent over the entire concentration range.

The same type of bonds, similar crystal-chemical structure, and favourable "size" factor determine a possibility to form a continuous series of solid solutions between $A^{IV}B^{V}$ compounds. In [53, 54], it was shown that the formation of solid solutions with cation substitution is extremely difficult. The formation of solid solutions between silicon and germanium phosphides and arsenides, in contrast, can be performed quite easily [55, 56]. A feature of the directed synthesis of ternary solid solutions is the need to simultaneously control the composition by two parameters: such properties as bandgap, the lattice constant, etc. can be varied by altering the molarity of the solid solution; and the deviation from stoichiometry allows controlling the type and the concentration of the carriers. Therefore, there is a need in a comprehensive study of phase diagrams of the A^{IV}-As-P ternary systems which would include the analysis of defect formation processes in ternary solid solutions. This involves examining the nature of the interaction between the elements of group V.

P-T-x diagrams for the Sb – As and As – P systems were constructed with the help of a combination of differential thermal analysis and the static manometric method [57–62]. Due to very high values of saturated vapour pressure, it is extremely difficult to measure it directly along the three-phase equilibrium line. In [60], this problem was solved as follows. Lead was introduced into the system. It acted as an indifferent solvent which reduced the phase transition temperature. The authors measured the vapour pressure in liquidus points for sections with different quantities of lead and then extrapolated these values so that the content of lead was zero in the alloy with different

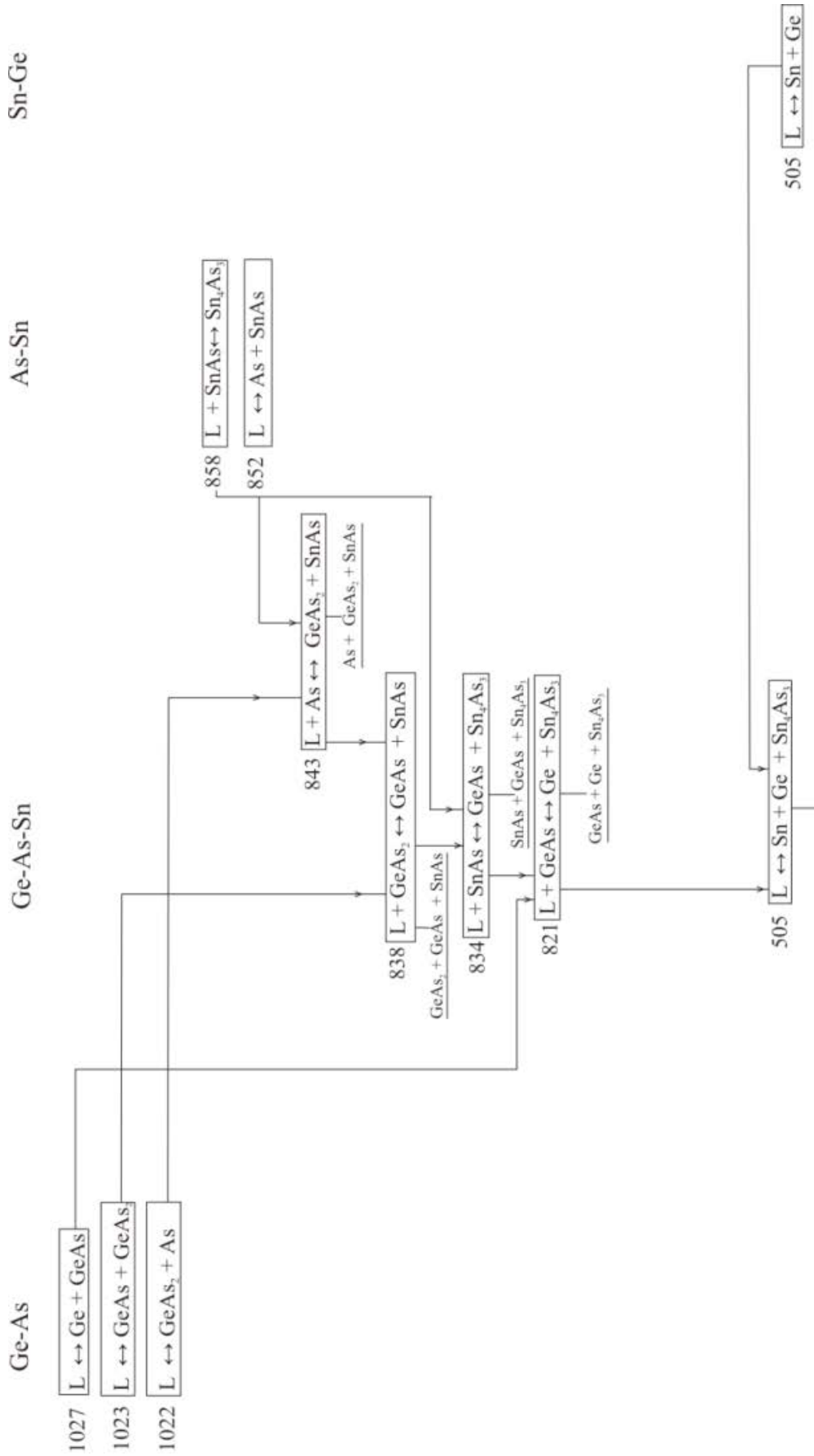

Fig. 2. A topological scheme of the equilibria in the Sn–As–Ge system

ratios of arsenic and phosphorus. This allowed establishing the coordinates of the three-phase equilibrium line in the P–As system. According to these data, the system has an intermediate berthollide phase which melts with a peritectic reaction. However, the nature of this phase was not discussed and there was no information about the parameters of the crystal lattice. To support this version the authors of [60–62] provided data of a thermographic study, according to which *T-x* diagram has two horizontals corresponding to invariant processes of the γ-phase formation from the arsenic-based melt and solid solution of L + β ↔ γ and phosphorus-based α-solid solutions: L + γ ↔ α. This was also indicated by the results of tensimetric studies according to which groups of *P-T*-curves that coincide within the experimental error tolerance can be distinguished. *P-x* isotherms constructed at 773, 823, and 873 K confirmed the presence of two heterophase areas in the P – As system.

There is another version regarding the nature of the phase equilibria, according to which the P – As system has limited solid solutions based on the components, however, the specific feature of the experiment was that alloys were prepared in the presence of metallic mercury [63, 64]. This contributed to the transition of phosphorus into its orthorhombic modification (black phosphorus). In fact, the experiment described phase relations under completely different conditions.

Recently, a huge interest in layered structures, and the orthorhombic modification of phosphorus in particular, has provided new results in the study of pnictogens and systems formed by them [65–68]. For example, [69] described an attempt to obtain orthorhombic modifications of phosphorus and arsenic under conditions close to normal. It showed the mutual influence of arsenic and phosphorus on the possibility to form different allotropes. On the one hand, arsenic promotes the crystallisation of amorphous red phosphorus. On the other hand, it promotes the formation of the orthorhombic modification even in the absence of catalysts of the process (e.g. mercury or PbI_2). The sample with the $As_{0.7}P_{0.3}$ composition was prepared by heating the amorphous red phosphorus and grey (rhombohedral) arsenic. Tensimetric studies showed that at 723 K phosphorus crystallises to its violet modification (Hittorf's phosphorus). Both phases are metastable, since their pressures are higher than the pressure of black phosphorus vapour. At 773 K, the pressure drops and an orthorhombic modification is formed, i.e. solid solution of arsenic and phosphorus. Using the results of the X-ray diffraction analysis of the samples of the P – As system, we established that at concentrations of 55–85 mol% of As there is a heterophasic mixture of a solid solution of phosphorus in α-As and a phase with an orthorhombic crystal lattice with the parameters of a = 3.48, b = 4.42, c = 10.81 A. Therefore, the phase with a structure identical to that of black phosphorus is formed in the P – As system without the addition of catalysts or the use of high pressure. The nature of the phase relations in the P – As system requires further research.

The analysis based on the experimental studies of a number of polythermal cross sections of phase diagrams of the Ge – As – P, Si – As – P ternary systems [70-75] showed that in case of anionic substitution solid solutions are formed without any notable difficulties. Solid solutions are formed in the GeAs – GeP system over the entire range of concentrations, whereas in the Si – As – P ternary system there is a peritectic mixture of silicon phosphide and arsenide-based solid solutions and the heterogeneous region extends from 45 to 60 mol% of SiP at 1300 K. To obtain crystals of solid solutions homogeneous along the length of the ingot in the Ge – As – P system, it was proposed to use the method of two-temperature synthesis followed by directed crystallisation of the melt and to use As – P melts as a source of volatile components. Using alloys which are a heterophasic mixture of the intermediate γ-$As_{1-x}P_x$ (x = 0.3 ÷ 0.4) and a phosphorus or arsenic-based solid solution allows growing homogeneous crystals of solid solutions under the conditions of controlled vapour pressure of the two volatile components. The composition of the resulting $GeAs_{1-x}P_x$ solid solutions can be varied by changing the temperature of the source zone [70].

The investigation of phase equilibria in the Sn – As – P system is challenging, not only due to difficulties of working with volatile components, phosphorus and arsenic, but also to a large number of intermediate phases. In such complex systems, triangulation is normally conducted

and it is divided into simpler individual systems, but in this case it is not possible because of the wide regions of solid solutions, based both on individual components and on intermediate phases. In this case, we can talk about phase subsolidus demarcation.

The study of the Sn – As – P systems in the regions of high tin concentrations established a continuous series of solid solutions between arsenide and phosphide with the composition of Sn_4B_3 (α-solid solutions) [76].

X-ray diffraction analysis of the alloys whose compositions belong to the polythermal cross sections of SnAs–$Sn_{0.43}P_{0.57}$, Sn_4As_3–$Sn_{0.43}P_{0.57}$, and SnAs–$Sn_{0.5}P_{0.5}$ revealed that in addition to the α-phase the samples have solid solutions based on tin monoarsenide and tin phosphide SnP_3 [77, 78]. The formation of solid solutions based on tin monoarsenide (β-solid solutions) is indicated by a shift of the characteristic lines of the SnAs spectra toward greater angles. What is more, the shift increases with an increase in the molar fraction of phosphorus. In contrast, the alloys of the investigated polythermal cross sections with a content of phosphorus of more than 70 mol% for the SnP_3 reflexes demonstrate a natural increase in the interplanar spaces which indicates the replacement of phosphorus atoms with arsenic atoms whose radius is greater. Solid solutions based on SnP_3 tin phosphide (γ-solid solutions) are formed [79].

The study of the SnAs–SnP_3 polythermal cross section in the Sn–As–P ternary system by X-ray diffraction analysis revealed that the region of solid phase solubility based on tin monoarsenide extends up to 30 mol% of SnP_3 [80]. The analysis of the obtained data in combination with the results of the study of alloys with lower tin contents allowed establishing the presence of four-phase equilibria of the peritectic type with the participation of the melt and solid solutions based on tin monoarsenide, tin phosphide SnP_3, and the $As_{0.6–0.7}P_{0.4–0.3}$ intermediate phase. It was found that in the region of the Sn – As – P phase diagram with the tin content below 50 mol% in addition to four-phase equilibria $L \leftrightarrow \alpha + \beta + \gamma$ (818 K) at a temperature of 824 K there is an invariant equilibrium of the peritectic type with the participation of solid solutions based on tin monoarsenide, tin phosphide SnP_3, and the intermediate δ-phase $As_{1-x}P_x$: $L + \delta \leftrightarrow \beta + \gamma$ (Fig. 3).

We would like to draw attention to the fact that a deep understanding of the processes occurring in multicomponent systems is impossible without the development of methods of phase diagrams construction and determining

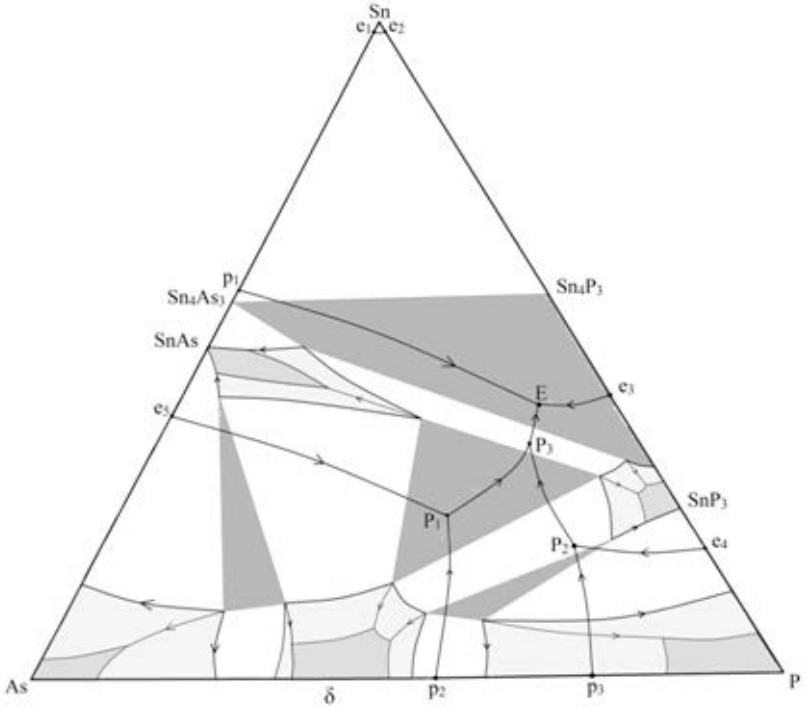

Fig. 3. Scheme of phase equilibria in the Sn–As– P system

regions of condensed phases. *Tensimetric* (and in particular, *manometric*) methods which study the dependence of pressure on temperature or composition of condensed phases equilibrium with vapour are considered to be the most direct and appropriate methods to solve such tasks.

It should be noted that *P T x* diagrams of the Ge – As, Si – As, Ge – P, and Si – As binary systems and the $A^{IV} – B^{V} – C^{V}$ ternary systems were defined with the help of manometric *tensimetry,* i.e. using a quartz null-manometer with a flat membrane [6 – 18]. These studies were greatly facilitated due to the absolutely incongruent nature of silicon and germanium phosphides and arsenides evaporation (sublimation), wherein only phosphorus or arsenic transit to the vapour phase mainly in the form four-atom molecules. Definite vapour composition allowed the composition of the equilibrium condensed matter to be reliably and easily determined at known values of temperature (*T*), pressure (*P*), the volume of the reaction chamber (*V*), and the initial amounts of components used to prepare the sample of silicon or germanium phosphides or arsenides ($n°A^{IV}$), ($n°B^{V}$).

The results of tensimetric experiments allowed not only defining a set of intermediate phases in the $A^{IV}– B^{V}$ systems but also establishing unusual variation of homogeneity ranges of germanium and silicon diarsenides with temperature changes [18]. The authors [18] associated this feature with autointercalation of $SiAs_2$ and $GeAs_2$ by arsenic at premelting temperatures. In the transfer to the $A^{IV} – B^{V} – C^{V}$ ternary systems it was still possible to calculate the composition of vapour and solid phases despite a more complex vapour composition due to the formation of mixed molecules of P_xAs_{4-x} in the vapour.

The next stage was to validate the identified peculiarities of silicon and germanium phosphides and arsenides using the compounds of $A^{III}B^{VI}$, indium and gallium monochalcogenides. These compounds are $A^{IV}B^{V}$ isoelectronic phases. They are similar to them in the structure and nature of chemical bonds. Also, similar to $A^{IV}B^{V}$ compounds, the practical application of $A^{III}B^{VI}$ compounds is experiencing a surge of interest. Basically, this interest is related directly to graphite-like quasi-2D-structure of indium and gallium monochalcogenides [81-84]. Of no less interest is the application of sesquichalcogenides (of type Ga_2S_3), structures with a great concentration of stoichiometric vacancies in the cation sublattice (up to 1/3 of the number of nodes) [85]. However, the phase diagrams of the $A^{III} – B^{VI}$ systems need to be detailed. The study of these systems is complicated by low values of vapour pressure over indium and gallium chalcogenides and the complex composition of the vapour, which makes it impossible to use classical manometric methods.

For this reason, the auxiliary component method (AC) was developed for systems with unsuitable (generally very small for the experiment) values of vapour pressure. It should be noted that the possibilities regarding the application of this method are quite wide and are not limited to the $A^{III}B^{VI}$ compounds for which it was originally designed.

3. A new method for studying phase diagrams and phase equilibria: the auxiliary component method

The idea of the method is to bypass equilibrium (1) between the *X component*, which was a part of the X_nY_m condensed phase, and its vapour

$$X'' \underset{\leftarrow}{\overset{\rightarrow}{}} X' \quad (1)$$

and to create a suitable for the study equilibrium with an auxiliary component additionally introduced into the system. For example,

$$X'' + qZ \underset{\leftarrow}{\overset{\rightarrow}{}} XZ_q, \quad (2)$$

where *Z* is the auxiliary component, and at least one of the *Z* and XZ_q substances has to be volatile and form a vapour. In equations (1), (2) and hereinafter, the symbol "″" corresponds to the component in the condensed state, and the symbol "′" corresponds to the component in the state of vapour.

The principles of this approach have been used in the past. There are several works in the literature, where a number of oxide or sulphide systems was studied with the help of hydrogen or carbon (X = O or S, $Z = H_2$ or $C^{<graphite>}$, volatile forms of XZ_q – H_2O, H_2S or CS_2). However, there has been no systematic research in this area and the possibilities of the AC method have not been thoroughly studied.

First of all, let us analyse various possibilities of the auxiliary component method. The results of this analysis can be used for the selection of the optimal strategy to solve research objectives

and directed synthesis of new inorganic materials with a set composition, and, consequently, with set properties.

3.1. The role of the auxiliary component (AC) vapour in tasks aimed at the study of phase diagrams. The $K_P^{\#}$ value and its informative value. The indicating function of the AC

Our analysis only considered the situation when the auxiliary component was only present in vapour and condensed phases belonged to a binary system. Obviously, when *Z* substance is made to contact the X_nY_m condensed phase, the number of components in the system will increase by one. However, approaching the complete insolubility of the *Z* component in the studied condensed phases, a subsystem can be singled out which only contains studied phases *with the original components*. Relative to this subsystem, its remaining part with the auxiliary component will play the role of an *external body*. The latter, in addition to other properties, is an indicator of the state of the studied phases. In particular, the indicator vapour phase allows "reading" condensed phase information about chemical potentials of their constituent components. For example, when investigating low-volatile inorganic sulphides by means of hydrogen, there is the equilibrium

$$S'' + H_2' \underset{\leftarrow}{\rightarrow} H_2S', \quad (3)$$

for which the necessary equilibrium conditions

$$\mu_S'' + \mu_{H_2}' - \mu_{H_2S}' = 0, \quad (4)$$

give

$$\mu_S'' = RT \ln K_P^{\#} + F, \quad (5)$$

where in (4) and (5), μ_S'' are chemical potentials of bound sulphur in sulphide, μ_{H_2}' and μ_{H_2S}' are chemical potentials of hydrogen and hydrogen sulphide in the vapour, $K_P^{\#}$ is the value, which is often called the constant of heterogeneous equilibrium, and the element *F*, which only depends on the temperature, represents the difference between standard chemical potentials of molecular forms of gas:

$$F = \mu_{H_2S}'^{\circ} - \mu_{H_2}'^{\circ}. \quad (7)$$

The $K_P^{\#}$ value connects the partial pressures of gases as

$$K_P^{\#} = \frac{p_{H_2S}}{p_{H_2}}, \quad (6)$$

Since $K_P^{\#}$, according to (5), depends both on temperature and composition and slightly on pressure, it would be more correct to call it *pseudo-constant* of heterogeneous equilibrium. We will show below that $K_P^{\#}$ is a convenient experimental value. Equation (5) is also valid for a more general case of (2), naturally the respective components in the above expression need to be replaced.

3.2. The possibility to obtain and study such conditions of condensed phases in which these phases cannot coexist with their own vapours. The contractive function of the AC

It is important to note that in contrast to the equilibrium "condensed phase - its own saturated vapour", the equilibria with the participation of an auxiliary component will involve such states of condensed phases in which these phases do not coexist with their own vapours.

By "their own vapours" we understand such vapours that are present in heterogeneous equilibria *without the participation* of an auxiliary component.

For example, carbon placed in a closed and initially evacuated system with free volume will give way to the equilibrium "graphite – carbon vapour" (it is obvious that the last phase at temperatures below 2000 °C will be extremely sparse). However, diamond can never act as a condensed phase in such equilibrium since in the phase diagram of a single-component system diamond at any temperatures does not coexists with the vapour in the subcritical region. However, a gas consisting of carbon oxides may well coexist with diamond in the equilibrium at sufficiently high pressures

$$C^{diamond} + CO_2' \underset{\leftarrow}{\rightarrow} 2CO' \quad (8)$$

In this case, vapour with an auxiliary component plays an important role and acts both as the indicator phase and the contractive medium.

For such problems, as far as it is actually known by the authors of this work, the auxiliary component method has not been used yet. It should also be noted that almost all instrumental methods of investigation of solids are directly (classical tensimetric methods) or indirectly (electrophysical methods) associated with the investigation of phases in the region of their coexistence with their own vapour. On the contrary, for the study of solids

in the regions where the coexistence with saturated vapour is not possible, there is a very limited number of methods. What is more, most of them are not very accurate (for example, the method of thermal electromotive force). Therefore, the considered approach may be useful, for example, for solid-state chemistry or high-pressure materials science.

If the dependence of the chemical potential of the condensed phase on the pressure is substantial, the correct construction of *T-x - sections* including a detailed description of the homogeneity ranges, is only possible with the help of the auxiliary component method. This statement is even true for such cases when the phase allows for the possibility of direct tensimetric measurements. The demand for such studies will be apparent if it is necessary, for example, to compare the range of homogeneity of a phase at very different pressures (for example, 1 and 10 000 atm).

3.3. The construction of phase diagrams of binary systems using an AC. Retrieving thermodynamic information. The amplifying function of the AC

Another area of application of the auxiliary component is ideologically opposite to the approach described above. It is based on the thesis that chemical potentials of the condensed phase components are typically not very sensitive to pressure changes if they do not exceed hundreds or thousands of atmospheres. Then, the state of the condensed phase equilibrium with the vapour of the auxiliary component can be considered the same as in the equilibrium with its own saturated vapour. Applying this to equation (5) it can be expected that the temperature dependence of the $K_P^{\#}$ value for various compositions of condensed phases should be very close to the classical *p-T* diagram. For example, [86, 87] present the results of a null-manometer study of the phase diagram of the Ga – S and Ga – Se systems using the equilibrium

$$2\mathrm{Ga}'' + \mathrm{GaHal}_3' \rightleftarrows 3\mathrm{GaHal}' \quad (\mathrm{Hal} = \mathrm{Cl, I}), \qquad (9)$$

$$K_P^{\#} = \frac{p_{\mathrm{GaHal}}^3}{p_{\mathrm{GaHal3}}}.$$

In Fig.1, in the temperature dependence of the $K_P^{\#}$ value ($Ga_{(liq)}$ – *V*, GaSe – L_{Ga} – *V*, GaSe – Ga_2Se_3 – *V* equilibrium) lines similar to lines of the monovariant equilibrium for the *p-T* diagrams are clearly visible. As expected, the position of these lines does not depend on

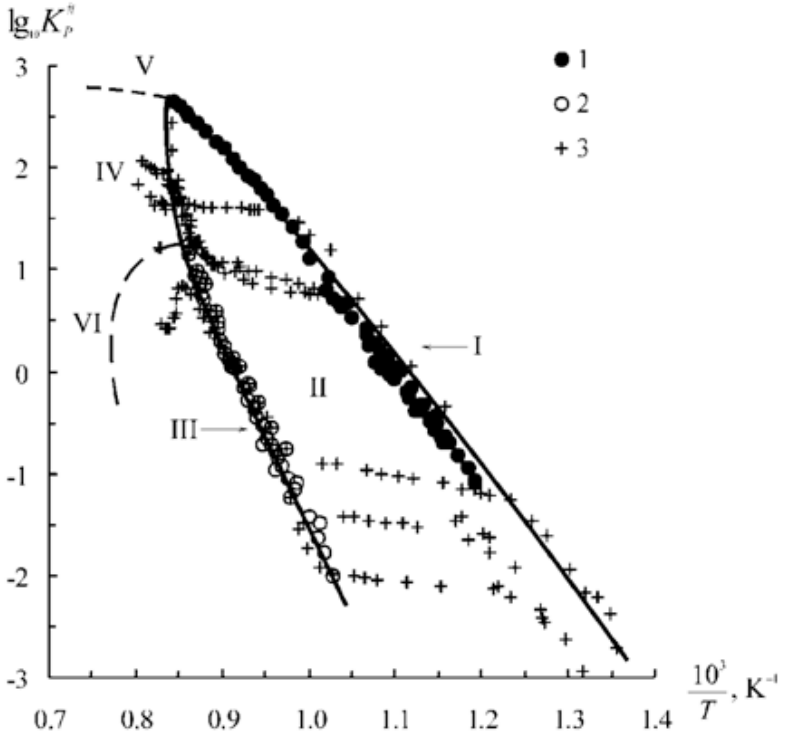

Fig. 4. The temperature dependence of the $K_P^{\#}$ value for heterogeneous equilibria of different natures: I – equilibrium line: $Ga_{(l)}$ – $GaSe_{(s)}$ – $V_{GaI+GaI3}$; II – the $GaSe_{(s)}$ $V_{GaI+GaI3}$ equilibrium region; III – the $GaSe_{(s)}$ – $Ga_2Se_{3(s)}$ – $V_{GaI+GaI3}$ equilibrium region; IV, V, VI – a schematic representation of the regions: IV – $GaSe_{(s)}$ $L_{GaSe\text{-}based}$ – $V_{GaI+GaI3}$; V – $L_{Ga\text{-}based}$ $L_{GaSe\text{-}based}$ $V_{GaI+GaI3}$; VI – $Ga_2Se_{3(s)}$ L – $V_{GaI+GaI3}$; 1 – 7 – experimental curves in the area of equilibrium II

the bulk composition of the GaSe alloy, on the weight of the sample, and the total pressure P ($P \approx p_{GaI} + p_{GaI3}$; vapour unsaturated in relation to gallium iodides, pressure range: from 0.1 to 0.7 MPa). In [86, 87], it was also shown that the homogeneity range of the GaSe phase sharply expands and shifts toward selenium in a narrow temperature range (from ~0.2 mol % at 1100 K to 0.8 mol% at 1180 K). It also has a retrograde solidus for selenium.

Since the chemical potential of the condensed phase component is associated with the (pseudo) constant of the heterogeneous equilibrium $K_P^{\#}$, the analysis of the latter value as a function of the thermodynamic variables gives a lot of information not only about boundaries but also about the behaviour of the phase within its homogeneity range. For example, [88-90] described the results of the study of the In – S system with the help of hydrogen. The dependence of the $K_P^{\#}$ value (see equilibrium 3) on the sulphur concentration for the $In_{3-x}S_4$ phase at T = const (Fig. 5) shows that the $In_{3-x}S_4$ homogeneity range has a tendency to break up into separate phases with similar stoichiometry.

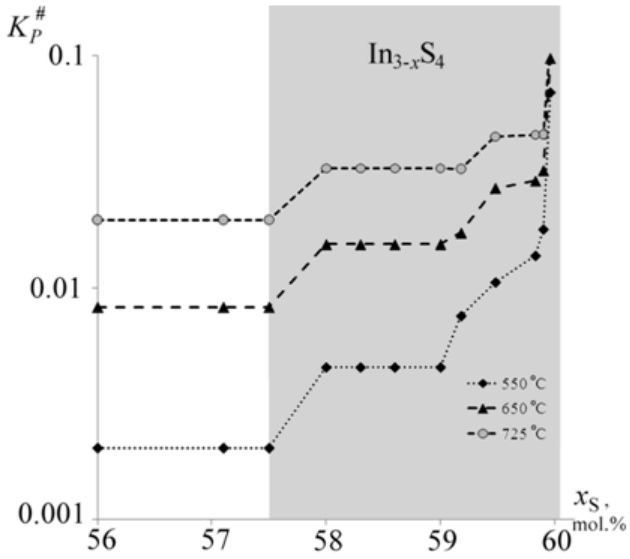

Fig. 5. Isotherms of the $K_P^{\#}$ dependencies of the sulphur content in the $In_{3-x}S_4$ phase. The $K_P^{\#}$ value refers to the S″ +H_2′ = H_2S′ equilibrium where S″ refers to the sulphur chemically bound in condensed phases of the In – S system

3.4. Calculation of partial pressures and p-T diagram

The approach associated with the approximation regarding the negligible impact of pressure on the chemical potential of the condensed phase components can be applied to calculate *p-T* diagrams of the original system under study. As a consequence of this approximation the introduction of the AC does not shift heterogeneous equilibria associated with self-sublimation of the components of the studied phase. In other words, the partial pressures of their own vapours in systems with an AC and without this component should not differ if the two systems are in the same conditions. Furthermore, the partial pressures may be calculated for known values of (pseudo) constant of the heterogeneous equilibrium $K_P^{\#}$. The details of such calculations are described in depth in [87, 88].

It should be noted that the determination of the partial pressure values allows comparing data obtained using *different* auxiliary components or comparing data of experiments with an AC with the results of *direct study* (for example, mass spectrometry). Thus, in the above-mentioned work [87], practically identical results for the pressure of gallium vapour over gallium selenides were obtained using iodine and chlorine (in the form of GaI_3 and $GaCl_3$) as auxiliary components. It should also be noted that the calculated pressures may be so small that they cannot even be determined by mass spectrometry. For example, the partial pressure of gallium vapours for the GaSe – Ga_2Se_3 – V equilibrium calculated at a temperature of 700 K is $1.7 \cdot 10^{10}$ Pa [87]. In such cases, we can say that the auxiliary component plays the role of an amplifier of the signal sent to the external device by a very small value of the partial pressure of a low-volatile component.

3.5. Possibility to calculate thermodynamic quantities

In the case of independent experimental determination (up to a certain constant) of chemical potential of the second component (μ_Y) of the X_mY_n phase, the value $K_P^{\#}$ allows finding the molar Gibbs energy of the formation of this phase ($\Delta_f G$). If it is impossible to experimentally determine the potential of the second component, the value of the Gibbs energy may be determined by the Gibbs–Duhem equation. Further, the $\Delta_f G$

data will allow calculating other molar properties: entropy, enthalpy, volume, heat capacity, etc.

3.6. Using the auxiliary component for fine tune regulation of the composition (nonstoichiometry) of inorganic solid bodies of variable composition

The AC method can be used not only for research purposes, but to solve problems relating to the regulation of the composition (nonstoichiometry) of inorganic compounds. For such cases, the discussed method is close to classical *chemical* (*gas*) *transport reactions* (CTRs). It is different from traditional CTRs in the fact that in this case the original sample is not exposed to oversublimation: due to the strict selectivity of the reaction of type (2), only a change in the ratio of components occurs in the sample.

The main idea of the method is that depending on conditions the selective chemical gas transport reaction can occur in the forward direction (extraction of the component from the sample) or in the reverse direction (saturation of the sample with a transported component [91-95]. The regulation of the content is carried out in a closed system (ampoule) where the sample and the batch are placed. The latter serves as a source or a getter of the transported component. The vapour in the ampoule consists of vapours of different forms of the transport component which provide for the selective transport. According to the findings in [91, 94, 95], the direction of the *selective chemical gas transport reaction* (SSCTR) should *only* be regulated by the temperatures of the sample (T_1) and the batch (T_2) and the composition of the batch (x_1). The evolution of the formulations of the sample and the batch is completed when the system reaches the steady state where there is no mass transfer. It can be said that the composition of the sample "adjusts" to the variables: T_2, T_1, and x_1. The following condition can be the empirical criterion to achieve the steady state:

$$K_P^{\#}(1) = K_P^{\#}(2), \quad (10)$$

where

$$K_P^{\#}(1) = f(T_1, x_1); K_P^{\#}(2) = f(T_2, x_2) \text{ ([91, 94])}. \quad (11)$$

Both for problems relating to the research of phase diagrams and equilibria and for the practical regulation of the composition the right choice of the auxiliary components is only possible if it meets a number of requirements [86, 87, 91, 94, 95]:

1. Comparable amounts of Z and Xzq_q molecular forms in the vapour in equilibrium (2).

2. The absence of binary or ternary compounds between the transport component Z and the second (non-transported) component Y of the sample and the batch (the condition of the third component indifference in relation to the second component).

3. Almost complete insolubility of the Z component in the studied or adjusted X_mY_n phase.

4. Preservation of the non-volatility of the condensed X_mY_n sample under the experimental conditions.

The SSCTR method can be especially useful when the material with the required structure is relatively easy to synthesise, however, it is difficult to precisely control its composition (e.g. due to low volatility). Thus, in [91-98], we demonstrated the possibility of fine tuning the nonstoichiometric composition and properties of gallium, indium, and copper selenides and sulphides.

It should be noted that it is not always possible to separate the "applied" and "research" possibilities of the auxiliary component method. For example, it was shown in [93, 95] that the selenium-enriched part of the homogeneity range of the gallium monoselenide (GaSe) has two phases: γ-modification of GaSe at high temperatures (> 1000 K) and ε-GaSe at low temperatures. The composition of the phase within the homogeneity range was set by the SSCTR method. Apparently, constrained kinetics and the difficulties in regulating the GaSe composition by traditional methods did not allow detecting the enantiotropic transition εGaSe ↔ γGaSe earlier. Therefore, the *T-x-* chart of the Ga Se system should have two phases closely spaced by their composition and separated by a narrow heterogeneous region (which is supported by the independent thermal analysis data [99]).

The adjustment of the composition of intermediate phases conducted for the sake of studying the phase diagram was also carried out in the In – S system. This adjustment was performed using a modified (considering the specific nature of equilibria in the In – Cl system) SSCTR method [96]. As a result, it was possible to show in [88, 90, 96] that the $In_{3-x}S_4$ cubic phase (with a structural type of defect reversed spinel) has a wide range of homogeneity (from ~58.0 to~59.9 mol% of S) that

changes little with temperature. As has already been noted above, the behaviour of the chemical potential of indium in the homogeneity range indicates a tendency to break the homogeneity range into individual phases. The attempts to obtain compositions with a greater content of sulphur at temperatures below 415 °C led to a phase change with symmetry decreased to tetragonal and the formation of the α-In_2S_3 independent phase which almost exactly corresponded to the related stoichiometry. The data relating to the phase equilibria in the In – S system were verified by independent methods without using an AC [100].

In recent papers [101, 102], we were able to develop a method of chemical transport reactions to regulate the composition of the binary phases and to apply it to obtain single crystals of ferric sulphides with a controlled phase and non-stoichiometric composition. The novelty of the developed and applied technique was that a liquid phase based on iron dihalogenide melts was used as a carrier medium for the transported component (iron). Apart from the nature of the transport agent (melt) and the temperature, the composition of ferric sulphides was adjusted by the pressure of sulphur vapour. It should be noted that the substance transfer through the liquid phase in reactions similar in chemistry to gas transfer is very rare in experimental chemistry.

In our opinion, it is also promising to use the auxiliary component to create *catalytic materials*. It is known that highly disordered metals with high chemical and catalytic activity are often called skeleton metals (Ni, Cu, Ag, etc.). To produce them, first a metallide is normally synthesised which is formed by a *d*-metal remaining thereafter in the "skeleton" and by the second chemically active component (Al, Si, etc.). The latter is then removed by leaching. However, this method is unsuitable in some cases: primarily for reactions that must occur under anhydrous conditions.

[103, 104] considered a "dry" method to create activated metals based on the SSCTR method. The main idea of the method is to remove the active component from the metallide into the gas phase. For example:

$$Al'' \text{<from the alloy>} + AlI_3' = 3AlI' \quad (12)$$

or

$$Ga'' \text{<from the alloy>} + GaI_3' = 3GaI'. \quad (13)$$

Metallides in the Cu–Ge, Ni–Ga, Cu–Ga systems were used to show the selective removal of the active component. Gallium or germanium were removed from alloys by means of transport reactions with the participation of germanium and gallium iodides and chlorides. To create a catalyst, the active component was removed in the obviously nonequilibrium conditions: in the vapour *flow* of the transport agent. Further, [104] compared the catalytic activities of nickel materials produced by a conventional method (Al leaching from the $NiGa_4$ phase by the KOH solution) and substances produced by using the SSCTR method. Reactions of the reduction of nitrobenzene to aniline by means of hydrazine and conversion of benzyl alcohol vapours to toluene (benzene) and benzaldehyde were used as test reactions. For the latter conversion the content of decomposition products was studied depending on the process conditions (temperature, vapour flow rate) and the conditions of the catalyst's preparation. [104] also showed the possibility to increase the catalytic activity of nickel by introducing a transport agent directly into the reaction mixture that had been passed through a metallide. NH_4Cl and n-C_4H_9Cl were used as such activator agents. [105] showed the possibility of activating the surface of the nickel-containing material, which involved, on the contrary, a partial removal of nickel atoms from the near-surface region by a selective reaction with the formation of nickel carbonyl:

$$Ni'' \text{<from the alloy>} + CO' = [Ni(CO)_4]' \quad (14)$$

Most recently, the development of *the auxiliary component method* has been based on the spectrophotometric experimental resources. Scanning the vapour absorption spectra with the participation of the AC allows independently determining the concentrations (partial pressures) of various AC forms in the vapour (for example, GaI and GaI_3) instead of the total vapour pressure in classical manometric methods. To calculate the $K_P^{\#}$ value, which is a key value for the measurements, the *partial* pressure data are necessary. An important feature of the newly developed experimental capabilities is an in-situ study of the spectra, i.e. the study of the vapour that is in contact with a condensed phase should be conducted

directly under experimental conditions: at high temperatures (up to 900 °C) and pressures other than the atmospheric pressure (up to $3 \cdot 10^5$ Pa). The considered spectrophotometric method with the application of an AC was used to verify homogeneous and heterogeneous equilibria in the Ga – I [106], In – Cl [107] systems and to specify the phase diagram of the Ga – S system in the high-temperature region (> 800 °C) [108-110].

4. Conclusion

It should be noted that this review does not aim to cover all the areas in which the research has been conducted and the results have been achieved by that section of the scientific school of Ya A. Ugai which has been developing methods for the research and synthesis of semiconductor materials with expressed bulk properties. Beyond the scope of this paper are the results of the study of the $A^{III}B^{V}$ binary and ternary diamond-like phases, new methods of thermal analysis (chromatographic analysis) and manometric methods (laser null-manometry), and a number of other achievements. The main focus of this article, as can be seen from the text, is on:

– the investigation of *P-T-x* diagrams of the $A^{IV} – B^{V}$, $A^{IV} – B^{V} – C^{V}$, and the $A^{III} – B^{VI}$ systems with emphasis on the study of the relationship between pressure (*P*) and other thermodynamic variables (*T, x*);

– the development of methods for the research and synthesis of intermediate phases with variable compositions (properties) in these systems.

Let us summarise the achievements in this area.

1. Using a set of complementary methods (the null-manometric method with two-way vacuuming of the membrane chamber, the differential thermal method with controlled vapour pressure, the extrapolation method with the introduction of an indifferent solvent, and standard methods of physico-chemical analysis), *P-T-x* diagrams of the $A^{IV} – B^{V}$ systems were constructed; the positions of regions of intermediate phases were defined, and their types of melting and corresponding coordinates (*P, T, x*) were determined. In particular, these methods in combination with structural studies were used to show that the monoarsenide (GeAs) and diarsenide ($GeAs_2$) in the Ge – As system are independent intermediate phases with similar but different structures.

Semiconductor silicon and germanium phosphides and arsenides are characterised by a pronounced layered structure, the atoms within a layer are bound by strong covalent bonds, however, between the layers there are weak van der Waals forces. Favourable size factor affects the antistructure disordering in these phases, which has a decisive influence on the defect formation mechanism. Thus, the dominant defects are ionised antistructural defects of the A'_B and $B^{\bullet}_A$ type. The study of micro- *P-T-x* diagrams of the corresponding systems served as the foundation for the development of modes of obtaining crystals with reproducible properties.

In systems with the participation of tin (Sn - B^{V}) the phases with stoichiometry close to Sn_4B_3 are stable. In addition, there are two more stable phases in the tin - phosphorus system, Sn_3P_4 and SnP_3. A similar crystal structure with the $R\bar{3}m$ space group similar to the structure of elements in the arsenic subgroup was revealed for all binary compounds. What is more, disparity of bonds is another characteristic feature of the structure. Such a layered crystalline structure allows for the intercalation of ions and molecules into the interlayer space.

The study of the temperature dependence of the saturated vapour pressure by means of optical-tensimetric methods in combination with the results of differential thermal analysis allowed constructing the *P-T-x* diagram of the Sn – P system. The coordinates of four-phase equilibria points: of the synthetic ($SSn_4P_3 + V + L_1 + L_2$) and eutectic ($L + V + Sn_4P_3 + SnP_3$) types were determined. It was shown that the Sn_3P_4 intermediate phase is only formed as a result of prolonged annealing of samples at a temperature below 673 K. The annealing of the Sn_3P_4 sample obtained by the two-temperature method at a temperature of 753–773 K leads to its complete decomposition into the adjacent phases, Sn_4P_3 and SnP_3. The detection of the $L \leftrightarrow Sn_4P_3 + SnP_3$ eutectic equilibrium ($T \approx 824$ K) in the Sn – P binary system suggests a significant difference of the obtained *T-x* diagram from the data available in the literature.

2. Compounds of the $A^{IV}B^{V}$ class are characterised by a similarity in the nearest atom coordination in compounds to their coordination

in simple substances. Thus, the structural motif of the anion former has a great impact on the crystal-chemical structure of phases. As a consequence, solid solutions are quite easily formed in ternary systems based on $A^{IV}B^{V}$ compounds with anionic substitution, while in the case of cation substitution, even prolonged homogenising annealing does not result in a noticeable region of solid phase solubility. Solid solutions are formed quite easily in Ge – As – P and Si – As – PGe systems, however, due to the different crystal-chemical structures of silicon phosphide and arsenide, the latter system has a heterogeneous region corresponding to the joint presence of the component-based solid solutions.

The Sn–As–P ternary system has a continuous series of solid solutions between tin phosphide and arsenide with the composition of Sn_4B_3 (α-solid solution). The *T-x* diagram of the Sn_4P_3–Sn_4As_3 polythermal cross section was constructed. The peritectic melting of tin arsenide and the decomposition of Sn_4P_3 by a synthetic schema resulted in three-phase regions in the diagram (Sn_4P_3 + SnAs + L) and (Sn_4P_3 + L_1 + L_2). The examination of a number of polythermal cross sections of the Sn–As–P system showed the existence of extended regions of solid phase solubility based on tin monoarsenide β-solid solutions) and the SnP_3 phase (γ-solid solutions).

Available data on phase diagrams make it easy to outline methods for growing single crystals of intermediate phases of solid solutions with set compositions and, therefore, with set properties in the A^{IV} – B^{V} and A^{IV} – B^{V} – C^{V} systems.

3. Physico-chemical foundations for a new manometric method to determine *P T x* diagrams of binary systems by using an auxiliary component (AC) were developed. The requirements for the AC and heterophase equilibria were formulated. The thermodynamic analysis of a number of systems established that the tensimetric study of equilibria with the participation of an AC can be used: *a)* to construct phase diagrams of binary systems; *b*) to scan homogeneity ranges; *c)* to calculate chemical potentials of the components; *d*) to determine integral thermodynamic properties. The validity of these conclusions was confirmed by experimental manometric research and the construction of phase diagrams of the Ga – Se, Ga – S, In – S binary systems. *T-x* and p_i-*T* μ_{Ga}-*T*-diagrams of these systems were determined. Integral thermodynamic characteristics of gallium monochalcogenides, GaS and GaSe, were calculated.

4. New types of diagrams ($K_P^{\#}$ – T, $K_P^{\#}$ – T – *x*) were proposed and determined for the Ga-Se-I and Ga-S-I systems which provide a basis for determining the conditions of the nonstoichiometry regulation by means of selective CTRs and are used to specify the boundaries of the homogeneity ranges of the binary phases. The homogeneity ranges of gallium monoselenide and monosulphide were determined. It was found that the data are consistent when different components (Cl, I) in **different** phase relations are used in the systems (the method of "the AC only in vapour" and "the method of gas solubility").

5. Tensimetric experiments **without the participation of the AC** were used to study phase diagrams and homogeneity ranges of the intermediate phases in the Si As and Ge As systems. Phase diagrams of silicon and germanium arsenides were compared with previously constructed diagrams of gallium and indium monochalcogenides based on the similarity of structures and the nature of chemical bonds in these groups of compounds. It was revealed that the following important peculiarity is common for the homogeneity ranges of these compounds: narrow over the entire range of temperatures homogeneity ranges of this compounds have sharp (up to a few percent) extensions in areas close to the maximum temperatures of phase melting. Such an extension in case of GaSe leads to the formation of a retrograde solidus in a narrow temperature range (~ 60 K). For germanium diarsenides such expansion of the homogeneity range (up to 1.8 mol% of As) occurs in an even smaller temperature range. A hypothesis was made according to which the peculiarities of homogeneity ranges of the considered layered phases similar in terms of structure are related to the formation of interlayer interstitial defects (i.e. autointercalation) at premelting temperatures.

6. A new method for nonstoichiometry regulation was developed and applied using non-destructive selective chemical transport reactions (i.e. with the participation of the AC). The method is based on the introduction or removal of one of the sample components by means of a selective

chemical transport reaction conducted in the **iso-** or **non-iso**thermal conditions. It was shown theoretically and experimentally that the direction of selective mass transfer, the introduction or removal of a component from the sample, is only determined by three parameters: temperatures (T_2, T_1) which *the sample* and *the batch* are exposed to (a donor or a getter of the component chemically transferred through the gas), and the batch composition (x_1). Transport stops when *stationary states* are achieved. What is more, the composition of the regulated sample (x_2) is determined by the same three parameters (T_2, T_1, x_1).

7. The method of selective chemical transport reactions was used to develop and apply a new method of directed synthesis of materials with the high reactivity based on the intermetallides of the GaNi system. It was shown that it is possible to increase the efficiency of the catalytic activity of such disturbed metals by introducing directly into the reaction process activator additives (n-C_4H_9Cl, NH_4Cl) which remove the residues of the activating component (Ga) from the material.

8. The new method of spectrophotometric studies based on the AC (hydrogen) equilibria quenching with indium sulphides was used to study the phase diagram of the InS system. It was proved that between the $In_{3-x}S_4$ and In_2S_3' phases (low-temperature modification) there is a narrow heterogeneous range which is limited from above by the temperature of the peritectic decomposition of the In_2S_3' phase (415 °C). The $In_{3-x}S_4$ homogeneity range extends from about ~58.0 mol% of S to ~59.9 mol% and is not particularly dependent on temperature (at $T \leqslant 725$ °C). A tendency to the decomposition of solid solutions based on the $In_{3x}S_4$ phase with extended homogeneity with a spinel structure was shown. Temperature dependences of sulphur vapour pressure (S_2) were determined in the equilibria of different nature with the participation of condensed indium sulphides. It was established that there is a good correlation between the results of spectrophotometric studies within the developed methodology and the mass spectrometric data.

9. As a result of applying the new *in situ* spectrophotometric method which involved using gallium iodides as an AC, and as a result of high-temperature X-ray studies, it was established that at temperatures below 825 °C the Ga – S system does not have intermediate solid phases but GaS and Ga_2S_3. In contrast, the high-temperature portion of the diagram of the Ga – S system is complex and comprises of two more phases with stoichiometries from 59 to 60 mol%.

We would like to conclude the review by mentioning the contributions of a number of employees involved in this collective work. An enormous contribution was made by the closest colleague of Ya. A. Ugai, Evgeny G. Goncharov. It is difficult to overestimate the importance of the contribution of the prematurely deceased A. E. Popov, whose works largely determined the achievements of the employees that surrounded him in the late 1980s - early 1990s. We would like to mention the works by the employees of the Faculty of Chemistry of Voronezh State University, T. P. Sushkova, A. V. Kosyakov, A. V. Naumov, E. Yu. Proskurina, and D. N. Turchen. Without the contributions of these professionals it would have been impossible to get the results presented herein. However, it has to be mentioned that all of these specialists worked in the direction laid by the founder of the scientific school, Ya. A. Ugai.

Author contributions

All authors made an equivalent contribution to the preparation of the publication

Conflict of interests

The authors declare that they have no known competing financial interests or personal relationships that could have influenced the work reported in this paper.

References

1. http://www.science.vsu.ru/resources/schools/ugai.pdf

2. Olesinski R. W., Abbaschian G. J. *Bulletin of Alloy Phase Diagrams*. 1985;6(3): 250–254. https://doi.org/10.1007/bf02880409

3. Massalski T. B. *Binary alloy phase diagrams*. ASM International: 1986; p. 187.

4. Miller L., Kannewurf C.R. Optical properties of single crystal silicon arsenides. *Journal of Physics and Chemistry of Solids*. 1970;31(4): 849–855. https://doi.org/10.1016/0022-3697(70)90218-0

5. Rau J. W., Kannewurf C. R. Optical absorption, reflectivity and electrical conductivity in GeAs. *Physical Review B*. 1977;3(8): 2581–2587. https://doi.org/10.1103/physrevb.3.2581

6. Ugai Ya. A., Gladyshev N. F., Goncharov E. G. Tenzimetricheskoe issledovanie sistemy Ge-As [Tensimetric study of the Ge-As system]. *Russian Journal of Inorganic*

Chemistry. 1978;23(4): 1065–1068. Available at: https://www.elibrary.ru/item.asp?id=29096579 (In Russ.)

7. Goncharov E. G., Gladyshev N. F., Ugai Ya. A. Fiziko-khimicheskaya priroda promezhutochnykh faz v sisteme germanii – mysh'yak [Physicochemical nature of intermediate phases in the germanium - arsenic system]. *Russian Journal of Inorganic Chemistry*. 1977;22(7): 1951–1956. Available at: https://www.elibrary.ru/item.asp?id=29091830 (In Russ.)

8. Ugai Ya. A., Miroshnichenko S. N., Goncharov E. G. Issledovanie *R-T-x* diagrammy sistemy Si-As [Study of the *P-T-x* diagram of the Si-As system]. *Izvestiya AN SSSR. Neorganicheskie materialy (Inorganic Materials)*. 1974;10(10): 174-1777. Available at: https://www.elibrary.ru/item.asp?id=29085699 (In Russ.)

9. Popov A. E., Zavrazhnov A. Yu., Averbakh E. M., Goncharov E. G. P-T-x diagramma diarsenida kremniya [P-T-x diagram of silicon diarsenide]. *Inorganic Materials*. 1993;29(11): 1458–1461. Available at: https://www.elibrary.ru/item.asp?id=29109931 (In Russ.)

10. Ugai Ya. A., Sokolov L. I., Goncharov E. G., Makarov V. S. R-T-x diagramma sostoyaniya i termodinamika fazovykh ravnovesii v sisteme kremnii – fosfor [P-T-x state diagram and thermodynamics of phase equilibria in the silicon - phosphorus system]. *Inorganic Materials*. 1987;32(5): 1198-1200. Available at: https://www.elibrary.ru/item.asp?id=29121653 (In Russ.)

11. Ugai Y. A., Semenova G. V., Sokolov L. I., Goncharov E. G. Thermal dissociation of silicon monophosphide. *Russian Journal of Inorganic Chemistry*. 1987;32(6): 875–877.

12. Ugai Ya. A., Sokolov L. I., Goncharov E. G. Termograficheskoe issledovanie razreza sistemy Ge-P-Pb [Thermographic study of the Ge-P-Pb system section]. *Izvestiya AN SSSR. Neorganicheskie materialy (Inorganic Materials*). 1973;9(8): 1445–1447. Available at: https://www.elibrary.ru/item.asp?id=29085659 (In Russ.)

13. Goncharov E. G., Sokolov L. I., Ugai Ya. A. Diagramma sostoyaniya i nekotorye termodinamicheskie parametry sistemy Ge-P [P-T-x diagram of the state of the Ge-P system]. *Russian Journal of Inorganic Chemistry*. 1975;20(9): 2452–2454. Available at: https://www.elibrary.ru/item.asp?id=29085724 (In Russ.)

14. Ugai Ya. A., Sokolov L. I., Goncharov E. G., Pshestanchik V. R. P-T-x diagramma sostoyaniya sistemy Ge-P i termodinamika vzaimodeistviya komponentov [P-T-x diagram of the state of the Ge-P system and the thermodynamics of the interaction of the components]. *Russian Journal of Inorganic Chemistry*. 1978;23(7): 1907–1911. Available at: https://www.elibrary.ru/item.asp?id=29096578 (In Russ.)

15. Ugai Ya. A., Popov A. E., Goncharov E. G. Oblast' gomogennosti arsenida germaniya [Homogeneity region of germanium arsenide]. *Russian Journal of Inorganic Chemistry*. 1982;27(7): 1782–1787. Available at: https://www.elibrary.ru/item.asp?id=29096104 (In Russ.)

16. Zavrazhnov A. Yu., Turchen D. N., Goncharov E. G., Fedorova M. V. P-T-X phase diagram of the Ge-As system near germanium diarsenide. *Inorganic Materials*. 1998;34(7): 637–641.

17. Ugai Ya. A., Popov A. E., Goncharov E. G., Lukin A. N., Samoilov A. M. Elektrofizicheskie svoistva i oblast' gomogennosti arsenida germaniya [Electrophysical properties and homogeneity region of germanium arsenide]. *Izvestiya AN SSSR. Neorganicheskie materialy (Inorganic Materials)*. 1983;19(2): 190–192. Available at: https://www.elibrary.ru/item.asp?id=29095704 (In Russ.)

18. Goncharov E. G., Popov A. E., Zavrazhnov A. Yu. Poluprovodnikovye fosfidy i arsenidy kremniya i germaniya [Semiconductor phosphides and arsenides of silicon and germanium]. *Inorganic Materials*. 1995;31(5): 579–591. Available at: https://www.elibrary.ru/item.asp?id=29113633 (In Russ.)

19. Lukin A. N. Elektricheskie svoistva monoklinnykh kristallov gruppy $A^{IV}B^{V}$. *Fiziko-khimicheskie protsessy v poluprovodnikakh i na ikh poverkhnosti* [Electrical properties of monoclinic crystals of the AIVBV group. In: *Physicochemical processes in semiconductors and on their surfaces* / Collection of articles]. Voronezh: VSU Publ.; 1981. p. 148–151. (In Russ.)

20. Lukin A. N., Sokolov L. I., Kavetskii V. S. Elektrofizicheskie i opticheskie svoistva fosfida germaniya. *Khimiya i tekhnologiya fosfidov i fosforosoderzhashchikh splavov* [Electrophysical and optical properties of germanium phosphide. In: *Chemistry and technology of phosphides and phosphorus-containing alloys* / Collection of articles] Kiev: 1979. p. 133–135. (In Russ.)

21. Schmetterer C. Interaction of Sn-based sSolders with Ni(P)-Substrates: The Ni–P, P–Sn and Ni–P–Sn phase diagrams: Diss. Dr. rer. Nat. Wien: 2009. 143 p.

22. Schmetterer C., Ganesan R. Ipser H. Interaction of Sn-based solders with Ni(P) substrates: phase equilibria and thermochemistry. In*: Lead-Free Solders: Materials Reliability for Electronics*. 2012. p. 71–118. https://doi.org/10.1002/9781119966203.ch4

23. Shevelkov A. V. Thermoelectric materials: an introduction. *Dalton Trans*. 2010;39(4): 977–977. https://doi.org/10.1039/b924863n

24. Hashimoto K., Kato Z., Kumagai N., Kamio K., Hirose K. Sn – P alloys for rapid and stable production of tin solution for tin plating. *ECS Transactions*. 2006;1(4): 525–532. https://doi.org/10.1149/1.2215536

25. Kim Y., Hwang H., Yoon C. S., Kim M. G., Cho J. Reversible lithium intercalation in teardrop-shaped ultrafine $SnP_{0.94}$ particles: anode material for lithium-ion batteries. *Advanced Materials*. 2007;19(1): 92-96. https://doi.org/10.1002/adma.200600644

26. Kim Y., Kim Y., Choi A., Woo S., Mok D., Choi N.-S., … Lee K. T. Tin phosphide as a promising anode material for Na-ion Batteries. *Advanced Materials*. 2014;26(24): 4139-4145. https://doi.org/10.1002/adma.201305638

27. Liu S., Zhang H., Xu L., Ma L. Synthesis of hollow spherical tin phosphides (Sn_4P_3) and their high adsorp-

tive and electrochemical performance. *Journal of Crystal Growt*. 2016;438: 31–37. https://doi.org/10.1016/j.jcrysgro.2015.12.018

28. Liu S., Zhang H., Xu L., Ma L. Solvothermal preparation of tin phosphide as a long-life anode for advanced lithium and sodium ion batteries. *Journal of Power Sources*. 2016;304: 346–353. https://doi.org/10.1016/j.jpowsour.2015.11.056

29. Ueda A., Nagao M., Inoue A., et al. Electrochemical performance of all-solid-state lithium batteries with Sn_4P_3 negative electrode. *Journal of Power Sources*. 2013;244: 597–600. https://doi.org/10.1016/j.jpowsour.2013.01.061

30. Liu S., Li S., Li M., Yan L., Li H. Synthesis of tin phosphides (Sn_4P_3) and their high photocatalytic activities. *New Journal of Chemistry*. 2013;37(3): 827–833. https://doi.org/10.1039/C2NJ41068K

31. Usui H., Sakata T., Shimizu M., Sakaguchi H. Electrochemical Na-insertion/extraction properties of Sn–P anodes. *Electrochemistry*. 2015;83(10): 810–812. https://doi.org/10.5796/electrochemistry.83.810

32. Doh C. VASP calculation on lithium reaction to tin phosphides. In: *ECS Meeting Abstracts***.** 2014. 255 p. https://doi.org/10.1149/ma2014-01/2/255

33. Vivian A. C. The tin-phosphorus system. *Journal of the Institute of Metals*. 1920;23: 325–336.

34. Sushkova T. P., Kononova E. Yu., Savinova Yu. A., Dorokhina E. S., Semenova G. V. Intermediate phases in Sn - P system. *Kondensirovannye sredy i mezhfaznye granitsy = Condensed Matter and Interphases*. 2014;16(1): 210–214. Available at: https://www.elibrary.ru/item.asp?id=21785802 (In Russ., abstract in Eng.)

35. Proskurina E. Yu., Semenova G. V., Zavrazhnov A. Yu., Kosyakov A. V. P-T-x diagram of Sn - P system. Condensed media and interphase boundaries. 2015;17(4): 498–509. Available at: https://www.elibrary.ru/item.asp?id=25946590 (In Russ., abstract in Eng.)

36. Sushkova T. P., Proskurina E. Yu., Semenova G. V., Zavrazhnov A. Yu. Thermal stability of tin monophosphide. In: *Science and Education: materials of the XI international research and practice conference*. Apr. 6^{th} – 7^{th}, 2016. Munich (Germany): 2016;1: 40–45.

37. Semenova G. V., Proskurina E. Yu., Sushkova T. P. T-x diagram of the Sn - P system. In: *XX Mendeleev Congress on General and Applied Chemistry. Fundamental problems of chemical science*. Abstracts. vol. 1. September 26-30, 2016. Yekaterinburg: 2016. p. 480. (In Russ.)

38. Zavrazhnov A. Yu., Semenova G. V., Proskurina E. Yu., Sushkova T. P. Phase diagram of the Sn - P system. In: *4th Central and Eastern European Conference on Thermal Analysis and Calorimetry (CEEC-TAC4)*. Abstracts. 28 - 31 August, 2017. Kishinev: 2017. p. 346.

39. Zavrazhnov A. Yu., Semenova G. V., Proskurina E. Yu., Sushkova T. P. Phase diagram of the Sn - P system. *Journal of Thermal Analysis and Calorimetry*. 2018;134(1): 475–481. https://doi.org/10.1007/s10973-018-7123-0

40. Shevelyuhina A. V., Semenova G. V., Sushkova T. P. Phase diagram of the Sn – P system at concentration of phosphorus over 70 mol%. In: *XVI International Conference on Thermal Analysis and Calorimetry* (RTAC). Abstracts. 6 July 2020, Moscow (Russia). Moscow: 2020. p. 194.

41. Guo J., Liu Y., Ma Y., Zhu E., Lee S., Lu Z., … Duan X. Few-layer GeAs field-effect transistors and infrared. *Advanced Materials*. 2018;30(21): 1705934. https://doi.org/10.1002/adma.201705934

42. Lee K., Synnestvedt S., Bellard M., Kovnir K. GeP and $(Ge_{1-x}Sn_x)(P_{1-y}Ge_y)$ (x ≈ 0.12, y ≈ 0.05): Synthesis, structure, and properties of two-dimensional layered tetrel phosphides. *ChemInform*. 2015;46(18): 62–70. https://doi.org/10.1002/chin.201518016

43. Lee K., Kamali S., Ericsson T., Bellard M., Kovnir K. GeAs: Highly anisotropic van der Waals thermoelectric material. *Chemistry of Materials*. 2016;28(8): 2776–2785. https://doi.org/10.1021/acs.chemmater.6b00567

44. Pomerantseva E., Resini C., Kovnir K., Kolen'ko Yu. Emerging nanostructured electrode materials for water electrolysis and rechargeable beyond Li-ion batteries. *Advances in Physics: X*. 2017;2 (2): 211–253. https://doi.org/10.1080/23746149.2016.1273796

45. Zhao T., Sun Y., Shuai Z., Wang D. $GeAs_2$: A IV–V group two-dimensional semiconductor with ultralow thermal conductivity and high thermoelectric efficiency. *Chemistry of Materials*. 2017;29(15): 6261–6268. https://doi.org/10.1021/acs.chemmater.7b01343

46. Proskurina E. Yu., Semenova G. V., Sushkova T. P. Phase equilibria in the Ge-As-Bi system. *Proceedings of Voronezh State University. Series: Chemistry. Biology. Pharmacy*. 2018;4: 27–34. Available at: https://www.elibrary.ru/item.asp?id=36664319 (In Russ., abstract in Eng.)

47. Semenova G. V., Kononova E. Yu., Sushkova T. P. Polythermal section Ge-SnAs of the Sn-As-Ge system. *Russian Journal of Inorganic Chemistry*. 2014;59(12): 1517-1521. https://doi.org/10.1134/s0036023614120225

48. Semenova G. V., Sushkova T. P., Proskurina E. Yu. Polythermal section Sn - GeAs of the Sn - As - Ge system. *Proceedings of Voronezh State University. Series: Chemistry. Biology. Pharmacy*. 2015;1: 49–53. Available at: https://www.elibrary.ru/item.asp?id=23478462 (In Russ., abstract in Eng.)

49. Proskurina E. Yu., Semenova G. V., Sushkova T. P. Topological scheme of phase equilibria in the Sn - As - Ge system. *Kondensirovannye sredy i mezhfaznye granitsy = Condensed Matter and Interphases*. 2016;18(2): 241–247. Available at: https://www.elibrary.ru/item.asp?id=26023376 (In Russ., abstract in Eng.)

50. Proskurina E. Yu., Makagonov V. A, Semenova G. V., Sushkova T. P. Alloying with tin of the germanium monoarsenide. *Proceedings of Voronezh State University. Series: Chemistry. Biology. Pharmacy*. 2018;2: 41–47. Available at: https://www.elibrary.ru/item.asp?id=35350430 (In Russ., abstract in Eng.)

51. Semenova G., Proskurina E., Sushkova T., Semenov V. Phase diagram of the Sn–As–Ge system. *Acta*

Chimica Slovenica. 2018;65(3): 662–669. https://doi.org/10.17344/acsi.2018.4333

52. Semenova G. V., Zabakhidze G. E., Goncharov E. G. Polythermal section SiAs-GeAs. *Russian Journal of Inorganic Chemistry*. 1997;42(10): 1596–1597.

53. Semenova G. V., Zabakhidze G. E., Goncharov E. G. Analysis of phase equilibria in the Si-Ge-As system. *Russian Journal of Inorganic Chemistry*. 1998;43(9): 1435–1437.

54. Ugai Ya. A., Muravyova S. N., Goncharov E. G. Diagramma sostoyaniya sistemy GeAs-GeP [State diagram of the GeAs-GeP system]. *Izvestiya AN SSSR. Neorganicheskie materialy (Inorganic Materials)*. 1972;8(9): 1665–1666. (In Russ.)

55. Meshchaninova L. N., Goncharov E. G., Ugai Ya. A. R-T-x diagramma sostoyaniya sistemy SiAs-SiP [P-T-x state diagram of the SiAs-SiP system]. *Russian Journal of Inorganic Chemistry*. 1980;25(11): 3084–3088. Available at: https://www.elibrary.ru/item.asp?id=29096734 (In Russ.)

56. Ugai Ya. A., Goncharov E. G., Semenova G. V., Lazarev V. B. *Fazovye ravnovesiya mezhdu fosforom, mysh'yakom, sur'moi i vismutom* [Phase equilibria between phosphorus, arsenic, antimony and bismuth]. Moscow: Nauka Publ.; 1989. 233 p. (In Russ.)

57. Ugai Ya. A., Semenova G. V., Goncharov E. G. P-T-x diagramma sostoyaniya sistemy sur'ma - mysh'yak [P-T-x diagram of the state of the antimony - arsenic system]. *Russian Journal of Inorganic Chemistry*. 1985;30(6): 1532–1535. Available at: https://www.elibrary.ru/item.asp?id=28991560 (In Russ.)

58. Ugai Ya. A., Semenova G. V., Samoilov A. M., Goncharov E. G. Analiz fazovykh ravnovesii v sisteme Sb – As [Analysis of phase equilibria in the Sb - As system]. *Izvestiya AN SSSR. Neorganicheskie materialy (Inorganic Materials)*. 1987;23(9): 1434–1437. Available at: https://www.elibrary.ru/item.asp?id=29030335 (In Russ.)

59. Ugai Ya. A., Semenova G. V., Goncharov E. G., Berendt E. Issledovanie P-T-x diagrammy sistemy fosfor - mysh'yak ekstrapolyatsionnym metodom [Study of the P-T-x diagram of the phosphorus – arsenic system by the extrapolation method]. *Russian Journal of Inorganic Chemistry*. 1979;24(12): 3344–3346. Available at: https://www.elibrary.ru/item.asp?id=28999582 (In Russ.)

60. Ugai Ya. A., Semenova G. V., Goncharov E. G. Raschet sostava para v sisteme fosfor - mysh'yak [Calculation of the composition of steam in the phosphorus - arsenic system]. *Russian Journal of Physical Chemistry A*. 1979;53(4): 1019–1020. Available at: https://www.elibrary.ru/item.asp?id=28998458 (In Russ.)

61. Ugai Ya. A., Semenova G. V., Goncharov E. G. Termodinamicheskii analiz fazovykh ravnovesii v sisteme fosfor - mysh'yak [Thermodynamic analysis of phase equilibria in the phosphorus - arsenic system]. *Russian Journal of Physical Chemistry A*. 1986;60(12): 2952–2954. Available at: https://www.elibrary.ru/item.asp?id=29003620 (In Russ.)

62. Krebs H., Weitz H., Worms K. H. Uber die strukture und eigenschaften der halbmetalls. *Zeitschrift for anorganische und allgemeine Chemie*. 1955;280(1/3): 119–133. https://doi.org/10.1002/zaac.19552800110

63. Krebs H., Holz W., Worms K. H. Eine neue rhombische arsen modifikation und ihre mischkristallbildunf mit schwarzen phosphor. *Chemische Berichte*. 1957;90(6): 1031–1037. https://doi.org/10.1002/cber.19570900624

64. Pang J., Bachmatiuk A., Yin Y., Trzebicka B. Applications of phosphorene and black phosphorus in energy conversion and storage devices. *Advanced Energy Materials*. 2018;8(8): 1702093. https://doi.org/10.1002/aenm.201702093

65. Zeng J., Cui P., Zhang Z. Half layer by half layer growth of a blue phosphorene monolayer on a GaN(001) substrate. *Physical Review Letters*. 2017;118(4): 46101. https://doi.org/10.1103/PhysRevLett.118.046101

66. Niu T. New properties with old materials: Layered black phosphorous. *Nano Today*. 2017;12: 7–9. https://doi.org/10.1016/j.nantod.2016.08.013

67. Zhu Z., Tománek D. Semiconducting layered blue phosphorus: A computational study. *Physical Review Letters*. 2014;112(17): 176802. https://doi.org/10.1103/PhysRevLett.112.176802

68. Osters O., Nilges T., Bachhuber F., Pielnhofer F, Weihrich R., Schöneich M., Schmidt P. Synthesis and identification of metastable compounds: Black arsenic – science or fiction? *Angewandte Chemie International Edition*. 2012;51(12): 2994–2997. https://doi.org/10.1002/anie.201106479

69. Goncharov E. G., Semenova G. V., Kalyuzhnaya M. I. Termograficheskoe issledovanie fazovoi diagrammy sistemy Ge-As-P [Thermographic study of the phase diagram of the Ge-As-P system]. *Russian Journal of Inorganic Chemistry*. 1992;37(8): 1895–1897. Available at: https://www.elibrary.ru/item.asp?id=29031293 (In Russ.)

70. Semenova G. V., Morozova A. A., Goncharov E. G., Dolgopolova E. A. Ge-As-P system. *Russian Journal of Inorganic Chemistry*. 1997;42(2): 266–268.

71. Semenova G. V., Morozova A. A., Goncharov E. G. Termodinamicheskii analiz R-T-kh- u fazovoi diagrammy sistemy Ge-As-P [Thermodynamic analysis of the P-T-x-y phase diagram of the Ge-As-P system]. *Russian Journal of Inorganic Chemistry*. 1993;38(12): 2023–2025. Available at: https://www.elibrary.ru/item.asp?id=29029850 (In Russ.)

72. Goncharov E. G., Semenova G. V. Kalyuzhnaya M. I., Solov'ev N. E. Politermicheskii razrez SiAs – SiP [Polythermal section SiAs - SiP]. *Russian Journal of Inorganic Chemistry*. 1993;38(4): 709–710. Available at: https://www.elibrary.ru/item.asp?id=29029856 (In Russ.)

73. Semenova G. V., Sushkova T. P., Dolgopolova E. A., Morozova A. A. Tverdye rastvory v sisteme SiAs – SiP [Solid solutions in the SiAs - SiP system]. *Russian Journal of Inorganic Chemistry*. 2003;48(4): 582–584. Available at: https://www.elibrary.ru/item.asp?id=17278755 (In Russ.)

74. Semenova G. V., Morozova A. A., Goncharov E. G. Analiz fazovykh ravnovesii v sisteme Si-As-P [Analysis of phase equilibria in the Si-As-P system]. *Russian Journal of Inorganic Chemistry*. 1995;40(4): 658–660. Available at: https://www.elibrary.ru/item.asp?id=29053410 (In Russ.)

75. Semenova G. V., Goncharov E. G. Tverdye rastvory s uchastiem elementov pyatoi gruppy [Solid solutions with the participation of elements of the fifth group]. Moscow: Izd. MFTI Publ.; 2000. 160 p. (In Russ.)

76. Semenova G. V., Kononova E. Yu., Sushkova T. P. Polythermal section Sn_4P_3-Sn_4As_3. *Russian Journal of Inorganic Chemistry*. 2013;58(9): 1112–1114. https://doi.org/10.1134/S0036023613090192

77. Kononova E. Yu. , Sinyova S. I., Semenova G. V. , Sushkova T. P. Phase equilibria in the Sn–As–Ge and Sn–A–P systems. *Journal of Thermal Analysis and Calorimetry*. 2014;117(3):1171–1177. https://doi.org/10.1007/s10973-014-3883-3

78. Semenova G. V., Sushkova T. P., Zinchenko E. N., Yakunin S. V. Solubility of phosphorus in tin monoarsenide. *Kondensirovannye sredy i mezhfaznye granitsy = Condensed Matter and Interphases*. 2018;20(4): 644–649. https://doi.org/10.17308/kcmf.2018.20/639 (In Russ., abstract in Eng.)

79. Semenova G. V., Sushkova T. P., Tarasova L. A., Proskurina E. Yu. Phase equilibria in a Sn – As – P system with a tin concentrations less than 50 mol%. *Kondensirovannye sredy i mezhfaznye granitsy = Condensed Matter and Interphases*. 2017;19(3): 408–416. https://doi.org/10.17308/kcmf.2017.19/218 (In Russ., abstract in Eng.)

80. Sushkova T. P., Sheveljuhina A. V., Semenova G. V., Proskurina E. Yu. The SnAs–P polythermic section of Sn–As–P ternary system. *Kondensirovannye sredy i mezhfaznye granitsy = Condensed Matter and Interphases*. 2019;21(2): 287–295. https: //doi.org/10.17308 /kcmf.2019.21/766

81. Liu C.-W., Dai J.-J., Wu S.-K., Diep N.-Q., Huynh S.-H., Mai T.-T., … Luc H.-H.. Substrate-induced strain in 2D layered GaSe materials grown by molecular beam epitaxy. *Scientific Reports*. 2020;10(1): 12972. https://doi.org/10.1038/s41598-020-69946-4

82. Zhou X., Cheng J., Zhou Y., Cao T., Hong H., Liao Z., … Yu D. Strong second-harmonic generation in atomic layered GaSe. *Journal of the American Chemical Society*. 2015;137(25): 7994–7997. https://doi.org/10.1021/jacs.5b04305

83. Olmstead M. A., Ohuchi F. S., Group III selenides: Controlling dimensionality, structure, and properties through defects and heteroepitaxial growth. *Journal of Vacuum Science & Technology A*. 2021;39(2): 020801. https://doi.org/10.1116/6.0000598

84. Marvan P., Mazánek V., Sofer Z. Shear-force exfoliation of indium and gallium chalcogenides for selective gas sensing applications. *Nanoscale*. 2019;11(10): 4310–4317 https://doi.org/10.1039/C8NR09294J

85. Woods-Robinson R., Han Y., Zhang H., Ablekim T., Khan I., Persson K. A., Zakutayev A. Wide band gap chalcogenide semiconductors. *Chemical Reviews*. 2020;120(9): 4007–4055. https://doi.org/10.1021/acs.chemrev.9b00600

86. Zavrazhnov A. Yu, Turchen D. N, Goncharov Eu. G., Zlomanov V. P. Manometric method for the study of P-T-X diagrams. *Journal of Phase Equilibria*. 2001;22(4): 482–490. https://doi.org/10.1361/105497101770333063

87. Zavrazhnov A. Yu. Design of P-T-x diagrams for gallium chalcogenides with the use of an ancillary component. *Russian Journal of Inorganic Chemistry*. 2003;48(10): 1577–1590.

88. Kosyakov A. V., Zavrazhnov A. Yu., Naumov A. V., Sergeeva A. S. Specification of the phase diagram of system In-S according to spectrophotometric researches of balance between sulfide of indium and hydrogen. *Proceedings of Voronezh State University. Series: Chemistry. Biology. Pharmacy*. 2009;2: 28–39. Available at: https://www.elibrary.ru/item.asp?id=12992199 (In Russ., abstract in Eng.)

89. Kosyakov A. V., Zavrazhnov A. Y. Naumov A. V . Refinement of the In-S phase diagram using spectrophotometric characterization of equilibria between hydrogen and indium sulfides. *Inorganic Materials*. 2010;46(4): 343–345 (2010). https://doi.org/10.1134/S0020168510040035

90. Zavrazhnov A. Y., Kosyakov A. V., Naumov A. V., Sergeeva A. V., Berezin S. S. Study of the In–S phase diagram using spectrophotometric characterization of equilibria between hydrogen and indium sulfides. *Thermochimica Acta Journal*. 2013;566: 169–174. https://doi.org/10.1016/j.tca.2013.05.031

91. Zavrazhnov A. Y., Turchen D. N., Naumov A. V., Zlomanov V. P. Chemical transport reactions as a new variant of the phase composition control. *Journal of Phase Equilibria*. 2003;24(4): 330–339. https://doi.org/10.1361/105497103770330316

92. Zavrazhnov A. Y., Turchen D. N., Naumov A. V., Zlomanov V. P. Chemical vapor transport as a means of controlling the composition of condensed phases. *Inorganic Materials*. 2004;40(2): 101–127. https://doi.org/10.1007/s10789-005-0056-6

93. Sidei V. I., Naumov A. V, Turchen D. N., Chukichev V. M. Upravlenie sostavom monoselenida galliya v predelakh oblasti gomogennosti i diagnostika nestekhiometrii GaSe [Controlling the composition of gallium monoselenide within the homogeneity region and diagnostics of GaSe nonstoichiometry]. *Kondensirovannye sredy i mezhfaznye granitsy = Condensed Matter and Interphases*. 2004;6(4): 322–325. Available at: https://www.elibrary.ru/item.asp?id=29833369 (In Russ.)

94. Zavrazhnov A. Yu., Zartsyn I. D., Naumov A. V., Zlomanov V. P., Davydov A. V. Composition control of low-volatile solids through chemical vapor transport reactions. I. Theory of selective chemical vapor transport. *Journal of Phase Equilibria and Diffusion*. 2007;28(6): 510–516. https://doi.org/10.1007/s11669-007-9200-0

95. Zavrazhnov A., Naumov A., Sidey V., Pervov V. Composition control of low-volatile solids through

chemical vapor transport reactions. III. The example of gallium monoselenide: Control of the polytypic structure, non-stoichiometry and properties. *Thermochimica Acta Journal*. 2012;527: 118124. https://doi.org/10.1016/j.tca.2011.10.012

96. Zavrazhnov A. Yu., Naumov A., Riazhskikh M., Pervov V. Chemical vapor transport for the control of composition of low-volatile solids: II. The composition control of indium sulfides: Technique of the charge dilution. *Thermochimica Acta Journal*. 2012;532: 96102. https://doi.org/10.1016/j.tca.2010.10.004

97. Zavrazhnov A. Y., Naumov A. V., Sergeeva A. V., Sidey V. I. Selective chemical vapor transport as a means of varying the composition of nonstoichiometric indium sulfides. Inorg Mater 2007;43(11): 1167–1178. https://doi.org/10.1134/S0020168507110039

98. Zavrazhnov A. Yu., Naumov A., Sergeeva A., Semenov V., Pervov V. Novel approach to the design of optoelectronic heterostructures based on copper and indium sulfides. *J. Fudan University (Fudan Xuebao, China)*. 2007;46(5): 730.

99. Kosyakov A. V., Nekrylov I. N., Brezhnev N. Yu., Berezin S. S., Malygina E. N., Zavrazhnov A. Yu. Tx diagram of the Ga - Se system in the composition range from 48.0 to 61.5 % Se according to thermal analysis data. *Kondensirovannye sredy i mezhfaznye granitsy = Condensed Matter and Interphases*. 2019;21(4): 519–527. https://doi.org/10.17308/kcmf.2019.21/2363 (In Russ., abstract in Eng.)

100. Berezin S. S., Berezina M. V., Zavrazhnov A. Y., Kosyakov A. V., Sergeeva A. V., Sidei V. I. Phase transformations of indium mono- and sesquisulfides studied by a novel static thermal analysis technique. *Inorganic Materials*. 2013;49: 555–563. https://doi.org/10.1134/S0020168513060010

101. Berezin S. S., Spesivtseva A. P., Zavrazhnov A. Yu., Okushko A. I. Iron sulfides crystal growth at controlled sulfur pressure with the use of metal-halogenide melts. 2015;17(4): 412–416. Available at: https://www.elibrary.ru/item.asp?id=25946576 (In Russ., abstract in Eng.)

102. Zavrazhnov A. Y., Naumov A., Kosyakov A., Berezin S., Volkov V., Sergeeva A. The iron sulfides crystal growth from the halide melts. *Materials Research*. 2018;21(4): e20170648 . https://doi.org/10.1590/1980-5373-mr-2017-0648

103. Zavrazhnov A., Naumov A., Kosykov A., Kovygin Y. New way of the skeletal metal synthesis. *J. Fudan University (Fudan Xuebao, China)*. 2007;46(5): 786.

104. Kosyakov A. V., Zavrazhnov A. Y., Naumov A. V., Nazarova A. A., Zlomanov V. P. Chemical vapor transport: A viable approach to controlling the composition of intermetallic phases promising for catalyst engineering. *Inorganic Materials*. 2007;43(11): 1199–1205. https://doi.org/10.1134/S0020168507110088

105. Kosyakov A. V., Zavrazhnov A. Yu. Equilibrium in the reaction between nickel or gallium in nickel solid solutions and of with carbon monoxide *Kondensirovannye sredy i mezhfaznye granitsy = Condensed Matter and Interphases*. 2017;19(1): 68–79. Available at: https://www.elibrary.ru/item.asp?id=29033318 (In Russ., abstract in Eng.)

106. Zavrazhnov A. Yu., Kosyakov A. V., Sergeeva A. V., Berezin S. S., Chernenko K. K. High-temperature in situ vapor spectrophotometry as a static variant of tensimetric method equilibria in the Ga-I system. *Kondensirovannye sredy i mezhfaznye granitsy = Condensed Matter and Interphases*. 2015;17(4): 417–436. Available at: https://www.elibrary.ru/item.asp?id=25946578 (In Russ., abstract in Eng.)

107. Zavrazhnov A. Yu., Naumov A. V., Malygina E. N., Kosyakov A. V. Indium monochloride vapor pressure: the vapor-gauge and spectrophotometric experimaental data. *Kondensirovannye sredy i mezhfaznye granitsy = Condensed Matter and Interphases*. 2019;21(1): 60–71. https://doi.org/10.17308/kcmf.2019.21/717

108. Berezin S. S. Fazovye ravnovesiya v sistemakh Fe-S, Ga-S i sintez sul'fidov galliya i zheleza s ispol'zovaniem galogenidov FeX_2 (X≠F) *и* GaI_3. *Diss. Cand. Chem. Sciences* / Voronezh: Voronezh State University; 2018. 239 p. Available at: https://www.dissercat.com/content/fazovye-ravnovesiya-v-sistemakh-fe-s-ga-s-i-sintez-sulfidov-galliya-i-zheleza-s-ispolzovanie (In Russ.).

109. Zavrazhnov A. Y., Berezin S. S., Kosykov A., Naumov A., Berezina M., Brezhnev N. The phase diagram of the Ga–S system in the concentration range of 48.0–60.7 mol%. *Journal of Thermal Analysis and Calorimetry*. 2018;134(1): 483–492 https://doi.org/10.1007/s10973-018-7124-z

110. Volkov V. V., Sidey V. I., Naumov A. V., Nekrylov I. N., Brezhnev N. Yu.; Malygina E. N., Zavrazhnov A. Yu. The cubic high-temperture modification of gallium sulphide (xS = 59 mol%) and the T, x-diagram of the Ga – S system *Kondensirovannye sredy i mezhfaznye granitsy = Condensed Matter and Interphases*. 2019;21(1): 37–50. https://doi.org/10.17308/kcmf.2019.21/715

Information about the authors

Galina V. Semenova, DSc in Chemistry, Professor, Department of General and Inorganic Chemistry, Voronezh State University, Voronezh, Russian Federation; e-mail: semen157@chem.vsu.ru. ORCID iD: htpps://orcid.org/0000-003-3877-985X.

Alexander Yu. Zavrazhnov, DSc in Chemistry, Professor, Department of General and Inorganic Chemistry, Voronezh State University; Voronezh, Russian Federation; e-mail: Alzavr08@rambler.ru. ORCID iD: htpps://orcid.org/ 0000-0003-0241-834X.

Received 24 June 2021; Approved after reviewing 15 July 2021; Accepted 15 August 2021; Published online 25 September 2021.

Translated by Irina Charychanskaya
Edited and proofread by Simon Cox

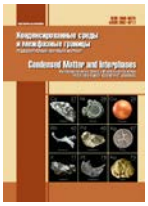

ISSN 1606-867X (Print)
ISSN 2687-0711 (Online)
Condensed Matter and Interphases
Kondensirovannye Sredy i Mezhfaznye Granitsy
https://journals.vsu.ru/kcmf/

Original articles

Research article
https://doi.org/10.17308/kcmf.2021.23/3528

Technological features of the method of liquid-phase epitaxy when growing InP/GaInAsP heterostructures

M. G. Vasil'ev✉, A. M. Vasil'ev, A. D. Izotov✉, Yu. O. Kostin, A. A. Shelyakin

Kurnakov Institute of General and Inorganic Chemistry of the Russian Academy of Sciences,
31 Leninsky prospect, Moscow 119991, Russian Federation

Abstract

Semiconductor devices of quantum electronics based on InP/GaInAsP heterostructures require the creation of non-defective chips for emitting devices and photodetectors. The production of such chips is impossible without a thorough technological study of the growth processes of epitaxial structures. One of the important problems in relation to the growth of such structures is the growth defects associated with the process of dissociation of indium phosphide on the surface during their growth. The aim of the work was the investigation of the process and mechanism of destruction (dissociation) of the surface of indium phosphide substrates in the range of growth temperatures of structures, as well as the study of methods and techniques that allow minimize the process of dissociation of surface of indium phosphide.

The work provides studies of the growth processes of InP/GaInAsP heterostructures, from the liquid phase, taking into account the degradation processes of the growth surface and the mechanisms for the formation of dissociation defects. The schemes of the dissociation process of the InP on the surface of the substrate and the formation of the defective surface of the substrate were analysed. At the same time, technological methods allowing to minimize the dissociation of the surface compound during the process of liquid-phase epitaxy were shown. The original design of a graphite cassette allowing to minimize the dissociation of the indium phosphide substrate in the process of liquid-phase epitaxy was proposed.

Keywords: Heterostructures, Growth defects, Laser diodes, Indium phosphide, Buried heterostructures, Channel in the substrate

Acknowledgements: the work was supported by the Ministry of Science and Higher Education of Russia as part of the state assignment of Kurnakov Institute of General and Inorganic Chemistry of the Russian Academy of Sciences.

For citation: Vasil'ev M. G., Vasil'ev A. M., Izotov A. D., Kostin Yu. O., Shelyakin A. A. Technological features of the method of liquid-phase epitaxy when growing InP/GaInAsP heterostructures. *Kondensirovannye sredy i mezhfaznye granitsy = Condensed Matter and Interphases*. 2021; 23 (3): 374–379. https://doi.org/10.17308/kcmf.2021.23/3528

Для цитирования: Васильев М. Г., Васильев А. М., Изотов А. Д., Костин Ю. О., Шелякин А. А. Технологические особенности метода жидкофазной эпитаксии при выращивании гетероструктур InP/GaInAsP. *Конденсированные среды и межфазные границы*. 2021;23(3): 374–379. https://doi.org/10.17308/kcmf.2021.23/3528

✉ Mikhail G. Vasil'ev, e-mail: mgvas@igic.ras.ru
✉ Alexander D. Izotov, e-mail: izotov@igic.ras.ru
© Vasiliev M. G., Vasiliev A.M., Izotov A.D., Kostin Yu. O., Shelyakin A.A., 2021.

The content is available under Creative Commons Attribution 4.0 License.

1. Introduction

The process of liquid-phase epitaxial growth is a heterogeneous process occurring at the liquid-solid interface. The analysis of the conditions of contact between the substrate and the nonequilibrium liquid or gas phase [1–3] indicates the complexity of the contact phenomena occurring at the interface. In this regard, the preparation of indium phosphide substrates for epitaxial growth can be of decisive importance for the growth of structures [4, 5] required for manufacturing of devices of quantum electronics. InGaAsP solid solutions are widely used for the production of devices for quantum electronics, laser diodes, superluminescent radiation sources, and photodetectors [6-10]. The main area of application of these devices is systems for transmitting optical signals through quartz fiber [11, 12], fiber-optic sensors for environmental monitoring [12, 13], optical coherence tomography [14, 15], navigation and instrumentation systems [16, 17]. The creation of such devices requires the production of high-quality epitaxial layers of InP/GaInAsP heterostructures on indium phosphide substrates, which, in turn, makes it necessary to pay special attention to the quality of the growth surface of the substrates before epitaxial growth. Such structures are mainly grown as isoperiodic on InP. Particular attention should be paid to the state of the initial InP substrate before and during the liquid-phase epitaxy process in the temperature range of 675–600 °C. Due to the fact that indium phosphide contains a highly volatile phosphorus component in its composition, epitaxial growth leads to dissociation of the substrate with the appearance of characteristic defects in the form of faceted depressions with indium drops (Fig. 1). In the course of epitaxial growth, these defects grow into the epitaxial structure, which leads to the low quality of the manufactured devices.

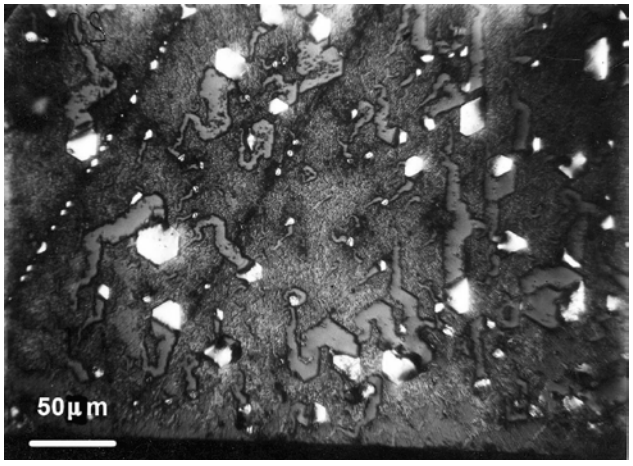

Fig. 1. Dissociation of the indium phosphide on the surface of the plate

The aim of this study was the investigation of the process and mechanism of destruction (dissociation) of the surface of indium phosphide substrates in the temperature range of growth of structures, as well as the study of methods and techniques allowing to minimize the process of dissociation of the surface of indium phosphide.

2. Experimental

Microscopic studies prove the existence of the effect of solution-melt dissolution (SMD) of the indium phosphide substrate during the growth of InP and InGaAsP epitaxial layers by liquid-phase epitaxy (LPE). The SMD effect can manifest itself in the form of depressions with In droplets or grooves with In droplets on the surface of both InP substrates and on layers grown in the InP/InGaAsP system. Subsequently, this effect negatively affects the production of layers in InP/InGaAsP heterostructures. The process of creating semiconductor chips for laser diodes, photodiodes and light-emitting diodes includes the operations required for the application of dielectric masking coatings. Dielectric coatings are used in the manufacture of strip-line laser diodes [18]. It is known [19] that the intensification of phosphate formation on the InP surface leads to the formation of nanosized dielectric films, the resistivity of which reaches 10^{10} Ohm· cm, which sharply reduces the leakage currents through the insulating film and leads to an increase in the quantum efficiency of laser diode radiation and a decrease in dark currents in photodiodes based on InP/GaInAsP heterostructures.

In this regard, it becomes obvious that the surface quality of the grown InP/GaInAsP epitaxial heterostructures becomes decisive in the design of chips for devices.

The formation of a multilayer heterostructure in the InP/InGaAsP system by LPE method starts with an increase in the temperature inside the quartz reactor to 675 °C in an atmosphere of H_2. The substrate is located in a graphite cassette (Fig. 2)

Fig. 2. Graphite cassette for growing layers on InP/InGaAsP on InP substrates

in a substrate holder. The rise in temperature in the range of 600-675 °C occurs in 10 minutes. Then, for 30 minutes, exposure at 675 °C and the onset of a isothermal mode are performed. Then, for 20 minutes, cooling by 10-15 degrees to the onset of growth, which is a temperature of 660 °C. The substrate is kept at an elevated temperature for ~1 hour in an atmosphere of dry H_2 with a dew point of –80 °C.

The InP compound has a crystal structure of the sphalerite type, in the lattice of which, due to the alternation of two types of atoms, there is no inversion symmetry. This leads to the fact that in crystals with the <111> directions axes are polar, which in turn leads to a difference between the A (111) and B (111) planes. The {111} crystallographic plane consists of two geometric planes, each of which contains atoms of only one type, as a result of which atoms of either 3 or 5 groups emerge on the outer surface of the crystallographic planes. Atoms of group 5 (surface B) use only three of the available five valence electrons for the formation of bonds with the lattice and thus have two electrons capable of interacting with particles of the outer phase. Group 3 atoms of surface A use all three valence electrons for the formation of bonds with the lattice. In this regard, B surfaces are more reactive than A surfaces, which leads to the dissociation of indium phosphide during epitaxial growth processes.

The dissociation process is shown in Fig. 3. In the course of experimental work on the growth of heterostructures, we discovered that the formation and movement of an indium drop occurs in a certain direction. In this case, the depression or groove is faceted by the {111} A and {111} B planes simultaneously. In practice, after high-temperature exposure, the substrate is covered with a micro-profile in the form of etching pits resulting from the dissociation of indium phosphide. The effect of the formation of a depression or groove at an elevated temperature as a result of the loss of phosphorus by the surface and the release of a drop of indium will be called the solution-melt dissolution "SMD" effect. The "SMD" effect is shown schematically in Fig. 4. Studies carried out in [20] showed that the {001} A and {111} B planes will grow at a rate of 0.2 μm/°C and 0.4 μm/°C, respectively, and the {111} A plane will grow only at a rate of 0.1 μm/°C. Thus, planes {111} A will prevent the overgrowing of depressions and grooves and facet them along the entire thickness of the grown layer. In this case, from one depression or one groove, two depressions located symmetrically against each other, will be formed (Fig. 5). This is shown schematically in Fig. 6.

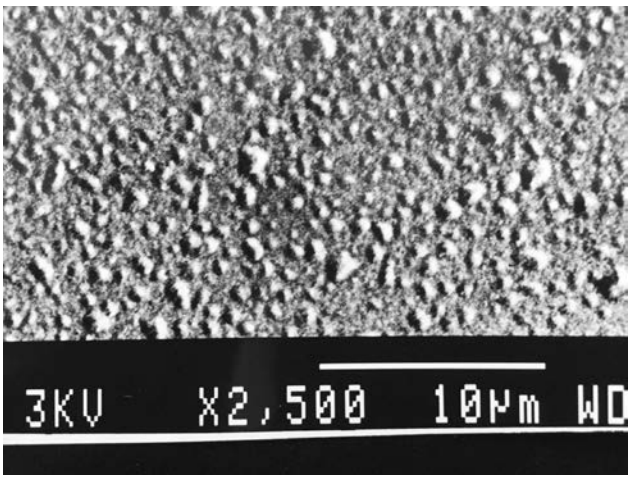

Fig. 3. Indium drops on the surface of InP substrate

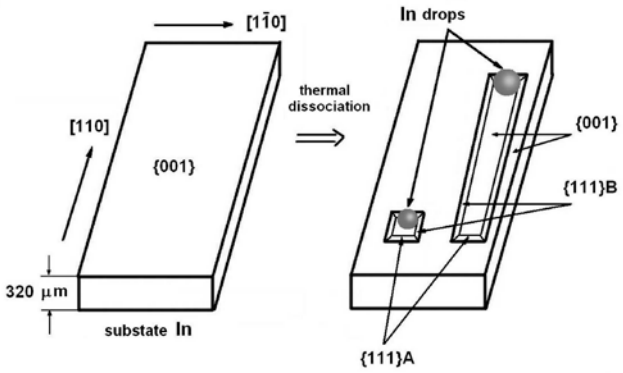

Fig. 4. Scheme of the dissociation of InP on the surface of the substrate

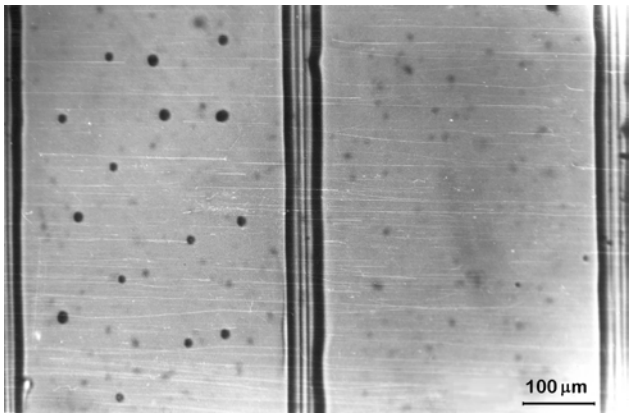

Fig. 5. Growing of InP buffer layer on the surface of the substrate, with dissociation traces

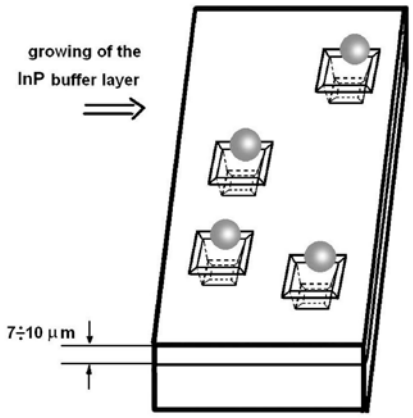

Fig. 6. Scheme of the formation of depressions in the process of growing the InP buffer layer

In order to eliminate the "SMD" effect, a number of technological methods were proposed:

– a decrease in the growth temperature of growing epitaxial heterostructures in the InP/InGaAsP system from 675 to 610 °C without affecting the structural properties of epitaxial layers and the electrophysical parameters of future devices;

– optimization of current consumption of H_2 from 10 l/h to 2-4 l/h;

– optimization of the design of the graphite container, which makes possible the provision of an additional quasi-closed volume for the creation of partial pressure of phosphorus during the growth of the InP/GaInAsP heterostructure;

– rapid cooling of the growth system with a growth cassette.

It is known [21] that indium phosphide has significant solubility in the tin melt. In this regard, a special solution-melt of indium phosphide in tin was prepared, placed in a quasi-closed volume of the growth cassette (Fig. 7) and it served as a source of the partial pressure of phosphorus during epitaxial growth. In addition, immediately before the start of the growth process, the indium phosphide substrate was etched with a 50% diluted In-InP melt solution, which allowed the etching of 3 to 5 μm from the damaged indium phosphide layer.

After the end of the growth process, in order to reduce the dissociation of the grown epitaxial layers, the graphite cassette was abruptly cooled at a cooling rate of 20–30 degrees per minute by shifting the heating furnace. The proposed technological process allowed to obtain mirror-smooth layers with a density of growth defects not more than $5 \cdot 10^2$ cm^{-2}.

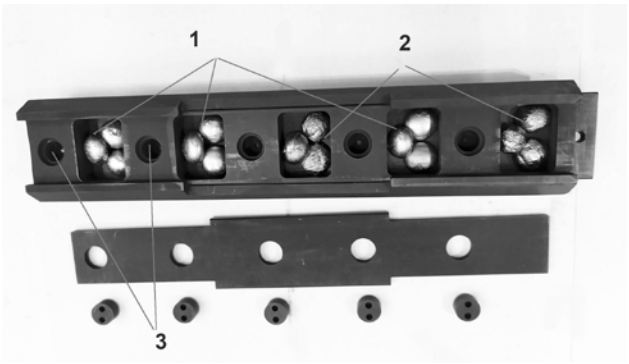

Fig. 7. Graphite cassette with quasi-closed volumes: *1* – solution-melt InP; *2* – solution-melt InGaAsP; *3* – reservoirs for increasing the partial pressure of phosphorus

3. Conclusion

The solution-melt dissolution (SMD) effect is present throughout the growth process by liquid-phase epitaxy in the InP/InGaAsP system on InP substrates. This effect is extremely undesirable and caused by the polarity of the {111} A and {111} B planes, which is clearly manifested during the growth of InP buffer layers. The family of planes {001} and {111} B aligns the depressions and grooves, and the family of planes {111} A with planes {001} and {111} B facets them. As a result of the joining of the {111} planes in the depression, they are cut faceted from both sides by the {111} A planes to the height of the buffer layer. One depression produces two smaller symmetrical depressions. As a result, these depressions permeate the entire grown structure. This leads to

structural defects in the epitaxial layers and short circuits of *p-n* transitions. Such heterostructures lead to a high rate of rejection in the manufacture of semiconductor devices and non-reproducibility of electrophysical parameters over the area of the epitaxial plate.

Author contributions

All authors made an equivalent contribution to the preparation of the publication.

Conflict of interests

The authors declare that they have no known competing financial interests or personal relationships that could have influenced the work reported in this paper.

References

1. *Uspekhi v khimii i khimicheskoi tekhnologii* [Advances in chemistry and chemical technology]. In: Collection of scientific papers. 2016; XXX.6(175). Moscow: RKhTU im. D. I. Mendeleeva Publ.; 2016. 118 p. (In Russ.)

2. Klyndyuk A. I. *Poverkhnostnye yavleniya i dispersnye sistemy: uchebnoe posobie dlya studentov khimiko-tekhnologicheskikh spetsial'nostei* [Surface phenomena and dispersed systems: a textbook for students of chemical and technological specialties]. Minsk: BGTU Publ.; 2011. 317 p. ISBN 978-985-530-054-1. (In Russ.)

3. Saidov A. S., Usmonov Sh. N., Saidov M. S. Liquid-phase epitaxy of the $(Si_2)_{1-x-y}(Ge_2)_x(GaAs)_y$ substitutional solid solution ($0 \leqslant x \leqslant 0.91$, $0 \leqslant y \leqslant 0.94$) and their electrophysical properties. *Semiconductors*. 2015;49(4): 547–550. https://doi.org/10.1134/s106378261504020x

4. Alfimova D. L., Lunin L. S., Lunina M. L., Kazakova A. E., Pashchenko A. S. Liquid-phase synthesis and properties of constant lattice parameter AlGaInAsP solid solutions on indium phosphide substrates. *Inorganic Materials*. 2019;55(6): 533–541. https://doi.org/10.1134/S0020168519060013

5. Vasil'ev M. G., Vasil'ev A. M., Izotov A. D., Shelyakin A. A. Preparation of indium phosphide substrates for epilayer growth. *Inorganic Materials*. 2018;54(11): 1109–1112. https://doi.org/10.1134/S0020168518110158

6. Leshko A. Yu., Lyutetskii A. V., Pikhtin N. A., Slipchenko S. O., Sokolova Z. N., Fetisova N. V., Golikova E. G., Ryaboshtan Yu. A., Tarasov I. S. High power single-mode (λ=1.3–1.6 μm) laser diodes based on quantum well InGaAsP/InP heterostructures. *Semiconductors*. 2002;36(11): 1308–1314. https://doi.org/10.1134/1.1521236

7. Dikareva N. V., Zvonkov B. N., Samartsev I. V., Nekorkin S. M., Baidus N. V., Dubinov A. A. GaAs-based laser diode with InGaAs waveguide quantum wells. *Semiconductors*. 2019;53(12): 1709–1711. https://doi.org/10.1134/S1063782619160085

8. Ladugin M. A. Gultikov N. V., Marmalyuk A. A., Konyaev V. P., Solov'eva A. V. Continuous-wave laser diodes based on epitaxially integrated InGaAs/AlGaAs/GaAs heterostructures. *Quantum Electronics*. 2019;49(10): 905–908. https://doi.org/10.1070/qel17089

9. Zhuravlev K. S., Gilinskii A. M., Chistokhin I. B., Valisheva N. A., Dmitriev D. V., Toropov A. I., Aksenov M. S., Chizh A. L., Mikitchuk K. B. Moshchnye SVCh-fotodiody na osnove geterostruktur InAlAs/InGaAs, sinteziruemykh metodom molekulyarno-luchevoi epitaksii [High-power microwave photodiodes based on InAlAs / InGaAs heterostructures synthesized by molecular beam epitaxy]. *Zhurnal tekhnicheskoi fiziki (Technical Physics)*. 2021;91(7): 1158–1163. https://doi.org/10.21883/JTF.2021.07.50957.347-20 (In Russ.)

10. Mintairov S. A., Nakhimovich M. V., Salii R. A., Shvarts M. Z., Kalyuzhnyi N. A. Uvelichenie koeffitsienta poleznogo deistviya fotopreobrazovatelei lazernogo izlucheniya diapazona 520–540 nm na osnove geterostruktur GaInP/GaAs [Increasing the efficiency of photoconverters for laser radiation in the 520–540 nm range based on GaInP / GaAs heterostructures]. *Pis'ma v zhurnal tekhnicheskoi fiziki (Technical Physics Letters)*. 2021;(6): 29–31. https://doi.org/10.21883/PJTF.2021.06.50755.18619 (In Russ.)

11. Zhukov A. E., Kovsh A. R. Quantum dot diode lasers for optical communication systems. *Quantum Electronics*. 2008;38(5): 409–423. https://doi.org/10.1070/qe2008v038n05abeh013817

12. Marmalyuk A. A., Ivanov A. V., Kurnosov V. D., Ladugin M. A., Lobintsov A. V., Padalitsa A. A., Romatsevich V. I., Ryaboshtan Yu. L., Sapozhnikov S. M., Svetogorov V. N., Simakov V. A. AlGaInAs/InP semiconductor lasers with an increased electron barrier. *Quantum Electronics*. 2019;49 (6): 519–521. https://doi.org/10.1070/qel17032

13. Borda C., DuToit D., Duncan H., Nikles M. External pipeline leak detection based on fiber optic sensing for the kinosis 12″–16″ and 16″–20″ pipe-in-pipe system. External pipeline leak detection based on fiber optic sensing for the kinosis 12″–16″ and 16″–20″ pipe-in-pipe system. In: *Volume 1: Design and Construction; Environment; Pipeline Automation and Measurement. 10th International Pipeline Conference*. 2014;IPC2014–33375: V001T09A016. https://doi.org/10.1115/ipc2014-33375

14. Song J. H., Cho S. H., Han I. K., Hu Y., Heim P. J. S., Johnson F. G., Stone, D. R., Dagenais M. High-power broad-band superluminescent diode with low spectral modulation at 1.5-μm wavelength. *IEEE*

Photonics Technology Letters. 2000;12(7): 783-785. https://doi.org/10.1109/68.853499

15. Han I. C., Jaffe G. J. Evaluation of artifacts associated with macular spectral-domain optical coherence tomography. *Ophthalmology*. 2010;117(6): 1177–1174. https://doi.org/10.1016/j.ophtha.2009.10.029

16. Jiao Y. G., Nishiyama N., van der Tol J., van Engelen J., Pogoretskiy V., Reniers S., Abbas Kashi A., Wang Y., Calzadilla V. D., Spiegelberg M. Show InP membrane integrated photonics research. *Semiconductor Science and Technology*. 2021;36(1): 013001. https://doi.org/10.1088/1361-6641/abcadd

17. Hou C. -C., Chen H. -M., Zhang J. -C., Zhuo N., Huang Y.-Q., Hogg R. A., Childs D. TD, Ning J. -Q., Wang Z.-G., Liu F. -Q., Zhang Z. -Y. Near-infrared and mid-infrared semiconductor broadband light emitters. *Light: Science & Applications*. 2018;(7): 17170. https://doi.org/10.1038/lsa.2017.170

18. Svetikov V. V., Kononov M. A. Generation of a broad-area laser diode in an asymmetrical V-cavity possessing a spectrally nonselective feedback mirror. *Quantum Electronics*. 2018;48(8): 706–710. https://doi.org/10.1070/qel16706

19. Mittova I. Ya., Sladkopevtcev B. V., Samsonov A. A., Tomina E. V., Andreenko S. Yu., Kostenko P. V. Growth and properties of nanofilms produced by the thermal oxidation of MnO_2/InP under the effect of $Mn_3(PO_4)_2$. *Inorganic Materials*. 2019;55(9): 915–919. https://doi.org/10.1134/s0020168519090073

20. Vasil'ev M. G., Izotov A. D., Marenkin S. F., Shelyakin A. A. Preparation of shaped indium phosphide surfaces for edge-emitting devices. *Inorganic Materials*. 2019;55(1): 105–108. https://doi.org/10.1134/s0020168519010175

21. Suchikova Y. Porous indium phosphide: preparation and properties. In: Aliofkhazraei M., Makhlouf A. (eds). *Handbook of Nanoelectrochemistry*. Springer, Cham.: 2015. p. 283–305. https://doi.org/10.1007/978-3-319-15266-0_28

Information about the authors:

Mikhail G. Vasil'ev, DSc in Technical Sciences, Professor, Head of the Laboratory of Semiconductor and Dielectric Materials, Kurnakov Institute of General and Inorganic Chemistry of the Russian Academy of Sciences, Moscow, Russian Federation, e-mail: mgvas@igic.ras.ru. ORCID iD: https://orcid.org/0000-0002-4279-1707.

Anton M. Vasil'ev, Researcher Fellow, Kurnakov Institute of General and Inorganic Chemistry of the Russian Academy of Sciences, Moscow, Russian Federation e-mail: toto71@bk.ru. ORCID iD: https://orcid.org/0000-0002-9901-5856.

Alexander D. Izotov, DSc in Chemistry, Corresponding Member of the Russian Academy of Sciences, Chief Researcher of the Laboratory of Semiconductor and Dielectric Materials, Kurnakov Institute of General and Inorganic Chemistry of the Russian Academy of Sciences, Moscow, Russian Federation, e-mail: izotov@igic.ras.ru. ORCID iD: https://orcid.org/0000-0002-4639-3415.

Yuriy O. Kostin, PhD in Technical Science, Senior Researcher, Kurnakov Institute of General and Inorganic Chemistry of the Russian Academy of Sciences, Moscow, Russian Federation, e-mail: temptelam@yandex.ru. ORCID iD: https://orcid.org/0000-0001-8172-3988.

Alexey A. Shelyakin, PhD in Technical Science, Senior Researcher of the Laboratory of Semiconductor and Dielectric Materials, Kurnakov Institute of General and Inorganic Chemistry of the Russian Academy of Sciences, Moscow, Russian Federation, e-mail: alekssche liakin@gmail.com. ORCID iD: https://orcid.org/0000-0003-0028-005X.

Received 8 June 2021; Approved after reviewing 21 June 2021; Accepted for publication 15 August 2021; Published online 25 September 2021.

Translated by Valentina Mittova
Edited and proofread by Simon Cox

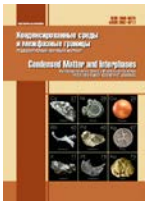

ISSN 1606-867X (Print)
ISSN 2687-0711 (Online)
Condensed Matter and Interphases
Kondensirovannye Sredy i Mezhfaznye Granitsy
https://journals.vsu.ru/kcmf/

Original articles

Research article
https://doi.org/10.17308/kcmf.2021.23/3529

A 3D computer model of the CaO-MgO-Al_2O_3 *T-x-y* diagram at temperatures above 1300 °C

V. P. Vorob'eva, A. E. Zelenaya✉, V. I. Lutsyk, M. V. Lamueva

Institute of Physical Materials Science, Siberian Branch of the Russian Academy of Sciences,
6 Sakhianova ul., Ulan-Ude 670047, Russian Federation

Abstract

The research analyses the controversies surrounding the technique for the formation of a CaO-Al_2O_3 binary system and the nature of melting of compounds in it, i.e. whether the 12:7 compound is technically possible and whether the 1:1 and 1:2 compounds are congruently or incongruently melting compounds. It also discusses whether in the CaO-MgO-Al_2O_3 ternary system the following compounds can be formed: a 3:1:1 compound alone or, in addition to it, two more compounds of 1:2:8 and 2:2:14. A 3D model of the *T-x-y* diagram was created for the most common version, with six binary and three ternary compounds. Its high-temperature portion (above 1300°C) consisted of 234 surfaces and 85 phase regions. Ternary compounds were formed as a result of three peritectic reactions. Besides them, six quasi-peritectic and three eutectic invariant reactions occurred in the system with the participation of the melt. The principle of construction for a three-dimensional model involved a gradual transition from a phase reaction scheme (which is transformed into a scheme of uni- and invariant states) presented in a tabulated and then in a graphical form (a template of ruled surfaces and isothermal planes corresponding to invariant reactions) to a *T-x-y* diagram prototype (graphic images of all liquidus, solidus, and solvus surfaces). The design was concluded with the transformation of the prototype into a 3D model of the real system after the input of the base points coordinates (concentrations and temperatures) and the adjustment of curvatures of lines and surfaces. The finished model provides a wide range of possibilities for the visualisation of the phase diagram, including the construction of any arbitrarily assigned isothermal sections and isopleths. The 3D model was designed with the help of the author's software PD Designer (Phase Diagram Designer). To assess the quality of the 3D model, two versions of an isothermal section at 1840 °C were compared: model section and a fragment of an experimental section near Al_2O_3.

Keywords: Phase diagram, Computer simulation, Oxides of calcium, magnesium, and aluminium

Acknowledgements: The work was carried out in accordance with the state assignment of the Institute of Physical Materials Science, Siberian Branch of the Russian Academy of Science for 2017-2020 (project No. 0336-2019-0008) and was partially supported by the Russian Foundation for Basic Research (project 19-38-90035).

For citation: V. P. Vorob'eva, A. E. Zelenaya, V. I. Lutsyk, M. V. Lamueva. A 3D computer model of the CaO-MgO-Al_2O_3 *T-x-y* diagram at temperatures above 1300 °C. *Kondensirovannye sredy i mezhfaznye granitsy = Condensed Matter and Interphases*. 2021;23(3): 380–386. https://doi.org/10.17308/kcmf.2021.23/3529

Для цитирования: Воробьева В. П., Зеленая А. Э., Луцык В. И., Ламуева М. В. 3D компьютерная модель *T-x-y* диаграммы CaO-MgO-Al_2O_3 при температурах выше 1300 °C. *Конденсированные среды и межфазные границы*. 2021;23(3): 380–386. https://doi.org/10.17308/kcmf.2021.23/3529

✉ Anna E. Zelenaya, e-mail: zel_ann@mail.ru
© V. P. Vorob'eva, A. E. Zelenaya, V. I. Lutsyk, M. V. Lamueva, 2021

The content is available under Creative Commons Attribution 4.0 License.

1. Introduction

The information about phase transformations in the CaO-MgO-Al_2O_3 system, including the subsolidus area, is important for the study of petrological objects, since this system is a component of the CaO-MgO-Al_2O_3-SiO_2 quaternary system which, in its turn, serves as the foundation for the description of deep-seated rock minerals [1–2]. In addition, the prediction and the study of the properties of magnesium aluminate spinel-based cements and technical ceramics are of great importance [3].

Therefore, works dedicated to the experimental study of the CaO-MgO-Al_2O_3 system, thermodynamic calculations, and simulations of its *T-x-y* diagram are of great interest. However, while two of its constituent binary systems, CaO-MgO and MgO-Al_2O_3, have been interpreted unambiguously, there are many controversies in the literature surrounding the third binary system of CaO-Al_2O_3, as well as the ternary system formed by them. As a result, the understanding of the geometric structure of the *T-x-y* diagram, at least with regard to its liquidus surfaces, has been challenged due to many possible interpretations of certain fragments of the diagram.

A spatial (three-dimensional (3D)) computer model of the phase diagram, based at least on one of the most common versions (which can be used to present other simpler versions) can be helpful for the formal description of the T-x-y diagram.

Before constructing the 3D model, it was necessary to redesignate the initial and formed components in the compound system. This is a requirement of the PD Designer software, which was used to construct 3D models of the *T-x-y* phase diagrams [4-6].

Thus, the CaO-MgO-Al_2O_3 system was redesignated as A-B-C.

The binary CaO-MgO (A-B) system is a simple eutectic one [7–9].

According to [10, 11], in the MgO-Al_2O_3 (B-C) binary system a 1:1 or MgO·Al_2O_3 congruently melting compound (designated as R6 in the 3D model) is formed which splits it into an eutectic MgO-MgO·Al_2O_3 (B-R6) and peritectic MgO·Al_2O_3-Al_2O_3 (R6-C) subsystems. What is more, minimums are recorded on the liquidus and solidus lines in the peritectic subsystem.

The structure of the CaO-Al_2O_3 (A-C) system has been debated a lot, the differences relate to the quantity and the nature of the formed compounds and the type of binary dots. For example, [7], with reference to [12], presents a version of the *T-x* diagram where five compounds are formed: the $3CaO·Al_2O_3$ (R1) and $CaO·6Al_2O_3$A (R5) incongruently melting compounds and $12CaO·7Al_2O_3$ (R2), $CaO·Al_2O_3$ (R3), and $CaO·2Al_2O_3$A (R4) congruently melting compounds. Therefore, the system is divided into two eutectic systems: $12CaO·7Al_2O_3$-$CaO·Al_2O_3$ (R2-R3), $CaO·Al_2O_3$-$CaO·2Al_2O_3$ (R3-R4), and two eutectic-peritectic systems: CaO-$12CaO·7Al_2O_3$ (A-R2), $CaO·2Al_2O_3$-Al_2O_3 (R4-C) which are accompanied by the formation of the incongruently melting $3CaO·Al_2O_3$ (R1) and $CaO·6Al_2O_3$ (R5) compounds, respectively. This most complex version of the structure of the CaO-Al_2O_3 (A-C) *T-x* diagram was used to construct a 3D computer model of the *T-x* diagram.

However, according to [13], the $12CaO·7Al_2O_3$ (R2) compound is actually a $Ca_{12}Al_{14}O_{32}(OH)_2$ hydrate and therefore it cannot be found in the CaO-Al_2O_3 system. As a result, instead of five compounds there are four compounds (without $12CaO·7Al_2O_3$) in the system. What is more, the nature of melting of $CaO·Al_2O_3$ (R3), $CaO·2Al_2O_3$ (R4) is also considered to be incongruent, similar to the $3CaO·Al_2O_3$ (R1) and $CaO·6Al_2O_3$ (R5) compounds. In this case, these four compounds are formed as a result of peritectic reactions. Moreover, $3CaO_3·Al_2O_3$ (R1) and $CaO·Al_2O_3$ (R3) interact as a result of an eutectic reaction. The same version of the T-x diagram structure was generated as a result of thermodynamic calculations [14, 15], and was confirmed by the latest experimental research [16].

Based on the published data analysis, [8, 9, 17–19] claimed that the versions of the CaO-Al_2O_3 structure dependent on humidity and the concentration of oxygen in the furnace atmosphere. Depending on this, the $5CaO·3Al_2O_3$ stoichiometry can be attributed to the $12CaO·7Al_2O_3$ compound. According to this version of the phase diagram structure, only one compound, $12CaO·7Al_2O_3$ (R2), melts congruently, while the remaining four, $3CaO·Al_2O_3$ (R1), $CaO·Al_2O_3$ (R3), $CaO·2Al_2O_3$ (R4), and $CaO·6Al_2O_3$ (R5), melt incongruently as a result

of four peritectic reactions. The $12CaO{\cdot}7Al_2O_3$ (R2) compound interacts with the $3CaO{\cdot}Al_2O_3$ (R1) and $CaO{\cdot}Al_2O_3$ (R3) as a result of two eutectic reactions. More recent thermodynamic calculations regarding the CaO-Al_2O_3 system [20] confirm this version of the phase diagram structure. Additionally, the authors emphasised that earlier thermodynamic calculations [15] did not consider the $12CaO{\cdot}7Al_2O_3$ phase since it is not strictly anhydrous. In a conventional air humidity and within a temperature range of 950-1350°C, the $12CaO{\cdot}7Al_2O_3$ absorbs a small amount of water (no more than 1.3 wt%) [20].

In cement systems, the $12CaO{\cdot}7Al_2O_3$ compound was regarded as an aluminate phase, in other words, it was considered to be anhydrous and was included in the diagrams [18, 19]. The $12CaO{\cdot}7Al_2O_3$ compound has been found in the form of a natural mineral and has been called meionite [21]. It is of practical importance for the production of dense ceramics [22].

As for the CaO-MgO-Al_2O_3 ternary system, earlier works [23] did not record the formation of ternary compounds. [24] discussed the formation of three ternary compounds: $3CaO{\cdot}MgO{\cdot}Al_2O_3$ (R7), $CaO{\cdot}2MgO{\cdot}8Al_2O_3$ (R8), and $2CaO{\cdot}2MgO{\cdot}14Al_2O_3$ (R9). The thermodynamic calculations [10] did not consider the $C_{12}A_7$ binary compound What is more, the configuration of the internal field of liquidus that corresponds to the $3CaO{\cdot}MgO{\cdot}Al_2O_3$ (R7) compound is characterised by the fact that its boundaries are formed by four invariant points, whereas in [24] this field is triangular in shape.

Therefore, the aim of this work was to construct a 3D computer model of the CaO-MgO-Al_2O_3 *T-x-y* diagram, including all its surfaces: liquidus, solidus, solvus, ruled surfaces, and the horizontal plane corresponding to the invariant transformations in the ternary system up to a temperature of 1300 °C.

2. Modelling

The computer 3D model of the CaO-MgO-Al_2O_3 (A-B-C) *T-x-y* diagram was constructed using the data from [24] considering the formation of six binary compounds: $3CaO{\cdot}Al_2O_3$ (R1), $CaO{\cdot}6Al_2O_3$ (R5) (incongruently melting), $12CaO{\cdot}7Al_2O_3$ (R2), $CaO{\cdot}Al_2O_3$ (R3), $CaO{\cdot}2Al_2O_3$ (R4), $MgO{\cdot}Al_2O_3$ (R6) (congruently melting), and ternary compounds: $3CaO{\cdot}MgO{\cdot}Al_2O_3$ (R7), $CaO{\cdot}2MgO{\cdot}8Al_2O_3$ (R8), $2CaO{\cdot}2MgO{\cdot}14Al_2O_3$ (R9) (Fig. 1).

For a better display and understanding of the geometric structure of the *T-x-y* diagram, first its prototype was constructed in which the base points were spaced for a better visualisation, however, their temperature coordinates were set according to the temperature range (Fig. 1c).

As can be seen from the prototype, the ternary system involved three peritectic reactions leading to the formation of ternary compounds:

P1: L+B+R3→R7, P2: L+R6+R9→R8,
P3: L+R5+R6→R9

six quasi-peritectic:

Q1: L+A→B+R1, Q2: L+R6→B+R3,
Q3: L+R4→R3+R6, Q4: L+R5→R4+R9,
Q5: L+R9→R4+R8, Q6: L+C→R5+R6

and four eutectic:

E1: L→B+R1+R2, E2: L→B+R2+R7,
E3: L→R2+R3+R7, E4: L→R4+R6+R8

invariant reactions. Since the 3D model was designed in a limited temperature range, above 1300 °C, it did not reflect the processes that occurred in the subsolidus.

The prototype can be used to claim that the *T-x-y* diagram consists of 12 liquidus surfaces corresponding to the beginning of crystallisation of the three initial components, 9 compounds (I = A, B, C, R1-R9), and 12 solidus surfaces conjugated with them between which the L+I two-phase regions are found. Each of the 13 complex planes corresponding to the invariant reactions (three peritectic reactions (P), six quasi-peritectic reactions (Q), and four eutectic reactions (E)) are divided into four simplexes. All 24 invariant liquidus lines (Fig. 1d), together with the 48 solidus lines associated with them pair wisely, function as 72 directing curves for the ruled surfaces which form the boundaries for 24 L+I+J three-phase regions. Accordingly, in this high temperature portion of the diagram 24 I+J two-phase regions and 24 conjugated solvus surfaces should be expected. The boundaries for each of these 13 three-phase regions I+J+K without the liquid are represented by three ruled surfaces, the total number of which is 39.

Therefore, the *T-x-y* diagram is formed by 234 surfaces and 85 phase regions (Fig. 1a).

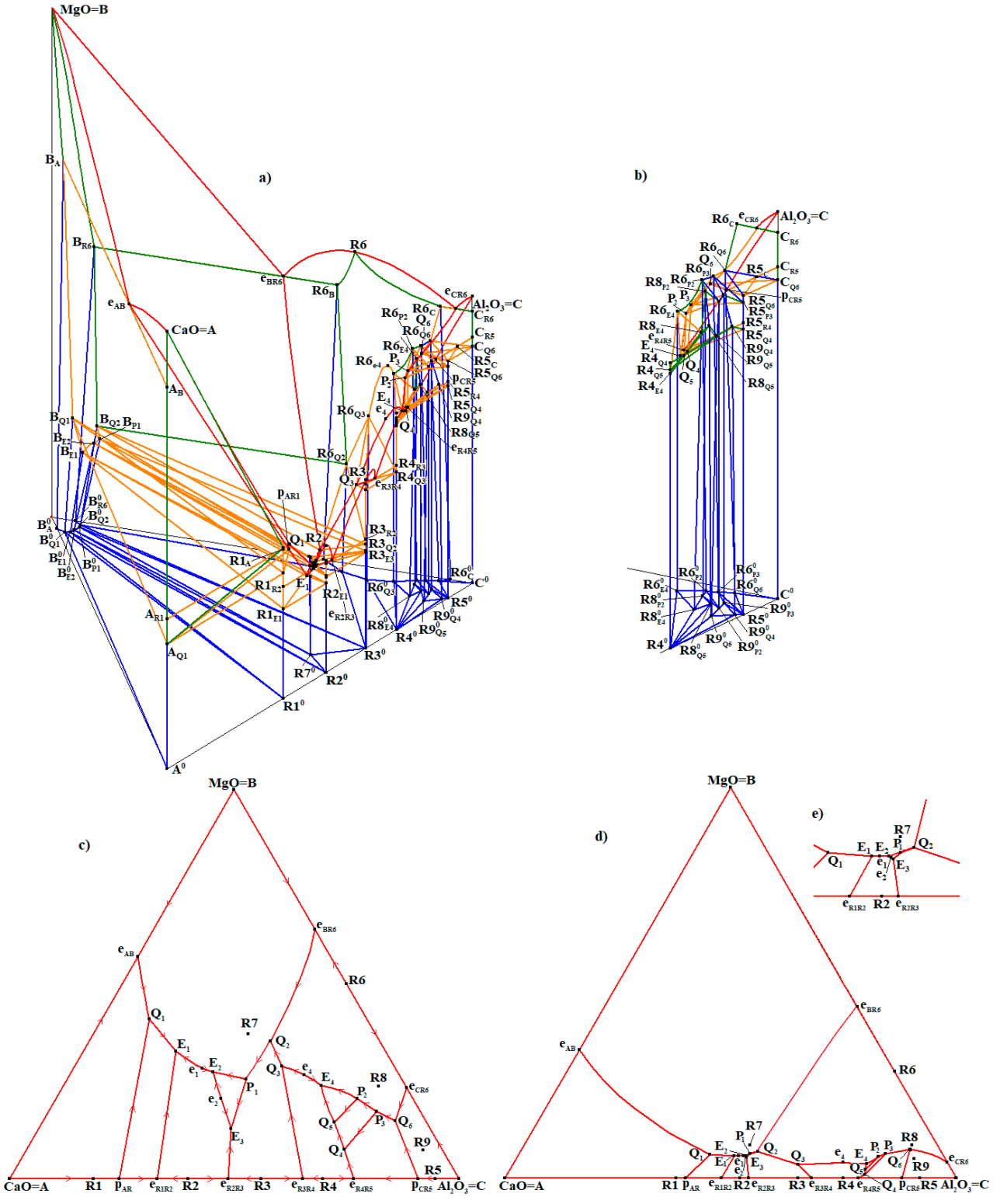

Fig. 1. 3D model of the CaO-MgO-Al_2O_3 (A-B-C) *T-x-y* diagram (a) and an enlarged fragment near Al_2O_3 (b), *x-y* projections of the liquidus surfaces: of the prototype (c), of the real system (d), and its enlarged fragment (e)

3. Results and discussion

The 3D computer model was constructed by assembling the above-mentioned surfaces and phase regions. First, a prototype was formed (Fig. 1b.), i.e. 13 horizontal (isothermal) planes were constructed using the PD Designer: 3 peritectic (P) triangles, 6 quasi-peritectic (Q) quadrangles, 4 triangles which included points E. Then, directing lines were brought to them and ruled surfaces were formed. Thus boundaries for 24 three-phase regions with the melt and 13 solid phase regions were set. The resulting frame was completed with unruled liquidus, solidus, and solvus surfaces.

Next, the prototype was transformed into a 3D model of the phase diagram of the real system. To achieve this, the base points were given real values of concentrations and temperatures and the curvatures of lines and surfaces were adjusted (Fig. 1d).

As a result, a spatial computer model of the *T-x-y* diagram was obtained which has a wide range of visualisation possibilities: the model can be rotated, viewed from arbitrary angles, split into pieces (separate groups of phase regions), arbitrary set sections can also be obtained.

The quality of the resulting model can be assessed by comparing the model sections (Fig. 2a) with the experimental sections (Fig. 2b). The observed isothermal section at 1840 °C is 10 °C lower than the invariant point of the highest temperature Q6 (1850 °C) and higher than point P3 (1830 °C) (Fig. 1a), that is why the crossing traces of the Al_2O_3 phase regions and the melt are not displayed. [24] considered a fragment of the section adjacent to the Al_2O_3 angle, which displayed the section lines limiting the L+R5, L+R6, L+R5+R6, R5, C+R5, R5+R6, C+R5+R6 phase regions (Fig. 2b). The model section was fully calculated and the fragment adjacent to Al_2O_3 was marked (Fig. 2a). Since it was assumed during the construction of the model that the R5 binary compound has a constant composition, the phase regions corresponding to R5 and C+R5 coincided with the edge of the prism, whereas for the spinel R6, on the contrary, a limited solubility was taken into account. Nevertheless, the section topology corresponded to the section presented in [24] (Fig. 2b).

4. Conclusions

A three-dimensional computer model of the CaO-MgO-Al_2O_3 *T-x-y* diagram was constructed.

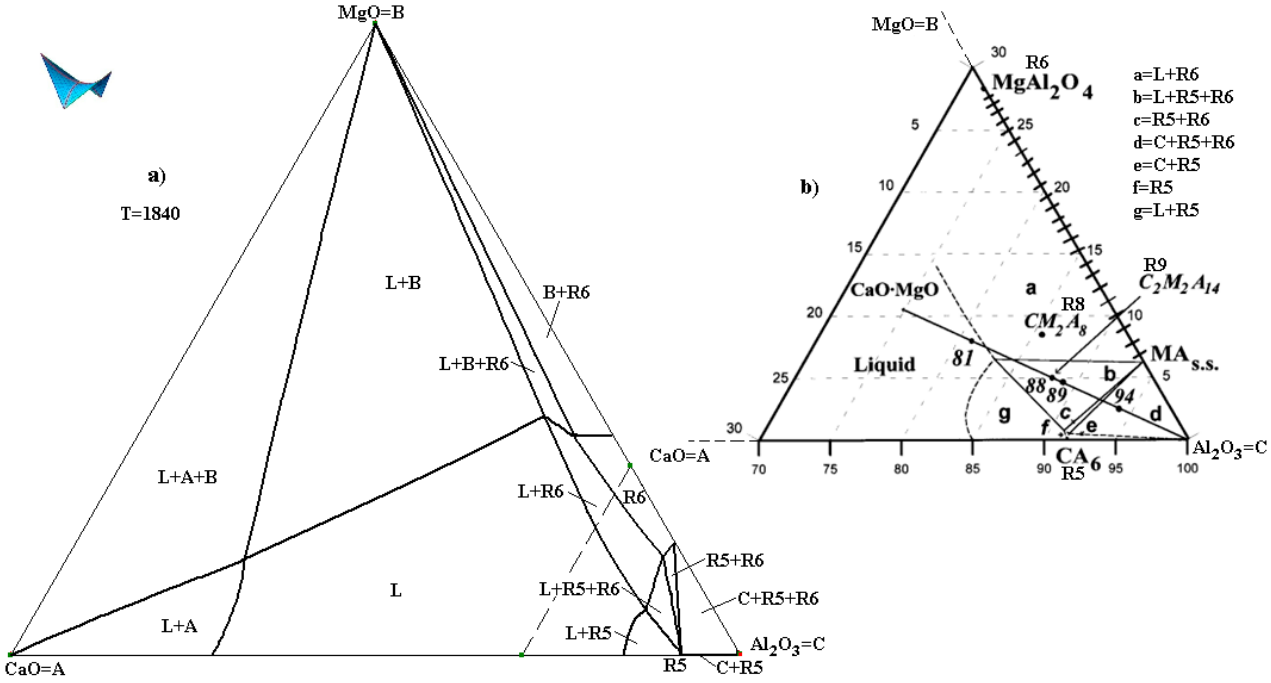

Fig. 2. Isothermal section at 1840°C: 3D models (a), experimentally studied fragment near Al_2O_3 [24] (b) (in [24] the CaO·6Al_2O_3 (R5) compound has a region of limited solubility, and the MgO·Al_2O_3 (R6) compound has a region of permanent composition, in 3D models this is vice versa)

It was shown that its high-temperature fragment (above 1300 °C) in the most complex version, i.e. as a result of the formation of six binary: $3CaO{\cdot}Al_2O_3$, $CaO{\cdot}6Al_2O_3$ (incongruently melting), $12CaO{\cdot}7Al_2O_3$, $CaO{\cdot}Al_2O_3$, $CaO{\cdot}2Al_2O_3$, $MgO{\cdot}Al_2O_3$ (congruently melting) and three ternary $3CaO{\cdot}MgO{\cdot}Al_2O_3$, $CaO{\cdot}2MgO{\cdot}8Al_2O_3$, $2CaO{\cdot}2MgO{\cdot}14Al_2O_3$ compounds, it consists of 234 surfaces and 85 phase regions. To assess the quality of the model its sections were compared with the sections constructed using the experimental data.

Author contributions

All authors made an equivalent contribution to the preparation of the publication.

Conflict of interests

The authors declare that they have no known competing financial interests or personal relationships that could have influenced the work reported in this paper.

References

1. Surkov N. V., Gartvich Y. G. Modeling of deep-seated high-alumina parageneses on the basis of the stability fields of corundum- and spinel-normative assemblages of the system CaO-MgO-Al_2O_3-SiO_2. *Russian Geology and Geophysics*. 2012;53(1): 51–61. https://doi.org/10.1016/j.rgg.2011.12.004

2. Banushkina S. V., Gartvich Yu. G., Golitsyna Z. F., Surkov N. V. Experimental study of monovariant melting possibilities in the forsterite-normative part of the CaO-MgO-Al_2O_3-SiO_2 system in connection with the formation of spinel peridotitis. *Mezhdunarodnyy nauchno-issledovatel'skiy zhurnal = International Research Journal*. 2017;66(12): 153–161. https://doi.org/10.23670/IRJ.2017.66.050 (In Russ., abstract in Eng.)

3. Shabanova G. N., Korogodskaya A. N. Physical and chemical bases of spinel cements containing. Part 1. Subsolidus structure of aluminate oxide systems. *Ogneupory i tekhnicheskaya keramika = Refractories and technical ceramics*. 2014;6: 3–7. Available at: https://www.elibrary.ru/item.asp?id=23998838 (In Russ., abstract in Eng.)

4. Lutsyk V. I., Vorob'eva V. P. Computer models of eutectic-type *T–x–y* diagrams with allotropy. *Journal of Thermal Analysis and Calorimetry*. 2010;101(1): 25–31. https://doi.org/10.1007/s10973-010-0855-0

5. Vorob'eva V. P., Zelenaya A. E., Lutsyk V. I., Sineva S. I., Starykh R. V., Novozhilova O. S. High-temperature area of the Fe-Ni-Co-Cu diagram: experimental study and computer design. *Journal of Phase Equilibria and Diffusion*. 2021;42(2): 175-193. https://doi.org/10.1007/s11669-021-00863-3

6. Lutsyk V. I., Zelenaya A. E., Zyryanov A. M. Multicomponent systems simulation by the software of «Diagrams Designer». *Journal Materials, Methods & Technologies. International Scientific Publications*. 2008;2(1): 176–184. Available at: https://www.scientific-publications.net/download/materials-methods-and-technologies-2008.pdf

7. Levin E. M., Robbins C. R., McMurdie H. F. *Phase Diagrams for Ceramists*. Ohio: American. Ceramic Society; 1964. 600 p.

8. Berezhnoi A. S. *Mnogokomponentnyye sistemy okislov* [Multicomponent systems of oxides]. Kiev: Naukova dumka Publ.; 1970. 542 p. (In Russ.)

9. Toropov N. A., Barzakovsky V. P., Lapshin V. V., Kurtseva N. N. *Diagrammy sostoyaniya silikatnykh sistem. Spravochnik. Vyp. pervyy. Dvoynyye sistemy* [State diagrams of silicate systems. Reference book. Issue first. Binary systems]. Leningrad: Science, Leningrad Branch Publ.; 1969. 822 p. (In Russ.)

10. Jung I. -H., Decterov S. A., Pelton A. D. Critical thermodynamic evaluation and optimization of the MgO-Al_2O_3, CaO-MgO-Al_2O_3, and MgO-Al_2O_3-SiO_2 systems. *Journal of Phase Equilibria and Diffusion*. 2004;25(4): 329–345. https://doi.org/10.1007/s11669-004-0151-4

11. Zienert T., Fabrichnaya O. Thermodynamic assessment and experiments in the system MgO-Al_2O_3. CALPHAD. 2013;40: 1–9. https://doi.org/10.1016/j.calphad.2012.10.001

12. Lea F. M., Desh C. H. *The chemistry of cement and concrete*. 2d ed., London: Edward Arnoid & Co; 1956.

13. Nurse R. W., Welch J. H., Majumdar A. J. The CaO-Al_2O_3 system in a moisture-free atmosphere. *Transactions of the British Ceramic Society*. 1965;64: 409–418.

14. Berman R. G., Brown T. H. *A* Thermodynamic model for multicomponent melts, with application to the system CaO-$A1_2O_3$-SiO_2. *Geochimica et Cosmochimica Acta*. 1984;48(4): 661–678. https://doi.org/10.1016/0016-7037(84)90094-2

15. Mao H., Selleby M., Sundman B. A re-evaluation of the liquid phases in the CaO-Al_2O_3 and MgO-Al_2O_3 systems. *CALPHAD*. 2004;28(3): 307–312; https://doi.org/10.1016/j.calphad.2004.09.001

16. Jerebtsov D. A., Mikhailov G. G. Phase diagram of CaO-Al_2O_3 system. *Ceramics International*... 2001;27(1): 25–28. https://doi.org/10.1016/S0272-8842(00)00037-7

17. Smirnov G. S., Chatterjee A. K., Zhmoidin G. I. The phase equilibrium diagram of the ternary subsystem CaO-CaO·Al_2O_3-11CaO·$7Al_2O_3$·CaF_2. *Journal of Materials Science*. 1973;8(9): 1278–1282. https://doi.org/10.1007/BF00549342

18. Taylor H. F. W. *Cement chemistry*. London: Thomas Telford; 1997. 459 p.

19. Lea F. *Lea's chemistry of cement and concrete*. London: Elsevier Ltd; 1998. 1057 p.

20. De Noirfontaine M. -N., Tusseau-Nenez S., Girod-Labianca C., Pontikis V. CALPHAD formalism for portland clinker: Thermodynamic models and databases. *Journal of Materials Science*. 2012;47(3): 1471–1479. https://doi.org/10.1007/s10853-011-5932-7

21. Hentschel G. Mayenit $12CaO{\cdot}7Al_2O_3$ und brownmillerit, $2CaO{\cdot}(Al,Fe){\cdot}2O_3$, zwei neue minerale in den kalksteineinschlüssen der lava des ettringer bellerberges. *Neues Jahrbuch für Mineralogie, Monatshefte*. 1964: 22–29.

22. Tolkacheva A. S., Shkerin S. N., Plaksin S. V., et al. Synthesis of dense ceramics of single-phase mayenite $(Ca_{12}Al_{14}O_{32})O$. *Russian Journal of Applied Chemistry*. 2011;84(6): 907–911. https://doi.org/10.1134/S1070427211060012

23. Rankin G. A., Merwin H. E. The ternary system $CaO\text{-}Al_2O_3\text{-}MgO$. *Journal of the American Chemical Society*. 1916;38(3): 568–88; https://doi.org/10.1021/ja02260a006

24. De Aza A. H., Iglesias J. E., Pena P., De Aza S. Ternary system Al_2O_3–MgO–CaO: Part II, Phase relationships in the subsystem $Al_2O_3\text{-}MgAl_2O_4\text{-}CaAl_4O_7$. *Journal of the American Chemical Society*. 2000;83(4): 919–27. https://doi.org/10.1111/j.1151-2916.2000.tb01295.x

Information about the authors

Vera P. Vorob'eva, DSc in Physics and Mathematics, Leading Researcher at the Sector of Computer Materials Design, Institute of Physical Materials Science, Siberian Branch of the Russian Academy of Sciences, Ulan-Ude, Russian Federation; e-mail: vvorobjeva@mail.ru. ORCID iD: https://orcid.org/0000-0002-2714-3808.

Anna E. Zelenaya, PhD in Physics and Mathematics, Senior Researcher at the Sector of Computer Materials Design, Institute of Physical Materials Science, Siberian Branch of the Russian Academy of Sciences, Ulan-Ude, Russian Federation; e-mail: zel_ann@mail.ru. ORCID iD: https://orcid.org/0000-0001-5232-8567.

Vasily I. Lutsyk, DSc in Chemistry, Head of the Sector of Computer Materials Design, Institute of Physical Materials Science, Siberian Branch of the Russian Academy of Sciences, Ulan-Ude, Russian Federation; e-mail: vluts@ipms.bscnet.ru. ORCID iD: https://orcid.org/0000-0002-6175-0329.

Marina V. Lamueva, post-graduate student of Sector of Computer Materials Design, Institute of Physical Materials Science SB RAS, Ulan-Ude, Russian Federation, e-mail: marina_bgu@mail.ru. ORCID iD: https://orcid.org/0000-0001-8347-1753.

Received 31 May 2021; Approved after reviewing 23 June 2021; Accepted for publication 15 July 2021; Published online 25 September 2021.

Translated by Irina Charychanskaya
Edited and proofread by Simon Cox

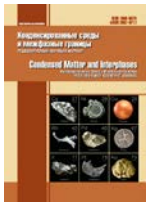

ISSN 1606-867X (Print)
ISSN 2687-0711 (Online)
Condensed Matter and Interphases
Kondensirovannye Sredy i Mezhfaznye Granitsy
https://journals.vsu.ru/kcmf/

Original articles

Research article
https://doi.org/10.17308/kcmf.2021.23/3530

Synthesis of bulk crystals and thin films of the ferromagnetic MnSb

M. Jaloliddinzoda✉[1], S. F. Marenkin[1,2], A. I. Ril'[2], M. G. Vasil'ev[2], A. D. Izotov[2], D. E. Korkin[2]

[1]National University of Science and Technology MISIS,
4 Leninskiy prospekt, Moscow 119049, Russian Federation

[2]Kurnakov Institute of General and Inorganic Chemistry of the Russian Academy of Sciences,
31 Leninsky prospekt, Moscow 119991, Russian Federation

Abstract

High-temperature ferromagnets are widely used on a practical level. Based on them, magnetic memory for computers and various types of magnetic field sensors are created. Therefore, bulk ingots and thin-film samples of ferromagnet manganese antimonide (MnSb) with a high Curie point are of great interest, both from the practical and fundamental sides. Manganese antimonide films are obtained in hybrid structures using molecular-beam epitaxy. The thickness of the films does not exceed tens of nanometers. Despite their high sensitivity to magnetic fields, their small thickness prevents them from being used as magnetic field sensors. The aim of this work was to synthesise thick bulk ingots of manganese antimonide crystals and films with a thickness of ~ 400 nm on sitall and silicon substrates.

MnSb crystals were synthesised using the vacuum-ampoule method and identified using XRD, DTA, and microstructural analysis. The results of studies of bulk samples indicated the presence of an insignificant amount of antimony in addition to the MnSb phase. According to the DTA thermogram of the MnSb alloy, a small endothermic effect was observed at 572 °C, which corresponds to the melting of the eutectic on the part of antimony in the Mn-Sb system. Such composition, according to previous studies, guaranteed the production of manganese antimonide with the maximum Curie temperature. A study of the magnetic properties showed that the synthesised MnSb crystals were a soft ferromagnet with the Curie point ~ 587 K. Thin MnSb films were obtained by an original method using separate sequential deposition in a high vacuum of the Mn and Sb metals with their subsequent annealing. To optimise the process of obtaining films with stoichiometric composition, the dependences of the thickness of metal films on the parameters of the deposition process were calculated.

The temperature range of annealing at which the metals interact with the formation of ferromagnetic MnSb films was established, the films were identified, and their electrical and magnetic properties were measured.

Keywords: High-temperature soft ferromagnets, XRD, DTA, Thin films, Microstructure analysis, Manganese antimonide (MnSb)

Acknowledgments: the work was supported by the Russian Science Foundation as part of the project No. 21-73-20220**.** The authors are grateful to the Centre for Collective Use of Physical Research Methods of Kurnakov Institute of General and Inorganic Chemistry of the Russian Academy of Sciences.

For citation: Jaloliddinzoda M., Marenkin S. F., Ril' A. I., Vasil'ev M. G., Izotov A. D. Synthesis of bulk crystals and thin films of the ferromagnetic MnSb. *Kondensirovannye sredy i mezhfaznye granitsy = Condensed Matter and Interphases.* 2021;23(3): 387–395. https://doi.org/10.17308/kcmf.2021.23/3530

Для цитирования: Джалолиддинзода М., Маренкин С. Ф., Риль А. И., Васильев М. Г., Изотов А. Д., Коркин Д. Е. Синтез объемных кристаллов и тонких пленок ферромагнетика MnSb. *Конденсированные среды и межфазные границы*. 2021;23(3): 387–395. https://doi.org/10.17308/kcmf.2021.23/3530

✉ Jaloliddinzoda Muhammadyusuf, e-mail: muhammad.9095@mail.ru
© Jaloliddinzoda M., Marenkin S. F., Ril' A. I., Vasil'ev M. G., Izotov A. D., 2021

The content is available under Creative Commons Attribution 4.0 License.

1. Introduction

According to the phase diagram, manganese antimonide has a wide range of homogeneity and forms two polymorphic modifications, a hexagonal and a tetragonal one [1–5]. The first modification is a soft ferromagnet with the high Curie temperature (T_C). The Curie temperature of manganese antimonide changes significantly in the range of homogeneity from 300 to 587 K and depends on the content of manganese in a crystal lattice ($P6_3/mmc$) from 55 to 50 at% Mn [6–7]. The compositions of 50 at% Mn and Sb have the highest Curie point [8,9]. As for the melting point of MnSb, which is ~ 840 °C, there is no decisive answer as to whether MnSb melts peritectically or not [10–12].

Different areas of application of manganese antimonide were studied, both as bulk crystals and thin films [13, 14]. Manganese antimonide in the form of bulk crystals is considered to be a promising material for creating high-temperature microrefrigerators based on the magnetocaloric effect [15, 16]. MnSb films obtained on semiconductor substrates of the $A^{III}B^{V}$ group are considered to be promising materials for spintronics devices. Thus, it was of interest to synthesise bulk crystals and obtain thin films of manganese antimonide.

Molecular-beam epitaxy is a traditional way to obtain thin MnSb films [17, 18]. However, this method is complex and it does not allow obtaining films that are thicker than 20 nm. Due to the low concentration of manganese antimonide, the films have low magnetic field sensitivity. It was of interest to synthesise films with greater thickness using vacuum thermal sputtering [19–22]. However, the use of this method was limited due to the incongruent nature of the evaporation of manganese antimonide. To solve this problem, the separate sequential production of Mn and Sb films of a certain thickness was used with further thermal annealing, which ensured their stoichiometric composition. The aim of this work was to synthesise thick bulk ingots of manganese antimonide crystals and films with a thickness of ~ 400 nm on sitall and silicon substrates.

2. Experimental

Bulk single crystals were synthesised from high-purity elements. We used antimony N5 and manganese N3. Mn was subjected to resublimation in a high vacuum for additional purification. The crystals were obtained using the vacuum-ampoule method at a temperature 5 °C lower than the melting point of MnSb. To obtain samples with the maximum Curie point, a small excess of antimony was introduced to the stoichiometric composition of antimony. To protect the walls of the quartz ampoule from exposure to manganese, they were graphitised.

We used quartz ampoules with the thickness of the walls from 1.5 to 2 mm. The ampoules were purified using the solution of aqua regia, washed with distilled water, and dried. Mn and Sb were placed in the ampoules that were then pumped out to 10^{-1} Pa and unsoldered. We synthesised MnSb in the furnace at a temperature of 835 °C with a heating rate of 60 deg/hour. The temperature was controlled and regulated with an accuracy of ± 1 °C using a Termodat-16E3. For the purpose of homogenisation, the melt was kept at a temperature of 835 °C for at least 25 hours with further cooling in the switched-off furnace. As a result, thick ingots were obtained and identified using XRD, DTA, microstructural analysis, and other methods.

XRD was conducted in the Kurnakov Institute of General and Inorganic Chemistry of the Russian Academy of Sciences, using a Bruker D8 Advance powder diffractometer. The obtained diffraction patterns confirmed the formation of MnSb phase of the space group $P6_3/mmc$, corresponding to the composition 50 at% Mn (Fig. 1). The X-ray patterns also showed reflections of an insignificant amount of Sb.

The synthesised samples were examined using DTA on the equipment with the software for heating and cooling processes. Fig. 2 shows a thermogram of the heating and cooling of a bulk sample of MnSb. Two thermal effects were noted on the thermogram. The high-temperature effect was related to the melting of MnSb, while the low-temperature effect was due to the melting of the eutectic of MnSb + Sb.

According to the thermogram, endothermic effects were observed: the first one at 572 °C was related to the melting of the eutectic (MnSb + Sb), the second one at 792 °C was due to the melting of MnSb, which corresponds to the XRD data on the presence of a small excess of

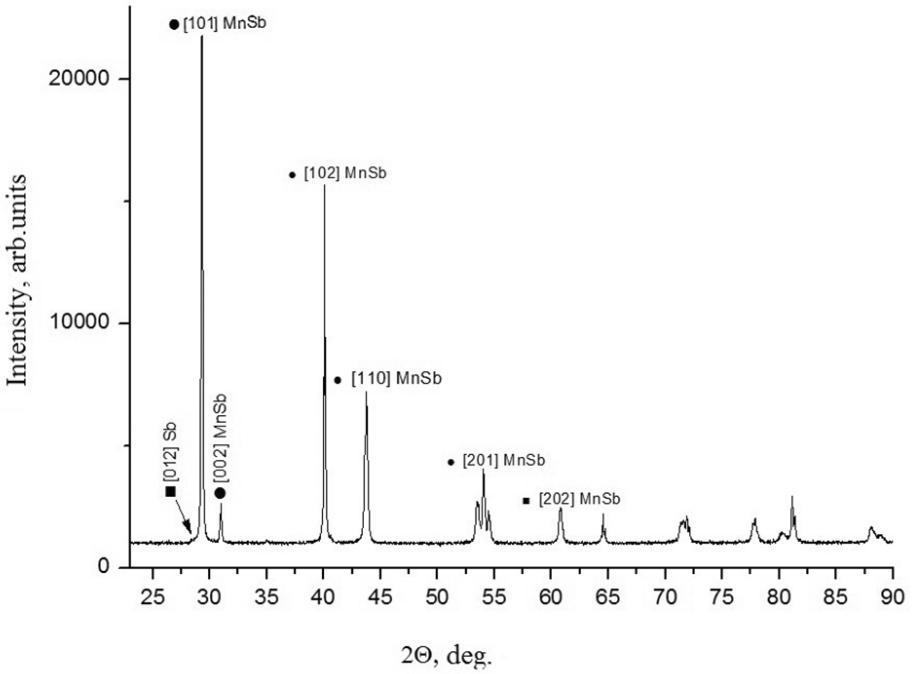

Fig. 1. Diffraction pattern of the synthesised MnSb sample

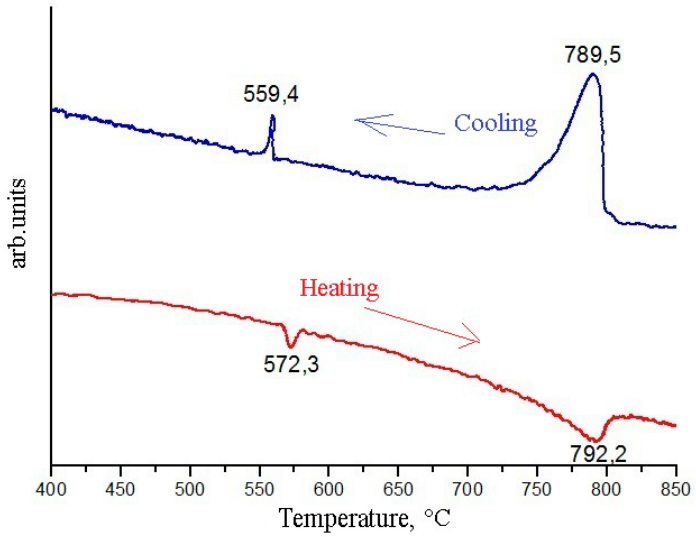

Fig. 2. Thermogram of the heating and cooling of MnSb

antimony in the samples. The examination of temperature dependences of the magnetisation (Fig. 3) showed that the synthesised samples were soft ferromagnets with the Curie point of 587 K, which corresponds well with the previous studies. The study of changes in the magnetisation due to the value of the magnetic field showed that coercive force was H_c = 5.9 Oe (Fig. 4). The magnetisation value in the magnetic saturation field was *Ms* = 84 emu/g with the value of residual magnetisation being 0.9 emu/g.

Manganese antimonide films were synthesised using sequential separate vacuum-thermal deposition of Mn and Sb films on sitall and silicon substrates with their further thermal annealing. To optimise obtaining the stoichiometric composition of MnSb films, we calculated the flux density and the rate of condensation of vapours of Mn and Sb metals. The calculations were made under conditions of molecular evaporation using the Langmuir equation [23]. Based on the results of temperature dependences of the evaporation

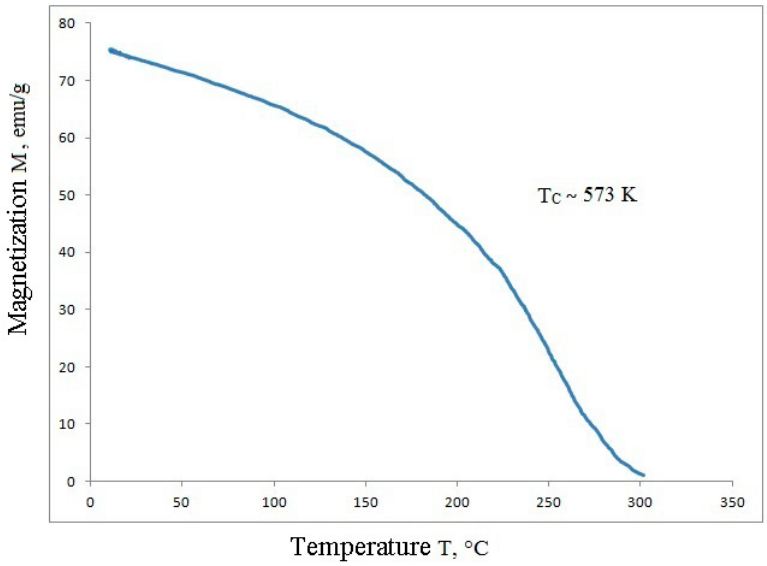

Fig. 3. Temperature dependences of the magnetisation of MnSb samples

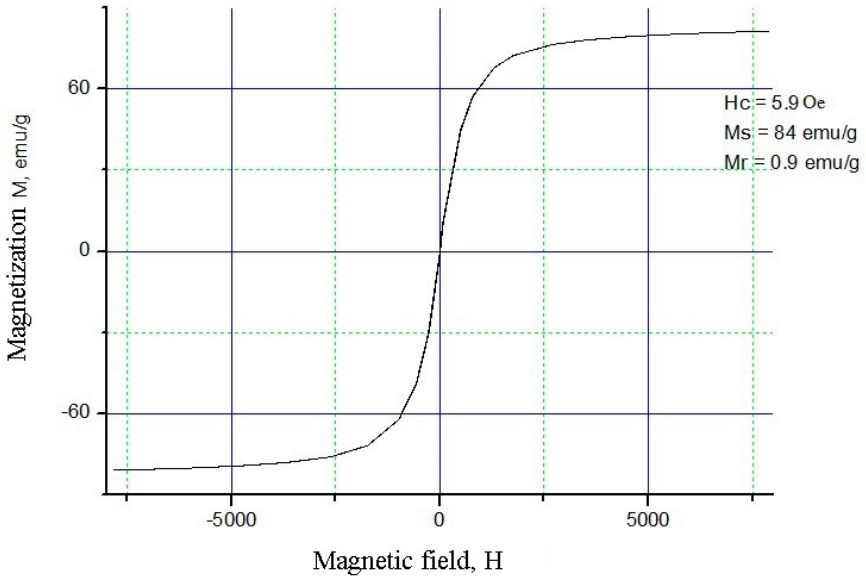

Fig. 4. Dependence of the magnetisation of bulk samples on the value of the magnetic field at T = 300 K

rates of antimony and manganese in the range of 900–1700 K, the distance from the evaporator to the substrate varied from 3 to 15 cm. The calculation results are presented in Figs. 5, 6.

The metals were evaporated in vacuum ($5 \cdot 10^{-4}$ Pa) on a substrate made of single-crystal silicon. We used high-purity metals Mn (5N) and Sb (5N). Conical resistive heaters, pre-annealed in a high vacuum, were used as the source of evaporation. We chose the temperature of the evaporator and the distance between the evaporator and the substrate based on the calculated densities of fluxes and the rate of evaporation. The time of evaporation was chosen so that the thickness of the films was ~ 200 nm.

The samples of metals for the synthesis of manganese antimonide with a stoichiometric composition contained 0.020 g of manganese and 0.032 g of antimony respectively. The films were deposited using a vacuum universal post (VUP-5). The sputtering was conducted with a ~ 10^{-4} Pa vacuum. Conical resistive heaters were

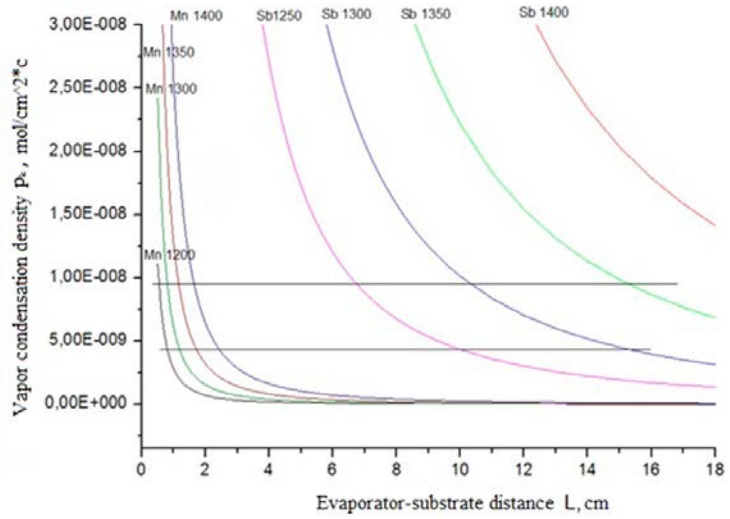

Fig. 5. Dependence of the condensation flux density on the evaporator-substrate distance

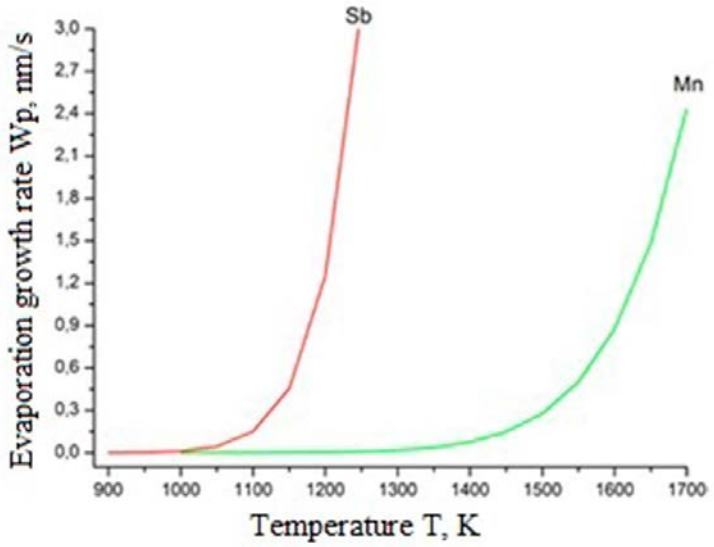

Fig. 6. Temperature dependence of the rate of condensation of Mn and Sb on the substrate 2θ

used as the evaporator. The distance between the evaporator and the substrate was at least 10 cm. The size of the substrates was 10x5x0.5 mm. The composition of the films was studied using XRD and scanning electron microscopy (SEM). Fig. 7a shows a diffraction pattern of the Sb film on a sitall substrate where only reflections related to antimony and sitall were observed. Fig. 7b shows the diffraction pattern of the Sb film on silicon substrates.

Manganese films were sputtered on antimony films. The MnSb films were synthesised by thermal annealing in vacuumed ampoules placed in the isothermic section of an electrical furnace. According to XRD data (Fig. 8) and microstructural analysis (Fig. 9), phase synthesis of MnSb started at a temperature of 380 °C.

The optimal temperature of synthesis was ~ 400 ± 20 °C with an annealing time of 2 hours. A further increase of the temperature resulted in the disruption of the mechanical strength and detachment of the films from the substrate. Fig. 10 shows the temperature dependence of the resistivity within the temperature range of 100 – 300 K, according to which the films had metal conductivity. It should also be noted that the resistivity of the annealed films was 3-4 times higher as compared to the unannealed ones. This

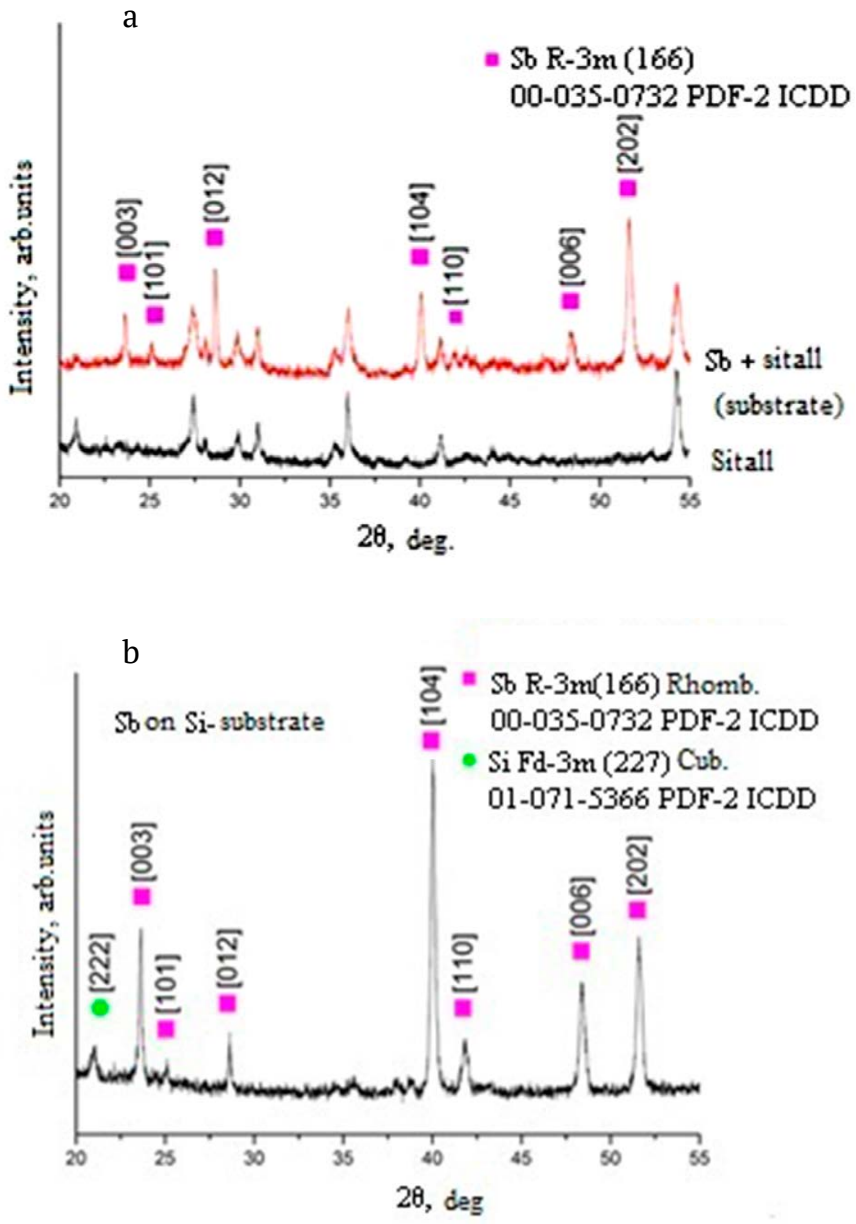

Fig. 7. X-ray diffraction patterns of Sb films on substrates made of sitall (a) and single-crystal silicon (b)

also proves the interaction between manganese and antimony metals with the formation of a manganese antimonide film (MnSb).

4. Conclusion

Using the vacuum-ampoule method, we synthesised thick bulk samples of manganese antimonide, which are soft ferromagnets with T_c = 587 K. The high chemical activity of nanostructured Mn and Sb metal films allows synthesising the MnSb compound at low temperatures by annealing in a high vacuum. We found optimal conditions for the synthesis of MnSb from Mn and Sb films.

Author contributions

All authors made an equivalent contribution to the preparation of the publication.

Conflict of interests

The authors declare that they have no known competing financial interests or personal relationships that could have influenced the work reported in this paper.

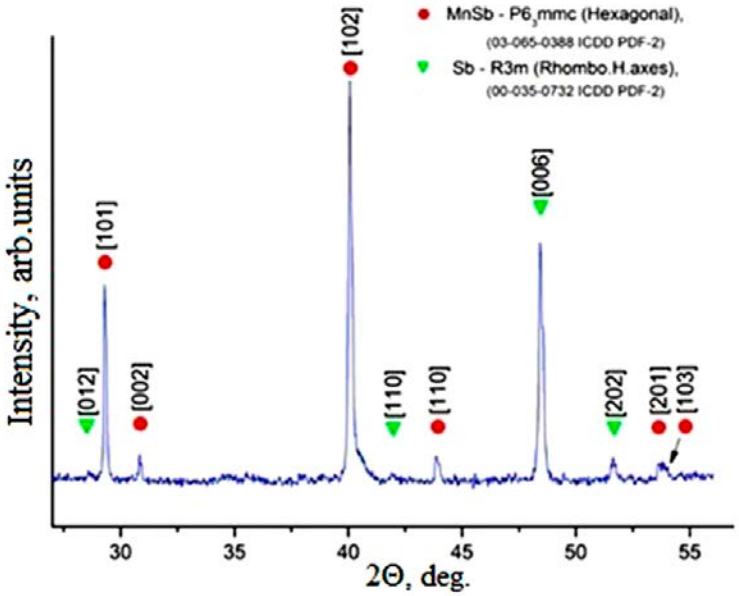

Fig. 8. Diffraction patterns of Mn + Sb films after annealing at T = 400 ° C

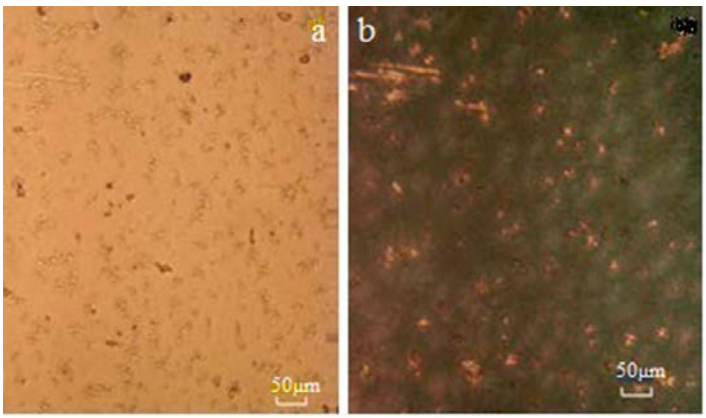

Fig. 9. Microstructure of a film with Mn and Sb layers, before annealing (a), after annealing at 400 °C (b)

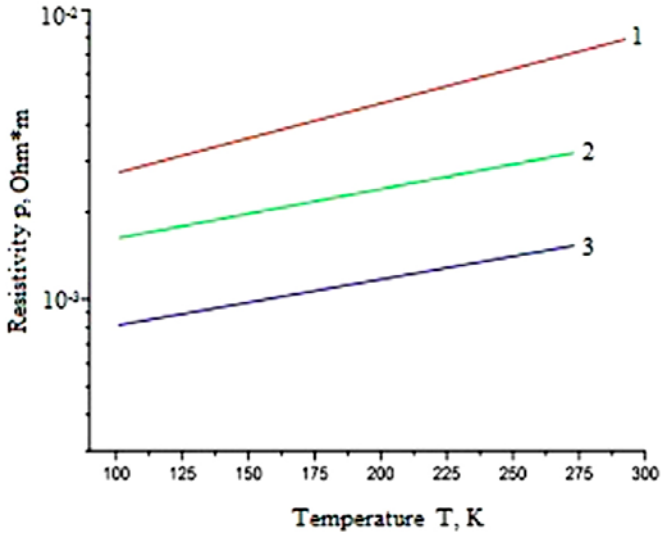

Fig. 10. Temperature dependence of the resistivity of films with a temperature range of 100-300 K: *1* – annealed MnSb film on sitall; *2* – Mn + Sb, unannealed on sitall; *3* – unannealed Mn + Sb on silicon

References

1. Ugai Ya. A. *Obshchaya i neorganicheskaya khimiya* [General and inorganic chemistry]. Moscow: Vysshaya shkola Publ., 5th ed.; 2007. 526 p.

2. Kainzbauer P., Richter K.W., Ipser H. Experimental investigation of the binary Mn-Sb phase diagram. *Journal of Phase Equilibria and Diffusion*. 2016;37(4): 459–468. https://doi.org/10.1007/s11669-016-0470-2

3. Halla H., Nowotny H., X-ray Investigation in the system manganese-antimony. *Zeitschrift für Physikalische Chemie*. 1936;34: 141–144. https://doi.org/10.1515/zpch-1936-3409

4. *Binary alloy phase diagrams*. Okamoto H., Schlesinger M. E.; Mueller E. M. (eds.). ASM International, vol. 3: 2016. p. 2598. https://doi.org/10.31399/asm.hb.v03.9781627081634

5. Yamashita T., Takizawa H., Sasaki T., Uheda K., Endo T. Mn3Sb: A new $L1_2$-type intermetallic compound synthesized under high-pressure. *Journal of Alloys and Compounds*. 2016;348(1-2): 220–223. https://doi.org/10.1016/S0925-8388(02)00834-4

6. Marenkin S. F., Kochura A. V., Izotov A. D., Vasil'ev M. G. Manganese pnictides MnP, MnAs, and MnSb are ferromagnetic semimetals: preparation, structure, and properties. *Russian Journal of Inorganic Chemistry*. 2018;63(14): 1753–1763. https://doi.org/10.1134/S0036023618140036

7. Han G. C., Ong C. K., Liew T. Y. F. Magnetic and magneto-optical properties of MnSb films on various substrates. *Journal of Magnetism and Magnetic Materials*. 1999;192(2): 233–237. https://doi.org/10.1016/S0304-8853(98)00545-9

8. Teramoto I., Van Run A. M. J. G. The existence region and the magnetic and electrical properties of MnSb. *Journal of Physics and Chemistry of Solids*. 1968;29: 347–352. https://doi.org/10.1016/0022-3697(68)90080-2

9. Chen T., Stitius W., Allen J. W., Steward G. R. Magnetic and electric properties of MnSb. *AIP Conference Proceedings*. 1976;29: 532–535. https://doi.org/10.1063/1.30431

10. Lyakisheva N. P. *Diagrammy sostoyaniya dvoinykh metallicheskikh system* [State diagrams of binary metal systems]: Handbook: vol. 3. Moscow: Mashinostroenie Publ.; 2001. 872 p.

11. Grazhdankina N. P., Medvedeva I. V., Pasheev A. V., Bersenev Yu. S. Magnetic properties of alloys MnSb and $Mn_{1.11}Sb$ after subjection to high pressures and temperatures. *Journal of Experimental and Theoretical Physics*. 1981;54(3): 564–567. Available at: http://www.jetp.ac.ru/cgi-bin/dn/e_054_03_0564.pdf

12. Zhang H., Kushvaha S.S., Chen S., Gao X., Wang S. Synthesis and magnetic properties of MnSb nanoparticles on Si-based substrates. *Applied Physics Letters*. 2007;90(20): 202503. https://doi.org/10.1063/1.2737908

13. Marenkin S. F., Izotov A. D., Fedorchenko I. V., Novotortsev V. M. Manufacture of magnetic granular structures in semiconductor-ferromagnet systems. *Russian Journal of Inorganic Chemistry*. 2015;60(3): 295–300. https://doi.org/10.1134/S0036023615030146

14. Dmitriev A. I., Talantsev A. D., Koplak O. V., Morgunov R. B. Magnetic fluctuations sorted by magnetic field in MnSb clusters embedded in GaMnSb thin films. *Journal of Applied Physics*. 2016;119(7): 073905. https://doi.org/10.1063/1.4942005

15. Hanna T., Yoshida D., Munekata H. Preparation characterization of MnSb–GaAs spin LED. *Journal of Crystal Growth*. 2011;323(1): 383–386. https://doi.org/10.1016/j.jcrysgro.2010.11.146

16. Moya X., Kar-Narayan S., Mathur N. Caloric materials near ferroic phase transitions. *Journal of Nature Materials*. 2014;13(5): 439–450. https://doi.org/10.1038/nmat3951

17. Burrows C., Dobbie A., Myronov M., Hase T., Wilkins S.,Walker M. Heteroepitaxial growth of ferromagnetic MnSb(0001) films on Ge/Si(111) virtual substrates. *Crystal Growth Design*. 2013;13(11): 4923-4929. https://doi.org/10.1021/cg4011136

18. Mousley P. J., Burrows C. W., Ashwin M. J., Takahasi M., Sasaki T., Bell G. R. In situ X-ray diffraction of GaAs/MnSb/Ga(In)As heterostructures. *Physica Status Solidi*. 2017;254(2): 1600503. https://doi.org/10.1002/pssb.201600503

19. Matsui T., Ando E., Morii K., Nakayama Y. Development of (001) texture of MnSb in thin films prepared by interdiffusion of Mn/Sb multilayers. *Materials Science and Engineering*. 1994; B(27): 109–115. https://doi.org/10.1016/0921-5107(94)90131-7

20. Dai R., Chen N., Zhang X. W., Peng C. Net-like ferromagnetic MnSb film deposited on porous silicon substrates. *Journal of Crystal Growth*. 2007;299(1): 142–145. https://doi.org/10.1016/j.jcrysgro.2006.11.132

21. Kushvaha S. S., Zhang H. L., Yan Z, Wee A. T. S., Wang X. Growth of self-assembled Mn, Sb and MnSb nanostructures on highly oriented pyrolytic graphite. *Thin Solid Films*. 2012;520(23): 69096915. https://doi.org/10.1016/j.tsf.2012.07.099

22. Marenkin S. F., Ril A. I., Rabinovich O., Fedorchenko I., Didenko S. MnSb ferromagentic films synthesized by vacuum thermal evaporation. *Journal of Physics: Conference Series*. 2020;1451: 012022. https://doi.org/10.1088/1742-6596/1451/1/012022

23. Nesmeyanov A. N. *Davlenie para khimicheskikh elementov* [Vapor pressure of chemical elements] Moscow: AN SSSR Publ.; 1961. 396 p.

Information about the authors

Muhammadyusuf Jaloliddinzoda, PhD student, Department of Electronic materials technology, National University of Science and Technology "MISIS", Moscow, Russian Federation; e-mail: muhammad.9095@mail.ru. ORCID iD: https://orcid.org/0000-0002-5187-5136.

Sergey F. Marenkin, DSc in Chemistry, Professor, Chief Researcher of the Laboratory of Semiconductor and Dielectric Materials, Kurnakov Institute of General and Inorganic Chemistry of the Russian Academy of Sciences, Moscow, Russian Federation; email: marenkin@rambler.ru. ORCID iD: https://orcid.org/0000-0003-2577-6481.

Alexey I. Ril', Junior Researcher at the Laboratory of Semiconductor and Dielectric Materials, Kurnakov Institute of General and Inorganic Chemistry of the Russian Academy of Sciences, Moscow, Russian Federation; e-mail: ril_alexey@mail.ru. ORCID iD: https://orcid.org/0000-0002-7745-2529.

Mikhail G. Vasil'ev, DSc in Technical Sciences, Professor, Head of the Laboratory of Semiconductor and Dielectric Materials, Kurnakov Institute of General and Inorganic Chemistry of the Russian Academy of Sciences, Moscow, Russian Federation; e-mail: mgvas@igic.ras.ru. ORCID iD: https://orcid.org/0000-0002-4279-1707.

Alexander D. Izotov, DSc in Chemistry, Corresponding Member of Russian Academy of Sciences, Chief Researcher at the Laboratory of Semiconductor and Dielectric Materials, Kurnakov Institute of General and Inorganic Chemistry of the Russian Academy of Sciences, Moscow, Russian Federation; e-mail: izotov@igic.ras.ru. ORCID iD: https://orcid.org/0000-0002-4639-3415.

Denis E. Korkin, Technologist at the Laboratory of Semiconductor and Dielectric Materials, Kurnakov Institute of General and Inorganic Chemistry of the Russian Academy of Sciences, Moscow, Russian Federation; e-mail: disa5566@yandex.ru. ORCID iD: https://orcid.org/0000-0001-6838-3974.

Received 8 June 2021; Approved after reviewing 17 June 2021; Accepted for publication 15 August 2021; Published online 25 September 2021.

Translated by Marina Strepetova
Edited and proofread by Simon Cox

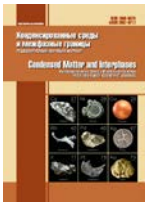

ISSN 1606-867X (Print)
ISSN 2687-0711 (Online)
Condensed Matter and Interphases
Kondensirovannye Sredy i Mezhfaznye Granitsy
https://journals.vsu.ru/kcmf/

Original articles

Research article
https://doi.org/10.17308/kcmf.2021.23/3531

TSF-MOCVD – a novel technique for chemical vapour deposition on oxide thin films and layered heterostructures

A. R. Kaul[1], R. R. Nygaard✉[1], V. Yu. Ratovskiy[1], A. L. Vasiliev[2,3,4]

[1]*Lomonosov Moscow State University,*
1 Leninskie Gory, Moscow 119991, Russian Federation

[2]*National Research Center "Kurchatov University",*
1 pl. Akademika Kurchatova, Moscow 123182, Russian Federation

[3]*Shubnikov Crystallography Institute of the Russian Academy of Sciences,*
59 Leninskiy prospect, Moscow 119333, Russian Federation

[4]*Moscow Institute of Physics and Technology,*
9 Institutskiy Pereulok, Moscow Region, Dolgoprudny, 141701, Russian Federation

Abstract

A new principle for supplying volatile precursors to MOCVD gas-phase chemical deposition systems is proposed, based on a two-stage evaporation of an organic solution of precursors from a soaked cotton thread, which passes sequentially through the zones of evaporation of the solvent and precursors. The technological capabilities of TSF-MOCVD (Thread-Solution Feed MOCVD) are demonstrated based on examples of obtaining thin epitaxial films of CeO_2, h-LuFeO3 and thin-film heterostructures β-Fe_2O_3/h-$LuFeO_3$. The results of studying the obtained films by X-ray diffraction, energy dispersive X-ray analysis, and high- and low-resolution transmission microscopy are presented. Using the TSF module, one can finely vary the crystallisation conditions, obtaining coatings of the required degree of crystallinity, as evidenced by the obtained dependences of the integral width of the h-$LuFeO_3$ reflection on the film growth rate. Based on the TEM and XRD data, it was concluded that β-Fe_2O_3 grows epitaxially over the h-$LuFeO_3$ layer. Thus, using TSF-MOCVD, one can flexibly change the composition of layered heterostructures and obtain highly crystalline epitaxial films with a clear interface in a continuous deposition process.

Keywords: Thread-solution feed, TSF, MOCVD, Epitaxy, Thin films, Heterostructures

Acknowledgements: the work was carried out within the framework of project No 19-33-90289 supported by Russian Foundation for Basic Research.

For citation: Kaul A. R., Nygaard R. R., Ratovskiy V. Yu., Vasiliev A. L. TSF-MOCVD – a novel technique for chemical vapour deposition on oxide thin films and layered heterostructures. *Kondensirovannye sredy i mezhfaznye granitsy = Condensed Matter and Interphases*. 2021;23(3): 396–405. https://doi.org/10.17308/kcmf.2021.23/3531

Для цитирования: Кауль А. Р., Нигаард Р. Р., Ратовский В. Ю., Васильев А. Л. TSF-MOCVD – новый способ осаждения оксидных тонких пленок и слоистых гетероструктур из газовой фазы. *Конденсированные среды и межфазные границы*. 2021;23(3): 396–405. https://doi.org/10.17308/kcmf.2021.23/3531

✉ Roy Nygaard, e-mail: rnygaard@mail.ru
© Kaul A. R., Nygaard R. R., Ratovskiy V. Yu., Vasiliev A. L., 2021

The content is available under Creative Commons Attribution 4.0 License.

1. Introduction

Thin-film technologies underlie the development of many scientific and technical fields, and their continuous improvement gives rise to new possibilities for creating modern materials and thin-film devices with a precisely specified architecture and physical properties. Along with high-vacuum physical methods for producing thin films, chemical vapour deposition (CVD) is widely used. [1–3]. Thus, the MOC-hydride epitaxy method has taken a leading position in the production of planar semiconductor structures $A^{III}B^{V}$, $A^{II}B^{VI}$ and solid solutions based on them [4], and metal-organic precursor vapour deposition (MOCVD) is successfully used to obtain a wide range of oxide coatings, as well as in the development of functional materials for oxide electronics [5]. The MOCVD method started to be intensively developed at the end of the 80s of the last century due to the need to obtain thin HTSC films [6]. Over the years, this method has been demonstrated to be extremely flexible in producing films of a wide variety of compositions and purposes, as well as the ability to deposit coatings with high uniformity and over large areas. [7]. Both highly-crystalline epitaxial functional layers and heterostructures with clear interfaces with a thickness of several nanometres [8], and polycrystalline coatings with a thickness of tens of microns can be obtained using MOCVD [9].

In the deposition of multicomponent films, along with the traditional approach, which consists in the evaporation/sublimation of the precursor of each component from an individual source heated to the required temperature [7], a more convenient single source is used successfully [10, 11]. In this case, the mixture of precursors is sharply heated to a temperature providing the simultaneous transition of all precursors into a vapour, including the least volatile of them. This approach can be implemented in two ways, which differ in the aggregate states of the mixture of precursors: either an aerosol of an organic solution of a mixture of precursors [10, 11], or a fine mechanical mixture of solid precursors are used [12, 13]. Both schemes have advantages and disadvantages. For example, liquid-phase MOCVD systems are technically simpler than solid state systems and provide a continuous and smoother feed of precursors into the reactor. However, it is important to understand that the total concentration of precursor solutions is usually in the order of 10^{-1} M, from which it follows that the vapour in the reactor is formed mainly by the organic solvent. The solvent vapour, as well as the vapour of the precursors, undergoes pyrolysis and oxidation near the substrate heated to a high temperature, which increases the concentration of residual carbon in the films, reduces and makes the partial pressure of oxygen in the deposition zone undefined [14]. It is clear that this method is of little use for the reproducible production of films of easily reducible oxides, oxides with a narrow region of oxygen homogeneity, and other films with functional properties sensitive to residual carbon.

MOCVD systems, in which the reactor is fed by the flash evaporation of micro-portions of a mixture of solid precursors, are free from these fundamental disadvantages. [12, 15], however, instead of them, there are problems with the uniformity of vapour supply to the reactor and the limited amount of precursor substances loaded into the feeder of the setup for a single experiment. The disadvantages of this approach in the implementation of the MOCVD process also include the technical complexity of setups, especially those designed specifically for the production of thin-film heterostructures. [16, 17].

This article highlights a new principle of supplying liquid precursors to chemical vapour deposition systems, which combines the advantages of known liquid-phase and solid state power supply systems and is devoid of their disadvantages [18]. Moreover, it allows obtaining thin-film structures consisting of layers of different chemical compositions within a single deposition run, as well as thin films with a vertical composition gradient.

2. Experimental

All samples were obtained using MOCVD setup with TSF module for precursor feed and a vertical hot-walled reactor. The scheme of MOCVD setup with TSF module, in which the new principle was applied, is shown in Fig. 1. During its operation, the following stages were carried out: a cotton thread (11) passed through a solution of precursors in a low-boiling solvent (6), which

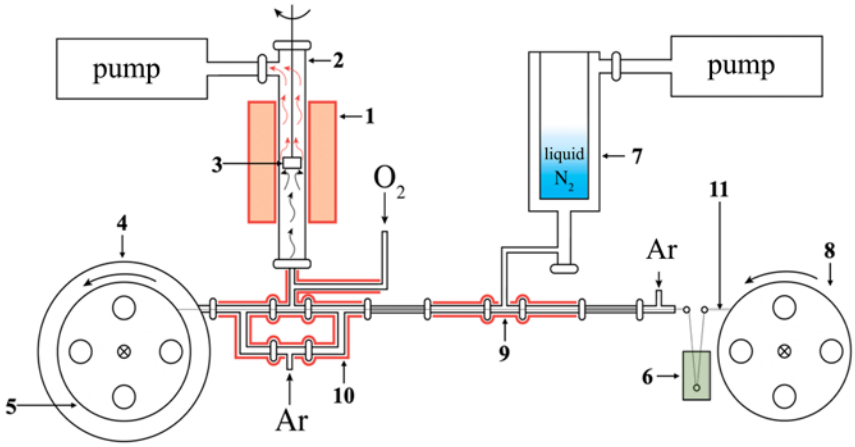

Fig. 1. The scheme of MOCVD setup with TSF module, *1* – reactor furnace, *2* – quartz reactor, *3* – substrate holder, *4* – vacuum container for the receiving reel, *5* – receiving reel, *6* – precursor reservoir, *7* – nitrogen trap, *8* – feeding reel, *9* – cold zone of the TSF module, *10* – hot zone of the TSF module, *11* – cotton thread

evaporated in the solvent distilling zone (9). After distilling off the solvent, the thread, covered with small crystals of precursors, continued to move towards the hot zone (10), where the precursors were sublimated, and the resulting vapours were transferred to the reactor (2) by heated argon flow. Directly at the inlet to the heated quartz reactor, oxygen was introduced into the gas mixture of argon with precursor vapours in a predetermined proportion. In the reactor zone, the precursor vapours decomposed in the substrate zone, which led to the formation of a thin oxide film. Throughout the entire deposition, the substrate holder (3) was rotated constantly for a more uniform heating and a more symmetrical arrangement of the substrates with respect to the gas flow directed along the normal to their surface.

During the entire deposition process, the reservoir with the precursor solution was outside the vacuum system and was accessible to the experimenter, therefore, by replacement of the solution in the reservoir (6), one could optionally change the chemical composition of the deposited oxide layers by gradual addition of additional precursors. It allowed to control the structure of the interface, making the transition between phases either abrupt or smooth, depending on the task. The proposed scheme also allowed the extremely fine variation of the film growth rate, which is an important condition for crystallisation. It can be changed by altering either the concentration of precursors in the solution, or the speed of drawing the thread, or the absorption capacity of the thread.

The described setup was used to synthesize the following objects:

a) epitaxial CeO_2 thin films on R-sapphire,

b) epitaxial hexagonal $LuFeO_3$ (h-$LuFeO_3$) thin films on the (111) and (100) surfaces of YSZ single-crystal,

c) thin-film heterostructures with an architecture of β-Fe_2O_3(100)//h-$LuFeO_3$ (001)// YSZ(100) and β-Fe_2O_3 (111)//h-$LuFeO_3$ (001)// YSZ(111).

Metal-organic volatile complexes of $Ce(thd)_4$, $Lu(thd)_3$ and $Fe(thd)_3$ (thd = 2,2,6,6-tetramethylheptanedionate 3,5) dissolved in toluene were used as precursors. In all cases, a temperature of 190 °C was set in the hot zone of the TSF module (10) for sublimation of the precursors. CeO_2 thin films were deposited at temperatures of 850 and 900 °C in the reactor. The total pressure in the reactor was 10 mbar and the partial pressure of oxygen in the reactor was 2, 3, 4, 5, 6, and 8 mbar. The depositions were carried out on single-crystalline r-sapphire with a surface orientation (10–12), which before deposition were annealed at a temperature of 900 °C for 30 min for the purification of the surface from the residues of adsorbed organic contaminants.

The molar ratio of precursors (Lu:Fe) in a toluene solution varied from 1 to 2 for the production of h-$LuFeO_3$ single-phase thin films of the required stoichiometry. It has been found that the optimal Lu:Fe ratio in the solution is 2.

h-$LuFeO_3$ thin films were obtained at a reactor temperature of 900 °C, a total pressure in the reactor of 10 mbar and the oxygen partial pressure in the reactor of 1 mbar. The deposition was carried out on single-crystalline YSZ [$ZrO_2(Y_2O_3)$] substrates with the (111) and (100) orientations of the growth surface. Before deposition, these substrates were annealed in air at a temperature of 1100 °C for 24 h, while the defects in the structure of the surface layer, damaged by the polishing of the substrates by the manufacturer, were eliminated.

Deposition of β-Fe_2O_3 layers on the h-$LuFeO_3$ buffer layers was carried out at a temperature in the reactor of 900 °C, the total pressure in the reactor of 10 mbar, and the partial pressure of oxygen in the reactor of 0.1 mbar.

The epitaxial growth of all films and layers was confirmed by X-ray diffraction (2θ-ω scanning) using a Rigaku Miniflex diffractometer with a copper anode ($\lambda K\alpha$ = 1.54046 Å), a power of 600 W, and a beta filter. The cationic composition of h-$LuFeO_3$ films was determined by energy dispersive X-ray analysis using a Carl Ziess Leo SUPRA 50 VP scanning electron microscope with an X-ray system (Oxford Instruments INCA Energy+).

Cross sections of β-Fe_2O_3/h-$LuFeO_3$/YSZ thin-film heterostructures were prepared for transmission electron microscopy using a focused ion beam (FIB) on a Helios Nanolab 660 scanning electron microscope (ThermoFisher Scientific, USA) equipped with an Omniprobe micromanipulator (Omniprobe, USA). The cut lamellae were examined using a Titan 80-300 TEM/STEM device (FEI, USA) equipped with a C_S corrector at an accelerating voltage of 300 kV. The microscope is equipped with an EDX Si (Li) spectrometer (EDAX, USA), a high angular annular dark-field detector (HAADF) (Fischione, USA), and a Gatan Image Filter (GIF) (Gatan, USA).

3. Results and discussion

3.1. CeO_2 thin films

Epitaxial CeO_2 thin films are a very popular material with multiple applications; in particular, they are used as a buffer layer in the deposition of HTS films. CeO_2 can grow in two different orientations on R-sapphire: in one of them, the crystallographic axis [100] is directed along the normal to the substrate plane, and in the other, the [111] axis is oriented in this direction. The [100] orientation is thermodynamically more favourable, since the R-plane of the sapphire has a rectangular motif, which promotes the growth of the cubic CeO_2 face. The growth in the [111] direction is due to kinetic reasons: as is known, this direction is the direction of the rapid growth of crystals with a fluorite structure. Our goal was to achieve the growth of films in which the fraction of (100)-oriented crystallites is maximal. The key condition for success in this case is fast surface diffusion, which promotes the crystallisation of the thermodynamically favourable (100) orientation. For acceleration of the surface diffusion, two ways were used: the first was an increase in the deposition temperature, and the second was the heterovalent doping of CeO_2 films with yttrium oxide. In the second case, diffusion is activated due to the appearance of oxygen vacancies in the growing film.

The texture coefficient (T) of the (100) orientation, calculated by equation (1), which allows estimating its share among all other orientations, taking into account the structural data was used as a quantitative characteristic of the quality of the obtained films.

$$T(100) = \frac{\frac{I_{exp}^{200}}{I_{st}^{200}} + \frac{I_{exp}^{400}}{I_{st}^{400}}}{\frac{I_{exp}^{200}}{I_{st}^{200}} + \frac{I_{exp}^{400}}{I_{st}^{400}} + \frac{I_{exp}^{111}}{I_{st}^{111}} + \frac{I_{exp}^{222}}{I_{st}^{222}}}. \quad (1)$$

For the calculation, we used the intensities of the (100) and (111) reflections in the obtained films $\left(I_{exp}^{hkl}\right)$ determined by profile analysis of the corresponding reflections, as well as their reference intensities taken from the powder diffractogram stored in the crystallographic data base. Thus, the closer the texture coefficient is to 1, the more grains in the film are oriented with the (100) plane parallel to the substrate plane, and the more perfect is the film.

It can be seen, that the character of the texture coefficient dependence upon the oxygen partial pressure changes dramatically with an increase in temperature: at 850 °C the trend was downward (black line in Fig. 2a), while at 900 °C (black line in Fig. 2b) it changed to an upward trend.

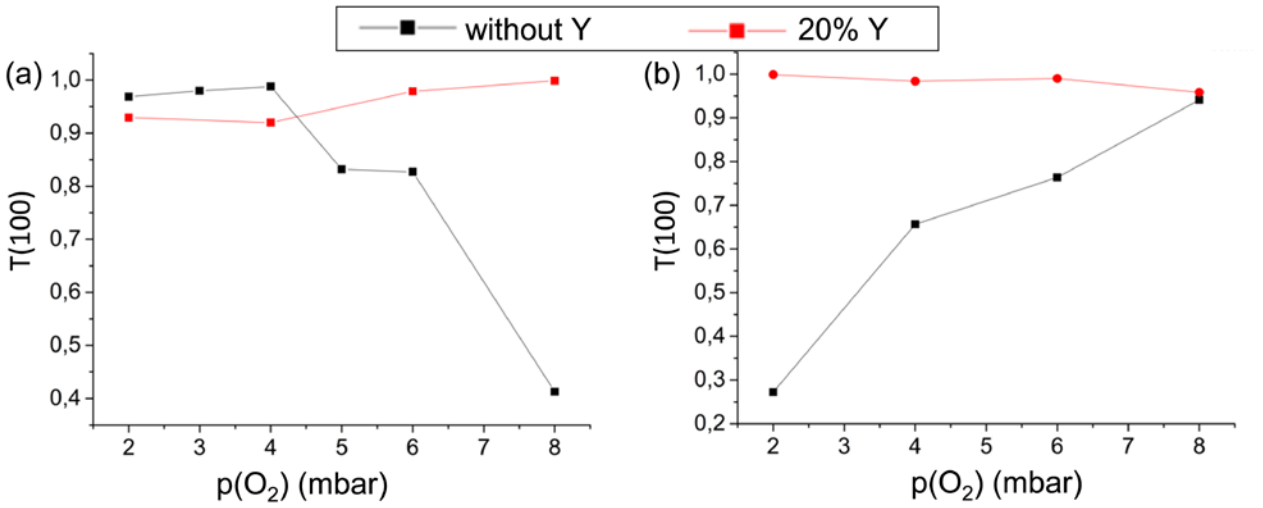

Fig. 2. Dependence of the texture orientation coefficient (100) of CeO_2 on $p(O_2)$ and the content of the doping component (yttrium oxide) at the deposition temperature a) 850 °C and b) 900 °C

This fact can be explained as follows: at 850 °C, an increase in $p(O_2)$ increased the deposition rate making the surface diffusion flow insufficient, which led to the formation of a larger proportion of grains with the (111) orientation. The rate of surface diffusion exponentially depends on the temperature and at a temperature of 900 °C it already becomes sufficient for the equilibrium crystallisation of the film from the substance approaching the substrate surface. However, at this temperature, the system approaches pO_2-T conditions for the dissociation of CeO_2, and phase stabilization of this oxide requires an increase in pO_2. Dissociation occurs with the formation of an equilibrium Ce_7O_{12} [19] phase which crystallises in the rhombohedral space group *R3,c* unit cell parameter a = 6.785 (1) Å and angle α = 99.42 (1) [20]. The emergence of the secondary phase nuclei limits the epitaxial growth of the main CeO_2 phase in the equilibrium (100) orientation, as a result of which the (111) orientation and other polycrystalline orientations develop. This should be prevented by increasing the pO_2 in the reactor.

As we noted above, the second method for activating of surface diffusion to facilitate the achievement of the thermodynamic equilibrium is the heterovalent doping of cerium oxide with yttrium oxide, which leads to the formation of oxygen vacancies in the films:

$$\frac{1}{2}Y_2O_{3(\rightarrow CeO_2)} = Y'_{Ce} + \frac{3}{2}O_O^{\times} + \frac{1}{2}V_O^{\circ\circ},$$

the concentration of which is many orders of magnitude higher than the equilibrium concentration of thermal vacancies, which, in turn, leads to a sharp increase of the surface diffusion flow. As a consequence, the dependence of the texture coefficient (red line in Figs. 2a and 2b), both on the partial pressure of oxygen and on temperature, disappears, since under any deposition conditions implemented in this study, the system has sufficient diffusion mobility to reach the most energetically favourable (thermodynamically stable) variant of film growth. This result confirms the conclusions of the study [21].

3.2. h-$LuFeO_3$ thin films

Thin films of h-$LuFeO_3$ were more complex object obtained using the proposed precursor feed method. It should be noted that under the conditions of conventional solid state synthesis, $LuFeO_3$ crystallises with orthorhombically distorted perovskite structure [22]. Formation of the hexagonal ferrite LuFeO3, which is isostructural to the hexagonal manganite $LuMnO_3$, becomes possible due to epitaxial stabilization on a structurally coherent substrate [23]. The low energy of the film – substrate interface leads to a decrease in the free energy of the system and the stabilization of phases structurally coherent to the substrate and unstable in the autonomous state [24]. In this study, YSZ(111) and YSZ(100) were used as such substrates.

For demonstration of the possibility of controlling the crystallisation conditions using the new precursor feed system, a series of depositions were carried out, varying the film growth speed by changing the thread passing speed. The X-ray diffraction results (Figs. 3a and 3b) showed that in all cases the films are h-$LuFeO_3$.

As can be seen from the dynamics of changes in the integral width of (002) reflection of the h-$LuFeO_3$ (Fig. 4), the crystallinity of the films decreased with an increase in the growth rate, which is quite a logical observation. In this case, a decrease in crystallinity can be associated not only with an insufficiently active surface diffusion flux, but also with a deviation of the system from the required stoichiometry Lu: Fe = 1: 1, leading to the formation of secondary phases enriched in iron and interfering the epitaxial growth of h-$LuFeO_3$. Their reflections can not be seen on the presented XRD patterns probably due to absence of the clearly defined growth direction.

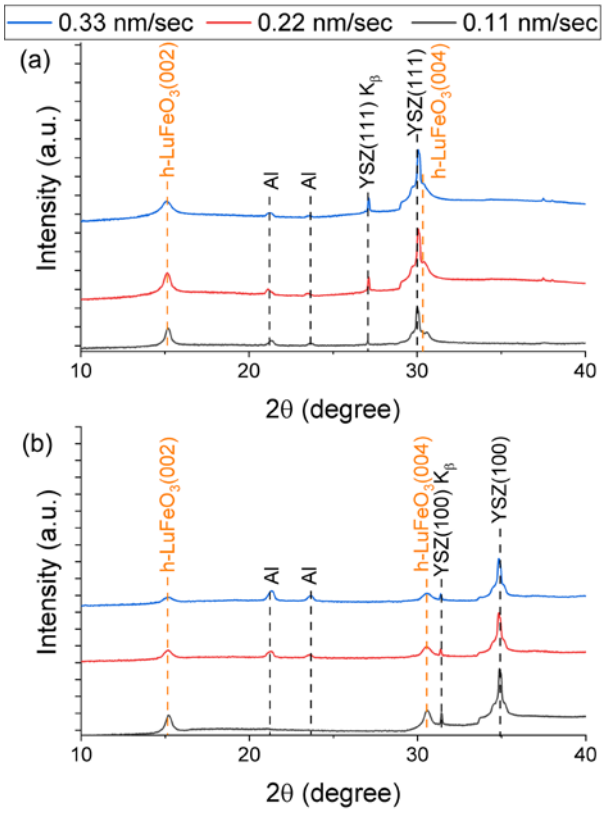

Fig. 3. Diffraction patterns of h-$LuFeO_3$ films obtained at different deposition rates on (a) YSZ (111) and (b) YSZ (100) substrates

An interesting feature is that the integral width of the h-$LuFeO_3$ reflection formed on the YSZ(100) surface in all cases was higher than that of h-$LuFeO_3$ on the YSZ(111) surface. The reason for this may be that the stabilizing effect of the (100) surface on h-$LuFeO_3$ is lower than that for the (111) surface due to the lower structural correspondence of the YSZ(100) surface to the hexagonal crystal structure of the forming film(25).

3.3. Thin-film heterostructures h-$LuFeO_3$+β-$Fe2O_3$

The possibility of the deposition of layers of various chemical compositions was demonstrated on the example of obtaining thin-film heterostructures h-$LuFeO_3$ with iron oxide on single-crystalline substrates YSZ(111) and YSZ(100). It can be seen from the diffraction patterns (Fig. 5) that the iron oxide layer growing on top the h-$LuFeO_3$ surface is an unusual cubic modification β-Fe_2O_3. It should be noted that this phase is unstable under the implemented synthesis conditions. There is information in the literature on its transition to α-Fe_2O_3 already at 650 °C [26], while in this study, the deposition temperature of the iron oxide layer was 900 °C. The absence of phases other than β-Fe_2O_3 and the presence of only one family of reflections of this phase indicated the strong epitaxial stabilization of β-Fe_2O_3 by the h-$LuFeO_3$ sublayer. It should be noted that epitaxial stabilization also changes the equilibrium characteristic phase relations between Fe_2O_3 and $LuFeO_3$: it is well known that in mixtures of powders of this and similar systems

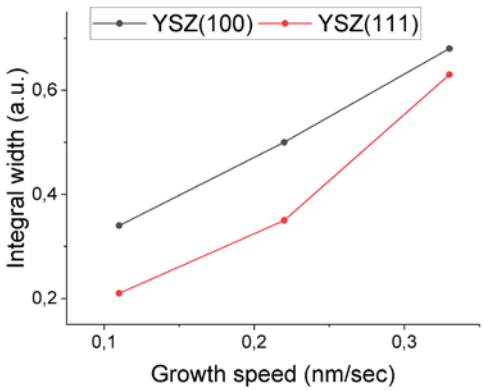

Fig. 4. Dependence of the integral width of the h-$LuFeO_3$ (002) reflection on the deposition rate

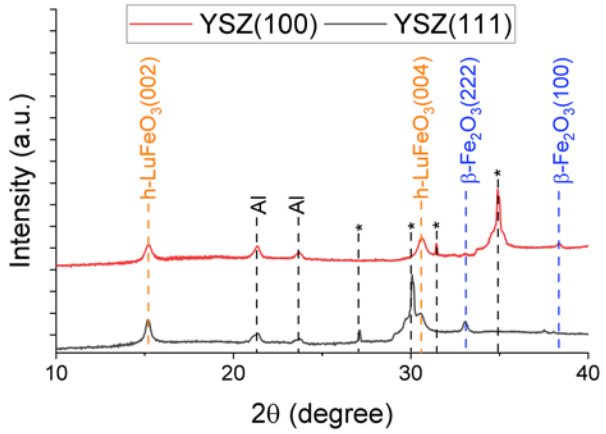

Fig. 5. Diffraction patterns of thin-film β-Fe_2O_3/h-$LuFeO_3$ heterostructures on YSZ (111) and YSZ (100) substrates. Reflexes of substrates are marked with *

(REE = Nd–Yb), Fe_2O_3, and $RFeO_3$ REE oxides react with each other forming garnet phases [27]. However, thanks to the epitaxial contact of thin films of these substances, the chemical reaction was suppressed. Similar changes in phase relations as a result of epitaxial stabilization have been described for other oxide systems as well [24].

Also, the difference in the orientation of the epitaxially growing β-Fe_2O_3 film on YSZ surfaces with different indices should be noted: in the heterostructure deposited on the YSZ(111) substrate, the oriented growth of the β-Fe_2O_3 phase was observed in the [111] direction perpendicular to the plane of the substrate, while in the heterostructure on the YSZ(100) substrate it was observed in the [100] direction perpendicular to the plane of the substrate. The results of local electron diffraction and transmission microscopy of the cross section of the obtained heterostructures confirmed the phase composition and orientation of the layers, which were determined based on the results of X-ray diffraction. Microphotographs of β-Fe_2O_3/h-$LuFeO_3$/YSZ heterostructure cross-sections (Fig. 6 a, c) indicate a higher uniformity and less surface roughness of the h-$LuFeO_3$ layer grown on YSZ(111) substrate compare to one deposited on YSZ(100). This observation can be explained by the previously described in-plane variant growth of h-$LuFeO_3$ on YSZ(100), which results in the formation of a films with microstructure fragmented into nanoscale domains [25]. The closer examination of images of heterostructure β-Fe_2O_3(001)//h-$LuFeO_3$(001)//YSZ(100) revealed that h-$LuFeO_3$ had not formed located uniformly in one direction: its (001) planes were aligned parallel to both (001) and (111) planes of the YSZ substrate. The former growth variant is observed near the substrate surface and continues up to film thickness of roughly 25 nm where the growth direction is switched to the later variant. The presence of the side orientation of h-$LuFeO_3$ in the YSZ(100) heterostructure is very interesting and can be a factor explaining the difference in the growth direction of the β-Fe_2O_3 on different substrates. Thus, in the heterostructure on YSZ(111) substrate the stabilizing surface for β-Fe_2O_3 is h-$LuFeO_3$ with its (001) plane parallel to the substrate plane while in case of YSZ(100) substrate β-Fe_2O_3 is stabilized on h-$LuFeO_3$ with its (001) plane inclined by 54.7o relative to the substrate plane (54.7 is the angle between <111> and <100> directions in the cubic cell). This substantiation of the β-Fe_2O_3 growth is also reinforced by the fact that the angle between the crystallographic directions of β-Fe_2O_3 in heterostructures on different substrates (<111> on YSZ(111) and <100> on YSZ(100)) is also 54.7°.

Grains of β-Fe_2O_3 with clearly visible grain boundaries are clearly seen on microphotographs of heterostructures deposited on both substrates, which indicates Volmer–Weber type (island) growth. The growth of iron oxide layer with a thickness of about 5 nm on the surface of the β-Fe_2O_3 in the heterostructure on the YSZ(111) substrate should be noted (Fig. 6b). According to the Fourier spectrum, this nanolayer can be described by a cubic syngony with a lattice parameter of 8.4 Å, which can correspond to the Fe_3O_4 phase with a lattice parameter of 8.396 nm (ICDD PDF-2 database). Its appearance in this heterostructure and, on the contrary, its absence in the heterostructure on the YSZ(100) substrate (Fig.6c, d) can be explained by the fact that, in the former case, the critical thickness of the β-Fe_2O_3 film is exceeded, above which the energy lowering of β-Fe_2O_3 (111)//h-$LuFeO_3$ (001) epitaxial contact turns out to be insufficient to stabilize this metastable modification of iron oxide. At the same time, in the heterostructure on the YSZ(100) substrate, β-Fe_2O_3 grows in a different orientation relative to h-$LuFeO_3$, which obviously

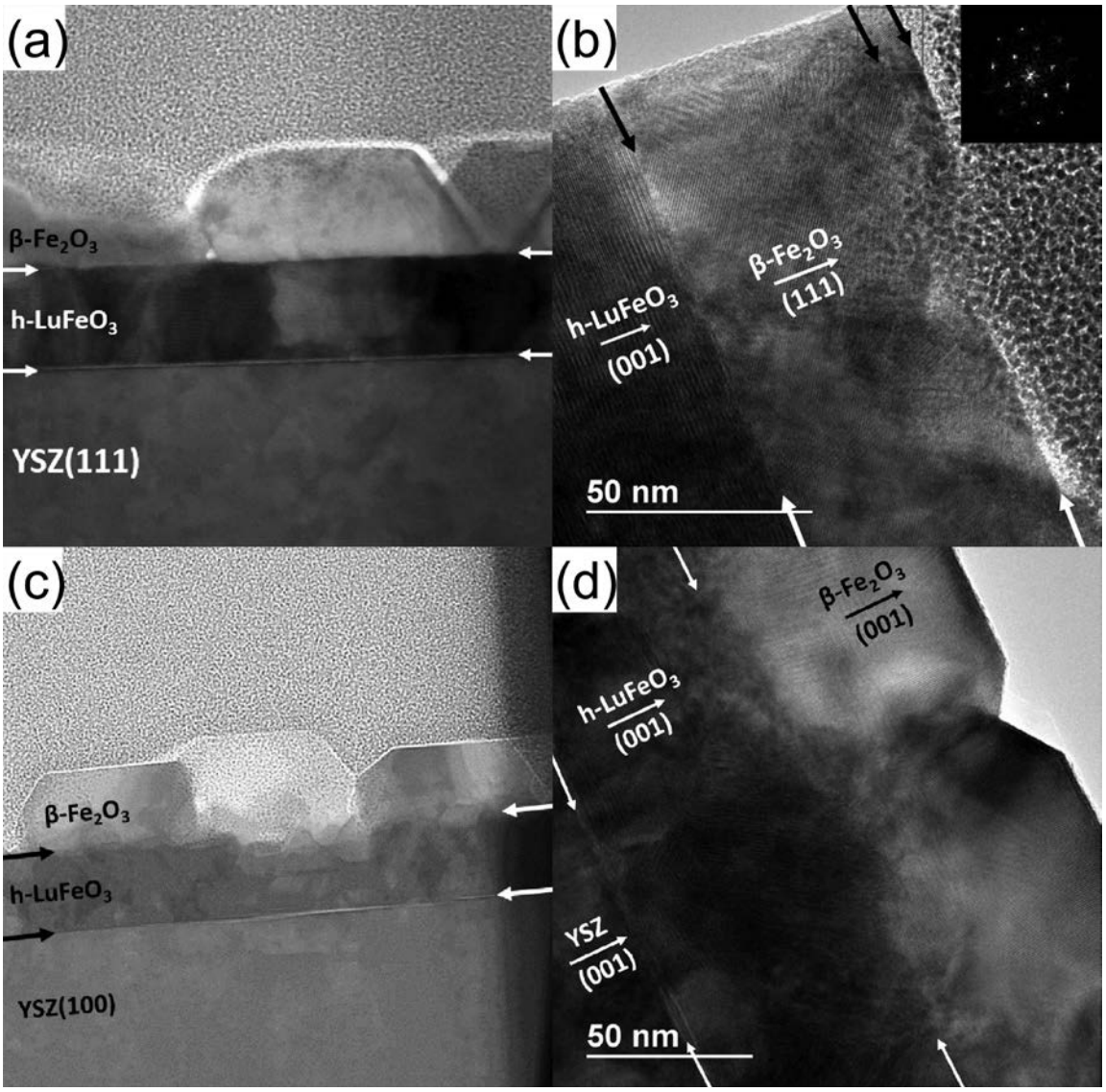

Fig. 6. Results of cross-section TEM of heterostructures (a, b) β-Fe_2O_3 (111)//h-$LuFeO_3$ (001)//YSZ (111) and (c, d) β-Fe_2O_3 (001)//h-$LuFeO_3$ (001)//YSZ (100)

leads to an increase in the critical thickness of this epitaxially stabilized layer. This interesting aspect, the dependence of the critical thickness on the orientetion of epitaxially stabilized phase, will be clarified by further calculations of the interface energies using the algorithm described by us in [25].

4. Conclusions

Thus, we have implemented a new version of the MOCVD with an original method for supplying volatile precursors to the reactor, called TSD-MOCVD, which combines the advantages of liquid-phase and solid-state single-source MOCVD variants. The deposition occurs at a low total pressure in the reactor, the precursor solution is available to the operator throughout the experiment, which allows one to change the composition of the solution and/or its concentration, make a cyclic change, and to add new components to it. The new method was used for the deposition of CeO_2 films, the possibility of a smooth change in the deposition rate, its effect, as well as the effect of heterovalent doping on the texture of the films are shown. The great preparative capabilities of the proposed method for the growth of epitaxial heterostructures with a clear interface were based on the examples of β-Fe_2O_3(111)//h-$LuFeO_3$(001)//YSZ(111) and β-Fe_2O_3(001)//h-

$LuFeO_3$(001)//YSZ(100). The possibility of the epitaxy of metastable β-Fe_2O_3 polymorph on the surface of hexagonal lutetium ferrite was revealed for the first time The existence of both phases is explained within the framework of the phenomenon of epitaxial stabilization. Such film composites will be further investigated for possible multiferroic properties.

Author contributions

Kaul A. R. – scientific leadership, research concept, text writing. Nigaard R. R. and Ratovskiy V. Yu. – conducting experiments on gas-phase deposition of thin films and heterostructures, processing the results of X-ray diffraction and transmission electron microscopy, text writing. Vasiliev A. L. – carrying out transmission electron microscopy and discussion of its results.

Conflict of interests

The authors declare that they have no known competing financial interests or personal relationships that could have influenced the work reported in this paper.

References

1. Blocher J. Coating by chemical vapor deposition (CVD). *SAE Technical Paper Series*. 1973;82: 1780–6. https://doi.org/10.4271/730543

2. Pierson H. *Handbook of chemical vapor deposition*. 2nd ed. Noyes Publications; 1999. 506 p. https://doi.org/10.1016/B978-081551432-9.50005-X

3. Syrkin V. G. CVD- metod. *Khimicheskaya parofaznaya matellizatsiya* [CVD-method of chemical vapor-phase metallization]. Nauka Publ.; 2000. 495 p. (In Russ.)

4. Akchurin R. H., Marmalyuk A. A. *MOS-gidridnaya epitaksiya v tekhnologii materialov fotoniki i elektroniki* [MOC-hydrid epitaxy in the technology of materials for photonics and electronics]. Technosphera Publ.; 2018. 488 p. (In Russ.)

5. Wright P. J., Crosbie M. J., Lane P. A., Williams D. J., Jones A. C., Leedham T. J., Davies H. O. Metal organic chemical vapor deposition (MOCVD) of oxides and ferroelectric materials. *Journal of Materials Science: Materials in Electronics*. 2002;13(11): 671–678. https://doi.org/10.1023/a:1020618411750

6. Wahl G., Arndt J., Stadel O. Chemical vapor deposition of superconductor and oxide films. In: *Chemical physics of thin film deposition processes for micro- and nano-technologies*. Springer; 2002. p. 145–170. https://doi.org/10.1007/978-94-010-0353-7_7

7. Choy K. L. Chemical vapour deposition of coatings. *Progress in Materials Science*. 2003;48(2): 57–170. https://doi.org/10.1016/s0079-6425(01)00009-3

8. Dubourdieu C., Rosina M., Audier M., Weiss F., Sénateur J. P., Dooryhee E., Hodeau J. L. Application of pulsed liquid-injection MOCVD to the growth of ultrathin epitaxial oxides for magnetic heterostructures. *Thin Solid Films*. 2001;400(1–2): 81–84. https://doi.org/10.1016/s0040-6090(01)01457-2

9. Samoilenkov S.V., Stefan M. A., Wahl G. MOCVD of thick YSZ coatings using acetylacetonates. *Surface and Coatings Technology*. 2005;192(1): 117–123. https://doi.org/10.1016/j.surfcoat.2004.03.019

10. Weiss F., Audier M., Bartasyte A., Bellet D., Girardot C., Jimenez C., ... Ternon C. Multifunctional oxide nanostructures by metal-organic chemical vapor deposition (MOCVD). *Pure and Applied Chemistry*. 2009;81(8): 1523–1534. https://doi.org/10.1351/pac-con-08-08-10

11. Sénateur J.-P., Dubourdieu C., Galindo V., Weiss F., Abrutis A. Application of pulsed injection MOCVD to the deposition of oxide single layers and superlattices. In: *Innovative processing of films and nanocrystalline powders*. 2002. p. 71–105 https://doi.org/10.1142/9781860949623_0003.

12. Kartavtseva M. S., Gorbenko O. Y., Kaul A. R., Akbashev A. R., Murzina T. V., Fusil S., Barthélémy A., Pailloux F. $BiFeO_3$ thin films prepared by MOCVD. *Surface and Coatings Technology*. 2007;201(22-23): 9149–9153. https://doi.org/10.1016/j.surfcoat.2007.04.099

13. Bibes M., Gorbenko O., Martínez B., Kaul A., Fontcuberta J. Alkaline-doped manganese perovskite thin films grown by MOCVD. *Journal of Magnetism and Magnetic Materials*. 2000;211(1-3): 47–53. https://doi.org/10.1016/s0304-8853(99)00712-x

14. Decker W., Erokhin Y., Gorbenko O., Graboy I., Kaul A., Nurnberg A., Pulver M., Stolle R., Wahl G.. Low-pressure single aerosol source MOCVD of YBCO thin films. *Journal of Alloys and Compounds*. 1993;195(C): 291–294. https://doi.org/10.1016/0925-8388(93)90742-6

15. Kaul A. R., Seleznev B. V. New principle of feeding for flash evaporation MOCVD devices. *Le Journal de Physique IV*. 1993;3(3): 375–378. https://doi.org/10.1051/jp4:1993351

16. Menushenkov A. P., Ivanov V. G., Chepikov V. N., Nygaard R., Soldatenko A., Rudnev I. A., ... Monteseguro V. Correlation of local structure peculiarities and critical current density of 2G MOCVD YBCO tapes with $BaZrO_3$ nanoinclusions. *Superconductor Science and Technology*. 2017;30(4): 045003. https://doi.org/10.1088/1361-6668/aa599c

17. Shukin A. E., Kaul. A. R., Vasiliev A. L., Rudnev I. A. Synthesis, structure and superconducting

properties of laminated thin film composites $YBa_2Cu_3O_{7-\delta}/Y_2O_3$ as the components of 2G HTS tapes. *Kondensirovannye sredy i mezhfaznye granitsy = Condensed Matter and Interphases*. 2021;23(1): 122–139. https://doi.org/10.17308/kcmf.2021.23/3313

18. Kaul A. R., Seleznev B. V., Sharovarov D. I., Nygaard R. R., Osipova Yu. A., Makarevich A. M., Sadykov I. I. Feeding system for supplying volatile compounds in reactors of chemical vapor-phase deposition: *Patent No 2722914 RF*. Claim. 03.12.2019. Publ. 04.06.2020. Byul. No 2019139340.

19. Niu G., Zoellner M. H., Schroeder T., Schaefer A., Jhang J. H., Zielasek V., ... Reichling M. Controlling the physics and chemistry of binary and ternary praseodymium and cerium oxide systems. *Physical Chemistry Chemical Physics*. 2015;17(38): 24513–2540. https://doi.org/10.1039/c5cp02283e

20. Kummerle E. A., Heger G. The structures of C-$Ce_2O_{3+\delta}$, Ce_7O_{12}, and $Ce_{11}O_{20}$. *Journal of Solid State Chemistry*. 1999;147(2): 485–500. https://doi.org/10.1006/jssc.1999.8403

21. Hayes W., Stoneham A. M. Defects and defect processes in nonmetallic solids. New York: John Wiley & Sons; 2004. 472 p.

22. Chowdhury U., Goswami S., Bhattacharya D., Rajput S. S., Mall A. K., Garg A., ... Bhattacharya D. Origin of ferroelectricity in orthorhombic $LuFeO_3$. *Physical Review B*. 2017;100(19): 1–5. https://doi.org/10.1103/physrevb.100.195116

23. Bossak A., Graboy I., Gorbenko O., Kaul A., Kartavtseva M., Svetchnikov V., Zandbergen H. W. XRD and HREM studies of epitaxially stabilized hexagonal orthoferrites $RFeO_3$ (R = Eu-Lu). *Chemistry of Materials*. 2004;16(9): 1751–1755. https://doi.org/10.1021/cm0353660

24. Kaul A. R., Gorbenko O. Yu., Kamenev A. A. The role of heteroepitaxy in the development of new thin-film oxide-based functional materials. *Russian Chemical Reviews*. 2004;73(9): 861–880. https://doi.org/10.1070/rc2004v073n09abeh000919

25. Markelova M, Nygaard R, Tsymbarenko D, Shurkina A, Abramov A, Amelichev V, ... Kaul A. Multiferroic h-$LuFeO_3$ thin films on (111) and (100) surfaces of YSZ substrates: An experimental and theoretical study. *ACS Applied Electronic Materials*. 2021;3(2): 1015–1022. https://doi.org/10.1021/acsaelm.0c01127

26. Zboril R., Mashlan M., Krausova D., Pikal P. Cubic β-Fe_2O_3 as the product of the thermal decomposition of $Fe_2(SO_4)_3$. Hyperfine Interact. 1999;120–121(1–8): 497–501. https://doi.org/10.1023/a:1017018111071

27. Manimuthu P., Manikandan M., Selvi M. M., Venkateswaran C. Multiferroic $Lu_3Fe_5O_{12}$ for magneto-dielectric applications. *AIP Conference Proceedings*. 2012;1447(1): 1205–1206. https://doi.org/10.1063/1.4710443

Information about the authors

Andrey R. Kaul, DSc in Chemistry, Full Professor at the Chair of Inorganic Chemistry, Lomonosov Moscow State University, Moscow, Russian Federation; arkaul@mail.ru. ORCID iD: https://orcid.org/0000-0002-3582-3467.

Roy R. Nygaard, Junior Research Fellow at the Chair of Inorganic Chemistry, Lomonosov Moscow State University, Moscow, Russian Federation; e-mail: rnygaard@mail.ru. ORCID iD:

Vadim Yu. Ratovskiy, student at the Higher School of Material Science, Lomonosov Moscow State University, Moscow, Russian Federation; e-mail: vratovskiy@bk.ru. ORCID iD: https://orcid.org/0000-0003-1657-110X.

Alexander L. Vasiliev, PhD in Physics and Mathematics, Associate Professor at the Faculty of NBICS, Moscow Institute of Physics and Technology, Moscow, Russian Federation; email: a.vasiliev56@gmail.com. ORCID iD: https://orcid.org/0000-0001-7884-4180.

Received 1 July 2021; Approved after reviewing 15 July 2021; Accepted for publication 15 August 2021; Published online 25 September 2021.

Translated by Valentina Mittova
Edited and proofread by Simon Cox

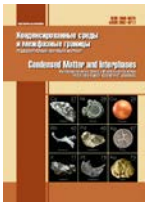

ISSN 1606-867X (Print)
ISSN 2687-0711 (Online)
Condensed Matter and Interphases
Kondensirovannye Sredy i Mezhfaznye Granitsy
https://journals.vsu.ru/kcmf/

Original articles

Research article
https://doi.org/10.17308/kcmf.2021.23/3532

Creation of thin films on the surface of InP with a controlled gas-sensitive signal under the influence of PbO + Y_2O_3 compositions

V. F. Kostryukov✉, **D. S. Balasheva, A. S. Parshina**

Voronezh State University,
1 Universitetskaya pl., Voronezh 394018, Russian Federation

Abstract

Thin-film objects with a reproducible temperature dependence of the resistance, thermally stable, and easy to obtain can be used as the sensitive elements in semiconductor gas sensors. The aim of this study was to create thin films on the InP surface under the influence of an oxide chemostimulator + inert component (PbO + Y_2O_3, respectively) compositions and to determine their gas-sensitive properties and their dependence on the formula of the composition.

Thin films were synthesised on the InP surface by the method of chemically stimulated thermal oxidation under the influence of various PbO + Y_2O_3 compositions. The thickness of the formed films, their elemental and chemical composition were determined (by laser ellipsometry, X-ray phase analysis, and infra-red spectroscopy). A number of experiments were carried out to establish the gas-sensitive properties of the obtained films with respect to ammonia with concentrations of 120, 100, and 80 ppm.

By chemically stimulated thermal oxidation, we obtained thin films with semiconductor properties on the InP surface. It was determined that the samples had n-type conductivity. A gas-sensitive response was detected in the presence of ammonia in the atmosphere. The ability to create thin films with a predetermined value of sensory response was demonstrated.

Keywords: Semiconductors, Indium phosphide, Thin films, Gas sensitivity, Thermal oxidation

Acknowledgements: the results of the research were obtained using the equipment of the Centre for the Collective Use of Scientific Equipment of Voronezh State University. URL: http://ckp.vsu.ru

For citation: Kostryukov V. F., Balasheva D. S., Parshina A. S. Creation of thin films on the surface of InP with a controlled gas-sensitive signal under the influence of PbO + Y_2O_3 compositions. *Kondensirovannye sredy i mezhfaznye granitsy = Condensed Matter and Interphases.* 2021;23(3): 406–412. https://doi.org/10.17308/kcmf.2021.23/3532

Для цитирования: Кострюков В. Ф., Балашева Д. С., Паршина А. С. Создание на поверхности InP тонких пленок с контролируемым значением газочувствительного сигнала под воздействием композиций PbO + Y_2O_3. *Конденсированные среды и межфазные границы*. 2021;23(3): 406–412. https://doi.org/10.17308/kcmf.2021.23/3532

✉ Victor F. Kostryukov, e-mail: vc@chem.vsu.ru
© Kostryukov V. F., Balasheva D. S., Parshina A. S., 2011

The content is available under Creative Commons Attribution 4.0 License.

1. Introduction

Currently, the creation of chemical sensors that can detect hazardous, toxic, and harmful gases is a topic of interest. Thus, it is necessary to develop new methods for creating gas-sensitive elements with a simple design, low cost, and high sensitivity and selectivity [1, 2].

The traditional way to increase the selectivity of the material is the search for the optimal microstructure of the material, dopants, and analysis temperature for each gas [3]. Numerous studies on improving the sensory parameters of materials are aimed at optimising the electronic properties or adsorption capacity of the material [4]. The main oxides for gas sensors are SnO_2 and In_2O_3 [5–11]. V_2O_5 [12], Ga_2O_3, and perovskite structures with various impurities [13–15] are also often used. The surface is modified in different ways: by preparing thin films of the In_2O_3 nanocolumn structure [16], by a porous microstructure in multilayer sensor structures SnO_2–CuO [17], through its doping, etc.

The aim of this study was to create thin films on the InP surface under the influence of an oxide chemostimulator + inert component (PbO + Y_2O_3, respectively) compositions, to determine their gas-sensitive properties and their dependence on the composition.

2. Experimental

Thin films on an InP surface were created by thermal oxidation under the influence of different compositions of PbO + Y_2O_3. The composition changed from one pure component to another with increments of 20 mol%. The samples were oxidised in a horizontal quartz reactor placed in an MTP-2M-50-500 resistance heating furnace at a temperature of 550 °C (± 1 °C). The oxygen flow rate was 30 l/h. Thermal oxidation of the samples was carried out for 60 minutes by postoxidation with a periodisation of 10 minutes. Such a temperature-time regime ensured the thin films formed on the InP surface had a thickness of 100–120 nm. Such values are required for the further study of their electrophysical characteristics (specific surface resistance). Indium phosphide plates (FIEO, orientation (100) with a concentration of major charge carriers of at least $5 \cdot 10^{16}$ cm^{-3} at 300 K and intrinsic n-type conductivity) were used as substrates. The mechanism of the formation of thin films in the processes of chemically stimulated thermal oxidation is considered in more detail in [18, 19].

The thickness of the resulting oxide films was determined using a LEF-754 laser ellipsometer (±2 nm). The elemental and chemical composition of the films was studied using a JEOL-6510LV unit with a Bruker energy dispersive microanalysis system and a Vertex 70 IR Fourier spectrometer, respectively. The specific surface resistance of the obtained thin films was measured by the Van der Pauw method using a TsIUS-4 system. The specific surface resistance of the oxide film samples was measured in air, as well as in the presence of the test gas (ammonia) at concentrations of 120, 100, and 80 ppm. When measuring the resistance, the air humidity was 55 %. The measurements were carried out in a steady-state system. The value of the sensory signal S was determined as the ratio of the resistance of the samples in air (R_a) to the resistance of the samples in the presence of NH_3 in the atmosphere (R_{tg}):

$$S = R_a / R_{tg} \quad (1)$$

3. Results and discussion

In order to determine the inertness of the oxides towards each other, the phase composition of the powders of the mixture after heat treatment was determined by the method of X-ray diffraction analysis (XRD). The heat treatment parameters corresponded to the regime of thermal oxidation of indium phosphide. An example of a diffraction pattern is shown in Fig. 1. The interplanar distances obtained as a result of the data analysis were compared with the reference values [20] of the interplanar distances of yttrium and lead oxides, as well as with the distances of possible mixed compounds of these oxides.

The absence of mixed phases of the oxides, as well as phases other than Y_2O_3 for yttrium oxide, indicates its inertness both to the second oxide of the composition (PbO) and to its own redox transformations. PbO, on the contrary, exhibits redox transformations at the experimental temperature (550 °C). Since the process takes place in a flow of oxygen, it is accompanied by the partial formation of mixed oxides Pb_2O_3 and Pb_3O_4.

The elemental composition of thin films grown on the InP surface was studied by local

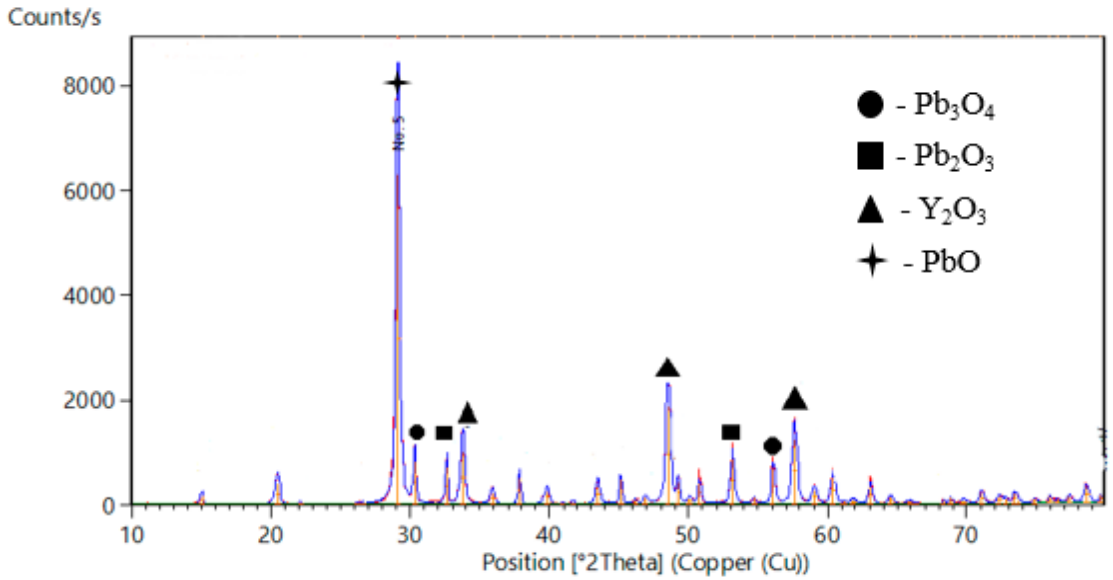

Fig. 1. Diffraction pattern of the $(Y_2O_3)_{0,6}$+$(PbO)_{0,4}$ composition after annealing at 550 °C for 10 min

electron probe microanalysis (EPMA). The obtained results are demonstrated in Table 1.

As follows from the obtained data, the main component of the film is indium. Its content is almost 2 times higher than the content of the second component of the substrate, phosphorus. Such a low phosphorus content in the resulting thin film on the InP surface is obviously due to its partial evaporation in the pentoxide form, which had also been observed in earlier studies [18, 21]. Moreover, for both of these elements, we can see practically no dependence on the various compositions of the oxides, under the influence of which the film on the semiconductor surface was formed. At the same time, the content of lead, which is another component of the film, shows a clear dependence on the composition. This dependence is considered in more detail below and shown in Fig. 2. Another component of the oxide composition, yttrium oxide, was not detected in the film at all. This confirms its inertness not only to the second oxide of the composition, but also to the process of thermal oxidation of InP in general. At the same time the total content of three elements is not 100 at%, which indicates that there is another component in the system. Since the film growth process takes place in a flow of oxygen, it is logical to assume that this is the missing component. Since the presence and amount of oxygen cannot be directly determined by EPMA, its content was calculated as the value lacking from 100 at%. The calculation showed significant oxygen content in the film (about 50 at%). Therefore, all other components of the film are in an oxidised state.

Using the data obtained by EPMA, we plotted a graph of the dependence of the lead content in the film on the composition (Fig. 2.)

As follows from Fig. 2, the dependence of the lead content in the film is almost linear. Such a dependence of the content of the film on the composition, under the influence of

Table 1. Elemental composition of thin films on the InP surface

Composition of the composition	Elemental composition of the films			
	In, at%	P, at%	Pb, at%	O, at%
$(PbO)_{0,2}(Y_2O_3)_{0,8}$	32.42	17.54	0.33	49.71
$(PbO)_{0.4}(Y_2O_3)_{0.6}$	34.54	16.87	0.88	47.71
$(PbO)_{0.6}(Y_2O_3)_{0.4}$	30.88	17.33	1.31	50.48
$(PbO)_{0.8}(Y_2O_3)_{0.2}$	31.66	17.55	1.61	49.15

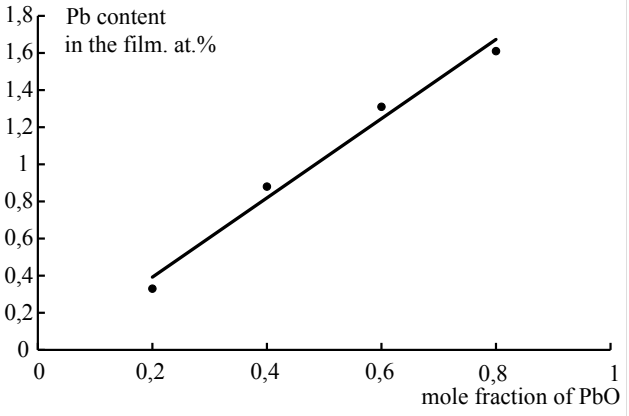

Fig. 2. Dependence of the chemostimulator content in the film on its molar fraction in the composition

which it was formed, makes it possible, using an inert component, to obtain oxide layers with the desired content of chemostimulator. It can help control various properties of the layers, including their electrophysical properties. The obtained result is similar to that achieved earlier [22] and confirms the versatility of using an inert component for the precise doping of thin films with an alloying component.

To confirm the presence of oxygen in the films on the InP surface, as well as the oxidation of the detected elements, the obtained samples were studied by IR spectroscopy. The results are presented in Table 2.

We can distinguish several characteristic absorption lines in the spectra of the samples. According to the literature data [23], frequencies of 565, 541, and 980 cm^{-1} correspond to the formation of In_2O_3 and $InPO_4$. Similar data were obtained during the intrinsic oxidation of indium phosphide. However, the spectra also contain absorption bands characteristic of the used oxide chemostimulator and the film obtained under the influence of the composition with the maximum PbO content, the compound with lead phosphate (538 cm^{-1}). It is necessary to note the absorption bands in the range of 430–440 and 620–630 cm^{-1}, associated with the background of the InP substrate. Thus, infrared spectroscopy was used to confirm the incorporation of lead oxide into the film growing on the InP surface and its interaction with the substrate components. Based on the EPMA data it also confirmed the conclusion that there was oxygen in the film on the InP surface and that all its other components were oxidised.

Table 2. The IR spectroscopic data for the films on the InP surface obtained under the influence of $PbO+Y_2O_3$ compositions

Composition	Absorption band, cm^{-1}	Compound
$(PbO)_{0.2}(Y_2O_3)_{0.8}$	430, 440, 630	InP
	565, 750	In_2O_3
	1025, 1242	$In(PO_3)_3$
	720	PbO
$(PbO)_{0.8}(Y_2O_3)_{0.2}$	430, 440, 620	InP
	500, 541, 980, 1080	$InPO_4$
	565. 750	In_2O_3
	720	PbO
	538	$Pb(PO_3)_2$

This allowed us to expect that the obtained films would have semiconductor properties.

Fig. 3 shows the temperature dependence (within the range of 20–400 °C) of the resistance in air of the samples prepared under the influence of the $PbO + Y_2O_3$ compositions. The dependences demonstrate a clear correlation between the composition of the oxide chemostimulator + inert component and the resistance of the oxide film on the InP surface obtained under its influence. The resistance increases with an increase in the PbO content in the films. The more PbO there is in the composition, the more PbO there is in the film. It results in a high oxide film thickness and, most likely, ensures the formation of films with high resistance parameters. In this case, the films themselves are semiconductors, as evidenced by the nature of the temperature dependence of the resistance.

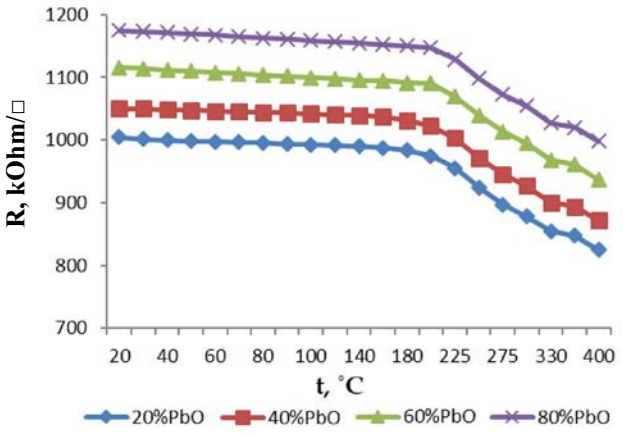

Fig. 3. Specific surface resistance of the samples in air

The gas to be detected in this study was ammonia. We carried out three series of experiments with different concentrations of ammonia: 120, 100, and 80 ppm. A typical temperature dependence of the resistance is shown in Fig. 4 for the lowest concentration studied.

The obtained surface resistance data were used to calculate the sensory signal according to equation (1). The results are shown in Fig. 5. All dependencies have a pronounced extreme character. The extremum corresponding to the maximum sensory signal of the obtained films, for all concentrations, corresponds to the same temperature, 225 °C. With an increase in concentration, the magnitude of the sensory signal increases slightly, but regularly. It is clearly demonstrated in Fig. 6 as an isothermal section at 225 °C.

In this range of gas concentrations, there is a linear dependency. In general, the operating range of the sensor is a logarithmic function. However, in our case it is a straight-line increasing dependence, which indicates that the operating range of the films is wider than the studied interval.

In addition to the dependence of the sensory signal of the film on the concentration of the detected gas, Fig. 5 shows its dependence on the synthesis conditions, namely, on the composition, which influenced the synthesis of this film. This dependence is shown more clearly in Fig. 7.

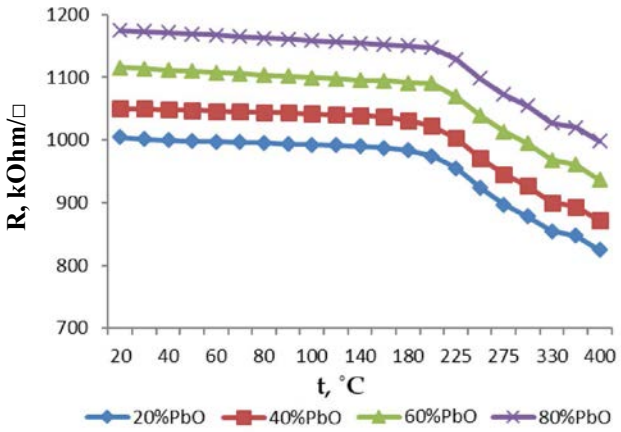

Fig. 4. Specific surface resistance of the samples measured in the presence of ammonia in the atmosphere with a concentration of 80 ppm

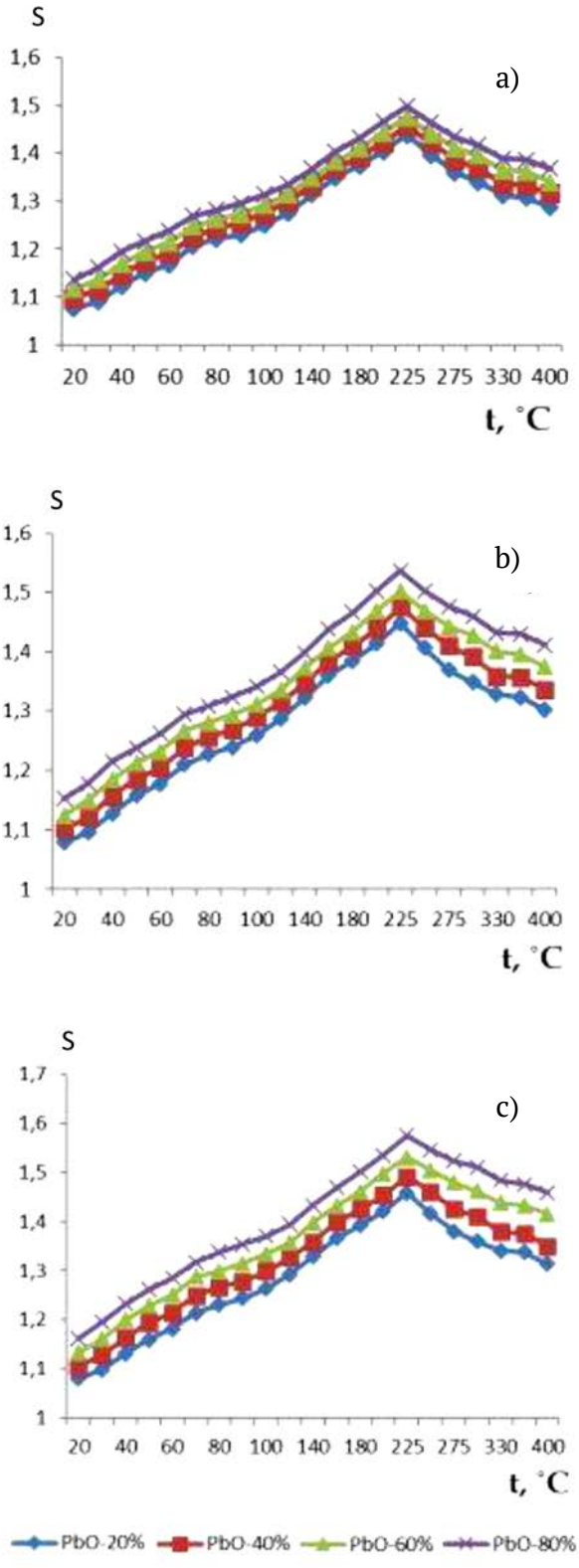

Fig. 5. Temperature dependence of the sensory signal of oxide films on the InP surface in the presence of ammonia in the atmosphere with a concentration of: a) 80 ppm; b) 100 ppm; c) 120 ppm

We chose a concentration of 120 ppm and a temperature of 225 °C, at which the magnitude of the sensory signal is maximum.

If we examine Figures 2 and 7 jointly, we can conclude that the use of oxide compositions, one of which is an inert component, as chemostimulators of the InP thermal oxidation process, makes it possible to obtain films with the desired content of the alloying component (in this case it was lead). This allows controlling the magnitude of the sensory signal formed on the surface of a thin film semiconductor.

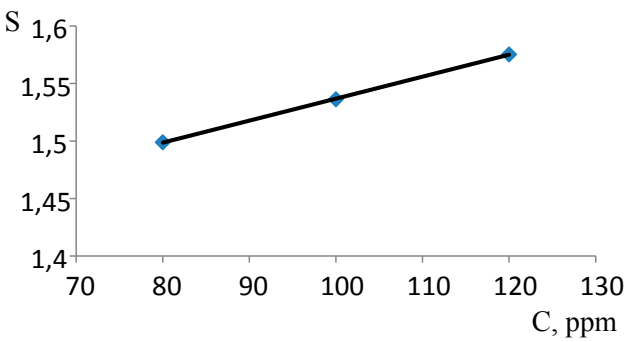

Fig. 6. Dependence of the sensory signal on the ammonia concentration

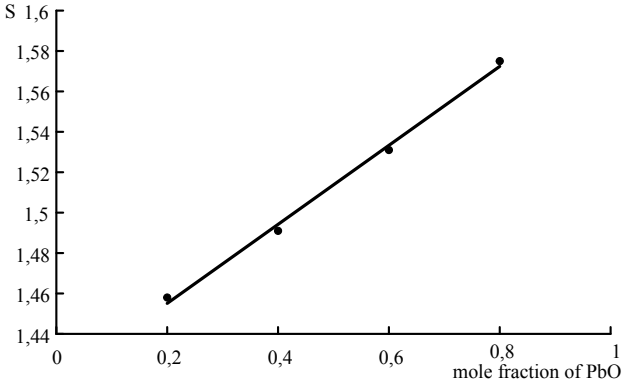

Fig. 7. Dependence of the sensory signal on the PbO content in the $PbO+Y_2O_3$ composition

4. Conclusions

Thin films were synthesized on the InP surface under the action of $PbO + Y_2O_3$ composites. The formed films predominantly consist of lead-containing substrate components in an oxidised state. Using the Van der Pauw method, we determined that the thin films were gas-sensitive and detected the presence of ammonia in the atmosphere. We revealed the possibility of precision doping of a thin film growing on the InP surface with a chemostimulator. It makes it possible to obtain films with a desired value of sensory signal.

Author contributions

All authors made an equivalent contribution to the preparation of the publication.

Conflict of interests

The authors declare that they have no known competing financial interests or personal relationships that could have influenced the work reported in this paper.

References

1. Kattrall R. V. *Khimicheskiye sensory* [Chemical sensors]. Moscow: Nauchnyy Mir Publ.; 2000. 144 p. (in Russ.)

2. Sproul W. D., Christie D. J., Carter D. C. Control of reactive sputtering processes. *Thin Solid Films*. 2005;491(1-2): 1-17. https://doi.org/10.1016/j.tsf.2005.05.022

3. *Nanostrukturnyye oksidnyye materialy v sovremennoy mikro-, nano- i optoelektronike* [Nanostructured oxide materials in modern micro-, nano- and optoelectronics]. V. A. Moshnikov, O. A. Aleksandrova (eds.). Saint Petersburg: Izd-vo SPbGETU "LETI" Publ., 2017. 266 p. (in Russ.)

4. Karpova S. S., Moshnikov V. A., Maksimov A. I., Mjakin S. V., Kazantseva N. E. Study of the effect of the acid-base surface properties of ZnO, Fe_2O_3 and $ZnFe_2O_4$ oxides on their gas sensitivity to ethanol vapor. *Semiconductors*. 2013;47(8): 1026–1030. https://doi.org/10.1134/S1063782613080095

5. Rumyantseva M. N., Makeeva E. A., Badalyan S. M., Zhukova A. A., Gas'kov A. M. Nanocrystalline SnO_2 and In_2O_3 as materials for gas sensors: the relationship between microstructure and oxygen chemisorption. *Thin Solid Films*. 2009;518(4): 1283–1288. https://doi.org/10.1016/j.tsf.2009.07.201

6. Rumyantseva M. N., Ivanov V. K., Rudyi Yu. M., Yushchenko V. V., Arbiol J., A. M. Gas'kov A. M. Microstructure and sensing properties of nanocrystalline indium oxide prepared using hydrothermal treatment. *Russian Journal of Inorganic Chemistry*. 2009;54(2): 163-171. https://doi.org/10.1134/s0036023609020016

7. Ohgaki T., Matsuoka R., Watanabe K., Matsumoto K., Adachi Y., Sakaguchi I., Hishita S., Ohashi N., Hanedaa H. Synthesizing SnO_2 thin films and characterizing sensing performances. *Sensors and Actuators B*. 2010;150(1): 99–104. https://doi.org/10.1016/j.snb.2010.07.036

8. Neria G., Bonavitaa A., Micalia G., Rizzoa G., Pinnab N. Effect of the chemical composition on the sensing properties of In_2O_3–SnO_2 nanoparticles

synthesized by a non-aqueous method. *Sensors and Actuators B*. 2008;130(1): 222–230. https://doi.org/10.1016/j.snb.2007.07.141

9. Singh N., Yan C., Lee P. S. Room temperature CO gas sensing using Zn-doped In_2O_3 single nanowire field effect transistors. *Sensors and Actuators B*. 2010;150(3): 19–24. https://doi.org/10.1016/j.snb.2010.07.051

10. Zeng Z., Wang K., Zhang Z., Chen J., Zhou W. The detection of H_2S at room temperature by using individual indium oxide nanowire transistors. *Nanotechnology*. 2009;20(4): 045503. https://doi.org/10.1088/0957-4484/20/4/045503

11. Elouali S., Bloor L. G., Binions R., Parkin I. P., Carmalt C. J., Darr J. A. Gas sensing with nano-indium oxides (In_2O_3) prepared via continuous hydrothermal flow synthesis. *Langmuir*. 2012;28(3):1879–1885. https://doi.org/10.1021/la203565h

12. Huotari J., Lappalainen J., Puustinen J. Gas sensing properties of pulsed laser deposited vanadium oxide thin films with various crystal structures. *Sensors and Actuators B*. 2013;187: 386–394. https://doi.org/10.1016/j.snb.2012.12.067

13. Fergus J. W. Perovskite oxides for semiconductor-based gas sensors. *Sensors and Actuators B*. 2007;123(2): 1169–1179. ttps://doi.org/10.1016/j.snb.2006.10.051

14. Frank J., Fleischer M., Meixner H. Gas-sensitive electrical properties of pure and doped semiconducting Ga_2O_3 thick films. *Sensors and Actuators B*. 1998;48(1-3): 318–321. https://doi.org/10.1109/7361.983471

15. Hoefer U., Frank J., Fleischer M. High temperature Ga_2O_3-gas sensors and SnO_2-gas sensors: a comparison. *Sensors and Actuators B*. 2001;78(1-3): 6–11. https://doi.org/10.1016/s0925-4005(01)00784-5

16. Han S. D., Noh M. S., Kim S. Versatile approaches to tune a nanocolumnar structure for optimized electrical properties of In_2O_3 based gas sensor. *Sensors and Actuators B*. 2017;248: 894-901. https://doi.org/10.1016/j.snb.2017.01.108

17. Verma M. K., Gupta V. A highly sensitive SnO_2-CuO multilayered sensor structure for detection of H_2S gas. *Sensors and Actuators B*. 2012;166-167: 378–385. https://doi.org/10.1016/j.snb.2012.02.076

18. Tomina E. V., Mittova I. Ya., Sladkopevtsev B. V, Kostryukov V. F., Samsonov A. A., Tretyakov N. N. Thermal oxidation as a method of formation of nanoscale functional films on $A^{III}B^{V}$ semiconductors: chemostimulated influence of metal oxides overview. *Kondensirovannye sredy i mezhfaznye granitsy* = *Condensed Matter and Interphases*. 2018;2(20): 184–203. https://doi.org/10.17308/kcmf.2018.20/522 (In Russ., abstract in Eng.)

19. Mittova I. Ya. Influence of the physicochemical nature of chemical stimulators and the way they are introduced into a system on the mechanism of the thermal oxidation of GaAs and InP. *Inorganic Materials*. 2014;50(9): 874–881. https://doi.org/10.1134/s0020168514090088

20. JCPDC PCPDFWIN: A windows retrieval / Display program for accessing the ICDD PDF – 2 Data base. *International Centre for Diffraction Data*; 1997.

21. Mittova I. Ya., Pshestanchik V. R., Kostryukov V. F. *Nelinejnye effekty v processah aktivirovannogo okisleniya GaAs* [Nonlinear effects in the activated oxidation of GaAs]. Voronezh, Izdatelsko-poligraficheskij centr Voronezhskogo gosudarstvennogo universiteta Publ.; 2008, 160 p. Available at: https://www.elibrary.ru/item.asp?id=21199148 (in Russ.)

22. Kostryukov V. F., Mittova I. Ya., Sladkopevtsev B. V. Method of precision doping thin films on InP surface: *Patent No 2632261 RF*. Claim. 17.12.2015. Publ. 03.10.2017. Byul. No.28.

23. Nakamoto K. Infrared and Raman spectra of inorganic and coordination compounds. New York: John Wiley; 1986. 479 p.

Information about the authors

Victor F. Kostryukov, DSc in Chemistry, Associate Professor, Associate Professor at the Department of Materials Science and the Industry of Nanosystems, Voronezh State University, Voronezh, Russian Federation; e-mail: vc@chem.vsu.ru. ORCID iD: https://orcid.org/0000-0001-5753-5653.

Dar'ya S. Balasheva, student at the Department of Materials Science and the Industry of Nanosystems, Voronezh State University, Voronezh, Russian Federation; e-mail: balasheva.98@mail.ru.

Anna S. Parshina, master's degree student, Department of Materials Science and the Industry of Nanosystems, Voronezh State University, Voronezh, Russian Federation; e-mail: anyuta_parshina@mail.ru.

Received 14 June 2021; Approved after reviewing 15 July 2021; Accepted for publication 15 August 2021; Published online 25 September 2021.

Translated by Anastasiia Ananeva
Edited and proofread by Simon Cox

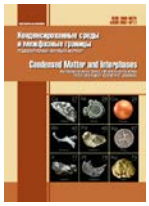

ISSN 1606-867X (Print)
ISSN 2687-0711 (Online)
Condensed Matter and Interphases
Kondensirovannye Sredy i Mezhfaznye Granitsy
https://journals.vsu.ru/kcmf/

Original articles

Research article
https://doi.org/10.17308/kcmf.2021.23/3533

Structure and chemical composition of grain boundaries in the magnetic semiconductor GaSb<Mn>

V. P. Sanygin, O. N. Pashkova, A. D. Izotov✉

Kurnakov Institute of General and Inorganic Chemistry of the Russian Academy of Sciences, 31 Leninsky prospekt, Moscow 119991, Russian Federation

Abstract

The structure and chemical composition of grain boundaries in GaSb<Mn> magnetic semiconductors have been investigated. We determined that quenching of the GaSb melt with 2% Mn results in the formation of a textured polycrystal (111). The grain boundaries of the texture are formed by split 60 degree dislocations with <110> dislocation lines. Microinclusions based on the ferromagnetic compound MnSb are located on the stacking faults of split dislocations. The chemical compositions of microinclusions differ, but their average composition is close to $Mn_{1.1}Sb$. The synthesized GaSb<Mn> is a soft ferromagnet with a coercive force of 10 Oe and a magnetic state approaching superparamagnetic.

Keywords: Magnetic semiconductors, Gallium antimonide, Crystal lattice defects, Magnetic clusters

Acknowledgements: The work was supported by the Ministry of Education and Science of the Russian Federation within the framework of the state order to Kurnakov Institute of General and Inorganic Chemistry of the Russian Academy of Sciences. The authors are grateful to the Centre for Collective Use of Physical Research Methods of IGIC RAS.

For citation: Sanygin V. P. Pashkova O. N., Izotov A. D. Structure and chemical composition of grain boundaries in the magnetic semiconductor GaSb<Mn>. *Kondensirovannye sredy i mezhfaznye granitsy = Condensed Matter and Interphases*. 2021;23(3): 413–420. https://doi.org/10.17308/kcmf.2021.23/3533

Для цитирования: Саныгин В. П., Пашкова О. Н., Изотов А. Д. Структура и химический состав межзеренных границ в магнитном полупроводнике GaSb<Mn>. *Конденсированные среды и межфазные границы*. 2021;23(3): 413–420. https://doi.org/10.17308/kcmf.2021.23/3533

✉ Alexander D. Izotov, e-mail: izotov@igic.ras.ru
© Sanygin V. P. Pashkova O. N., Izotov A. D., 2021

The content is available under Creative Commons Attribution 4.0 License.

1. Introduction

The production of spintronic devices requires materials that have both magnetic and semiconductor properties and are technologically compatible with common semiconductor devices. Recently, a large number of studies have focused on the search for new magnetic semiconductors in the form of solid solutions of manganese in III–V compounds, i.e. dilute magnetic semiconductors (DMS) [1].

All these studies employed the latest technologies, including molecular-beam epitaxy (MBE), laser irradiation, ion implantation, etc. Nevertheless, they did not manage to overcome the low solubility limit of manganese, because, according to the results of the studies, at room temperature and above ferromagnetism of $A^{III}B^{V}$ is explained by the formation of microinclusions based on Mn-V magnetic compounds [2–16].

At the same time, cluster magnetic semiconductors have certain advantages over dilute magnetic semiconductors. These materials are of practical importance since its is possible to control their magnetic properties by modifying the composition, the size, and the concentration of the forming magnetic microinclusions without using expensive technologies.

It is important to perform a comprehensive study of the effect of rapid melt crystallisation on the composition, structure, and properties of Mn-doped gallium antimonide. The article presents the results of the study of the structure and chemical composition of grain boundaries in GaSb<Mn> obtained by melt quenching.

2. Experimental

In order to obtain bulk samples of GaSb+2% Mn we used the following initial components: hole-conducting monocrystalline gallium antimonide and pure Mn (99.99%). The samples were prepared by melting the mixture in a vacuum quartz ampoule at T = 1200 K, incubating the melt at this temperature for 24 hours, and the following vertical quenching of the melt in a mixture of water and ice.

The samples were identified using X-ray phase analysis (XRD), performed using a BRUKER D8 ADVANCE diffractometer (CuK_{α}-radiation) at the Centre for Collective Use of Physical Research Methods of the Kurnakov Institute of General and Inorganic Chemistry of the Russian Academy of Sciences (CCU IGIC RAS). The angle range 2θ was from 10° to 80° with the scanning step Δ2θ = 0.014°. The XRD patterns were then analysed using the ICDD PDF-2 database.

The section surface was studied by means of scanning electron microscopy (SEM). Micrographs and chemical compositions of certain phases on the microstructure level were obtained at CCU IGIC RAS using a Carl Zeiss Nvision40 scanning electron microscope with an Oxford Instruments X-Max microprobe analyser.

The magnetic properties of the GaSb(2 % Mn) samples were studied at T = 4 K and T = 300 K in a magnetic field of up to H = 50 kOe using a PPMS-9 (Quantum Design) automated measurement system. When measuring the DC magnetization the absolute sensitivity was $\pm 2.5 \cdot 10^{-5}$ g/cm^3.

3. Results and discussion

In [16], we suggested that dislocations in semiconductors doped with magnetic impurities can be used as extensive linear magnetic circuits aligned in the same crystallographic direction. The concept of impurity-dislocation magnetism was inspired by the studies of the Cottrell atmosphere formation [17] and spheroid formation [18] performed by means of 3D imaging of impurity segregation near dislocations inside a crystal.

It was demonstrated that the impurity segregation in dislocations by means of atom diffusion inside the crystal is as intensive as the impurity segregation by means of decorating the dislocations on the surface. Therefore, we conducted a series of experiments, where III–V semiconductor compounds were doped with a *d*-element – manganese.

Namely, we analysed the samples of the semiconductor compound GaSb doped with 2 at% Mn.

Identically aligned dislocations were generated by quenching the melt at different coefficients of linear thermal expansion for GaSb ($\alpha \approx 6.7 \cdot 10^{-6}$ K^{-1} [19]) and quartz ($\alpha \approx 0.5 \cdot 10^{-6}$ K^{-1} [20]), with heat being removed radially from the cylindrical part of the melt-containing ampoule during the vertical quenching (Fig. 1a). Judging by the temperature dependence of the magnetization, the samples were ferromagnets with a Curie temperature T_C = ~560 K (Fig. 1b).

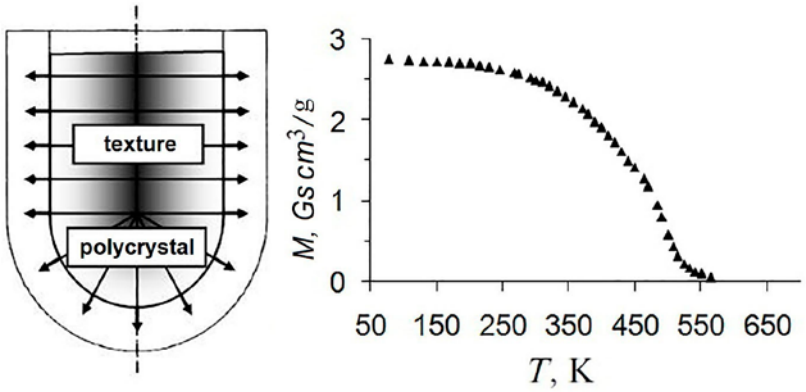

a b

Fig. 1. Diagram of an ampoule with the melt placed vertically during quenching (a) and the temperature dependence of the specific magnetization of the sample of GaSb + 2 % Mn (b)

Fig. 2a demonstrates a diffraction pattern of the synthesised GaSb<Mn> powder. Besides the peaks of polycrystalline GaSb, it shows peaks of the ferromagnetic compound $Mn_{1.1}Sb$ whose Curie temperature complies with the magnetic properties of the sample (Fig. 1b).

In order to further study the structural properties of the material, we produced a metallographic thin section of its ingot, whose diffraction pattern is given in Fig. 2b. It shows that the metallographic thin section of GaSb<Mn> is a texture, and therefore consists of blocks separated by low-angle grain boundaries formed by dislocations.

The (111) texture axis indicates that the dislocations controlling the grain formation are 60 degree edge dislocations with the (111) slip plane and the dislocation line <110>, which contradicts the generally accepted view that the structure of the sphalerite is formed by Lomer dislocations with (110) slip planes.

In order to see whether Lomer dislocations participate in the formation of the texture we synthesised a sample of a different III–V compound (InSb) by means of melt quenching. The diffraction pattern of the InSb powder is given in Fig. 2c. It demonstrated InSb peaks with the crystal structure of sphalerite type, identical to GaSb. However, the diffraction pattern of the crystallographic thin section of InSb corresponds to the texture with simple slip planes of type (110),

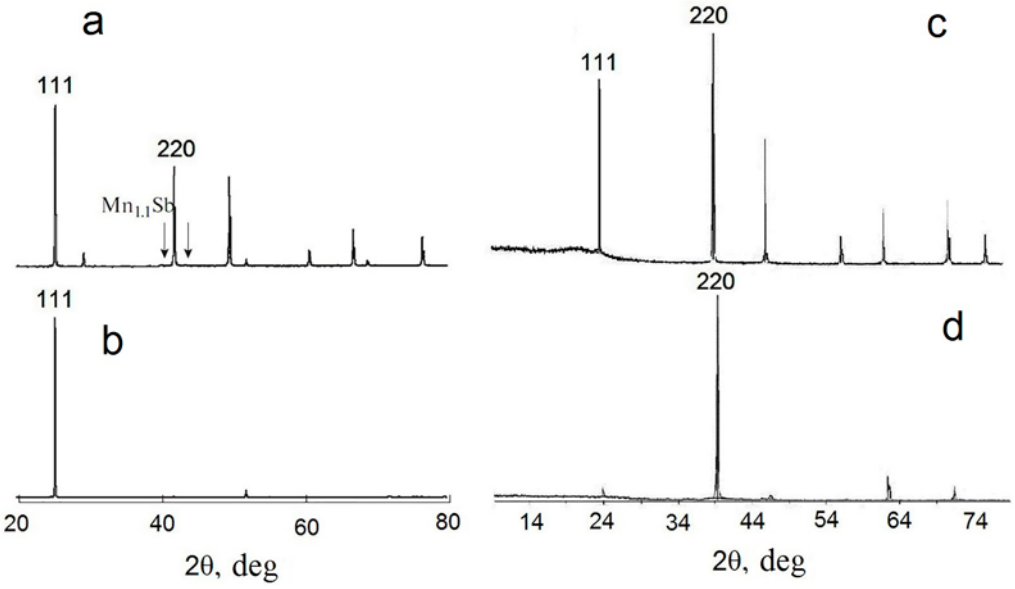

Fig. 2. X-ray diffraction patterns of (a) powder and (b) metallographic thin section of GaSb doped with Mn; powder (c) and metallographic thin section (d) of undoped InSb

which agrees well with the existing concepts.

Thus, in our study, we determined that the introduction of impurities during the melt quenching affects the orientation of the resulting ingots of III-V semiconductor compounds. To explain this phenomenon, let's consider the formation of a Lomer sessile dislocation.

Fig. 3a shows a simple 60 degree edge dislocation most common for a crystal structure of sphalerite type. Such dislocations are characterised by a (111) slip plane of the dislocation line along the crystallographic direction <110>; the family of the direction in the structure of the sphalerite is shown in Fig. 3b.

According to [21, 22], the formation of the Lomer sessile dislocation is a complex process including the following states of the material:

1 – formation of 60 degree edge dislocations in intersecting crystallographic planes;

2 – splitting of the edge dislocations into 30 and 90 degree dislocations, connected by a layer of stacking faults with two stacking faults moving towards each other until they meet at the planes intersection (Fig. 3b);

3 – formation of the Lomer sessile dislocation (Fig. 3c).

The possibility of all the stages taking place is quite high in pure semiconductors with a sphalerite structure. However, when an impurity is added to the crystal, the regions of hydrostatic compression and expansion around the extra half-plane of the edge dislocation begin to play a significant role. In Fig. 3a the region of hydrostatic compression is shaded. The impurity atoms intensively diffuse towards the regions of arising stresses, segregate around the extra half-plane, pin the dislocations to the crystal lattice of the material, and immobilise them.

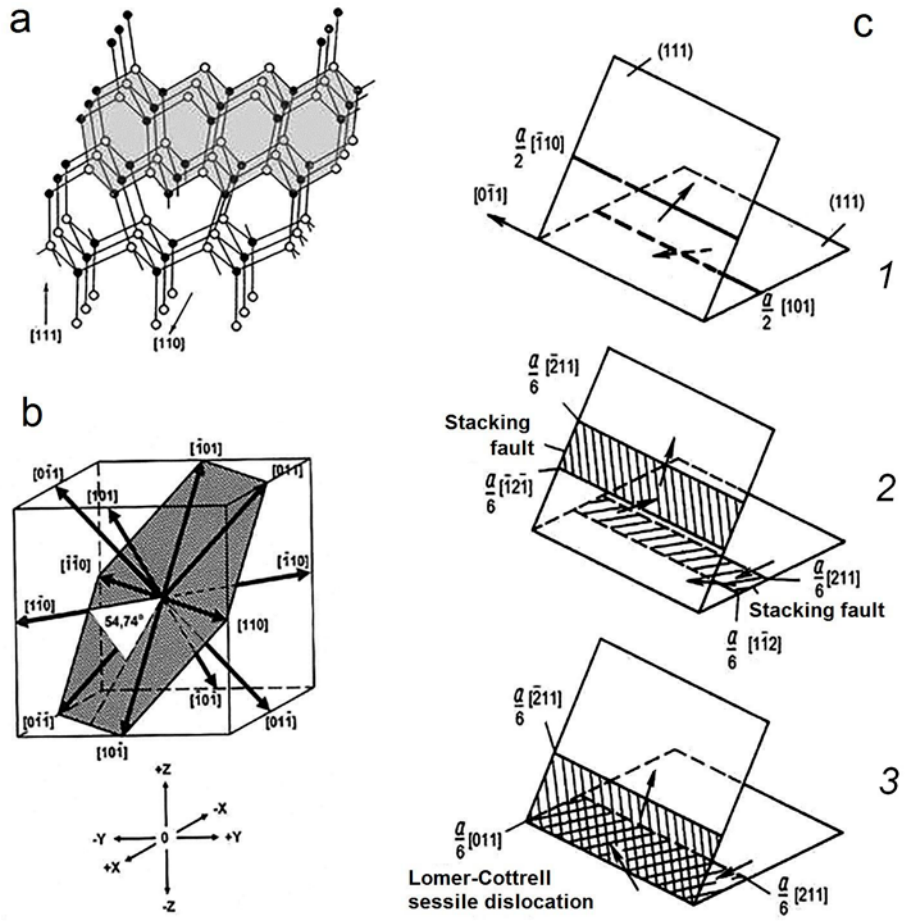

Fig. 3. Edge dislocation and Lomer sessile dislocation: a – initial 60 degree dislocation of GaSb with a shaded region of hydrostatic compression and a [110] dislocation line; b – the family of [110] directions in the sphalerite structure; c – a diagram of the formation of the Lomer sessile dislocation

If the diffusion rate is higher than the rate of formation of sessile dislocations, the latter do not appear. This is what happens when GaSb is doped with manganese. Of the two ways to hinder the dislocation motion, segregation of the impurity is the main one, and therefore the third stage of the formation of sessile dislocations does not occur.

Fig. 4a demonstrates a scheme and Fig. 4b shows the result of scanning electron microscopy of split dislocations of the surface of GaSb doped with Mn.

A split dislocation has the form of a stacking fault ribbon bounded by partial dislocations. The stretching of the stacking fault aims to pull the partial dislocations together, while pressing the microimpurities located between them (Fig. 4b), and limit their size.

The stacking fault ribbon is a two-dimensional crystal interlayer with incorrect alterations of the atomic close-packed layers of the FCC lattice and the formation of a thin interlayer of the hexagonal close-packed (HCP) structure. The split dislocation may consist of three, four, or more partial dislocations, and therefore of two, three, or more stacking fault ribbons, and come in the form of alternating regions of FCC and HCP lattices.

To determine the chemical composition of grain boundaries in GaSb<Mn>, we studied the chemical composition of the microinclusions on the dislocations controlling the grain formation by means of electron probe microanalysis. Since the region of X-ray excitation by an electronic probe is about 1 μm, we studied the inclusions of 1 μm size separated and surrounded by a relatively smooth surface of the semiconductor (Fig. 5a). We estimated the accuracy of identification to be ±2 at%.

The parameters of the chemical composition of the microinclusions were placed on the composition line of the state diagram Mn–Sb [23] (Fig. 5b). Then we performed phase identification

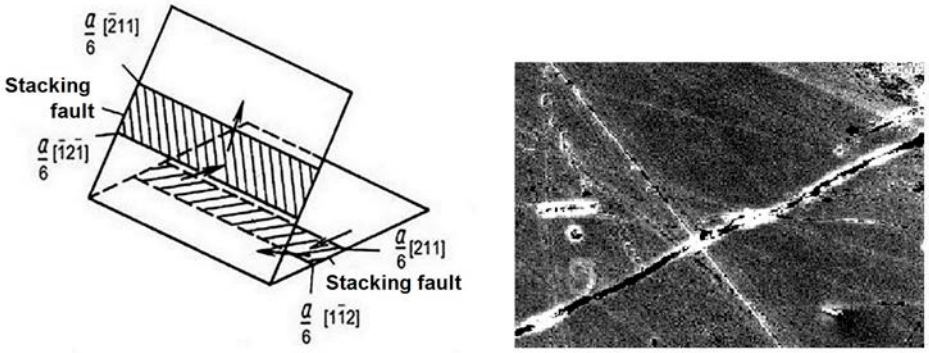

a b

Fig. 4. Scheme (a) and SEM images (b) of split dislocations on the surface of GaSb doped with manganese

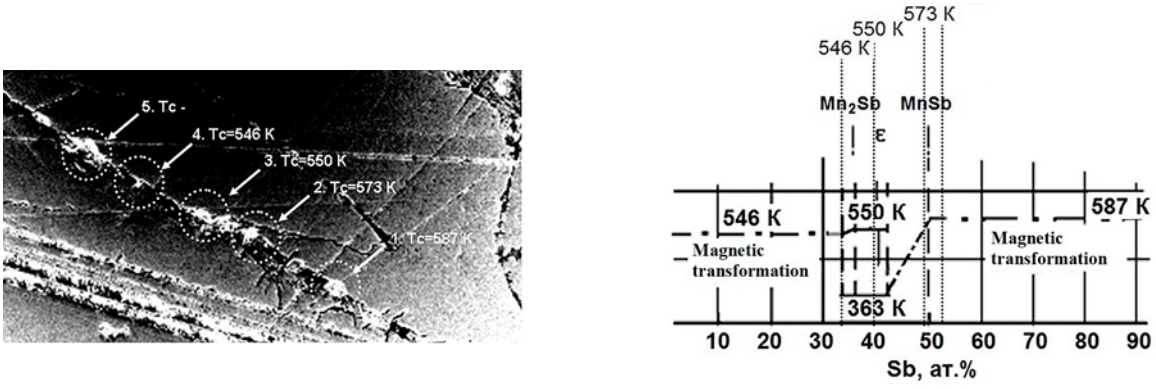

a b

Fig. 5. Dislocation outcrops on the surface of GaSb doped with Mn (a) and their compositions on the lines of magnetic transformations of the Mn-Sb phase diagram (b)

of the microinclusions and determined the type of magnetism and the Curie temperature for each of them. Fig. 5b shows that, although the chemical compositions of the microinclusions differ, their average composition is close to $Mn_{1.1}Sb$. The difference in the compositions is caused by the difference in the cooling rate during directional crystallisation of the melt from the surface to the centre of the ingot (in Fig. 1a the process is indicated by the gradual change in the contrast of the melt).

The temperature dependence of zero field cooled (ZFC) and field cooled (FC) magnetization of the GaSb<Mn> texture was the same at the cooling $T \approx 300$ K. This means that at temperatures above room temperature the ferromagnetic state is transformed into a superparamagnetic state, and $T \approx 300$ K is the blocking temperature for the ferromagnetic state of the texture.

Using the Bean–Livingston method [24] we can determine the dependency between the constant of the magnetic crystallographic anisotropy, the blocking temperature and the size of single-domain microinclusions in the diamagnetic matrix of GaSb.

Assuming that magnetic clusters are spherical, the maximum radius of the blocked effective clusters is about 180–200 nm.

Thus, the calculated maximum effective size of the blocked clusters $r \approx 200$ nm is close to the micron size of magnetic inclusions in dislocations (Fig. 4b).

The study of the magnetic properties demonstrated that at the temperature $T = 300$ K, sample GaSb<Mn> is still a ferromagnet with the coercive force of a soft magnetic material $H_c \approx 10$ Oe (Fig. 6).

The dislocation lines doped with magnetic impurities in a diamagnetic semiconductor matrix are artificially induced easy axes of magnetization. The magnetic moments of single-domain particles can be located along <110> or

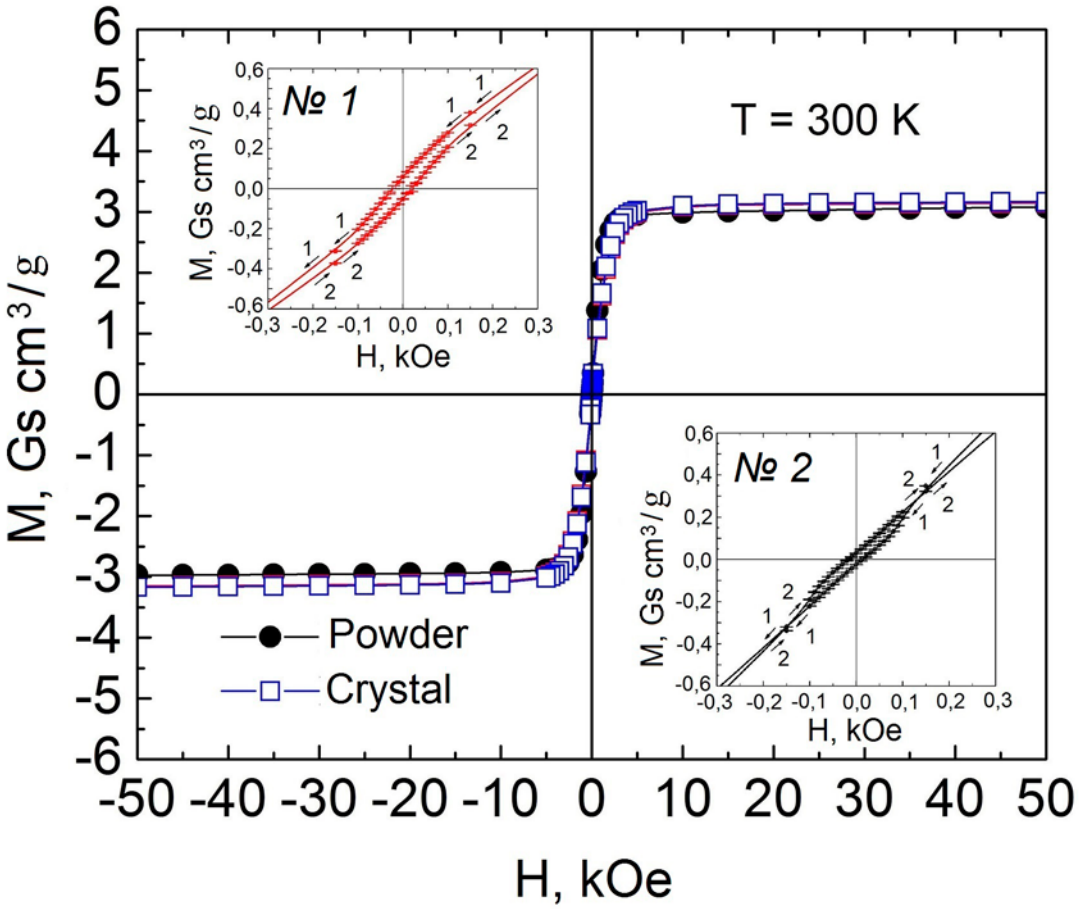

Fig. 6. Field dependences of the magnetization of the crystal and powder of GaSb doped with Mn. Inserts: No.1: the hysteresis loop region of the crystal, No.2: the hysteresis loop region of the powder

<–1–10> directions depending on the direction of the external magnetic field +*H* or –*H*. (Fig. 3b).

The characteristic feature of superparamagnetism is the merging of the demagnetization and magnetization curves, which means that hysteresis disappears. In this regard, it is interesting to compare the demagnetization and magnetization curves of the texture and its powder in the vicinity of a zero magnetic field. While the texture still has ferromagnetic properties (insert No.1, Fig. 6), in the case of its powder (insert No.2, Fig. 6) demagnetization and magnetization curves change places in the regions of magnetic tension H = ±0.15 kOe. With the magnetic tension being from –0.15 to +0.15 kOe, both curves merge (taking into account the measurement error) and form a region of superparamagnetic state.

4. Conclusions

As a result of our study we obtained samples of a semiconductor compound GaSb+2 at% Mn.

XRD analysis demonstrated that the main source of ferromagnetism in the obtained samples is the $Mn_{1.1}Sb$ phase with the Curie temperature T_C = ~560 K. The study also demonstrated the fundamental importance of the heat removal mode during the process of melt crystallisation and explained the formation of the <111> texture in GaSb that has a sphalerite crystal structure. We also determined that grain boundaries are formed by split edge dislocations.

SEM was used to determine the chemical compositions of microinclusions in stacking faults of split dislocations, perform their phase identification, and determine the type of magnetism and the Curie temperature for each of them.

The study of the magnetic properties showed that quenching of bulky samples of GaSb<Mn> results in the formation of a soft magnetic material. It also demonstrated the possibility of transition from the ferromagnetic to the superparamagnetic state.

Author contributions

All authors made an equivalent contribution to the preparation of the publication.

Conflict of interests

The authors declare that they have no known competing financial interests or personal relationships that could have influenced the work reported in this paper.

References

1. Ivanov V. A., Aminov T. G., Novotortsev V. M., Kalinnikov V. T. Spintronics and spintronics materials. *Russian Chemical Bulletin*. 2004;53(11): 2357-2405. https://doi.org/10.1007/s11172-005-0135-5

2. Pulzara-Mora C., Pulzara-Mora A., Forero-Pico A., Ayerbe-Samaca M., Marques-Marchan J., Asenjo A., Nemes, N. M., Arenas D., Saez Puche R. Structural, morphological and magnetic properties of GaSbMn/Si(111) thin films prepared by radio frequency magnetron sputtering. *Thin Solid Films*. 2020;705: 137971. https://doi.org/10.1016/j.tsf.2020.137971

3. Dmitriev A. I., Kochura A. V., Kuz'menko A. P., Parshina L. S., Novodvorskii O. A., Khramova O. D., Kochura E. P., Vasil'ev A. L., Aronzon B. A. Effect of Heat Treatment on the Dispersion of the Magnetic Anisotropy of MnSb Nanoinclusions Embedded in Thin GaMnSb Films. *Physics of the Solid State*. 2019;61(4): 523–529. https://doi.org/10.1134/S1063783419040073

4. Doria-Andrade J., Pulzara-Mora C., Bernal-Correa R., Rosales-Rivera A., Pulzara-Mora Á. Segregation of Mn into GaAsMn thin films prepared by magnetron sputtering. *Materia-Rio De Janeiro*. 2020;25(4): E-12884. https://doi.org/10.1590/s1517-707620200004.1184

5. Yokoyama M., Ogawa T., Nazmul A. M., Tanaka M. Large magnetoresistance (> 600 %) of a GaAs : MnAs granular thin film at room temperature *Journal of Applied Physics*. 2006;99(8): 08D502. https://doi.org/10.1063/1.2151817

6. Rednic L., Deac I. G., Dorolti E., Coldea M., Rednic V., Neumann M. Magnetic cluster developement in $In_{1-x}Mn_xSb$ semiconductor alloys. *Open Physics*. 2010;8(4): 620–627. https://doi.org/10.2478/s11534-009-0140-7

7. Tran L., Hatami F., Masselink W. T., Herfort J., Trampert A. Distribution of Mn in ferromagnetic (In,Mn)Sb films grown on (0 0 1) GaAs using MBE. *Journal of Crystal Growth*. 2011;323(1): SI 340–343 (Special Issue). https://doi.org/10.1016/j.jcrysgro.2010.10.127

8. Overberg M. E., Gila B. P., Thaler G. T., Abernathy C. R., Pearton S. J., Theodoropoulou N. A. et. al. Room temperature magnetism in GaMnP produced by both ion implantation and molecular-beam epitaxy. *Journal of Vacuum Science & Technology B: Microelectronics and Nanometer Structures*. 2002;20(3): 969–973. https://doi.org/10.1116/1.1477424

9. Sobolev N. A., Oliveira M. A., Rubinger R. M., Neves A. J., Carmo M. C., Lesnikov V.P., Podolskii V. V., Danilov Y. A., Demidov E. S., Kakazei G. N. Ferromagnetic resonance and Hall effect characterization of GaMnSb

layers. *Journal of Superconductivity and Novel Magnetism*. 2007;20(6): 399-403. https://doi.org/10.1007/s10948-007-0243-6

10. Hartmann Th., Lampalzer M., Klar P. J., Stolz W., Heimbrodt W., von Nidda H. A. K., Loidl A., Svistov L. Ferromagnetic resonance studies of (Ga,Mn) As with MnAs clusters. *Physica E: Low-dimensional Systems and Nanostructures*. 2002;13(2-4): 572–576. https://doi.org/10.1016/s1386-9477(02)00180-7

11. Chen C., Chen N., Liu L., Li Y., Wu J. $Ga_{1-x}Mn_xSb$ grown on GaSb substrate by liquid phase epitaxy. *Journal of Crystal Growth*. 2004;260(1-2): 50–53. https://doi.org/10.1016/j.jcrysgro.2003.08.022

12. Yoshizawa H., Toyota H., Nakamura S., Yamazaki M., Uchitomi N. Structural and ferromagnetic properties of InMnAs thin films including MnAs nanoclusters grown on InP substrates. *Thin Solid Films*. 2017;622: 136–141. https://doi.org/10.1016/j.tsf.2016.12.020

13. Novak J., Dujavova A., Vavra I., Hasenoehrl S., Reiffers M. Magnetic properties of InMnAs nanodots prepared by MOVPE. *Journal of Magnetism and Magnetic Materials*. 2013;327: 20-23. https://doi.org/10.1016/j.jmmm.2012.09.041

14. Liu J. D., Hanson M. P., Peters J. A., Wessels B. W. Magnetism and Mn Clustering in (In,Mn)Sb magnetic semiconductors. *ACS Applied Materials & Interfaces*. 2015;7(43): 24159–24167. https://doi.org/10.1021/acsami.5b07471

15. Yakovleva E. I., Oveshnikov L. N., Kochura A. V., Lisunov K. G., Lahderanta E., Aronzon B. A. Anomalous Hall effect in the In_{1-x} $Mn_{(x)}$ Sb dilute magnetic semiconductor with MnSb inclusions. *JETP Letters*. 2015;101(2): 130–135. https://doi.org/10.1134/s0021364015020149

16. Sanygin V. P., Tishchenko E. A., Shi D. H., Izotov A. D. Concept of impurity-dislocation magnetism in III-V compound semiconductors. *Inorganic Materials*. 2013;49(1): 6–13. https://doi.org/10.1134/s0020168513010147

17. Blavette D., Cadel E., Fraczkiewicz A., Menand A. Three-dimensional atomic-scale imaging of impurity to line defects. *Science*. 1999;286(5448): 2317–2319. https://doi.org/10.1126/science.286.5448.2317

18. Nechaev Yu. S. Metallic materials for the hydrogen energy industry and main gas pipelines: complex physical problems of aging, embrittlement, and failure. *Physics-Uspekhi*. 2008;51(7): 681–697. https://doi.org/10.1070/pu2008v051n07abeh006570

19. Strel'chenko S. S., Lebedev V. V. *Soedineniya A^3B^5*[Compounds A^3B^5] Moscow: Metallurgiya Publ.; 1984. 144 p. (In Russ.)

20. *Fizicheskie velichiny*. Spravochnik pod redaktsiei Grigor'eva I. S., Meilikhova E. Z. [Physical quantities. Handbook. I. S. Grigoriev, E.Z. Meilikhov (eds.)]. Moscow: Energoatomizdat Publ.; 1991. 1232 p. (In Russ.)

21. Osip'yan Yu. A. *Elektronnye svoistva dislokatsii v poluprovodnikakh* [Electronic properties of dislocations in semiconductors.]. Moscow: Editorial URSS Publ.; 2000. 314 p. (In Russ.)

22. Hull D. *Introduction to dislocations*. Oxford, New York: Pergamon Press; 1984. 257 p.

23. *Diagrammy sostoyaniya dvoinykh metallicheskikh sistem: Spravochnik: v 3 t. Kn. 1* [State diagrams of double metal systems: Handbook: In 3 vols. Book 1] / N. P. Lyakisheva (ed.). Moscow: Mashinostroenie Publ; 2001. 872 p. (In Russ.)

24. Bean C. P., Livingston J. D. Superparamagnetism. Journal of Applied Physics 1959;30: S120. https://doi.org/10.1063/1.2185850

Information about the authors

Vladimir P. Sanygin, PhD in Chemistry, senior research fellow, Laboratory of Semiconductor and Dielectric Materials, Kurnakov Institute of General and Inorganic Chemistry of the Russian Academy of Sciences, Moscow, Russian Federation; e-mail: sanygin@igic.ras.ru. ORCID iD: https://orcid.org/0000-0002-1261-6895.

Olga N. Pashkova, PhD in Chemistry, senior research fellow, Laboratory of Semiconductor and Dielectric Materials, Kurnakov Institute of General and Inorganic Chemistry of the Russian Academy of Sciences, Moscow, Russian Federation; e-mail: olg-pashkova@yandex.ru. ORCID iD: https://orcid.org/0000-0002-2102-1025.

Alexander D. Izotov, DSc in Chemistry, Associate Member of the Russian Academy of Sciences, Chief Researcher, Laboratory of Semiconductor and Dielectric Materials, Kurnakov Institute of General and Inorganic Chemistry of the Russian Academy of Sciences, Moscow, Russian Federation; e-mail: izotov@igic.ras.ru. ORCID iD: https://orcid.org/0000-0002-4639-3415.

Received 14 April 2021; Approved after reviewing 30 April 2021; Accepted for publication 15 May 2021; Published online 25.09.2021.

Translated by Yulia Dymant
Edited and proofread by Simon Cox

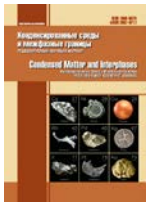

ISSN 1606-867X (Print)
ISSN 2687-0711 (Online)
Condensed Matter and Interphases
Kondensirovannye Sredy i Mezhfaznye Granitsy
https://journals.vsu.ru/kcmf/

Original articles

Research article
https://doi.org/10.17308/kcmf.2021.23/3527

Double molybdates of silver and monovalent metals

T. S. Spiridonova[1]✉, S. F. Solodovnikov[2], Yu. M. Kadyrova[1,3], Z. A. Solodovnikova[2], A. A. Savina[1,4], E. G. Khaikina[1,3]

[1]Baikal Institute of Nature Management, Siberian Branch of the Russian Academy of Sciences, 6 ulitsa Sakhyanovoy, Ulan-Ude, Republic of Buryatia 670047, Russian Federation

[2]Nikolaev Institute of Inorganic Chemistry, Siberian Branch of the Russian Academy of Sciences, 3 Akademika Lavrentieva prospekt, Novosibirsk 630090, Russian Federation

[3]Banzarov Buryat State University, 24a ulitsa Smolina, Ulan-Ude, Republic of Buryatia 670000, Russian Federation

[4]Skolkovo Institute of Science and Technology, 30, bld. 1 Bolshoy Boulevard, Moscow 121205, Russian Federation

Abstract

The Ag_2MoO_4–Cs_2MoO_4 system was studied by powder X-ray diffraction, the formation of a new double molybdate $CsAg_3(MoO_4)_2$ was established, its single crystals were obtained, and its structure was determined. $CsAg_3(MoO_4)_2$ (sp. gr. $P\bar{3}$, $Z = 1$, $a = 5.9718(5)$, $c = 7.6451(3)$ Å, $R = 0.0149$) was found to have the structure type of $Ag_2BaMn(VO_4)_2$. The structure is based on glaserite-like layers of alternating MoO_4 tetrahedra and $Ag1O_6$ octahedra linked by oxygen vertices, which are connected into a whole 3D framework by $Ag2O_4$ tetrahedra. An unusual feature of the Ag2 atom environment is its location almost in the centre of an oxygen face of the $Ag2O_4$ tetrahedron. Caesium atoms are in cuboctahedral coordination (CN = 12).

We determined the structures of the double molybdate of rubidium and silver obtained by us previously and a crystal from the solid solution based on the hexagonal modification of Tl_2MoO_4, which both are isostructural to glaserite $K_3Na(SO_4)_2$ (sp. gr. $P\bar{3}m1$). According to X-ray structural analysis data, both crystals have nonstoichiometric compositions $Rb_{2.81}Ag_{1.19}(MoO_4)_2$ ($a = 6.1541(2)$, $c = 7.9267(5)$ Å, $R = 0.0263$) and $Tl_{3.14}Ag_{0.86}(MoO_4)_2$ ($a = 6.0977(3)$, $c = 7.8600(7)$ Å, $R = 0.0174$). In the case of the rubidium compound, the splitting of the Rb/Ag position was revealed for the first time among molybdates. Both structures are based on layers of alternating MoO_4 tetrahedra and AgO_6 or (Ag, Tl)O_6 octahedra linked by oxygen vertices. The coordination numbers of rubidium and thallium are 12 and 10.

Keywords: Double molybdates, Silver, Monovalent metals, Binary systems, X-ray diffraction study, Structure, Glaserite

Acknowledgements: the authors are grateful to PhD Irina A. Prodan (Gudkova) and Ms Oksana A. Gulyaeva for recording and processing the X-ray diffraction data of the crystals on a Bruker X8 Apex CCD automated diffractometer. This research was supported by the Ministry of Science and Higher Education of the Russian Federation, projects No. 0273-2021-0008 (Baikal Institute of Nature Management, SB RAS), and No. 121031700313-8 (Nikolaev Institute of Inorganic Chemistry, SB RAS).

For citation: Spiridonova T. S., Solodovnikov S. F., Kadyrova Yu. M., Solodovnikova Z. A., Savina A. A., Khaikina E. G. Double molybdates of silver and monovalent metals. *Kondensirovannye sredy i mezhfaznye granitsy = Condensed Matter and Interphases*. 2021;23(3): 421–431. https://doi.org/10.17308/kcmf.2021.23/3527

Для цитирования: Спиридонова Т. С., Солодовников С. Ф., Кадырова Ю. М., Солодовникова З. А., Савина А. А., Хайкина Е. Г. Двойные молибдаты серебра и одновалентных металлов. *Конденсированные среды и межфазные границы*. 2021;23(3): 421–431. https://doi.org/10.17308/kcmf.2021.23/3527

✉ Tatyana S. Spiridonova, e-mail: spiridonova-25@mail.ru

© Spiridonova T.S., Solodovnikov S.F., Kadyrova Yu. M., Solodovnikova Z. A., Savina A.A., Khaikina E. G., 2021

The content is available under Creative Commons Attribution 4.0 License.

1. Introduction

Double molybdates of alkaline elements with divalent and trivalent metals are well known as promising phosphors [1–6], ferroelectrics and ferroelastics [7–9], solid electrolytes [10–13], electrode [14–19], laser [20–24], and other materials. A prominent place in the series of double molybdates is also occupied by phases formed in the M_2MoO_4–M'_2MoO_4 systems (M, M' – alkaline elements). The largest number of publications is devoted to M_2MoO_4–Li_2MoO_4 (M = K, Rb, Cs) systems and the double molybdates MLiMoO$_4$ formed in them. The compounds melt congruently and have developed polymorphism, and ferroelectric and ferroelastic properties [25–32]. Based on the results of studying the Na_2MoO_4–Li_2MoO_4 system by visual polythermic method, differential thermal analysis and X-ray powder diffraction, it was concluded in [25, 33, 34] that there are the phases with compositions 3:1 and 6:1 in the system; however, both compounds were not isolated and characterised. In the systems M_2MoO_4–Na_2MoO_4 (M = K, Rb, Cs), double molybdates $M_{2-x}Na_xMoO_4$ (M = K, Rb, Cs) were found [33, 35–39], which crystallize in the structure type of glaserite $K_3Na(SO_4)_2$ [40]. Unlike stoichiometric $Cs_3Na(MoO_4)_2$ [39], in the systems M_2MoO_4–Na_2MoO_4 (M = K, Rb) the glaserite-type phases have upper temperature limits of stability and noticeable homogeneity ranges: $K_{2-x}Na_xMoO_4$ ($0.40 \leqslant x \leqslant 1.0$) [36] and $Rb_{2-x}Na_xMoO_4$ ($0.50 \leqslant x \leqslant 0.67$) [37]. Another compound $RbNa_3(MoO_4)_2$ revealed in the Rb_2MoO_4–Na_2MoO_4 system is unstable at room temperature [37].

Until now, data on double molybdates of silver and monovalent metals were absent, although studies of the corresponding binary systems were undertaken. Thus, according to [41, 42], in the Ag_2MoO_4–Li_2MoO_4 system intermediate phases are not formed, while the authors of [43] on the base of the results of a visual polythermic analysis of the Ag_2MoO_4–Na_2MoO_4 system made a conclusion about formation of a continuous series of solid solutions with a minimum. The formation of continuous solid solutions of the spinel type was also confirmed by X-ray diffraction studies of the latter system [44]. One of the compositions of this solid solution ($NaAgMoO_4$) was studied in [45, 46]. The formation of boundary solid solutions was reported for the Ag_2MoO_4–Tl_2MoO_4 system [47, 48].

The first double molybdate of silver and an alkali metal was obtained by us when studying the Ag_2MoO_4–Rb_2MoO_4 system. The compound $Rb_3Ag(MoO_4)_2$ melts at 435 °C and has a glaserite structure type [49]. Later, in the similar potassium containing system, we obtained a hexagonal double molybdate, $K_{7-x}Ag_{1+x}(MoO_4)_4$ ($0 \leqslant x \leqslant 0.4$) [50], which crystallizes in its own structure type and at 334 °C undergoes a reversible first-order phase transition from the acentric form (sp. gr. $P6_3mc$) into centrosymmetric one.

In this study, we investigated the Ag_2MoO_4–Cs_2MoO_4 system and determined the crystal structure of the compound formed in it. In addition, the structure of double rubidium-silver molybdate was refined and an X-ray diffraction analysis of one of the members of the solid solution formed in the Ag_2MoO_4–Tl_2MoO_4 system on the base of the high-temperature modification of thallium molybdate [51] was performed.

2. Experimental

Commercially available $AgNO_3$, $TlNO_3$ (analytical reagent grade), MoO_3 (chemically pure grade), Cs_2CO_3 (extra-pure grade) reagents were used as starting materials. M_2MoO_4 (M = Ag, Tl) was obtained by calcining stoichiometric amounts of MNO$_3$ and MoO_3 with gradually increasing temperatures from 300–350 to 450 °C (in the case of silver) and up to 500 °C (in the case of thallium) for 50 h. Caesium molybdate was synthesised by the reaction $Cs_2CO_3 + MoO_3 = Cs_2MoO_4 + CO_2$ with annealing at 450–550 °C for 80 h. The thermal and crystallographic characteristics of the obtained compounds agreed with the literature data.

Powder X-ray diffraction (PXRD) analysis was carried out using a Bruker D8 ADVANCE automated powder diffractometer ($\lambda Cu K_\alpha$, secondary monochromator, scanning step $2\theta = 0.02076°$).

X-ray single crystal diffraction data for crystal structure determinations were taken at room temperature using Bruker-Nonius X8 Apex automated diffractometer with a two-dimensional CCD detector (MoK_α-radiation, graphite monochromator, φ-scanning with a scanning interval of 0.5°) in the hemisphere of reciprocal space. Calculations for solving and refinement of the structures were performed using the SHELX-97 software package [52].

3. Results and discussion

3.1. Cs_2MoO_4–Ag_2MoO_4 system and crystal structure of $CsAg_3(MoO_4)_2$

The Cs_2MoO_4–Ag_2MoO_4 system was studied by PXRD in the subsolidus region in the entire concentration range with a step of 5–10 mol% (2.5 mol% in some cases). The formation of an intermediate compound $CsAg_3(MoO_4)_2$ was established (the composition was found by single crystal structure determination). According to PXRD data, the formation of this compound begins at 300 °C; however, a single-phase $CsAg_3(MoO_4)_2$ sample was not obtained. An increase of the duration of reaction mixtures calcination (up to 500 h), an expansion of the temperature range (up to the limits of subsolidus temperatures), as well as the use of stoichiometric $AgNO_3$, Cs_2MoO_4, MoO_3 or Ag_2MoO_4, Cs_2CO_3, MoO_3 mixtures as starting components instead of simple silver and caesium molybdates, did not lead to a positive result.

Single crystals of $CsAg_3(MoO_4)_2$ suitable for X-ray structural analysis were obtained by spontaneous crystallization of the melt of a sintered sample of the compound, which was heated to 470 °C, kept at this temperature for 30 min and cooled at a rate of 4°/h down to 200 °C (then in a switched-off and cooling further). Crystal data and the structure refinement results are given in Table 1, the atomic coordinates and interatomic distances are listed in Tables 2 and 3.

The structure of $CsAg_3(MoO_4)_2$ was solved in the trigonal sp. gr. $P\bar{3}$ and it was found to be isostructural to $Ag_2BaMn(VO_4)_2$ [53]. The Mo atoms and 2/3 silver atoms (the Ag2 position) were tetrahedrally coordinated with the Mo–O distances 1.743(4)–1.776(2) Å, Ag2–O 2.314(2)–2.499(4) Å. An unusual feature of the Ag2 environment is its location almost in the centre of the oxygen face of $Ag2O_4$ tetrahedron (Fig. 1), which was also found in the $K_{6.68}Ag_{1.32}(MoO_4)_4$ structure [50]. The remaining third of silver atoms (Ag1) are located in octahedra with equal Ag1–O bond lengths of 2.446 (2) Å. The structure is based on glaserite-like layers of alternating MoO_4-tetrahedra and $Ag1O_6$-octahedra, which are linked by oxygen vertices and interconnected in a whole three-dimensional framework by $Ag2O_4$ tetrahedra (Fig. 1). The negative charge of the framework is compensated by caesium cations in cuboctahedral coordination (CN = 12); the Cs–O distances are 3.182(7)–3.451(1) Å.

3.2. Crystal structure of $Rb_{2.81}Ag_{1.19}(MoO_4)_2$

As we showed in [49], $Rb_3Ag(MoO_4)_2$ is the only intermediate compound of the Rb_2MoO_4–Ag_2MoO_4 system. A single-phase sample of the double rubidium-silver molybdate was synthesised by

Table 1. X-ray structure analysis data for $CsAg_3(MoO_4)_2$

Formula	$CsAg_3(MoO_4)_2$
Formula weight (g/mol)	776.40
Crystal system	Trigonal
Space group	$P\bar{3}$
Unit cell dimensions	a = 5.9718(5) Å, c = 7.6451(3) Å
V (Å^3) / Z	236.115(12) / 1
Calculated density (g cm^{-3})	5.460
Crystal size (mm)	0.15 × 0.06 × 0.06
μ(MoK_α), mm^{-1}	12.502
θ range (°)	5.328–61.126
Miller index ranges	$-8 \leqslant h \leqslant 8$, $-7 \leqslant k \leqslant 8$, $-10 \leqslant l \leqslant 10$
Reflections collected/unique	3234 / 490 [R_{int} = 0.0265]
Number of variables/constraints	24 / 0
Goodness-of-fit on F^2 (GOF)	1.158
Extinction coefficient	0.0087(6)
Final R indices [$I > 2\sigma(I)$] R indices (all data)	$R(F)$ = 0.0149, $wR(F^2)$ = 0.0349 $R(F)$ = 0.0158, $wR(F^2)$ = 0.0353
Largest difference peak / hole (e Å^{-3})	0.81/–1.15

Таблица 2. Координаты и эквивалентные изотропные тепловые параметры атомов в структуре $CsAg_3(MoO_4)_2$

Atom	*x/a*	*y/b*	*z/c*	U_{eq}(Å²)*
Mo	0.6667	0.3333	0.25304(5)	0.01327(11)
Ag1	0	0	0	0.02048(11)
Ag2	0.3333	0.6667	0.19216	0.02805(13)
Cs	0	0	0.5	0.02047(12)
O1	0.6667	0.3333	0.4810(5)	0.0306(9)
O2	0.7014(4)	0.631(4)	0.1792(3)	0.0242(4)

* $U_{eq} = 4(U_{11} + U_{22} + 0.75U_{33} - U_{12}) / 9$.

Table 3. Selected interatomic distances **(Å) in** $CsAg_3(MoO_4)_2$

Mo-tetrahedron		Ag1-octahedron	
Mo1–O1	1.743(4)	Ag1–O2	2.446(2) × 6
–O2	1.776(2) × 3		
<Mo1–O>	1.768		
Cs-polyhedron		**Ag2-tetrahedron**	
Cs–O2′	3.181(2) × 6	Ag2–O2	2.314(2) × 3
–O1	3.4509(2) × 6	–O1	2.499(4)
<Cs–O>	3.316	<Ag2–O>	2.360

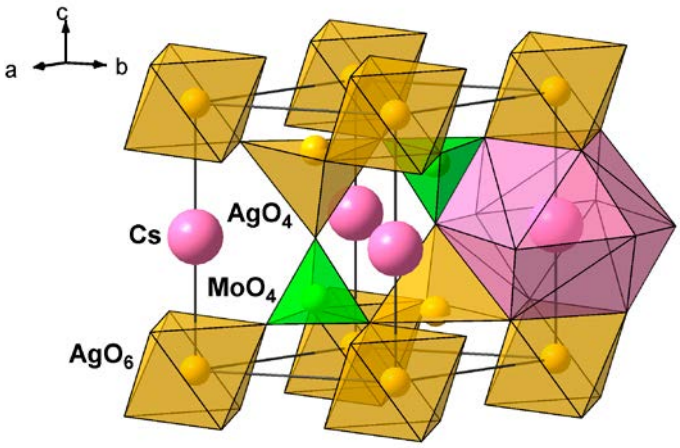

Fig. 1. Crystal structure of $CsAg_3(MoO_4)_2$

annealing a stoichiometric mixture of Ag_2MoO_4 and Rb_2MoO_4 at 380 °C for 100 h. Crystals suitable for X-ray structural analysis were obtained by spontaneous crystallisation from the melt. The preliminary results of X-ray structural analysis were previously published by us in [49]. In this study, the composition of the $Rb_{2.81}Ag_{1.19}(MoO_4)_2$ crystal and its structure were corrected and refined (Tables 4–6).

Note that the solid-state synthesis of a single-phase sample of the composition described above was not successful. After annealing the reaction mixtures of silver and rubidium molybdates, even at highest subsolidus temperatures, only $Rb_{3-x}Ag_{1+x}(MoO_4)_2$ ($0 \leqslant x \leqslant 0.10$) samples were single-phase. Probably, the found crystal composition has an extremely high silver content and can be obtained only from melts.

In the structure of $Rb_{2.81}Ag_{1.19}(MoO_4)_2$ (sp. gr. $P\bar{3}m1$) of the glaserite type $K_3Na(SO_4)_2$ [40], molybdenum atoms have tetrahedral oxygen coordination with the distances Mo–O 1.730(6)–1.773(3) Å. The Ag1 atoms are in octahedra with the equal bond lengths Ag–O 2.483(3) Å. The structure is based on layers of alternating MoO_4 tetrahedra and $Ag1O_6$ octahedra linked by

Table 4. X-ray structure analysis data for $Rb_{2.81}Ag_{1.19}(MoO_4)_2$ and $Tl_{3.14}Ag_{0.86}(MoO_4)_2$

Formula	$Rb_{2.81}Ag_{1.19}(MoO_4)_2$	$Tl_{3.14}Ag_{0.86}(MoO_4)_2$
Formula weight (g/mol)	688.42	1054.37
Crystal system	Trigonal	Trigonal
Space group	$P\bar{3}m1$	$P\bar{3}m1$
Unit cell dimensions	a = 6.1541(2) Å c = 7.9267(5) Å	a = 6.0977(3) Å c = 7.8600(7) Å
V (Å^3) / Z	259.99 (2) / 1	253.10 (3) / 1
Calculated density (g cm^{-3})	4.397	6.918
Crystal size (mm)	0.13 × 0.10 × 0.02	0.09 × 0.09 × 0.05
μ(MoK_α), mm^{-1}	3.645	53.840
θ range (°)	2.26–28.83	2.09–30.50
Miller index ranges	$-10 \leqslant h \leqslant 8$, $-10 \leqslant k \leqslant 7$, $-13 \leqslant l \leqslant 9$	$-5 \leqslant h \leqslant 8$, $-8 \leqslant k \leqslant 6$, $-11 \leqslant l \leqslant 10$
Reflections collected/unique	2370 / 504 [R_{int} = 0.0299]	2306 / 330 [R_{int} = 0.0314]
Number of variables/constraints	25 / 0	22 / 0
Goodness-of-fit on F^2 (GOF)	1.271	1.087
Extinction coefficient	0.0016 (3)	0.0035 (4)
Final R indices [$I > 2\sigma(I)$] R indices (all data)	$R(F)$ = 0.0263 $wR(F^2)$ = 0.0625 $R(F)$ = 0.0272 $wR(F^2)$ = 0.0627	$R(F)$ = 0.0174 $wR(F^2)$ = 0.0419 $R(F)$ = 0.0189 $wR(F^2)$ = 0.0425
Largest difference peak/hole (e Å^{-3})	1.00 / −1.21	0.87 / −0.87

Table 5. Coordinates and equivalent isotropic thermal parameters of atoms in the structure of $Rb_{2.81}Ag_{1.19}(MoO_4)_2$

Atom	Occ.	x/a	y/b	z/c	U_{eq} (Å^2)*
Mo	1	0.6667	0.3333	0.25304(5)	0.0149(2)
Ag1	1	0	0	0	0.0221(2)
Ag2	0.10(1)	0.3333	0.6667	0.179(5)	0.047(7)
Rb1	0.90(1)	0.3333	0.6667	0.1580(3)	0.0205(4)
Rb2	1	0	0	0.5	0.0296(3)
O1	1	0.6667	0.3333	0.4810(5)	0.055(2)
O2	1	0.7014(4)	0.631(4)	0.1792(3)	0.0321(7)

*$U_{eq} = 4(U_{11} + U_{22} + 0.75U_{33} - U_{12}) / 9$.

Table 6. Main interatomic distances (Å) in the structure of $Rb_{2.81}Ag_{1.19}(MoO_4)_2$

Mo-tetrahedron		Rb1-polyhedron	
Mo–O1	1.730(6)	Rb1–O1	2.705(7)
–O2	1.773(3) × 3	–O2	3.0990(5) × 6
		–O2′	3.296(4) × 3
<Mo–O>	1.762	<Rb1–O>	3.119
Ag1-octahedron		Rb2-polyhedron	
Ag1–O2	2.483(3) × 6	Rb2–O2	3.033(4) × 6
Ag2-polyhedron		–O1	3.5531(1) × 6
Ag2–O1	2.54(4)	<Rb2–O>	3.293
–O2	3.085(2) × 6		
<Ag2–O>	3.007		

common oxygen vertices (Fig. 2). The negative charge of the layers is compensated by two types of rubidium cations (CN = 12 and 10); the total range of Rb–O distances is 2.706(7) –3.553(1) Å. An additional position of silver (Ag2) near the Rb1 position (CN = 10) at the distance Rb1–Ag2 0.17(4) Å was found, which partially replaces rubidium in Rb1; the Ag2–O bond lengths are 2.54(4)–3.085(2) Å (CN = 7).

Splitting of the Rb/Ag position in molybdates was revealed for the first time. As for tungstates, it was found earlier in the structure $Ag_{3+x}Rb_{9-x}Sc_2(WO_4)_9$, ($x \approx 0.11$) [54], and a similar splitting of the K/Ag position was found by us in the structure of $Ag_{1.32}K_{6.68}(MoO_4)_4$ [50]. Such disordering and splitting of positions of large alkali cations is still rare. Examples are rubidium-containing defect pyrochlores $RbNb_2O_5F$ [55], $RbAl_{0.33}W_{1.67}O_6$ [56], ferroelectric solid electrolytes $RbTiOAsO_4$ [57] and $RbSbOGeO_4$ [58] of the $KTiOPO_4$ type. As a rule, this is considered as the ability of the structure to have potential ionic conductivity and/or ferroelectricity [59]. Indeed, some rubidium-containing defect pyrochlores and many members of the $KTiOPO_4$ family are bright examples of phases with these properties [58, 60]. This tendency is confirmed by the fact that the $Ag_{3+x}Rb_{9-x}Sc_2(WO_4)_9$ ($x \approx 0.11$) studied by us probably has rubidium ion conductivity [54], and nonstoichiometric phases of the glaserite type can also be solid electrolytes [61].

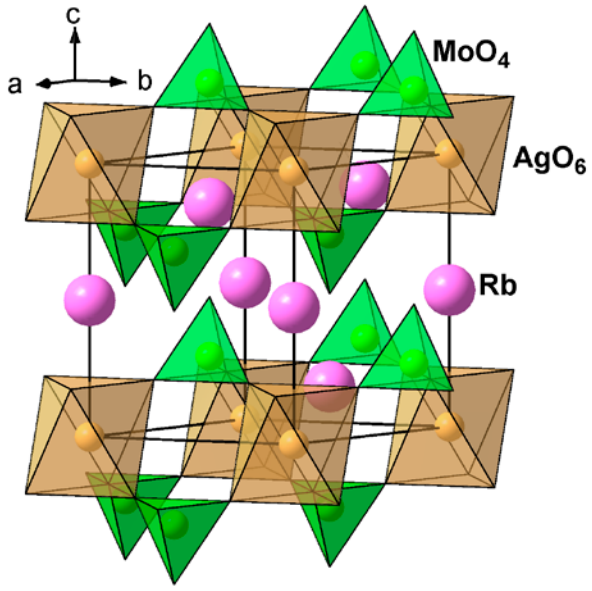

Fig. 2. General view of the $Rb_{2.81}Ag_{1.19}(MoO_4)_2$ structure

3.3. Crystal structure of $Tl_{3.14}Ag_{0.86}(MoO_4)_2$

According to [47, 48], in the Tl_2MoO_4–Ag_2MoO_4 system, boundary solid solutions are formed, including those based on the high-temperature hexagonal form α-Tl_2MoO_4 of the $K_3Na(SO_4)_2$ glaserite type [51]. Using spontaneous crystallisation of a molten sample of $Tl_3Ag(MoO_4)_2$ synthesized by solid-state reactions from a stoichiometric mixture of simple molybdates, we obtained crystals suitable for X-ray structural analysis from the region of the specified solid solution and refined their crystal structure.

The composition of the studied crystal of the glaserite type, $Tl_{3.14}Ag_{0.86}(MoO_4)_2$ (sp. gr. $P\bar{3}m1$), was determined by refinement of the site occupancies of the thallium and silver cations, which showed that the occupancy of thallium sites is 100 % within the experimental error limits, while the silver site contains an admixture of thallium. The correctness of this model is confirmed by a decrease in *R*-factor from 0.0235 to 0.0174, and the determined crystal composition fell into the range of the solid solution based on α-Tl_2MoO_4. The results of the structural refinement are given in Table 4, and the atomic coordinates and interatomic distances are shown in Tables 7 and 8.

In general, the structure of $Tl_{3.14}Ag_{0.86}(MoO_4)_2$ repeats the above-described structure of isostructural $Rb_{2.81}Ag_{1.19}(MoO_4)_2$ (Fig. 2). Molybdenum atoms are tetrahedrally coordinated with the distances Mo–O 1.760 (6)–1.765(3) Å, and the (Ag, Tl) atom has octahedral coordination with equal bond lengths (Ag, Tl)–O 2.535(4) Å, which is longer than the distance Ag1–O 2.483(3) Å in $Rb_{2.81}Ag_{1.19}(MoO_4)_2$ (see above) and is significantly shorter than the corresponding distance Tl1–O 2.769(10) Å in the structure of α-Tl_2MoO_4 [51]. Thallium atoms of two sorts with CN = 12 and 10 have the common distance range Tl–O 2.495(7)–3.5243(4) Å, which is close to the lengths of the corresponding bonds Tl–O 2.467(16)–3.682(16) Å in α-Tl_2MoO_4 [51].

4. Conclusions

The subsolidus region of the system Ag_2MoO_4–Cs_2MoO_4 was studied by PXRD, the compound with the composition $CsAg_3(MoO_4)_2$ crystallising in the structure type of $Ag_2BaMn(VO_4)_2$ (sp. gr. $P\bar{3}$, Z = 1) was revealed and its structure was determined.

Table 7. Coordinates and equivalent isotropic thermal parameters of atoms in the structure of $Tl_{3.14}Ag_{0.86}(MoO_4)_2$

Atom	Occ.	*x/a*	*y/b*	*z/c*	U_{eq} (Å²)*
Mo	1	0.6667	0.3333	0.29677(10)	0.0195(2)
(Ag, Tl)	0.877(5)Ag+0.123Tl	0	0	0	0.0282(3)
Tl1	1	0.3333	0.6667	0.16186(4)	0.0328(2)
Tl2	1	0	0	0.5	0.0316(2)
O1	1	0.6667	0.3333	0.5207(10)	0.062(3)
O2	1	0.8232(4)	0.6464(7)	0.2181(6)	0.0399(10)

*$U_{eq} = 4(U_{11} + U_{22} + 0.75U_{33} - U_{12}) / 9$.

Table 8. Main interatomic distances (Å) in the structure of $Tl_{3.14}Ag_{0.86}(MoO_4)_2$

Mo-tetrahedron		Tl1-polyhedron	
Mo–O1	1.760(8)	Tl1–O1	2.495(7)
–O2	1.765(4) × 3	–O2	3.0825(7) × 6
		–O2′	3.413(4) × 3
<Mo–O>	1.764	<Tl1–O>	3.123
(Ag, Tl)-octahedron		Tl2-polyhedron	
(Ag, Tl)–O2	2.535(4) × 6	Tl2–O2	2.898(4) × 6
		–O1	3.5243(4) × 6
		<Tl2–O>	3.211

We determined the structure and composition of double rubidium-silver molybdate, and performed X-ray structure analysis of a member of the solid solution on the base of the high-temperature form of thallium molybdate formed in the system Ag_2MoO_4–Tl_2MoO_4. It was confirmed that $Rb_{2.81}Ag_{1.19}(MoO_4)_2$ and $Tl_{3.14}Ag_{0.86}(MoO_4)_2$ (crystal compositions were determined by X-ray structure analysis) are of the glaserite structure type. In the case of the rubidium containing phase, splitting of the Rb/Ag position was revealed for the first time in molybdates. This phenomenon usually indicates the ability of the structure to have potential ionic conductivity and/or ferroelectricity.

Author contributions

All authors made an equivalent contribution to the preparation of the publication.

Conflict of interests

The authors declare that they have no known competing financial interests or personal relationships that could have influenced the work reported in this paper.

References

1. Fan W., He Y., Long L., Gao Y., Liu F., Liu J. Multiplexed excitations $KGd_{1-x}Eu_x(MoO_4)_2$ red-emitting phosphors with highly Eu^{3+} doping for white LED application. *Journal of Materials Science: Materials in Electronics*. 2021;32(5): 6239–6248. https://doi.org/10.1007/s10854-021-05339-1

2. Wang Y., Song M., Xiao L., Li Q. Upconversion luminescence of Eu^{3+} and Sm^{3+} single-doped $NaYF_4$ and $NaY(MoO_4)_2$. *Journal of Luminescence*. 2021;238: 118203. https://doi.org/10.1016/j.jlumin.2021.118203

3. Morozov V. A., Lazoryak B. I., Shmurak S. Z., Kiselev A. P., Lebedev O. I., Gauquelin N., Verbeeck J., Hadermann J., Van Tendeloo G. Influence of the structure on the properties of $Na_xEu_y(MoO_4)_z$ red phosphors. *Chemistry of Materials*. 2014;26(10): 3238–3248. https://doi.org/10.1021/cm500966g

4. Guo C., Gao F., Xu Y., Liang L., Shi F. G., Yan B. Efficient red phosphors $Na_5Ln(MoO_4)_4$: Eu^{3+} (*Ln* = La, Gd and Y) for white LEDs. *Journal of Physics D: Applied Physics*. 2009;42(9): 095407. https://doi.org/10.1088/0022-3727/42/9/095407

5. Zhao C., Yin X., Huang F., Hang Y. Synthesis and photoluminescence properties of the high-brightness Eu^{3+}-doped $M_2Gd_4(MoO_4)_7$ (*M* = Li, Na) red phosphors. *Journal of Solid State Chemistry*. 2011;184(12): 3190–3194. https://doi.org/10.1016/j.jssc.2011.09.025

6. Pandey I. R., Karki S., Daniel D. J., Kim H. J., Kim Y. D., Lee M. H., Pavlyuk A. A., Trifonov V. A. Crystal growth, optical, luminescence and scintillation characterization of $Li_2Zn_2(MoO_4)_3$ crystal. *Journal of Alloys and Compounds*. 2021;1860: 158510. https://doi.org/10.1016/j.jallcom.2020.158510 0925-8388

7. Isupov V. A. Binary molybdates and tungstates of mono and trivalent elements as possible ferroelastics and ferroelectrics. *Ferroelectrics*. 2005;321(1): 63–90. https://doi.org/10.1080/00150190500259699

8. Isupov V. A. Ferroelectric and ferroelastic phase transitions in molybdates and tungstates of monovalent and bivalent elements. *Ferroelectrics*. 2005;322(1): 83–114. https://doi.org/10.1080/00150190500315574

9. Tsyrenova G. D., Pavlova E. T., Solodovnikov S. F., Popova N. N., Kardash T. Yu., Stefanovich S. Yu., Gudkova I. A., Solodovnikova Z. A., Lazoryak B. I. New ferroelastic $K_2Sr(MoO_4)_2$: synthesis, phase transitions, crystal and domain structures, ionic conductivity. *Journal of Solid State Chemistry*. 2016;237: 64–71. https://doi.org/10.1016/j.jssc.2016.01.011

10. Savina A. A., Solodovnikov S. F., Basovich O. M., Solodovnikova Z. A., Belov D. A., Pokholok K. V., Gudkova I. A., Stefanovich S. Yu., Lazoryak B. I., Khaikina E. G. New double molybdate $Na_9Fe(MoO_4)_6$: synthesis, structure, properties. *Journal of Solid State Chemistry*. 2013;205: 149–153. https://doi.org/10.1016/j.jssc.2013.07.007

11. Savina A. A., Morozov V. A., Buzlukov A. L., Arapova I. Yu., Stefanovich S. Yu., Baklanova Ya. V., Denisova T. A., Medvedeva N. I., Bardet M., Hadermann J., Lazoryak B. I., Khaikina E. G. New solid electrolyte $Na_9Al(MoO_4)_6$: structure and Na^+ ion conductivity. *Chemistry of Materials*. 2017;29(20): 8901–8913. https://doi.org/10.1021/acs.chemmater.7b03989

12. Solodovnikov S. F., Solodovnikova Z. A., Zolotova E. S., Yudin V. N., Gulyaeva O. A., Tushinova Y. L., Kuchumov B. M. Nonstoichiometry in the systems Na_2MoO_4–$MMoO_4$ (*M* = Co, Cd), crystal structures of $Na_{3.36}Co_{1.32}(MoO_4)_3$, $Na_{3.13}Mn_{1.43}(MoO_4)_3$ and $Na_{3.72}Cd_{1.14}(MoO_4)_3$, crystal chemistry, compositions and ionic conductivity of alluaudite-type double molybdates and tungstates. *Journal of Solid State Chemistry*. 2017;253: 121–128. https://doi.org/10.1016/j.jssc.2017.05.031

13. Medvedeva N. I., Buzlukov A. L., Skachkov A. V., Savina A. A., Morozov V. A., Baklanova Ya. V., Animitsa I. E., Khaikina E. G., Denisova T. A., Solodovnikov S. F. Mechanism of sodium-ion diffusion in alluaudite-type $Na_5Sc(MoO_4)_4$ from NMR experiment and ab initio calculations. *Journal of Physical Chemistry C*. 2019;123(8): 4729. https://doi.org/10.1021/acs.jpcc.8b11654

14. Chen S., Duan H., Zhou Z., Fan Q., Zhao Y., Dong Y. Lithiated bimetallic oxide, $Li_3Fe(MoO_4)_3$, as a high-performance anode material for lithium-ion batteries and its multielectron reaction mechanism. *Journal of Power Sources*. 2020;476: 228656. https://doi.org/10.1016/j.jpowsour.2020.228656

15. Tamboli A. M., Tamboli M. S., Praveen C. S., Dwivedi P. K., Karbhal I., Gosavi S. W., Shelke M. V., Kale B. B. Architecture of $NaFe(MoO_4)_2$ as a novel anode material for rechargeable lithium and sodium ion batteries. *Applied Surface Science*. 2021;559: 149903. https://doi.org/10.1016/j.apsusc.2021.149903

16. Wang L., He Y., Mu Y., Wu B., Liu M., Zhao Y., Lai X., Bi J., Gao D. Sol-gel driving $LiFe(MoO_4)_2$ microcrystals: high capacity and superior cycling stability for anode material in lithium ion batteries. *Electronic Materials Letters*. 2019;15(2): 186–191. https://doi.org/10.1007/s13391-018-00115-6

17. Mikhailova D., Sarapulova A., Voss A., Thomas A., Oswald S., Gruner W., Trots D. M., Bramnik N. N., Ehrenberg H. $Li_3V(MoO_4)_3$: A new material for both Li extraction and insertion. *Chemistry of Materials*. 2010;22(10): 3165–3173. https://doi.org/10.1021/cm100213a

18. Begam K. M., Prabaharan S. R. S. Improved cycling performance of nano-composite $Li_2Ni_2(MoO_4)_3$ as a lithium battery cathode material. *Journal of Power Sources*. 2006;159(1): 319–322. https://doi.org/10.1016/j.jpowsour.2006.04.133

19. Serdtsev A. V., Medvedeva N. I. Ab initio insights into Na-ion diffusion and intercalation mechanism in alluaudite $Na_2Mn_2(MoO_4)_3$ as cathode material for sodium-ion batteries. *Journal of Alloys and Compounds*. 2019;808: 151667. https://doi.org/10.1016/j.jallcom.2019.151667

20. Voron'ko Yu. K., Zharikov E. V., Lis D. A., Popov A. V., Smirnov V. A., Subbotin K. A., Khromov M. N., Voronov V. V. Growth and spectroscopic studies of $NaLa(MoO_4)_2$:Tm^{3+} crystals: a new promising laser material. *Optics and Spectroscopy*. 2008;105(4): 538–546. https://doi.org/10.1134/S0030400X08100081

21. Gao S., Zhu Z., Wang Y., You Z., Li J., Wang H., Tu C. Growth and spectroscopic investigations of a new laser crystal Yb^{3+}-doped $Na_2Gd_4(MoO_4)_7$. *Optical Materials*. 2013;36(2): 505–508. https://doi.org/10.1016/j.optmat.2013.10.018

22. Loiko P., Pavlyuk A., Slimi S., Solé R. M., Salem E. B., Dunina E., Kornienko A., Camy P., Griebner U., Petrov V., Díaz F., Aguiló M., Mateos X. Growth, spectroscopy and laser operation of monoclinic Nd:$CsGd(MoO_4)_2$ crystal with a layered structure. *Journal of Luminescence*. 2021;231: 117793. https://doi.org/10.1016/j.jlumin.2020.117793

23. Iparraguirre I., Balda R., Voda M., Al-Saleh M., Fernandez J. Infrared-to-visible upconversion in $K_5Nd(MoO_4)_4$ stoichiometric laser crystal. *Journal of the Optical Society of America B*. 2002;19(12): 2911–2920. https://doi.org/10.1364/JOSAB.19.002911

24. Voron'ko Y. K., Subbotin K. A., Shukshin V. E., Lis D. A., Ushakov S. N., Popov A., Zharikov E. V. Growth and spectroscopic investigations of Yb^{3+}-doped $NaGd(MoO_4)_2$ and $NaLa(MoO_4)_2$: new promising laser crystals. *Optical Materials*. 2006;29(2-3): 246–252. https://doi.org/10.1016/j.optmat.2005.09.004

25. Hoermann F. Beitrag zur Kenntnis der Molybdate und Wolframate. Die binären Systeme: Li_2MoO_4–MoO_3, Na_2MoO_4–MoO_3, K_2MoO_4–MoO_3, Li_2WO_4–WO_3, Na_2WO_4–WO_3, K_2WO_4–WO_3, Li_2MoO_4–Na_2MoO_4, Li_2WO_4–Na_2WO_4, Li_2MoO_4–K_2MoO_4. *Zeitschrift für Anorganische und Allgemeine Chemie*. 1929;177(1): 145–186. https://doi.org/10.1002/zaac.19291770117

26. Bergman A. G., Kislova A. I., Korobka E. I. Issledovanie dvoinoi vzaimnoi sistemy diagonal'no-poyasnogo tipa iz sul'fatov i molibdatov litiya i kaliya [Investigation of the double reciprocal system of the diagonal-belt type of lithium and potassium sulfates and molybdates]. *Zhurnal Obshhej Khimii*. 1954;24(5): 1127–1135. (In Russ.)

27. Samuseva R. G., Bobkova M. V., Plyushchev V. E. Systems Li_2MoO_4–Rb_2MoO_4 and Li_2MoO_4–Cs_2MoO_4. *Zhurnal Neorganicheskoj Khimii (Russian Journal of Inorganic Chemistry*. 1969;14(11): 3140–3142. (In Russ.)

28. Klevtsova R. F., Klevtsov P. V., Aleksandrov K. S. Synthesis and crystal structure of $CsLiMoO_4$. *Doklady AN SSSR*. 1980;255(6): 1379–1382. Available at: http://www.mathnet.ru/links/615f6831862802e4f119568c63999bbe/ dan44135.pdf (In Russ.)

29. Okada K., Ossaka J. Crystal data and phase transitions of $KLiWO_4$ and $KLiMoO_4$. *Journal of Solid State Chemistry*. 1981;37(3): 325–327. https://doi.org/10.1016/0022-4596(81)90494-1

30. Aleksandrov K. S., Anistratov A. T., Melnikova S. V., Klevtsova P. F. Ferroelectricity in caesium lithium molybdate $CsLiMoO_4$ and related crystals $CsLiWO_4$ and $RbLiMoO_4$. *Ferroelectrics*. 1981;36(1): 399–402. https://doi.org/10.1080/00150198108218138

31. Kruglik A. I., Klevtsova P. F., Aleksandrov K. S. Crystal structure of new ferroelectric $RbLiMoO_4$. *Doklady AN SSSR*. 1983;271(6): 1388–1391. Available at: http://www.mathnet.ru/links/b19a6f8fab3efdda809632d278dc8cb9/dan46252.pdf (In Russ.)

32. Melnikova S. V., Voronov V. N., Klevtsov P. V. Phase transitions in $RbLiMoO_4$. *Kristallografiya*. 1986;31(2): 402–404. (In Russ.)

33. Ding Y., Hou N., Chen N., Xia Y. Phase diagrams of Li_2MoO_4–Na_2MoO_4 and Na_2MoO_4–K_2MoO_4 systems. *Rare metals*. 2006;25(4): 316–320. https://doi.org/10.1016/S1001-0521(06)60060-0

34. Bergman A. G., Korobka E. I. Fusibility diagram of a ternary reciprocal system of lithium and sodium sulfates and molybdates. *Zhurnal Neorganicheskoj Khimii (Russian Journal of Inorganic Chemistry)*. 1959;4(1): 110–116. (In Russ.)

35. Fabry J., Petricek V., Vanek P., Cisarova I. Phase transition in $K_3Na(MoO_4)_2$ and determination of the twinned structures of $K_3Na(MoO_4)_2$ and $K_{2.5}Na_{1.5}(MoO_4)_2$ at room temperature. *Acta Crystallographica Section B*. 1997;53(4): 596–603. https://doi.org/10.1107/s0108768197002164

36. Gulyaeva O. A., Solodovnikova Z. A., Solodovnikov S. F., Yudin V. N., Zolotova E. S., Komarov V. Yu. Subsolidus phase relations and structures of solid solutions in the systems K_2MoO_4–Na_2MoO_4–$MMoO_4$ (M = Mn, Zn). *Journal of Solid State Chemistry*. 2019;272: 148–156. https://doi.org/10.1016/j.jssc.2019.02.010

37. Mokhosoev M. V., Khal'baeva K. M., Khaikina E. G., Ogurtsov A. M. Double sodium-rubidium molybdates. *Zhurnal Neorganicheskoj Khimii (Russian Journal of Inorganic Chemistry)*. 1990;35(8): 2126–2129. Available at: https://elibrary.ru/item.asp?id=22232925 (In Russ.)

38. Bai C., Lei C., Pan S., Wang Y., Yang Z., Han S., Yu H., Yang Y., Zhang F. Syntheses, structures and characterizations of $Rb_3Na(MO_4)_2$ (M = Mo, W) crystals. *Solid State Science*. 2014;33: 32–37. https://doi.org/10.1016/j.solidstatesciences.2014.04.011

39. Zolotova E. S., Solodovnikova Z. A., Yudin V. N., Solodovnikov S. F., Khaikina E. G., Basovich O. M., Korolkov I. V., Filatova I. Yu. Phase relations in the Na_2MoO_4–Cs_2MoO_4 and Na_2MoO_4–Cs_2MoO_4–$ZnMoO_4$ systems, crystal structures of $Cs_3Na(MoO_4)_2$ and $Cs_3NaZn_2(MoO_4)_4$. *Journal of Solid State Chemistry*. 2016;233: 23–29. https://doi.org/10.1016/j.jssc.2015.10.008

40. Okada K., Ossaka J. Structures of potassium sodium sulphate and tripotassium sodium disulphate. *Acta Crystallographica Section B*. 1980;36(4): 919–921. https://doi.org/10.1107/S0567740880004852

41. Belyaev I. N., Doroshenko S. S. Study of the interaction of sulfates and molybdates of lithium and silver in melts. *Zhurnal Neorganicheskoj Khimii (Russian Journal of Inorganic Chemistry)*. 1956;26(7): 1816–1820. (In Russ.)

42. Khal'baeva K. M., Khaikina E. G., Basovich O. M. Phase equilibria in lithium-silver(sodium)-bismuth molybdate systems. *Russian Journal of Inorganic Chemistry*. 2005;50(8): 1282–1284.

43. Belyaev I. N., Doroshenko A. K. Exchange decomposition in a reciprocal system of sodium and silver sulfates and molybdates in melts. *Zhurnal Obshhej Khimii*. 1954;24: 427–432. (In Russ.)

44. Zhou D., Li J., Pang L. X., Wang D. W., Reaney I. M. Novel water insoluble $(Na_xAg_{2-x})MoO_4$ ($0 \leqslant x \leqslant 2$) microwave dielectric ceramics with spinel structure sintered at 410 degrees. *Journal of Materials Chemistry. C*. 2017;5(24): 6086–6091. https://doi.org/10.1039/c7tc01718a

45. Rulmont A., Tarte P., Foumakoye G., Fransolet A.M., Choisnet J. The disordered spinel $NaAgMoO_4$ and its high-temperature, ordered orthorhombic polymorph. *Journal of Solid State Chemistry*. 1988;76(1): 18–25. https://doi.org/10.1016/0022-4596(88)90188-0

46. Zhou D., Pang L. X., Qi Z. M., Jin B. B., Yao X. Novel ultra-low temperature co-fired microwave dielectric ceramic at 400 degrees and its chemical compatibility with base metal. *Scientific Reports*. 2014;4(1): 5980. https://doi.org/10.1038/srep05980

47. Arkhincheeva S. I., Bazarova J. G., Munkueva S. D. Solid-phase interaction of thallium and silver molybdates (tungstates). *Vestnik BGU. Khimiya (BSU bulletin. Chemistry).* 2004;(1): 43–47. (In Russ.)

48. Grossman V. G., Bazarov B. G., Bazarova J. G. Phase formation in Tl_2MoO_4–Ag_2MoO_4 and Tl_2WO_4–Ag_2WO_4 systems. *Izvestia Vuzov. Prikladnaya Khimiya i Biotekhnologiya (Proceedings of Universitets. Applied Chemistry and Biotechnology)*. 2018;8(3): 142–147. https://doi.org/10.21285/2227-2925-2018-8-3-142-147 (In Russ.)

49. Kadyrova Yu. M., Solodovnikov S. F., Solodovnikova Z. A., Basovich O. M., Spiridonova T. S., Khaikina E. G. New silver-rubidium double molybdate. *Vestnik BGU (BSU bulletin. Chemistry. Physics)*. 2015;3: 21–25. (In Russ.)

50. Spiridonova T. S., Solodovnikov S. F., Savina A. A., Solodovnikova Z. A., Stefanovich S. Yu., Lazoryak B. I., Korolkov I. V., Khaikina E. G. Synthesis, crystal structures and properties of the new compounds $K_{7-x}Ag_{1+x}(XO_4)_4$ (X = Mo, W). *Acta Crystallographica Section C*. 2017;73(12): 1071–1077. https://doi.org/10.1107/s2053229617015674

51. Friese K., Madariaga G., Breczewski T. $T1_2MoO_4$ at 350 K. *Acta Crystallographica Section C*. 1999;55(11): 1753–1755. https://doi.org/10.1107/S0108270199008616

52. Sheldrick G. M. SHELX97, Release 97-2. – Göttingen, Germany: Univ. of Göttingen, 1997.

53. Rettich R., Müller-Buschbaum Hk., Zur Kristallchemie der Silber-Mangan-Oxovanadate $Ag_2BaMnV_2O_8$ und $(AgCa_2)Mn_2(VO_4)_3$. *Zeitschrift für Naturforschung*. 1998;53b: 291–295. Available at: https://zfn.mpdl.mpg.de/data/Reihe_B/53/ZNB-1998-53b-0291.pdf

54. Spiridonova T. S., Solodovnikov S. F., Savina A. A., Kadyrova Yu. M., Solodovnikova Z. A., Yudin V. N., Stefanovich S. Yu., Kotova I. Yu., Khaikina E. G., Komarov V. Yu. $Rb_{9-x}Ag_{3+x}Sc_2(WO_4)_9$: a new glaserite-related structure type, rubidium disorder, ionic conductivity. *Acta Crystallographica Section B*. 2020;76(1): 28–37. https://doi.org/10.1107/S2052520619015270

55. Fourquet J. L., Jacoboni C., de Pape R. Les pyrochlores $A^I_2X_6$: mise en evidence de l'occupation par le cation A^I de nouvelles positions cristallographiques dans le groupe d'espace $Fd3m$. *Materials Research Bulletin*. 1973;8(4): 393–404. https://doi.org/10.1016/0025-5408(73)90043-3

56. Thorogood G. J., Kennedy B. J., Peterson V. K., Elcombe M. M., Kearley G. J., Hanna J. V., Luca V. Anomalous lattice parameter increase in alkali earth aluminium substituted tungsten defect pyrochlores. *Journal of Solid State Chemistry*. 2009;182(3): 457–464. https://doi.org/10.1016/j.jssc.2008.11.014

57. Streltsov V. A., Nordborg J., Albertsson J. Synchrotron X-ray analysis of $RbTiOAsO_4$. *Acta Crystallographica Section B*. 2000;56(5): 785–792. https://doi.org/10.1107/S0108768100006285

58. Belokoneva E. L., Knight K. S., David W. I. F., Mill B. V. Structural phase transitions in germanate analogues of $KTiOPO_4$ investigated by high-resolution neutron powder diffraction. *Journal of Physics: Condensed Matter*. 1997;9(19): 3833–3851. https://doi.org/10.1088/0953-8984/9/19/005

59. Kalinin V. B., Golubev A. M. Splitting of cationic positions in crystal structures with special electrophysical properties. *Kristallografiya (Soviet Physics. Crystallography)*. 1990;35(6): 1472–1478. (In Russ.)

60. Astaf'ev A. V., Bosenko A. A., Voronkova V. I., Krasheninnikova M. A., Stefanovich S. Yu., Yanovskij V. K. Dielectric, optical properties and ionic conductivity of $TlNbWO_6$ and $RbNbWO_6$ crystals. *Kristallografiya (Soviet Physics. Crystallography)*. 1986;31(5): 968–973. (In Russ.)

61. Serdtsev A. V., Suetin D. V., Solodovnikov S. F., Gulyaeva O. A., Medvedeva N. I. Electronic structure and sodium-ion diffusion in glaserite-type $A_{3-x}Na_{1+x}(MoO_4)_2$ (A = Cs, K) studied with first-principles calculations. *Solid State Ionics*. 2020;357: 115484. https://doi.org/10.1016/j.ssi.2020.115484

Information about the authors

Tatiana S. Spiridonova, PhD in Chemistry, Researcher, Laboratory of Oxide Systems, Baikal Institute of Nature Management, Siberian Branch of the Russian Academy of Sciences (BINM SB RAS), Ulan-Ude, Russian Federation; e-mail: spiridonova-25@mail.ru. ORCID iD: https://orcid.org/0000-0001-7498-5103.

Sergey F. Solodovnikov, DSc in Chemistry, Professor, Leading Researcher, Laboratory of Crystal Chemistry, Nikolaev Institute of Inorganic Chemistry, Siberian Branch of the Russian Academy of Sciences (NIIC SB RAS), Novosibirsk, Russian Federation; e-mail: solod@niic.nsc.ru. ORCID iD: https://orcid.org/0000-0001-8602-5388.

Yulia M. Kadyrova, PhD in Chemistry, Researcher, Laboratory of Oxide Systems, Baikal Institute of Nature Management, Siberian Branch of the Russian Academy of Sciences (BINM SB RAS) and Senior Lecturer of the Department of General and Analytical Chemistry, Faculty of Chemistry, Banzarov Buryat State University (BSU), Ulan-Ude, Russian Federation; e-mail: yliychem@yandex.ru. ORCID iD: https://orcid.org/0000-0002-0106-8096.

Zoya A. Solodovnikova, PhD in Chemistry, Researcher, Laboratory of Crystal Chemistry, Nikolaev Institute of Inorganic Chemistry, Siberian Branch of the Russian Academy of Sciences (NIIC SB RAS), Novosibirsk, Russian Federation; e-mail: zoya@niic.nsc.ru. ORCID iD: https://orcid.org/0000-0001-5335-5567.

Alexandra A. Savina, PhD in Chemistry, Senior Researcher, Laboratory of Oxide Systems, Baikal Institute of Nature Management, Siberian Branch of the Russian Academy of Sciences (BINM SB RAS), Ulan-Ude, Russian Federation and Researcher, Skolkovo Institute of Science and Technology, Moscow, Russian Federation, e-mail: a.savina@skoltech.ru. ORCID iD: https://orcid.org/0000-0002-7108-8535.

Elena G. Khaikina, DSc in Chemistry, Professor, Chief Researcher, Laboratory Oxide Systems, Baikal Institute of Nature Management, Siberian Branch of the Russian Academy of Sciences (BINM SB RAS) and Professor of the Department of Inorganic and Organic Chemistry, Faculty of Chemistry, Banzarov Buryat State University (BSU), Ulan-Ude, Russian Federation; e-mail: egkha@mail.ru. ORCID iD: https://orcid.org/0000-0003-2482-9297.

Received 20 June 2021; Approved after reviewing 28 June 2021; Accepted for publication 15 July 2021; Published online 25 September 2021.

Translated by Valentina Mittova
Edited and proofread by Simon Cox

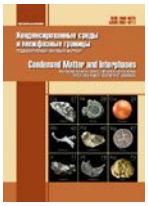

ISSN 1606-867X (Print)
ISSN 2687-0711 (Online)
Condensed Matter and Interphases
Kondensirovannye Sredy i Mezhfaznye Granitsy
https://journals.vsu.ru/kcmf/

Original articles

Research article
https://doi.org/10.17308/kcmf.2021.23/3534

Activation of film growth on indium phosphide by pulsed photon treatment

E. V. Tomina[1,2]✉, B. V. Sladkopevtsev[2], D. V. Serikov[3], I. Ya. Mittova[2]

[1]Morozov Voronezh State Forest Engineering University,
8 Timiryazeva ul., Voronezh 394087, Russian Federation

[2]Voronezh State University,
1 Universitetskaya pl., Voronezh 394018, Russian Federation

[3]Voronezh State Technical University,
14 Moskovsky prosp., Voronezh 394026, Russian Federation

Abstract

Photon activation of various physicochemical processes by the radiation of powerful pulsed xenon lamps (radiation range of 0.2-1.2 μm) is one of the promising areas of material science. The aim of this study was to determine the effect of pre-oxidative pulsed photon treatment on the process of thermal oxidation of indium phosphide with a nanosized layer of V_2O_5 on the surface, as well as its effect on the composition and morphology of the formed films.

We determined the optimal mode of pre-oxidative pulsed photon treatment of magnetron-formed V_2O_5/InP heterostructures with a radiation density of 15 J/cm^2. By laser and spectral ellipsometry methods, photon activation of V_2O_5/InP before thermal oxidation was found to increase the thickness of the formed films practically twofold. X-ray diffraction analysis confirms the intensification of the phosphate formation process. The morphological characteristics of the films were determined by atomic force microscopy.

Pre-oxidative pulsed photon treatment with an optimal radiation density of 15 J/cm^2 activates the thermal oxidation of V_2O_5/InP heterostructures. It is associated with the formation of new active centres and accelerated rearrangement of chemical bonds in the intermediate complexes of the V_2O_5 catalyst with semiconductor components.

Keywords: Indium phosphide, Vanadium (V) oxide, Thermal oxidation, Thermal oxidation, Pulsed photon treatment

Acknowledgements: Some of the research results were obtained using the equipment of Shared Scientific Equipment Centre of Voronezh State University. URL: http://ckp.vsu.ru. The study was partially supported by the Russian Foundation for Basic Research, project No. 18-29-11062 mk. The authors are grateful to V. M. Ievlev, Full Member of the Russian Academy of Sciences, for the opportunity to carry out pulsed photon treatment of the samples and assistance.

For citation: Tomina E. V., Sladkopevtsev B. V., Serikov D. V., Mittova I. Ya., Activation of film growth on indium phosphide by pulsed photon treatment. *Kondensirovannye sredy i mezhfaznye granitsy = Condensed Matter and Interphases.* 2021;23(3): 432–439. https://doi.org/10.17308/kcmf.2021.23/3534

Для цитирования: Томина Е. В., Сладкопевцев Б. В., Сериков Д. В., Миттова И. Я., Активация роста пленок на фосфиде индия импульсной фотонной обработкой. *Конденсированные среды и межфазные границы*. 2021;23(3): 432–439. https://doi.org/10.17308/kcmf.2021.23/3534

✉ Elena V. Tomina, e-mail: tomina-e-v@yandex.ru
© Tomina E. V., Sladkopevtsev B. V., Serikov D. V., Mittova I. Ya. 2021

The content is available under Creative Commons Attribution 4.0 License.

1. Introduction

Oxidation of $A^{III}B^{V}$ binary semiconductors is of great importance in various technological areas, such as designing optoelectronic devices, solar cells, and anti-reflective coatings, etc. [1–5]. Thermal oxidation of InP can be widely used in the development of cheap and highly efficient photoconverters of natural and linearly polarised radiation [6], it provides new approaches to the formation of MOS structures based on this semiconductor [7].

d-metal oxides are effective chemostimulators for the thermal oxidation of $A^{III}B^{V}$ semiconductors [8, 9]. Among them, vanadium (V) oxide has the highest potential. Deposited on the semiconductor surface even in a small amount, in the form of nanosized islands, it provides a catalytic mechanism for the thermal oxidation of indium phosphide [10].

The activation of physicochemical processes by irradiation with electrons, ions, and light is widely used to modify the subsurface layers of materials. One of the promising areas is pulsed photon treatment (PPT) by the radiation of powerful pulsed xenon lamps (radiation range of 0.2–1.2 μm) [11].

The aim of this study was to determine the effect of pre-oxidative PPT on the process of thermal oxidation of indium phosphide with a nanosized layer of V_2O_5 on the surface, as well as its effect on the composition and morphology of the formed films.

2. Experimental

For this study, we used monocrystalline indium phosphide plates (100), FIE-1A grade (indium phosphide, electronic conductivity), doped with tin, with the concentration of the main charge carriers no less than $5 \cdot 10^{16}$ cm^{-3}. The substrates were pre-treated in H_2SO_4 (92.80 %) : H_2O_2 (56 %) : H_2O = 2 : 1 : 1 for 10 min, then washed with distilled water. Nanosized layers of the chemostimulator, V_2O_5 oxide (~30 nm) were applied on the InP surface by magnetron sputtering (Covap II vacuum ion sputtering unit). The heterostructures were formed in a chamber vacuumised to a pressure of $2 \cdot 10^{-5}$ mm Hg. Metallic vanadium with a purity of 99.99 % was used as the initial target material, and O_2+Ar gases with a purity of 99.99 % were used as an ion source.

The process of thermal oxidation (TO) of the InP-based heterostructures was carried out in an MTP-2M-50-500 resistance heating furnace at a temperature of 530 °C for 1–60 minutes. Temperature was controlled by the TPM-10 unit with a precision of ± 1 °C. Oxidation was carried out in an oxygen flow (the volume flow rate was 30 l/h and the linear flow rate was 10 cm/min). Indium phosphide, oxidised in the same way without a chemostimulator, was used as a reference standard.

Pulsed photon treatment of the samples was carried out using a modernized UOLP-1M unit, designed for pulsed photon annealing of semiconductor materials. Heating was provided by the radiation of three INP 16/250 gas-discharge xenon lamps. The radiation dose for one treatment cycle was determined by the annealing time. It was regulated within the range of 0.02–20 s, which corresponds to 2–2000 unit pulses. The radiation dose varied from 15 to 120 J/cm^2.

To determine the thickness of the films of the formed heterostructures and films after TO (PPT), we used the methods of laser ellipsometry (LE, LEF-754) and spectral ellipsometry (SE, Ellips-1891).

To characterise the heterostructures and thin films formed on the semiconductor surface, a set of instrumental methods was used: X-ray diffraction analysis (XRD, ARL X'TRA diffractometer, Cu$K_{\alpha 1}$ with λ = 1.540562 Å); infrared spectroscopy (IRS, Vertex 70 IR Fourier spectrometer); atomic force microscopy (AFM, Solver P47 Pro (NT-MDT) scanning microscope with the HA_NC Etalon cantilever); scanning tunnelling microscopy (STM, Umka laboratory nanotechnology complex, based on the improved Umka-02-U scanning tunnelling microscope).

3. Results and discussion

A number of studies [12–15] revealed that the activating effect of PPT is expressed in the acceleration of diffusion processes, synthesis of thin films of the compounds, and recrystallisation. It is also associated with the decrease of temperature thresholds of phase formation, increase in the dispersity of synthesised structures, the formation of metastable phases, as well as nanocrystallisation of amorphous metal alloys. Nanocrystallisation leads to the increase in microhardness, while plasticity is preserved.

In order to select an optimal PPT mode for V_2O_5/InP heterostructures, a batch of samples were prepared. They underwent pulsed photon treatment at various radiation density values of 15, 30, 50, 60, and 90 J/cm^2. While optimising the PPT effect, we determined that the use of modes with a radiation dose of more than 50 J/cm^2 leaded to degradation of the surface of the heterostructure up to its complete destruction. We found out that a radiation density of 15 J/cm^2 can be considered optimal for the purposes of this study. Under these conditions the film grows most intensively with no degradation of the heterostructure.

Fig. 1 and Table 1 show the thickness values of the films formed by thermal oxidation of indium phosphide (intrinsic oxidation, reference standard), by the thermal oxidation of the V_2O_5/InP heterostructure without PPT, and upon pre-oxidative pulsed photon treatment carried out in the optimal mode.

The use of the Cauchy model for the interpretation of spectral ellipsometry data is confirmed by the good correlation (especially in the wavelength range above 500 nm) between the calculated and experimental spectra of the ellipsometric parameters Ψ and Δ (Fig. 2).

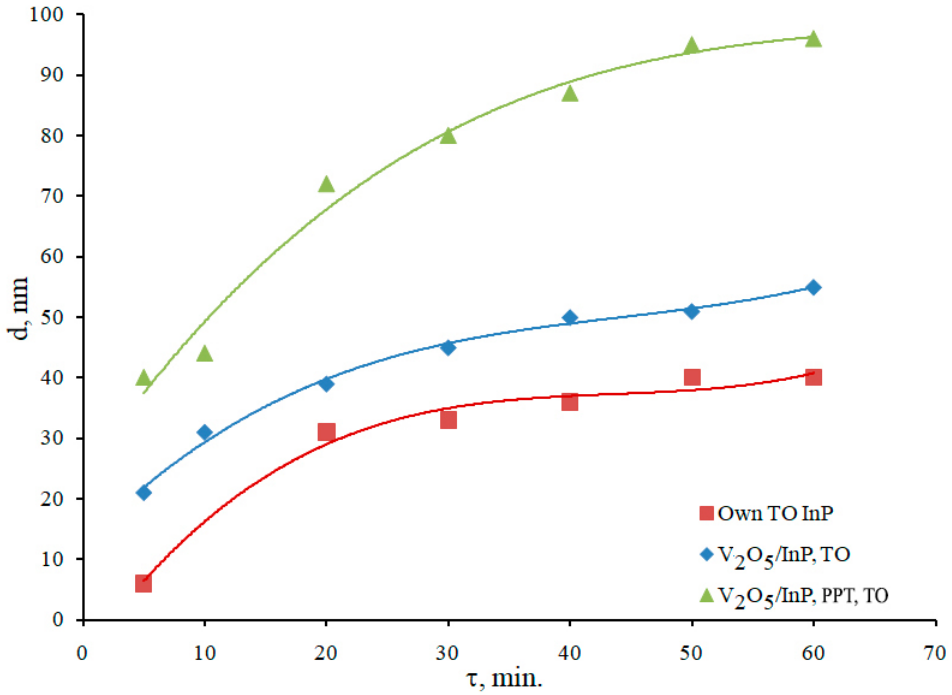

Fig. 1. Kinetic curves of the InP intrinsic thermal oxidation and the V_2O_5/InP heterostructures thermal oxidation, without PPT and upon PPT for 0.2 s. Oxidation temperature: 530 °C

Table 1. The thickness of the films formed by thermal oxidation of InP (reference) and V_2O_5/InP heterostructures without and with pre-oxidative PPT. Oxidation temperature: 530 °C

Oxidation time, min	Film thickness *d*, nm		
	InP intrinsic oxidation	V_2O_5/InP, thermal oxidation at 530 °C, without PPT	V_2O_5/InP, PPT 15 J/cm^2 and thermal oxidation at 530 °C
5	6	20	39
10	25	32	44
20	31	39	72
30	33	44	80
40	36	49	86
50	39	50	94
60	39	52	96

We had previously determined [8, 16] that thermal oxidation of InP with a magnetron-deposited nanoscale layer of V_2O_5 (25 nm) was carried out by the catalytic mechanism due to cyclic regeneration of V_2O_5 (the transition of vanadium from the oxidation state +5 (V_2O_5) to +4 (VO_2) and vice versa). We suggested the following "phase" evolution of the magnetron-formed V_2O_5/InP heterostructures during their thermal oxidation (Fig. 3).

At the initial stage of oxidation, due to the chemostimulating effect of V_2O_5 of the catalytic type, there is a sharp increase in the concentrations of oxides In_2O_3 and P_2O_5. In contrast to transition oxides (for example, NiO), which are consumed during the oxidation process, V_2O_5 is cyclically regenerated throughout the entire process. According to [17], this transition occurs quickly and with low energy consumption through the intermediate vanadium oxides V_3O_7

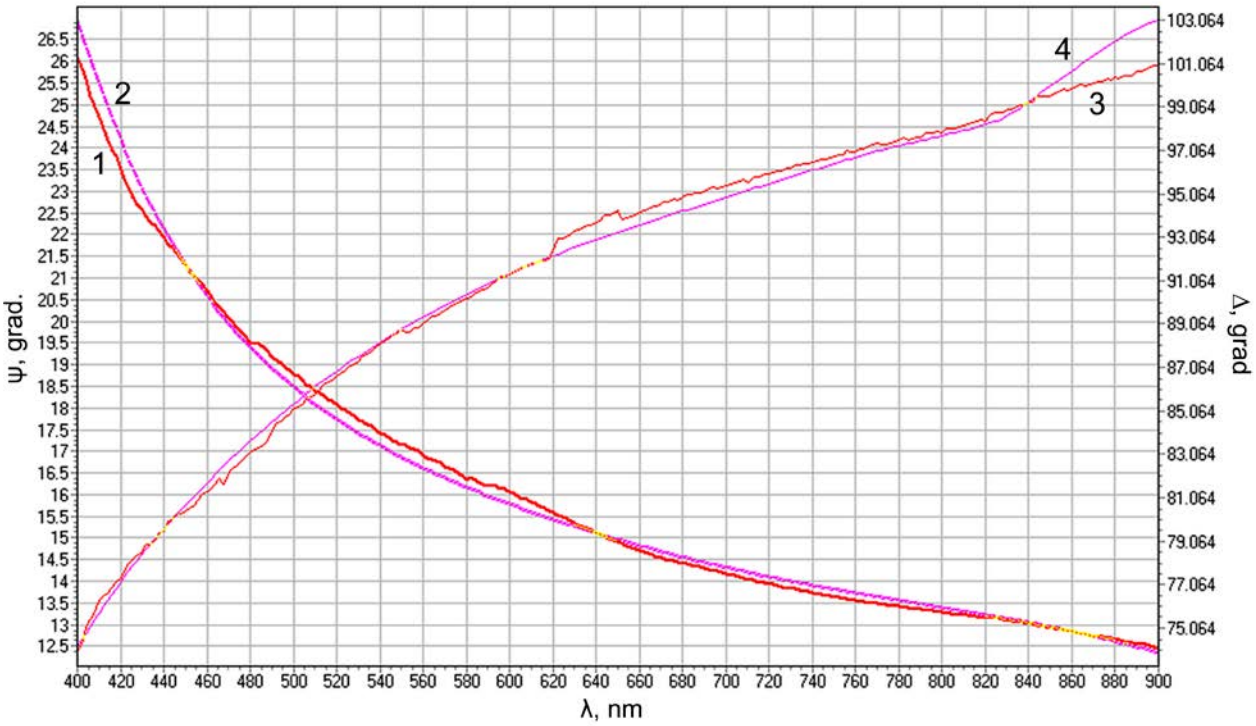

Fig. 2. Spectra of the ellipsometric parameters ψ (*1*,*2*) and Δ (*3*,*4*) of the V_2O_5/InP sample, which underwent preliminary PPT at 15 J/cm² and TO at 530 °C for 60 min (*1*,*3* – measured, *2*,*4* – calculated by the Cauchy model)

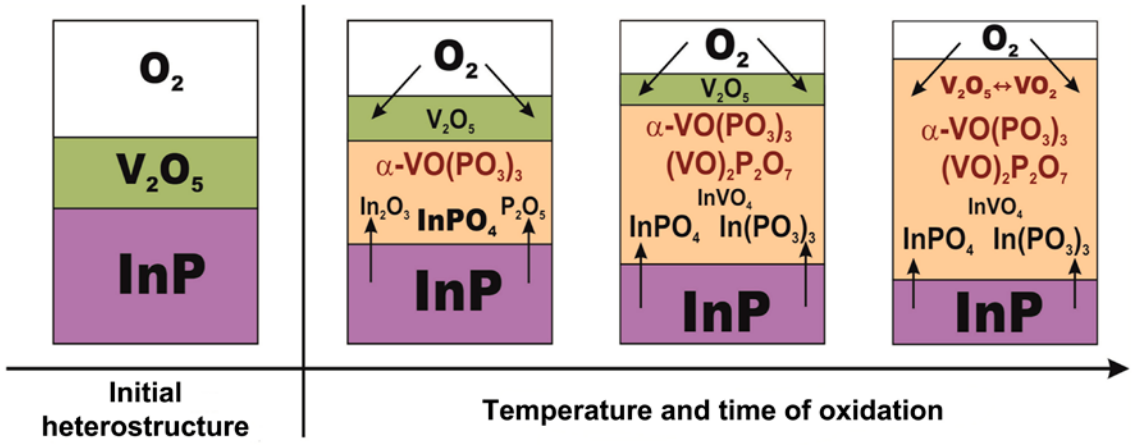

Fig. 3. Diagram of the evolution of V_2O_5/InP heterostructures during thermal oxidation

and V_4O_9, which were detected in the formed films by the XRD method. Thus, the chemostimulating effect of vanadium pentoxide, which involves the intensive oxidation of semiconductor components by the catalytic mechanism, persists throughout the entire thermal oxidation process. A rapid increase in the concentration of A^{III} and B^{V} oxides leads to the intensive development of secondary interactions in the system. They are accompanied with the formation of indium phosphate and are prominent due to the large acid-base difference between the A_2O_3 and B_2O_5 oxides. Due to the chemical nature of the vanadium (V) oxide, taking into account the isostructurality of vanadate ions with phosphate ions, vanadium in the form of vanadate is included in the forming phosphate framework of the films (in the form of $InVO_4$). Due to the electronic configuration V and the covalent type of chemical bonds between vanadium and oxygen, the metal is present in the films on the surface of indium phosphide in the form of vanadyl phosphates $VO(PO_3)_3$ and $(VO)_2P_2O_7$. It can be explained by the pronounced acidity of phosphorus oxide.

According to [17–19] the stepwise redox mechanism of catalytic oxidation at high temperatures is typical for most reactions where transition metal oxides act as catalysts, as the reduction and re-oxidation rates of the catalyst are rather high. Under other conditions of catalysis, for example, with a change in temperature, a transition from the stepwise mechanism to the associative mechanism is possible, when oxygen and the oxidised reagent interact simultaneously [17, 19]. The simultaneous presence of vanadium oxides exhibiting oxidation states +5 and +4 in the V_2O_5/InP heterostructures formed during the oxidation process, established by XRD and IRS methods, is an argument in favour of the stepwise oxidation mechanism. However, according to classical concepts [20], catalytic reactions, in the course of which the formation of an activated complex is preceded by the breaking of bonds in the initial reagent (dissociative mechanism), have high activation energy values, although lower as compared to the non-catalytic reaction. Low activation energy values are characteristic of catalytic reactions proceeding through an activated complex, which involves the particles of both reactants and the active centre of the catalyst at the same time (synchronous mechanism). For V_2O_5/InP heterostructures, the hard method of deposition (magnetron sputtering, exploding wire method) "imposes" the formation of interface intermediate complexes of the catalyst V_2O_5 with semiconductor components already in the synthesis process. That is, the weakening of the In-P bond and the beginning of the formation of the In-O and P-O bonds are simultaneous. Taking into account the low EAE values of the V_2O_5/InP thermal oxidation process, non-classical objects of study (solid reagent and catalyst, nanoscale state of the catalyst), it can be said these intermediate complexes are transformed by the mechanism of associative substitution by reactive oxygen species.

The pre-oxidative PPT of V_2O_5/InP heterostructures almost doubles the thickness of the films formed during thermal oxidation. According to [21], various physicochemical processes are activated by the PPT mainly due to the excess of a certain critical heating rate and athermal processes initiated by the interaction of the light flux with the substance. The effect of pulsed photon activation of the thermal oxidation process can be caused by an increase in the number of active centres. Interface intermediate complexes of the V_2O_5 catalyst with semiconductor components are formed on them, possibly, of a different chemical nature. In addition, a significant energetic effect on the heterostructure significantly facilitates the rearrangement of chemical bonds in intermediate complexes during oxidation and accelerates the formation of indium and phosphorus oxides, and, consequently, various phosphates. The XRD data for the film formed by thermal oxidation of the V_2O_5/InP heterostructure upon preliminary PPT (15 J/cm^2) indicate the formation of a pronounced phosphate and vanadate framework during oxidation (Fig. 4).

The pre-oxidative PPT of V_2O_5/InP heterostructures affects the morphological characteristics of the films formed by thermal oxidation. Thus, the surface of the film synthesised by oxidation of V_2O_5/InP at 530 °C for 60 min with preliminary PPT (E = 15 J/cm^2) is smooth, with no pronounced grain structure (Fig.5a). The difference in the relief height does not exceed 7 nm, the arithmetic mean roughness S_a is 0.4

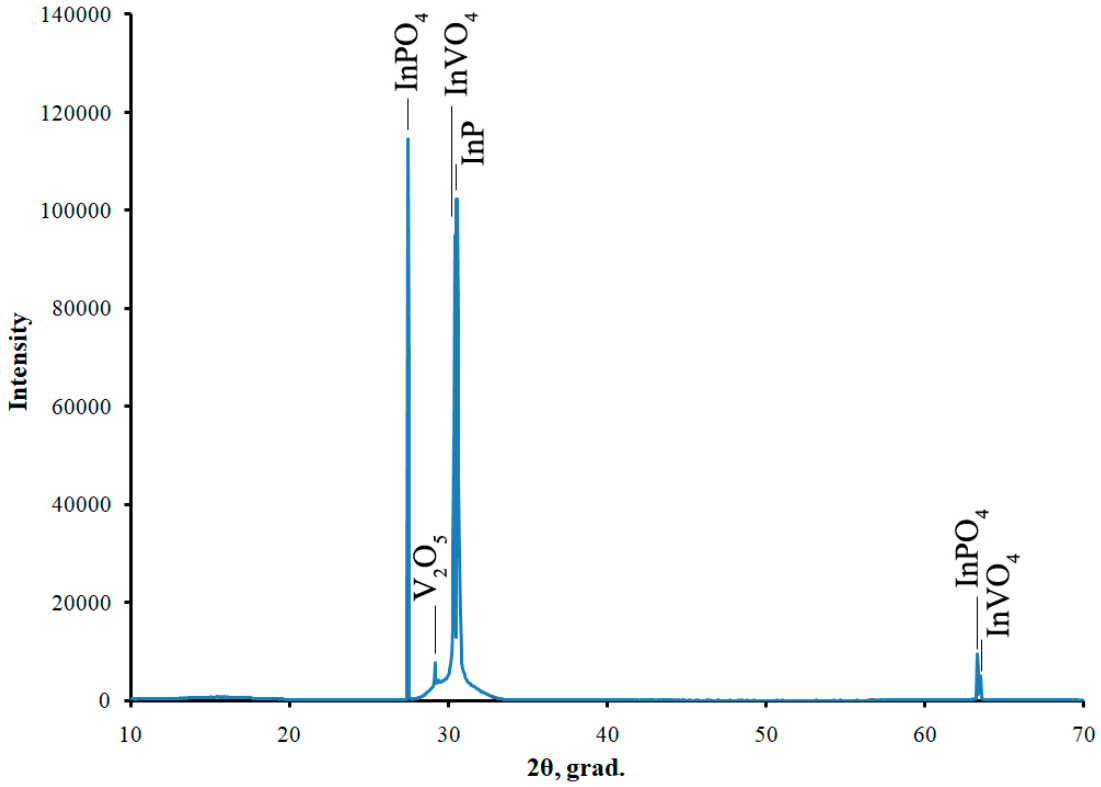

Fig. 4. Diffraction pattern of the V_2O_5/InP sample after preliminary PPT at 15 J/cm^2, followed by TO at 530 °C for 60 min

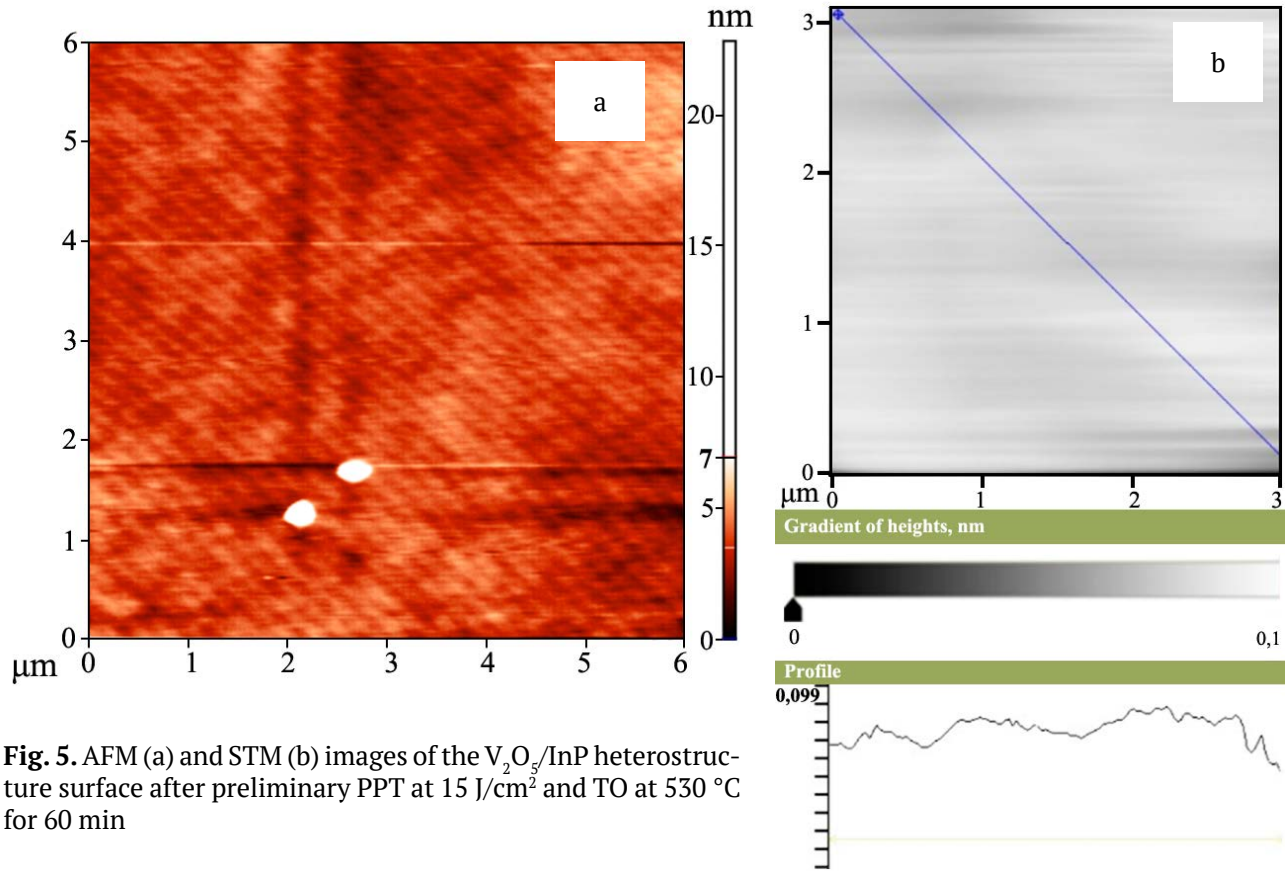

Fig. 5. AFM (a) and STM (b) images of the V_2O_5/InP heterostructure surface after preliminary PPT at 15 J/cm^2 and TO at 530 °C for 60 min

nm, the mean square roughness S_q is 0.6 nm. The STM data also confirm the high smoothness of these films (Fig. 5b). The height gradient does not exceed 10 nm.

4. Conclusions

Pre-oxidative PPT with an optimal radiation density of 15 J/cm^2 activates the thermal oxidation of the V_2O_5/InP heterostructures, resulting in an almost twofold increase in the thickness of the formed films. The PPT effect is associated with the formation of new active centres, where intermediate complexes of the catalyst V_2O_5 with semiconductor components are formed. The transformation of chemical bonds in these complexes also accelerates, resulting in the formation of indium and phosphorus oxides. Preliminary PPT stimulates the growth of films with a smooth surface, which arithmetic mean roughness S_a is 0.4 nm.

Author contributions

All authors made an equivalent contribution to the preparation of the publication.

Conflict of interests

The authors declare that they have no known competing financial interests or personal relationships that could have influenced the work reported in this paper.

References

1. Chistokhin I. B., Zhuravlev K. S. Microwave photodetectors for analog fiber optic communications. *Uspekhi prikladnoi fiziki (Advances in Applied Physics)*. 2015;3(1): 85–94. Available at: https://elibrary.ru/item.asp?id=22968188 (In Russ., abstract in Eng.)

2. Sheng S. Li. *Semiconductor physical electronics*. New York: Springer-Verlag; 2006. 708 p. https://doi.org/10.1007/0-387-37766-2

3. Arbiol J., Xiong Q. *Semiconductor nanowires: Materials, Synthesis, Characterization and Applications*. Elsevier Ltd.; 2015. 554 p.

4. Ahmad S. R., Cartwright M. *Laser ignition of energetic materials*. John Wiley & Sons Ltd; 2015. 425 p.

5. Ünlü H., Horing N. J. M., Dabowski J. *Low-dimensional and nanostructured materials and devices*. Springer Science LCC; 2015. 674 p. https://doi.org/10.1007/978-3-319-25340-4

6. Nikolaev Yu. A., Rud' Yu. V., Terukov E. I., Rud' V. Yu. Photosensitivity of heterojunctions obtained using thermal oxidation of indium phosphide. *Technical Physics Letters*. 2007;33(4): 313–315. https://doi.org/10.1134/S1063785007040128

7. Isakov D. S., Korobov P. P., Khabibullin I. M., Valyukhov D. P. *Issledovanie vzaimodeistviya kisloroda s poverkhnost'yu (110)* A^3V^5 [Study of the interaction of oxygen with the (110) A^3B^5 surface]. *Vestnik Severo-Kavkazskogo federal'nogo universiteta*. 2010;(2): 40–45. Available at: https://elibrary.ru/item.asp?id=15004240 (In Russ., abstract in Eng.)

8. Tomina E. V., Mittova I. Ya., Sladkopevtsev B. V., Kostryukov V. F., Samsonov A. A., Tretyakov N. N. Thermal oxidation as a method of formation of nanoscale functional films on $A^{III}B^V$ semiconductors: chemostimulated influence of metal oxides: overview. *Kondensirovannye sredy i mezhfaznye granitsy = Condensed Matter and Interphases*. 2018;20(2):184–203. https://doi.org/10.17308/kcmf.2018.20/522 (In Russ., abstract in Eng.)

9. Mittova I. Ya., Tomina E. V., Lapenko A. A., Khorokhordina A. O. Solid-state reactions during thermal oxidation of vanadium-modified GaAs surfaces. *Inorganic Materials*. 2004;40(5): 441–444. https://doi.org/10.1023/B:INMA.0000027588.78546.af

10. Mittova I. Y., Tomina E. V., Lapenko A. A., Sladkopevtsev B. V. Synthesis and catalytic performance of V_2O_5 nanoislands produced on the surface of InP crystals by electroexplosion. *Inorganic Materials*. 2010;46(4): 383–388. https://doi.org/10.1134/S0020168510040114

11. Ievlev V. M., Latyshev A. N., Selivanov V. N., Turaeva T. L., Sinel'nikov A. A. Effect of photon irradiation on the process of recrystallization of thin metallic films. *The Physics of Metals and Metallography*. 2007;103(1): 58–63. https://doi.o0rg/10.1134/S0031918X07010073

12. Ievlev V. M., Ilyin V. S., Kushev S. B., Soldatenko S. A., Lukin A. N., Belonogov E. K. Synthesis of nanostructured SiC films during pulsed photon treatment of Si in a carbon-containing atmosphere. *Journal of Surface Investigation: X-Ray, Synchrotron and Neutron Techniques*. 2009;3(5): 791–796. https://doi.org/10.1134/S102745100905022X

13. Ievlev V. M., Kannykin S. V., Kuschev S. B., Sinelnikov A. A., Soldatenko S. A. Rutile film synthesis activated by pulse photon treatment. *Physics and Chemistry of Materials Treatment*. 2011;(4): 5–9. Available at: https://elibrary.ru/item.asp?id=16757064 (In Russ., abstract in Eng.)

14. Vavilova V. V., Palii N. A., Ievlev V. M., Darinskii B. M., Yudin L. Y., Kalinin Y. E., Kushchev S. B., Pokazan'eva S. A. Effect of pulsed photon irradiation on the formation of a nanocrystalline structure in Fe-Pb-Nb amorphous alloys. *Russian Metallurgy (Metally)*. 2011;(5): 471–478. https://doi.org/10.1134/S0036029511050156

15. Gerasimenko Yu. V., Logacheva V. A., Babushkina E. V., Khoviv A. M. Struktura i opticheskie svoistva

plenok dioksida titana, legirovannykh lantanom [Structure and optical properties of lanthanum-doped titanium dioxide films]. *Kondensirovannye sredy i mezhfaznye granitsy = Condensed Matter and Interphases*. 2010;12(4): 348–354. Available at: https://journals.vsu.ru/kcmf/article/view/1132/1214 (In Russ.)

16. Mittova I. Ya., Tomina E. V., Lapenko A. A., Sladkopevtsev B. V. Kataliticheskoe deistvie vanadiya i ego oksida (V) v protsessakh oksidirovaniya poluprovodnikov $A^{III}B^{V}$ [Catalytic action of vanadium and its oxide (V) in the processes of oxidation of $A^{III}B^{V}$ semiconductors]. *Nanosystems: Physics, Chemistry, Mathematics*. 2012;3(2): 116–138. Available at: https://elibrary.ru/item.asp?id=17881315 (In Russ.)

17. Krylov O. V. *Geterogennyi kataliz* [Heterogeneous catalysis]. Moscow: FIZMATLIT Publ.; 2004. 679 p. (In Russ.)

18. Geits B., Kettsir Dzh., Shuit G. Gates B. C., Katzer J. R., Schult G. C. A. *Chemistry of catalytic processes*. New York: McGraw-Hill Book Company; 1979. 464 p.

19. Krylov O. V., Kiselev V. F. *Adsorbtsiya i kataliz na perekhodnykh metallakh i ikh oksidakh* [Adsorption and catalysis on transition metals and their oxides]. Moscow: Khimiya Publ .; 1981. 286 p. (In Russ.)

20. *Fizicheskaya khimiya* [Physical chemistry]: v 2-kh kn. / pod red. K. S. Krasnova. – Kn. 1: Stroenie veshchestva. Termodinamika. Moscow: Vysshaya shkola Publ.; 2001. 318 p. (In Russ.)

21. John T. Yates Jr. Photochemistry on TiO_2: Mechanisms behind the surface chemistry. *Surface science*. 2009;603(10): 1605–1612. https://doi.org/10.1016/j.susc.2008.11.052

Information about the authors

Elena V. Tomina, DSc in Chemistry, Associate Professor, Head of the Department of Chemistry, Morozov Voronezh State University of Forestry and Technologies, Voronezh, Russian Federation; e-mail: tomina-e-v@yandex.ru. ORCID iD: https://orcid.org/0000-0002-5222-0756.

Boris V. Sladkopevtsev, PhD in Chemistry, Associate Professor at the Department of Materials Science and Nanosystems Technologies, Voronezh State University, Voronezh, Russian Federation; e-mail: dp-kmins@yandex.ru. ORCID iD: https://orcid.org/0000-0002-0372-1941.

Dmitrii V. Serikov, engineer researcher of the Department of Solid-State Physics, Voronezh State Technical University, Voronezh, Russian Federation, e-mail: dmitriy.tut@mail.ru. ORCID iD: https://orcid.org/0000-0002-0464-3500.

Irina Ya. Mittova, DSc in Chemistry, Professor, Professor at the Department of Materials Science and Nanosystems Technologies, Voronezh State University, Voronezh, Russian Federation; e-mail: imittova@mail.ru. ORCID iD: https://orcid.org/0000-0001-6919-1683.

Received 6 June2020; Approved after reviewing 25. June2021; Accepted 15July 2021; Published online 25 September2021.

Translated by Anastasiia Ananeva
Edited and proofread by Simon Cox

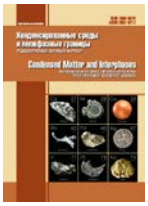

ISSN 1606-867X (Print)
ISSN 2687-0711 (Online)
Condensed Matter and Interphases
Kondensirovannye Sredy i Mezhfaznye Granitsy
https://journals.vsu.ru/kcmf/

Original articles

Research article
https://doi.org/10.17308/kcmf.2021.23/3535

An integral feature of porous silicon and its classification

A. M. Khort✉, **A. G. Yakovenko, Yu. V. Syrov**

MIREA – Russian Technological University. Institute of Physics and Technology,
78 Prospekt Vernadskogo, Moscow 119454, Russian Federation

Abstract

Porous silicon is currently one of the most studied materials which is used both in the areas traditional for silicon, such as electronics and optoelectronics, and in completely unconventional ones, such as catalysis, energetics, biology, and medicine. The multiple possibilities of the material are revealed due to the fact that its structure can be radically different depending on the properties of the initial silicon and the methods of obtaining porous phases. The use of any material inevitably leads to the need to classify its various forms. The purpose of the article was to find the most significant parameter that can be used as the basis for the classification of porous silicon.

Historically, the terminology defined by the IUPAC pore size classification has been used to classify porous silicon. Due to the authority of IUPAC, many researchers have considered this terminology to be the most successful and important, and the radial pore size has often been regarded as a main parameter containing the most important properties of porous silicon. Meanwhile, the unique properties and practical application of porous silicon are based on its developed inner surface. The method of nitrogen porosimetry, which is simple in its practical implementation, is often used in scientific literature to determine this value.

The most suitable integral parameter for the classification of porous silicon, regardless of its structure and morphology, is the total specific internal surface (cm^{-1}) that can be relatively easily established experimentally and is of fundamental importance for almost all applications of porous silicon. The use of this value does not exclude the use of other parameters for a more detailed classification.

Keywords: Porous silicon, Classification, Radial pore size, Nitrogen porosimetry, Ttotal specific internal surface area

For citation: Khort A. M., Yakovenko A. G., Syrov Yu. V. An integral feature of porous silicon and its classification. *Kondensirovannye sredy i mezhfaznye granitsy = Condensed Matter and Interphases.* 2021;23(3): 440–444. https://doi.org/10.17308/kcmf.2021.23/3535

Для цитирования: Хорт А. М., Яковенко А. Г., Сыров Ю. В. Интегральный признак и классификации пористого кремния. *Конденсированные среды и межфазные границы*. 2021;23(3): 440–444. https://doi.org/10.17308/kcmf.2021.23/3535

✉ Andrei M. Khort, e-mail: poristsil@yandex.ru
©Khort A. M., Yakovenko A. G., Syrov Yu. V., 2021

The content is available under Creative Commons Attribution 4.0 License.

1. Introduction

There are a great number of publications related to the study of porous silicon (PS), which shows increased interest to this material. The range of practical application of PS is potentially wide, from electronics, optoelectronics, and lithium-ion batteries to medicine [1, 6]. In simplistic terms, the properties of the material itself are determined by such parameters of porous layers as radial and axial pore size, interporous distances, and related density of pore distribution.

Currently, the following parameters are used in scientific literature to characterise the PS layers of various functional purpose: porosity, luminescence radiation wavelength, radial pore size, and some others. Certainly, each of these parameters describes the material only from the point of view of its functional use. At the same time, porosity is often mentioned as an "integral" parameter of PS which is the determining one for the properties of this material. However, this parameter is not significant for porous silicon, unlike most porous materials. It only indicates the correlation between the volume of the etched silicon and the full volume of silicon subjected to etching and is not related to the main properties of the material. This parameter is more likely to be applied to macrosystems and it carries certain functional information for the description of density and partly for the description of specific thermal and electric conductivity as well as mechanical properties, etc. The parameter is not so much informative for microsystems and especially for nanoscale systems. At the same time, such parameters as radial pore size, the density of their distribution, and growth direction are important on their own, although they rather describe the type of PS layers in the form of individual pores in the shape of a well and do not characterise any PS layers of other types. The International Union of Pure and Applied Chemistry (IUPAC) has accepted the size factor as the "classification parameter" of PS, so the pores are categorised by their size (micropores (d < 2 nm), mesopores (d = 20÷50 nm), and macropores (d > 50 nm)) [7, 8]. In our opinion, this classification is surely useful from the point of view of express classification of PS and is widely used in scientific literature, but it considers only its well-shaped structure and the underlying classification parameter of the radial pore size. This does not take into consideration such important parameters of PS layers as density of pore distribution, layer thickness, pore growth direction, and others. This does not allow determining general integral properties of PS layers and drawing conclusions about the possibility of their functional use. In fact, we can state that currently there is no integral feature that can characterise all or at least most types of PS layers.

2. Analysis of the parameters used in studies on porous silicon

PS layers have relatively varied structures [9] that depend both on the conditions of their production (duration of etching, current density, etching reagent composition, etc.) and on the parameters of the initial silicon (conductivity type, impurity type and concentration, crystallographic orientation of the initial silicon wafer, etc.). These parameters determine the places of the origin of pores and influence their development as well as the formation of layers with different morphology, for example, in the form of individual well-shaped pores, coral-like threads, rods, and other similar formations. Taking in consideration the aforementioned, we believe it is reasonable and important to choose some integral PS-characterising parameter which would indicate the specific features of almost all the formed layers while not depending much on their individual structure and morphology.

PS layers of any modification are characterised by a highly-developed surface of nanostructured layers being formed that in most cases are responsible for the practical significance of PS in the majority of the areas of practical use of PS (adsorption, medicine, energetics, etc.). It should be taken into account that the surface formed during the electrochemical etching of silicon contains different atomic groups such as Si-H_n, Si-OH, Si-O-Si, etc. [10] that can participate in various physicochemical processes determining the functional properties of the materials.

Thus, based on the aforementioned, we believe that the integral parameter is the total specific inner surface of PS which is able to characterise various obtained materials without specifying their structural individuality. The detailed

description of the types of characterisations of porous objects is presented in [11]. Total specific inner surface is often used when describing different porous materials. However, this parameter is very rarely used in the works related to porous silicon. This can be due to the fact that it is very laborious to determine it, and authors of the studies believe that this parameter can be fully replaced by porosity. At the same time, as it was mentioned above, a great number of properties of porous silicon depend on the behaviour of the pore surface, and the parameter we propose, the specific inner surface, seems to reflect the properties of porous silicon more comprehensively. This parameter surely depends on radial and axial pore sizes as well as the density of their distribution, as it contains the part of the total inner surface of PS that corresponds to these formations. Unlike the classification feature of IUPAC, this one allows characterising PS not by a particular parameter (radial pore size) but by the parameter that indicates the most important property for the use of this material which has a certain numeric value even in case when the pores of all size ranges from the IUPAC classification can be found in a PS layer at the same time.

The introduction of the parameter of total specific internal surface for the characterisation of PS is reasonable due to the fact that a great proportion of atoms in nanosized formations are located on the surface of particles and they participate in the implementation of surface phenomena. Table 1 shows these changes in the fraction of surface atoms depending on the number of atoms in the volume [12].

Table 1. Dependence of the fraction of surface atoms on the number of atoms in the volume of particles [12]

The number of atoms in the volume, cm^{-3}	10^6	10^5	10^4	10^3	10^2
Fraction of surface atoms, %	4	9	19	40	86

When the number of atoms in the volume decreases (that is, when the size of a particle decreases) from 10^6 to 10^2, the fraction of surface atoms increases to 86 %. The number of atoms in the volume 10^4 approximately corresponds to the lower size of a nanoparticle (2 nm). This is the state that determines an additional excess of surface energy, the so-called size effect typical for nanoformations.

The suggested classification parameter is the ratio of the total inner surface of PS to the volume of the etched material, and it has the dimension of the inverse length (cm^{-1}). The total area formed by the etching of the surface can be determined by the standard method of nitrogen porosimetry, and the volume with due consideration of density is calculated through the weight of silicon after etching which can be determined by a simple gravimetric method of weighing.

It should be noted that it is reasonable to use the suggested parameter not only because it can characterise PS in various fields of application, such as energy, sensory studies, optoelectronics, medicine, pharmacy, and biology, but also because it can classify and characterise the obtained nanoparticles based on PS. The practical significance of the suggested classification parameter can be confirmed by the analysis of scientific literature where, in addition to the IUPAC classification, the parameters related to the total specific internal surface of PS are used directly or indirectly [13–30].

It is reasonable to use this parameter for the classification of PS by its numeric values that determine the area of greatest effectiveness of application of this material. Such classification may include, for example, the display area of a quantum size effect (optoelectronics), or the area determined by the value of specific surface depending on the linear pore sizes or the density of their distribution (sensory studies and medicine), etc.

3. Conclusions

The introduction of a new classification feature, the total specific internal surface of PS layers, as an integral feature will allow defining the special characteristics and properties of various PS layers more comprehensively. The greater difficulty of its determination, as compared to the traditional parameters described above, is compensated for by its greater informational value, which makes it more preferable compared to other features. The use of this value does not exclude the use of other parameters for a more detailed classification.

Author contributions

All authors made an equivalent contribution to the preparation of the publication.

Conflict of interests

The authors declare that they have no known competing financial interests or personal relationships that could have influenced the work reported in this paper.

References

1. Canham L. (ed.). *Handbook of porous silicon*. Springer International Publishing Switzerland, 2014. 1024 p. https://doi.org/10.1007/978-3-319-05744-6

2. Ishchenko A. A., Fetisov G. V., Aslanov P. A. *Nanokremnii: svoistva, poluchenie, primenenie, metody ispol'zovaniya i kontrolya* [Nanosilicon: properties, production, application, methods of use and control]. Moscow: FIZMATLIT Publ., 2011. 648 p. Available at: https://biblioclub.ru/index.php?page=book&id=457660 (In Russ.)

3. Jia H., Li X., Song J. et al. Hierarchical porous silicon structures with extraordinary mechanical strength as high-performance lithium-ion battery anodes. *Nature Communications*. 2020;11(1): 1474. https://doi.org/10.1038/s41467-020-15217-9

4. Collins J., de Souza J. P., Hopstaken M., Ott J. A., Bedell S. W., Sadana D. K. Diffusion-controlled porous crystalline silicon lithium metal batteries. *iScience*. 2020;23(10): 101586. https://doi.org/10.1016/j.isci.2020.101586

5. Paczesny J., Richter Ł., Hołyst R. Recent progress in the detection of bacteria using bacteriophages. A Review. *Viruses*. 2020;12(8): 845. https://doi.org/10.3390/v12080845

6. Gongalsky M. B., Sviridov A. P., Bezsudnova Y. I., Osminkina L. A. Biodegradation model of porous silicon nanoparticles. *Colloids and Surfaces B: Biointerfaces*. 2020;190: 110946. https://doi.org/10.1016/j.colsurfb.2020.110946

7. Manual of symbols and terminology for physicochemical quantities and units. *Pure and Applied Chemistry*. 1979:51(1): 1–41. https://doi.org/10.1351/pac197951010001

8. *Compendium of chemical terminology gold book*. International union of pure and applied chemistry. Version 2.3.3 2014-02-24. IUPAC Compendium of Chemical Terminology. Available at: https://goldbook.iupac.org/files/pdf/goldbook.pdf

9. Yuzova V. A., Levitsky A. A., Harlashin P. A. Development technology of creation and research porous silicon. *Journal of Siberian Federal University. Engineering and Technologies*. 2011;4(1): 92–112. Available at: https://elibrary.ru/item.asp?id=15610067 (In Russ., abstract in Eng.)

10. Lenshin A. S., Kashkarov V. M., Seredin P. V., Spivak Yu. M., Moshnikov V. A. XANES and IR spectroscopy study of the electronic structure and chemical composition of porous silicon on *n*- and *p*-type substrates. *Semiconductors*. 2011;45: 1183. ttps://doi.org/10.1134/S1063782611090168

11. Fandeev V. P., Samokhina K. S. Research methods of porous structures. *Internet journal "Science Science"*. 2015;7(4). Available at: http://naukovedenie.ru/PDF/34TVN415.pdf (In Russ., abstract in Eng.)

12. Zimon A. D. *Karliki. Nanochasticy v populjarnom izlozhenii* [Dwarfs. Popular presentation of nanoparticles]. Moscow: Nauchnyj mir Publ., 2012. 160 p. (In Russ.)

13. Zharova Ju. A., Fedulova G. V., Astrova E. V., Baldycheva A. V., Tolmachev V. A., Perova T. S. Fabrication technology of heterojunctions in the lattice of a 2D photonic crystal based on macroporous silicon. *Semiconductors*. 2011;45(8): 1103-1110. https://doi.org/10.1134/s1063782611080239

14. Kashkarov V. M., Len'shin A. S., Seredin P. V., Agapov B. L., Cipenjuk V. N. Chemical modification of porous and corrugated silicon surfaces in polyacrylic acid solutions. *Journal of Surface Investigation. X-ray, Synchrotron and Neutron Techniques*. 2012;6(5): 776–781. https://doi.org/10.1134/S1027451012090078

15. Amdouni S., Rahmani M., Zaïbi M.-A, Oueslati M. Enhancement of porous silicon photoluminescence by electroless deposition of nickel. *Journal of Luminescence*. 2015;157: 93–97. https://doi.org/10.1016/j.jlumin.2014.08.041

16. Santos H. A, Bimbo L. M, Lehto V. P, Airaksinen A. J, Salonen J., Hirvonen J. Multifunctional porous silicon for therapeutic drug delivery and imaging. *Current Drug Discovery Technologies*. 2011;8(3): 228-249. https://doi.org/10.2174/157016311796799053

17. Lenshin A. S., Seredin P. V., Agapov B. L., Minakov D. A., Kashkarov V. M. Preparation and degradation of the optical properties of nano-, meso-, and macroporous silicon. *Materials Science in Semiconductor Processing*. 2015;30(2): 25-30. https://doi.org/10.1016/j.mssp.2014.09.040

18. Len'shin A. S., Kashkarov V. M., Turishchev S. Yu., Smirnov M. S., Domashevskaya E. P. Influence of natural aging on photoluminescence from porous silicon. *Technical Physics*. 2012;57(2): 305–307. https://doi.org/10.1134/s1063784212020156

19. Turishchev S. Yu., Terehov V. A., Nesterov D. N., Koltygina K. G., Parinova E. V., Kojuda D. A, Schleusener A., Sivakov V., Domashevskaya E. P. Electronic structure of silicon nanowires formed by the MAWCE method. *Kondensirovannye sredy i mezhfaznye granitsy = Condensed Matter and Interphases*. 2016;18(1): 130–141. Available at: https://elibrary.ru/item.asp?id=25946634 (In Russ., abstract in Eng.)

20. Travkin P. G., Vorontsova N. V., Vysotskiy S. A., Lenshin A. S., Spivak Yu. M., Moshnikov V. A. Study of regularities of porous silicon structure formation with multistage modes of electrochemical etching. *Proceedings of Saint Petersburg Electrotechnical University*. 2011;4: 3–8. https://elibrary.ru/item.asp?id=16313017 (In Russ.)

21. Len'shin A. S., Kashkarov V. M., Turishchev S. Yu., Smirnov M. S., Domashevskaya E. P. Effect of natural aging on photoluminescence of porous silicon. *Technical Physics Letters*. 2011;37(9): 789–792. https://doi.org/10.1134/s1063785011090124

22. Lenshin A. S., Kashkarov V. M., Seredin P. V., Minakov D. A., Agapov B. L., Kuznetsova M. A., Moshnikov V. A., Domashevskaya E. P. Study of the morphological growth features and optical characteristics of multilayer porous silicon samples grown on *n*-type substrates with an epitaxially deposited *p*+-layer. *Semiconductors*. 2012;46(8): 1079–1084. https://doi.org/10.1134/s1063782612080131

23. Khenkin M. V., Emelyanov A. V., Kazanskii A. G., Forsh P. A., Kashkarov P. K., Terukov E. I., Orekhov D. L., Roca i Cabarrocas P. Influence of the fabrication conditions of polymorphous silicon films on their structural, electrical and optical properties *Semiconductors*. 2013;47(9): 1271–1274. https://doi.org/10.1134/s1063782613090108

24. Lenshin A. S., Maraeva E. V. Studying specific surface area of perspective porous materials and nanostructures by nitrogen thermal desorption method. *Proceedings of Saint Petersburg Electrotechnical University*. 2011;6: 9–16. Available at: https://elibrary.ru/item.asp?id=16403450 (In Russ.)

25. Karnaukhov A. P. Adsorbtsiya. *Tekstura dispersnykh i poristykh materialov* [Adsorption. The texture of dispersed and porous materials]. Novosibirsk: Nauka Publ., 1999. 470 p. Available at: https://www.booksite.ru/localtxt/kar/nau/hov/text.pdf (In Russ.)

26. Levitskiy V. S., Lenshin A. S., Maximov A. I., Maraeva E. V., Moshnikov V. A. Investigation of formation porous structures in sol– gel systems by silicon oxide and oxides of metals. *Izvestiya Vysshikh Uchebnykh Zavedenii. Materialy Elektronnoi Tekhniki = Materials of Electronics Engineering*. 2012;4: 48–54. https://doi.org/10.17073/1609-3577-2012-4-48-53

27. Arroyo-Hernández M., Martín-Palma R. J., Torres-Costa V., Martínez Duar J. M. Porous silicon optical filters for biosensing applications. *Journal of Non-Crystalline Solids*. 2006;352(23-25): 2457–2460. https://doi.org/10.1016/j.jnoncrysol.2006.02.075

28. Tutov E. A., Pavlenko M. N., Tutov E. E., Protasova I. V., Bormontov E. N. Equilibrium and nonequilibrium electrode processes on porous silicon. *Technical Physics Letters*. 2006;32(13): 558–560. https://doi.org/10.1134/s1063785006070029

29. Sviridov A. P., Andreev V. G., Ivanova E. M., Osminkina L. A., Tamarov K. P., Timoshenko V. Y. Porous silicon nanoparticles as sensitizers for ultrasonic hyperthermia. *Applied Physics Letters*, 2013;103(19), 193110. https://doi.org/10.1063/1.4829148

30. Kotkovskiy G. E., Kuzischin Yu. A., Martynov I. L., Nabiev I. R., Chistyakov A. A. Fotofizicheskie svojstva poristogo kremnija i ego primenenie v tehnike i biomedicine [Photophysical properties of porous silicon and its application in engineering and biomedicine]. *Nuclear Physics and Engineering*. 2013;4(2): 174–192. https://doi.org/10.1134/s2079562913020073 (In Russ.)

Information about the authors

Andrey M. Khort, PhD in Chemistry, Associate Professor at the B. A. Dogadkin Department of Physics and Chemistry of Materials, MIREA – Russian technological university, Institute of Physics and Technology, Moscow, Russian Federation; e-mail: poristsil@yandex.ru. ORCID iD: https://orcid.org/0000-0001-8931-1793.

Anatoliy G. Yakovenko, DSc in Technical, Full Professor, Professor at the B. A. Dogadkin Department of Physics and Chemistry of Materials, MIREA – Russian technological university, Institute of Physics and Technology, Moscow, Russian Federation; e-mail: anavenko@yandex.ru. ORCID iD: https://orcid.org/0000-0001-9152-6566.

Yury V. Syrov, PhD in Physics and Mathematics, Associate Professor at the B. A. Dogadkin Department of Physics and Chemistry of Materials, MIREA – Russian technological university, Institute of Physics and Technology, Moscow, Russian Federation; e-mail: yvsyrov@yandex.ru. ORCID iD: https://orcid.org/0000-0003-2226-5790.

Received 9 June 2021; Approved after reviewing 8 July 2021; Accepted for publication 15 August 2021; Published online 25 September 2021.

Translated by Marina Strepetova
Edited and proofread by Simon Cox